



京都大学 防災研究所
Disaster Prevention Research Institute
Kyoto University

特定研究集会
2022C-01

スロー地震と海溝型巨大地震の関係はどこまで
明らかになり、今後、何を明らかにすべきか？：

南海トラフ巨大地震災害の軽減を目指して

**What do we know and what do we need to know about the
relation between slow earthquakes and megathrust
earthquakes?: Toward disaster mitigation of the Nankai
Trough earthquake**

令和5年5月

May, 2023

研究代表者 西川友章

Coordinator Tomoaki NISHIKAWA

特定研究集会（ 課題番号 : 2022C-01 ）

集会名：スロー地震と海溝型巨大地震の関係はどこまで明らかになり、今後、何を明らかにすべきか？：南海トラフ巨大地震災害の軽減を目指して（International Joint Workshop on Slow-to-Fast Earthquakes 2022）（共催）

主催：令和3～7年度 文部科学省 科学研究費助成事業 学術変革領域研究(A)「Slow-to-Fast 地震学」

共催：東京大学地震研究所共同利用研究集会「スロー地震から高速破壊まで全地震現象の包括的理解を目指して」

研究代表者：西川 友章

職 名 : 助教

所属機関名：京都大学防災研究所

開催日：令和 4 年 9 月 14 日 ～ 16 日

開催場所：奈良春日野国際フォーラム 麓（奈良県奈良市）

参加者数：240 名（防災研究所外 230 名、所内 10 名）

研究及び教育への波及効果のまとめ

将来の南海トラフ巨大地震発生を見据え、海溝型巨大地震とスロー地震の関係について最先端の知見を共有し、今後のスロー地震・海溝型地震研究の方向性や、研究成果の減災への活用について議論した。観測・解析・技術開発・実験・物理モデル・大規模計算等の多様なアプローチによる国内外の最新成果を一堂に集め、地震学・測地学・地質学・物理学・情報科学等の分野横断研究の促進を図った。本集会は、コロナ禍における数少ないハイブリッド型（対面・オンライン）国際研究集会であり、大学院生を含む若手研究者に対して、国内外の著名な研究者と対面で議論する貴重な機会を提供した。また、研究集会中の議論は英語で実施され、特に大学院生の語学力・国際性の向上に役立った。さらに、彼らの人的ネットワークの形成にも大きく貢献した。

研究集会報告

(1) 目的

本研究集会は、将来の南海トラフ巨大地震発生を見据え、海溝型巨大地震とスロー地震の関係について最先端の知見を共有し、今後のスロー地震・海溝型地震研究の方向性や、研究成果の減災への活用について議論することを目的とした。観測・解析・技術開発・実験・物理モデル・大規模計算等の多様なアプローチによる国内外の最新成果を集め、地震学・測地学・地質学・物理学・情報科学を横断するスロー地震・海溝型巨大地震研究の有機的結合を図った。

(2) 開催日および開催場所

令和4年9月14日～16日（3日間）

奈良春日野国際フォーラム 麓（奈良県奈良市）

(3) 成果のまとめ

スロー地震は、21世紀初頭に発見された新しい種類の断層すべり現象であり、過去20年間、活発に研究されてきた。さらに、近年では、東北地方太平洋沖地震等の巨大地震を契機に、海溝型巨大地震発生メカニズムとスロー地震の関連性が明らかになりつつある（Obara & Kato, Science, 2016）。

以上の背景を踏まえ、本研究集会では、科研費学術変革領域研究（A）「Slow-to-Fast 地震学」（代表：井出哲 東京大学教授）および東京大学地震研究所共同利用研究集会「スロー地震から高速破壊まで全地震現象の包括的理解を目指して」の参加者も交えて、世界各地の最新のスロー地震観測事例や、様々な分野の最新のスロー地震研究成果について、3日間にわたり研究発表を行った（口頭発表30件、ポスター発表112件）。本集会は、参加者240名という大規模対面国際研究集会となった。

また、本集会における研究発表に基づき、スロー地震と南海トラフ巨大地震等の海溝型巨大地震の関係性や、研究成果の巨大地震災害軽減への活用、今後解決すべき研究課題に関する最先端の議論を実施した。特に、南海トラフ地震の予測可能性に関しては、南海トラフ地震発生前に南海トラフ地域のスロー地震活動に変化が現れる可能性について議論が交わされた。また、スロー地震活動自体の予測の困難さについても指摘があった。

本研究集会では、さまざまな分野（地震学・測地学・地質学・物理学・情報科学等）および、さまざまな国・地域（米国、フランス、スイス、イギリス、ニュージーランド、メキシコ、チリ、中国、台湾等）から第一線の研究者を招き、コロナ禍における貴重な対面議論の機会を提供した。これにより、新たな分野横断研究コミュニティや国際研究コミュニティの形成を促進することができた。また、研究集会中の発表および議論は全て英語で実施し、大学院生をはじめとする若手研究者の語学力および国際性の向上に大きく貢献した。

(4) 研究成果の公表

研究集会の概要および予稿は、以下のWebページで公開されている。また、公表された予稿集は、本報告書末尾に掲載した。

日本語版 <https://sites.google.com/view/sf-earthquake-ws-2022/japanese>

英語版 <https://sites.google.com/view/sf-earthquake-ws-2022/english>

(5) プログラム
口頭発表 (30 件)

Oral				
Day 1 (14 Sep.)				
Opening Session/				
General Instructions	9:30	9:45	0:15	
O01	9:45	10:30	0:45	Satoshi IDE (Univ. Tokyo) Scaling fast and slow earthquakes
O02	10:30	10:45	0:15	Ahmed ELBANNA (Univ. Illinois Urbana Champaign) Off-fault Plasticity Controls the Spectrum of Fault Slip: From Slow to Fast and From Small to Large
O03	10:45	11:00	0:15	Yoshihiro KANEKO (Kyoto Univ.) Fault frictional heterogeneities can explain the observations of slow earthquake transitioning to fast rupture
Break				
O04	11:15	12:00	0:45	Daniel FAULKNER (Univ. Liverpool) The influence of heterogeneity on the strength and stability of faults
O05	12:00	12:15	0:15	Hideo AOCHI (ENS & BRGM) Earthquake scaling from dynamic rupture simulations
O06	12:15	12:30	0:15	Caroline MOUCHON (MIT) Slow Fault slip dynamics reproduced by sub daily low-frequency earthquake activity
Lunch				
Flash Talks	14:00	15:00	1:00	
Poster Core Time				
O07	16:30	16:45	0:15	Shukei OHYANAGI (Kyoto Univ.) Shallow tectonic tremor activity near the Japan Trench from 2016 to 2022: development of fully automated monitoring system and its application to the Off Sanriku and the Off Fukushima tremor clusters
O08	16:45	17:00	0:15	John TOWNEND (Victoria Univ. of Wellington) Interdisciplinary earthquake science on the late-interseismic Alpine Fault and opportunities for generalizable hypothesis-testing
O09	17:00	17:15	0:15	Victor M. CRUZ-ATIENZA (UNAM) Seismogenesis in the Guerrero Seismic Gap: A Slow and Fast Slip Swaying
O10	17:15	17:30	0:15	Vladimir KOSTOGLODOV (UNAM) Do Slow Slip Events on the La Venta-Chacalapa fault system (Mexico) conform the RSF law?
General Discussion				
	17:30	18:00	0:30	
Close				
	18:00			
Day 2 (15 Sep.)				
Online Poster Time				
	9:00			
O11	9:45	10:30	0:45	Zhongwen ZHAN & Jiaxuan LI(Caltech) The break of rupture asperities as resolved by distributed acoustic sensing
O12	10:30	10:45	0:15	Eiichiro ARAKI (JAMSTEC) Development on seafloor fiber optic sensing to capture slow process in the Nankai Trough megathrust
O13	10:45	11:00	0:15	Xiaowei CHEN (Texas A&M) Source parameter estimations using DAS and comparison with seismic stations
Break				
O14	11:15	12:00	0:45	Bertrand ROUET-LEDUC (Kyoto Univ.) Towards the automatic detection of slow slip events using machine learning
O15	12:00	12:15	0:15	Kate Huihsuan CHEN (National Taiwan Normal Univ.) Segmentation characteristics of tectonic tremors in Shikoku, Japan, using machine learning approaches
O16	12:15	12:30	0:15	Giuseppe COSTANTINO (ISTerre, Univ. Grenoble Alpes) Slow slip event detection from GNSS data using deep learning in the Cascadia subduction zone
Group Photo				
	12:30	12:35	0:05	
Lunch				
	12:35	14:00	1:25	
Beakout Session				
	14:00	15:00	1:00	
Break				
	15:00	15:30	0:30	
O17	15:30	15:45	0:15	Elizabeth SHERRILL (Indiana Univ.) The spatiotemporal distribution of aseismic and seismic slip at Nankai and Cascadia inferred from geodetic observations
O18	15:45	16:00	0:15	Akemi NODA (Japan Meteorological Agency) Energy-based scenarios for Nankai trough earthquakes: The impacts of aseismic slip events on strain energy accumulation
O19	16:00	16:15	0:15	Takeshi TSUJII(Univ. Tokyo) Geological features from trench to tectonic backstop controlling slip behaviors in the Nankai Trough
O20	16:15	16:30	0:15	Dan BASSETT (GNS Science) Crustal structure of the Nankai subduction zone revealed by two decades of onshore-offshore and ocean-bottom seismic data
Breakout Summary /				
General Discussion				
	16:30	17:00	0:30	
Online Poster Time				
	17:00	18:00	1:00	
Close				
	18:00			
Day 3 (16 Sep.)				
O21	9:00	9:45	0:45	Whitney M. BEHR (ETH Zurich) Rock record constraints on the structures, materials and environment of deep-seated slow slip and tremor
O22	9:45	10:00	0:15	Nelson PULIDO (NIED) Estimation of shear strength and fluid pressure in world subduction zones based on the earthquake energy budget
O23	10:00	10:15	0:15	Masaoki UNO (Tohoku Univ.) Development of geochemical machine-learning models to quantify silica transport in metamorphic rocks
Break				
	10:15	10:30	0:15	
O24	10:30	11:15	0:45	Cailey CONDIT (Univ. Washington) Geologic and petrologic constraints on fluid sources, pressures, and consequences for deep slow earthquakes in subduction zones
O25	11:15	11:30	0:15	Alexandre SCHUBNEL (CNRS / ENS-PSL Univ.) Mineral dehydrations at subduction zones conditions: experimental evidence of non volcanic tremors and high Vp/Vs ratio
O26	11:30	11:45	0:15	Shunya KANEKI(DPRI, Kyoto Univ.) What causes the local increase in pore-fluid pressure around the source region of shallow slow earthquakes?
Business Meeting for SFEQ				
	11:45	12:30	0:45	
Lunch				
	12:30	14:00	1:30	
Poster Core Time				
	14:00	15:30	1:30	
O27	15:30	15:45	0:15	Chengrui CHANG (Univ. Tokyo) Constitutive Properties and Frictional Behavior of Simulated Fault Zone of Halite Developed in Granular Medium
O28	15:45	16:00	0:15	Simone PUEL (Univ. Texas at Austin) A forward/inverse modeling framework for earthquake deformation problems
O29	16:00	16:15	0:15	Naofumi ASO (Tokyo Tech) Diffusional shear slip as the common mechanism for tectonic low-frequency earthquakes and volcanic deep-long-period earthquakes
O30	16:15	16:30	0:15	Yoshiyuki TANAKA (Univ. Tokyo) Temporal gravity anomalies in long-term slow slip areas along the Nankai Trough and Cascadia
General Discussion				
	16:30	17:00	0:30	
Closing				
	17:00			

45-min talks: Keynote speakers

ポスター発表 (112 件)

Poster		
In-Person (P001-P093)		
P001	Kazuki YOSHIDA	Transient fluid infiltration in the shallow mantle wedge recorded in the Oman Ophiolite
P002	Takumi AOKI	Dynamic simulations of coseismic slickenlines on non-planar and rough faults: Towards inferring the rupture directions of paleoearthquakes
P003	Asuka YAMAGUCHI	Forearc mylonite formed along a plate boundary of high temperature conditions related to Cretaceous ridge subduction
P004	Ayako TSUCHIYAMA	A systematic detection of intermediate-depth earthquakes within the Bucaramanga earthquake nest, Colombia
P005	Daya SHANKER	On The Seismic Hazard in the Western Himalayas Using PSHA Methodology
P006	Diana MINDALEVA	Temporal evolution of fluid flow along fractures in high-grade metamorphic rocks related to seismic events in the middle crust.
P007	Yoshitaka HASHIMOTO	Slip behavior, strain, and deformation mechanisms in a fossil earthquake fault in an exhumed accretionary complex
P008	Takane HORI	Numerical experiments using a friction law both for rapid and slow sliding
P009	Minoru IDENO	Estimation of 3D S-wave velocity model in the western Niigata area using surface wave analysis of microtremors
P010	Yoshihiro ITO	Insights into the occurrence and relationship between seismicity and a relief of plate interface near the trench at the western part of Guerrero seismic gap from a recent seafloor experiment
P011	Yusuke KAKIUCHI	Monitoring of seismic velocity change surrounding area of Mt. Fuji using ambient noise
P012	Tatsuhiko KAWAMOTO	Chemical composition of subduction-zone fluids
P013	KENICHI TSUDA	Incorporation of Experimental Data of Fault Material derived from Nankai Trough into Simulation of Dynamic Rupture Propagation
P014	Kazuya SHIRAISHI	Crustal structures and spatial correlation with seismic activities in the western Nankai Trough
P015	Ayumu MIYAKAWA	Relation between geological structure caused by seamount collisions and slow-earthquake insight from numerical geodynamic modeling.
P016	Makoto OTSUBO	Temporal changes in pore fluid overpressure during slow earthquake cycle estimated from foliation-parallel extension veins
P017	Pousali MUKHERJEE	Along-Strike Forearc and Subducted Upper Slab Structure beneath subduction regions of Alaska and Chile : Implications towards the occurrence of Slow Slip
P018	Pierre ROMANET	Fast 3D fully-dynamic earthquake cycle simulations on non-planar fault.
P019	Ryuta ARAI	Links between mud volcanoes, upper-plate fluid conduits and shallow slow earthquakes in the Hyuga-nada subduction zone
P020	Suguru YABE	Synthetic tests of joint CMT analysis using translation and strain data
P021	Tatsuhiko SAITO	Mechanical coupling on plate interfaces: Rupture scenarios of megathrust earthquakes and aseismic slips
P022	Ritsuya SHIBATA	Resolving slip directions in the finite fault with the radiation-corrected empirical Green's function
P023	Simon WALLIS	Fluid flow and silica transport along the subduction interface: example from the Franciscan metamorphic belt, USA
P024	Gaku KIMURA	Nankai Forearc Structural and Seismogenic Segmentation caused by a Magmatic Intrusion off the Kii Peninsula
P025	Gaku KIMURA	Slow Earthquake Gap on the Smoothed Decollement off the Kii Peninsula, Nankai Trough
P026	Takanori MATSUZAWA	Numerical modeling of SSEs in the Nankai region -Segments of short-term SSEs-
P027	Takayoshi NAGAYA	Serpentinite deformation mechanism in depths of deep slow earthquakes of the shallow wedge
P028	Takehito SUZUKI	Analytical understanding of condition of slow and fast earthquakes based on the BK model and the interaction among heat, fluid pressure and porosity
P029	Yohai MAGEN	The indirect triggering of a normal faulting earthquake sequence in the Ibaraki-Fukushima prefectural border, Japan by Mw9.0 Tohoku-Oki megathrust: the elusive role of low-angle normal fault slow-slip
P030	Yudong SUN	Propagation of Slow Slip Events on Rough Faults
P031	Gou FUJIE	Detailed seismic structure along the plate interface and its implication for the interplate seismic coupling in Nankai Trough off Cape Muroto
P032	Saeko KITA	Effects of long-term slow slip events on in-slab stresses and seismicity in Bungo Channel, Southwestern, Japan
P033	Keisuke ARIYOSHI	Precise monitoring of slow earthquakes around Nankai Trough toward early detecting crustal deformation
P034	Raymundo PLATA-MARTINEZ	Slip deficit and its correlation with slow and fast earthquakes at the Nankai subduction zone
P035	Ryosuke AZUMA	Shallow VLFE activity at the Japan-Kuril trench junction region revealed from a broadband OBS array and F-net observation
P036	Takahiko UCHIDE	Complexities in Earthquake Source Spectra Revealed by the Multiple Spectral Ratio Analyses
P037	Takeru MATSUDA	Data-driven decomposition of slow-to-fast earthquakes
P038	Rinya MIYAKAWA	Cluster formation of particles found in mixtures of viscoelastic fluids and particles under shear stress as an analog experiment for the spatio-temporal distribution of slow earthquakes and melange formation.
P039	Yuki SHINOHARA	Analog experiment of slow to fast earthquakes using viscoelastic fluid: fractures promoted by external shear strain
P040	Kojiro OTOGURO	Pattern formation during fluid injection into highly water absorbent granular media
P041	Shun ADACHI	Adjoint tomography of an accretionary wedge and shallow slow-slip regions in the North Island of New Zealand
P042	Amane SUGII	Development of classification methods for tectonic tremor, earthquake and noise using deep learning
P043	Taizo UCHIDA	A thermal event detected in a cataclastic seismogenic fault using paleomagnetic methods
P044	Takahiro HOSOKAWA	Geological constraints on dynamic changes of fluid pressure in seismic cycles
P045	Satoru BABA	Observation of slow earthquakes by distributed acoustic sensing off Cape Muroto, southwest Japan
P046	Ryota HINO	Quality of S-net seafloor pressure data in geodetic frequency band
P047	Takehiro HIROSE	Hydrothermal rotary-shearing apparatus in Kochi/JAMSTEC toward understanding slow to fast faulting processes
P048	Hitoshi HIROSE	Periodic changes in activity pattern of short-term slow slip events in the northern Kii Peninsula, Japan
P049	Yosuke ITO	Temporal correlation between seismic attenuation changes and slow-slip events
P050	Ryo ITO	Why do Gutenberg-Richter b-values decrease with time prior to large earthquakes? Insights from rate-and-state earthquake cycle simulations with frictional heterogeneities
P051	John BEDFORD	Experimental evidence for rapid fault healing after seismic slip

P052	Juan Carlos VILLEGAS	Heterogeneous interseismic coupling and aseismic slip event along the Peruvian subduction zone
P053	Koki MASUDA	Single-station detection of seismic slow earthquakes using their broadband characteristics
P054	Kodai SAGAE	Extraction of tremor migrations beneath Shikoku, southwest Japan, and their characteristics
P055	Kazuma MATSUMOTO	Swarms of microearthquakes associated with tectonic tremor bursts in the northern Japan Trench
P056	Kurama OKUBO	Calibration of AE sensors using ARX model used for estimating source properties of foreshocks during large-scale rock friction experiments
P057	Yukinojo KOYAMA	Nature of the plate boundary domain at the depth of deep slow earthquakes: evidence from the Sanbagawa belt
P058	Ryo KURIHARA	Various waveform characteristics of deep low-frequency earthquake in volcanic regions
P059	Liam MOSER	The down dip limit of the megathrust seismogenic zone: comparing thermal and lithological controls on frictional and viscous deformation
P060	Satoshi MATSUNO	Precise evaluation of element transfer in metabasalt with sample-based predictive uncertainty estimation using machine-learning
P061	Kazuki MASUDA	Investigation of earthquake source scaling laws using dynamic rupture simulations with a hierarchical patch structure
P062	Yanxue MA	Seismic structures and shallow tremor distributions in Hyuga-nada
P063	Madison FRANK	Deformation mechanisms and rheology of a mélangé shear zone associated with seamount subduction
P064	Mari HAMAHASHI	Tectono-sedimentary history of the Wharton Basin and its roles of subduction input at the northern Sunda Trench
P065	Yuta MITSUI	Comparison between deep learning, Kalman filtering, and classical methods for evaluating (quasi-)periodic signals
P066	Masaru NAKANO	Discriminating seismic events using 1D and 2D CNNs: applications to tectonic tremor and volcanic events
P067	Motoki NEGISHI	Shallow slow earthquake activity from December 2020 southeast off the Kii Peninsula inferred from dense ocean bottom seismometer array
P068	Tomoaki NISHIKAWA	Toward constructing a statistical model for slow earthquakes
P069	Takuya NISHIMURA	Earthquake swarm and transient crustal deformation in the Noto Peninsula, central Japan: Implication from combined analysis of multiple GNSS networks
P070	Hiroyuki NODA	Evolution of normal stress heterogeneity due to frictional heating and thermo-elastic effect: Implication for size effect in friction experiments
P071	Genki OIKAWA	Deep low frequency earthquakes evolve similarly to ordinary fast earthquakes
P072	Yutaro OKADA	Systematic detection of short-term slow slip events along the Japan and Kuril Trenches
P073	Hanaya OKUDA	Role of smectite-illite transition in the onset of seismogenic zone in subduction zones from experimental viewpoints
P074	Qing-Yu WANG	What makes low-frequency earthquakes low frequency?
P075	Yanfang QIN	Subsurface structural variations imaged by seismic reflection data along the Japan trench between 36–37.8°N: the overlapping of slow earthquake swarm and the rupture damping zone of 2011 Tohoku earthquake
P076	Ryosuke DOKE	Deformation of the seismogenic zone in the northeastern part of the Izu Peninsula, Japan, inferred from GNSS observations
P077	Rina FUKUCHI	Sediment properties of submarine mass movement deposits caused by subduction of topographic high at off Kumano region of the Nankai Trough
P078	Rosalie VERWIJS	The role of seamount subduction on the earthquake cycle
P079	Samuele PAPESCHI	Serpentinite carbonation produces rheological heterogeneities at the subduction interface
P080	Yasunori SAWAKI	Spatial Relationship of Shallow Slow Earthquake and Strong Negative Velocity Impedance at Hyuga-nada
P081	Kazuki SAWAYAMA	Relating permeability and geophysical properties with asperity contact
P082	Katsuhiko SHIOMI	Structural features of the uppermost Philippine Sea Plate beneath the Kii Peninsula, central Japan
P083	Shunsuke TAKEMURA	Detectability of very low frequency earthquakes in Nankai
P084	Tsukasa YAMAMOTO	Estimation of the crustal deformation using radiated energy of tectonic tremors in the northern Kii Peninsula, Nankai subduction zone
P085	Takehiro SATO	Spatio-temporal seismic velocity change near the Japan-Kuril trenches junction revealed from long-term dense-OBS network observation
P086	John WEBER	POSTER Strain Partitioning and Interseismic Fault Behavior Along the Caribbean-South American Transform Plate Boundary: Creeping and Locked Faults, and Fast and Slow (?) Earthquakes
P087	Qian XU	An improved method of mitigating orbital errors in multiple SAR interferometric pairs analysis for slow crustal deformation measurement
P088	Futoshi YAMASHITA	Slow stick-slips on a meter-scale laboratory fault
P089	Yohei HAMADA	Effect of fluid flow on fault healing
P090	Yuichi HIRAMATSU	Preliminary analysis of continuous gravity measurement data obtained in a slow slip area in the Ryukyu Trench
P091	Yusuke SHIMURA	Subduction–accretion–exhumation processes in the subduction zone: Example from the Cretaceous subduction complexes on the central Kii Peninsula, SW Japan
P092	Yusuke YOKOTA	Development of UAV technology to realize high-frequency GNSS-A observation: preparation
P093	Tetsuo YAMAGUCHI	Tremor-like behavior in nucleation of laboratory earthquakes
Online (P101-P119)		
P101	Kimihiro MOCHIZUKI	Seismicity of regular and slow events in relation to seamount subduction in the Hikurangi subduction margin, New Zealand
P102	Takeshi AKUHARA	Locating tectonic tremors with uncertainty estimates: optimizing inter-station measurements, wave propagation-based quality control, and Bayesian inversion
P103	Baoning WU	Explaining the First-order Source Characteristics of Slow Slip Events and Tremors with a Frictional-Viscous Faulting Model
P104	Grant CALDWELL	Can we use electrical conductivity to help understand the earthquake-induced stress-cycle in the ductile region beneath the Alpine Fault, New Zealand?
P105	Joan GOMBERG	The Evolution of Slip Events Inferred from Cascadia Tremor
P106	Junli ZHANG	Frictional properties of input sediments to the North Sumatra subduction zone
P107	Towako AOYAMA	Spatiotemporal distribution of tectonic tremors accompanying 2014 and 2019 SSE in the north of the Hikurangi Subduction Zone
P108	Atsushi OKAMOTO	Formation and transport of silica particles in supercritical and vapor conditions and its implications to fracture sealing
P109	Keishi OKAZAKI	“Stew and slide” friction and fluid-flow experiments on incoming sediments from the Japan trench
P110	Michiyo SAWAI	Frictional properties of basalt: Effects of the seamount subduction on earthquake generation

P111	Ryoko NAKATA	Numerical simulation with a multiscale circular patch model in the northern segment along the Japan Trench
P112	Yuki KODERA	Automatic classification of fast and slow earthquake signals from continuous records using an unsupervised machine learning algorithm
P113	Akiko TOH	Strongly scattering medium along slow earthquake fault zones, inferred by the new observations of short-duration tremors
P114	Kellen AZUA	Seismic and aseismic behavior in The Pichilemu crustal fault system during the post-seismic period of the 2010 Mw8.8 Maule Earthquake
P115	Anca OPRIS	Imaging the changes in the migration patterns of deep LFE caused by the occurrence of the 2010 L-SSE in Western Shikoku, Japan.
P116	Jingyi SUN	P-S travel time of low SNR events using polarization detection
P117	Wataru TANIKAWA	Determination of the non-slipperiest sand in Japan based on the double direct rotary shear experiment
P118	Yasuyuki NAKAMURA	Possible low velocity zone in the overriding plate beneath the Tosabae-Trough in the central-western Nankai Trough
P119	Zhen LIU	Investigate slow earthquakes variability and interaction with earthquake ruptures in Cascadia Subduction Zone

*Presentation status of each presenter is subject to change

(6) 参加者名簿

氏名	所属機関・部局名	職名
西川友章	京都大学防災研究所	助教
足立 舜	京都大学大学院理学系研究科	学生
青地秀雄	École normale supérieure, Bureau de Recherches Géologiques et Minières	上席・主任研究員
青木拓実	京都大学大学院理学系研究科	学生
新井隆太	海洋研究開発機構	研究員
荒木英一郎	海洋研究開発機構	上席・主任研究員
有吉慶介	海洋研究開発機構	上席・主任研究員
麻生尚文	東京工業大学	助教
東 龍介	東北大学大学院理学研究科	助教
馬場 慧	海洋研究開発機構	ポストドク研究員
Thorsten Becker	The University of Texas Institute for Geophysics	教授
John Bedford	海洋研究開発機構	ポストドク研究員
Whitney M. Behr	Eidgenössische Technische Hochschule Zürich	准教授
Chengrui Chang	東京大学大学院農学生命科学研究科	ポストドク研究員
Xiaowei Chen	Texas A&M University	准教授
Victor M. Cruz-Atienza	Institute of Geophysics, National Autonomous University of Mexico	上席・主任研究員
Sambuddha Dhar	東北大学大学院理学研究科	学生
道家涼介	神奈川県温泉地学研究所	上席・主任研究員
Daniel Faulkner	University of Liverpool	教授
Madison Frank	筑波大学	学生
藤江 剛	海洋研究開発機構	上席・主任研究員
福地里菜	鳴門教育大学	講師
濱田洋平	海洋研究開発機構高知コア研究所	研究員
浜橋真理	山口大学	講師
橋本善孝	高知大学	教授
日野亮太	東北大学大学院理学研究科	教授
平松祐一	東京大学	学生
廣瀬大洋	海洋研究開発機構	上席・主任研究員
堀 高峰	海洋研究開発機構	上席・主任研究員

細川貴弘	高知大学	学生
井出 哲	東京大学大学院理学系研究科	教授
出野 実	東京大学	学生
伊東 良	京都大学	学生
伊藤喜宏	京都大学防災研究所	准教授
伊藤陽介	東京工業大学	学生
陣出湧也	金沢大学	学生
垣内優亮	東京大学工学部システム創成学科	学生
金木俊也	京都大学防災研究所	ポストドク研究員
金子善宏	京都大学	准教授
加藤将行	東北大学	助教
川本竜彦	静岡大学理学部地球科学科	教授
木村 学	海洋研究開発機構	アドバイザー
北佐枝子	建築研究所	上席・主任研究員
小平秀一	海洋研究開発機構	教授
Vladimir Kostoglodov	National Autonomous University of Mexico	上席・主任研究員
小山雪乃丞	東京大学大学院 理学系研究科 地球惑星科学専攻	学生
栗原 亮	神奈川県温泉地学研究所	研究員
Yanxue Ma	東京大学地震研究所	学生
前原誠也	東京大学	学生
Yohai Magen	Department of Geophysics Tel-Aviv University	学生
増田和貴	京都大学	学生
増田滉己	東京大学	学生
松田孟留	理化学研究所	ユニットリーダー
松本一駿	東北大学	学生
松野哲士	東北大学大学院環境科学研究科	学生
松澤孝紀	防災科学技術研究所	上席・主任研究員
Diana Mindaleva	東北大学	助教
三井雄太	静岡大学	准教授
宮川歩夢	産総研地質調査総合センター	上席・主任研究員
宮川凜也	東京理科大学 理学研究科	学生
宮澤理絵	京都大学防災研究所	准教授
Liam Moser	Massachusetts Institute of Technology	学生
Caroline Mouchon	Massachusetts Institute of Technology	学生
Pousali Mukherjee	京都大学理学研究科	学生
棕平祐輔	東北大学	助教
永治方敬	東京大学	助教
中小路一真	京都大学理学部	学生
中野優	海洋研究開発機構	上席・主任研究員
根岸 幹	東京大学地震研究所	学生
西村卓也	京都大学防災研究所	准教授
西沢貴志	京都大学大学院理学研究科	学生

野田博之	京都大学防災研究所	准教授
大柳修慧	京都大学大学院理学研究科	学生
及川元己	東京工業大学	学生
岡田悠太郎	京都大学大学院理学研究科	学生
岡崎智久	理化学研究所	研究員
大久保蔵馬	防災科学技術研究所	ポスドク研究員
奥田花也	東京大学大気海洋研究所	学生
Anca Opris	海洋研究開発機構	ポスドク研究員
乙黒康次郎	東京理科大学	学生
大坪 誠	産業技術総合研究所	上席・主任研究員
Samuele Papeschi	海洋研究開発機構高知コア研究所	ポスドク研究員
Raymundo Plata-Martinez	海洋研究開発機構	ポスドク研究員
Simone Puel	The University of Texas at Austin	学生
Nelson Pulido	防災科学技術研究所	上席・主任研究員
Xu Qian	東京大学地震研究所	学生
Yanfang Qin	海洋研究開発機構	研究員
Pierre Romanet	防災科学技術研究所	ポスドク研究員
Bertrand Rouet-Leduc	京都大学防災研究所	助教
Alexis Saez	Swiss Federal Institute of Technology Lausanne	学生
寒河江皓大	国立研究開発法人産業技術総合研究所 地質調査総合センター	ポスドク研究員
齊藤竜彦	防災科学技術研究所	上席・主任研究員
佐藤豪大	東北大学	学生
佐脇泰典	京都大学理学研究科	学生
澤山和貴	京都大学	助教
Alexandre Schubnel	Centre national de la recherche scientifique, ENS-PSL University	上席・主任研究員
Daya Shanker	Indian Institute of Technology Roorkee, Department of Earthquake Engineering	准教授
Elizabeth Sherrill	Indiana University	学生
柴田律也	東京工業大学	学生
志村侑亮	産総研地質調査総合センター	研究員
篠原有輝	東京理科大学大学院理学研究科	学生
汐見勝彦	防災科学技術研究所	上席・主任研究員
杉井天音	金沢大学	学生
住野豊	東京理科大学	准教授
Jingyi Sun	東北大学流体科学研究所	学生
Yudong Sun	Massachusetts Institute of Technology	学生
鈴木岳人	青山学院大学	助教
鈴木貞臣	日本地震学会	退職（元教授）
波多野恭弘	大阪大学	教授
武村俊介	東京大学地震研究所	助教
田中愛幸	東京大学理学系研究科	准教授
利根川貴志	海洋研究開発機構	上席・主任研究員
John Townend	Victoria University of Wellington	教授

土山絢子	Massachusetts Institute of Technology	学生
津田健一	清水建設技術研究所	上席・主任研究員
辻 健	東京大学	教授
内田泰藏	高知大学	学生
内出崇彦	産業技術総合研究所	上席・主任研究員
上田 拓	京都大学防災研究所	ポストドク研究員
氏家恒太郎	筑波大学	准教授
宇野正起	東北大学	助教
Rosalie Verwijs	Massachusetts Institute of Technology	学生
ウォリス サイモン	東京大学	教授
Qingyu Wang	Massachusetts Institute of Technology and Earthquake Research Institute, the University of Tokyo	ポストドク研究員
John Weber	Grand Valley State University	教授
矢部優	産業技術総合研究所	研究員
山田真澄	京都大学防災研究所	助教
山口哲生	東京大学	准教授
山口飛鳥	東京大学大気海洋研究所	准教授
山本 史	金沢大学	学生
山下太	防災科学技術研究所	上席・主任研究員
横田裕輔	東京大学生産技術研究所	准教授
吉田一貴	東北大学	学生
加藤愛太郎	東京大学地震研究所	教授
野田朱美	気象庁気象研究所	研究員
南方昭寛	岡山大学	学生
竹尾明子	東京大学地震研究所	助教
藤並希子	東京大学理学系研究科	ポストドク研究員
小林昭夫	気象研究所	研究員
堤 昭人	京都大学大学院理学研究科	准教授
Ana Maria Restrepo Acevedo	The University of Texas at Austin	学生
Atikul Haque Farazi	京都大学大学院理学研究科	学生
岡本 敦	東北大学	教授
Audrey Chouli	Institut des Sciences de la Terre, Grenoble, France	学生
仲西理子	海洋研究開発機構	研究員
Baoning Wu	University of Southern California	ポストドク研究員
Cailey Condit	University of Washington	助教
Chunjing Wang	Southern University of Science and Technology	学生
Dan Bassett	GNS Science	上席・主任研究員
David Shelly	U.S. Geological Survey	研究員
福山英一	京都大学工学研究科	教授
Erika Moreno	神戸大学	ポストドク研究員
Giuseppe Costantino	ISTerre, Université Grenoble Alpes	学生
最首花恵	産業技術総合研究所	研究員
Haoran Meng	Southern University of Science and Technology	准教授

Hejun Zhu	The University of Texas at Dallas and University of Tokyo	准教授
内田嗣人	高知大学	学生
三宅弘恵	東京大学地震研究所	准教授
杉岡裕子	神戸大学	教授
坂上 啓	東京大学理学部	ポストドク研究員
Jiaxuan Li	California Institute of Technology	ポストドク研究員
Joan Gombert	US Geological Survey	研究員
中島淳一	東京工業大学	教授
Junli Zhang	MARUM, University of Bremen	ポストドク研究員
Kate Huihsuan Chen	National Taiwan Normal University	教授
太田和晃	防災科学技術研究所	ポストドク研究員
村松和紀	東京大学	学生
小原一成	東京大学地震研究所	教授
今西和俊	産業技術総合研究所	副研究部門長
白石和也	海洋研究開発機構	研究員
岡崎啓史	広島大学	准教授
矢野恵佑	統計数理研究所	准教授
Kellen Azua	University of Chile	学生
国吉健太郎	富山大学	学生
望月公廣	東京大学地震研究所	教授
溜湖功史	気象研究所	上席・主任研究員
福田孔達	東京大学地震研究所	学生
Kuanhung Chen	National Yang Ming Chiao Tung University, Taiwan	ポストドク研究員
Kuo-Fong Ma	Institute of Earth Sciences, Academia Sinica	教授
Lei Yang	東京大学地震研究所	ポストドク研究員
山谷里奈	防災科学技術研究所	ポストドク研究員
畑 真紀	東京大学地震研究所	ポストドク研究員
大谷真紀子	東京大学地震研究所	助教
大久保慎人	高知大学	准教授
木下正高	東京大学地震研究所	教授
米谷維康	住化エンバイロメンタルサイエンス (株)	会社員
澤井みち代	千葉大学	助教
小松美加	東京大学出版会	編集部員
高橋美紀	産業技術総合研究所 岩手層・火山研究部門	上席・主任研究員
大館未来	静岡大学	学生
西山直毅	産業技術総合研究所	上席・主任研究員
内田直希	東北大学	准教授
三反丸修	防災科学技術研究所	ポストドク研究員
Paul Caesar M. Flores	横浜国立大学, 海洋研究開発機構	学生
Qifeng Xie	University of Chinese academy of sciences	学生
小松理子	同志社大学	学生
縣 亮一郎	海洋研究開発機構	研究員

松本良一郎	株式会社大崎総合研究所	上席・主任研究員
中田令子	東京大学	ポスドク研究員
安藤亮輔	東京大学	准教授
田中佐千子	防災科学技術研究所	上席・主任研究員
Saruul Dorjpalam	大崎総合研究所	研究員
板場智史	産業技術総合研究所	上席・主任研究員
藤内智士	高知大学	講師
徐 世慶	南方科技大学	助教
副島祥吾	東京大学	学生
Shuang Zhao	東京大学	ポスドク研究員
鎌田俊一	北海道大学	教授
Soli Garcia	京都大学防災研究所	ポスドク研究員
Stephen Bannister	GNS Science	上席・主任研究員
前田純伶	防災科学技術研究所	ポスドク研究員
Syed Idros Bin Abdul Rahman	Earth observatory of Singapore	研究員
高部太来	東京大学地震研究所	学生
高田大成	東京大学理学系研究科	学生
悪原 岳	東京大学地震研究所	助教
飯沼卓史	海洋研究開発機構	上席・主任研究員
今寺琢朗	東京大学地震研究所	学生
久保田達矢	防災科学技術研究所	ポスドク研究員
Thomas Yeo	東北大学	学生
山田知朗	東大地震研	助教
井上智裕	京都大学理学系研究科	学生
比嘉友香	神戸大学	学生
青山都和子	東京大学地震研究所	学生
石川剛志	海洋研究開発機構	上席・主任研究員
谷川 亘	海洋研究開発機構	上席・主任研究員
William Frank	Massachusetts Institute of Technology	助教
Yanhan Chen	京都大学大学院理学系研究科	学生
岡田康男	大崎総合研究所	研究員
石原 靖	海洋研究開発機構	職員
中村恭之	海洋研究開発機構	上席・主任研究員
Yihe Huang	University of Michigan	准教授
木下陽平	筑波大学	助教
西尾嘉胡	高知大学	准教授
小寺祐貴	気象庁気象研究所	研究員
雨澤勇太	産業技術総合研究所地質調査総合センター	ポスドク研究員
前田裕太	名古屋大学	講師
Yuyun Yang	The Chinese University of Hong Kong	ポスドク研究員
Zhen Liu	Jet Propulsion Laboratory, California Institute of Technology	研究員
Zhongwen Zhan	California Institute of Technology	教授

生田領野	静岡大学	准教授
------	------	-----

Scaling fast and slow earthquakes

Satoshi Ide¹

¹Dept. EPS, Univ. Tokyo

Slow earthquakes have different names, such as low frequency earthquakes (LFEs), tectonic tremors, very low frequency earthquakes (VLFs), and slow slip events (SSEs), but these events can be considered as different manifestations of a single slow deformation process (Ide et al., 2007). Recent observations have proved that VLFs radiate very broadband seismic waves, from 0.01 to 10 Hz (e.g., Kaneko et al., 2018; Masuda et al., 2020) and the moment release of SSEs is synchronized well with the temporal change of tremor/LFE activity (Frank, 2016; Nakano et al., 2017). These observations are consistent with a Brownian slow earthquake model (Ide, 2008; Ide and Yabe, 2019), in which tiny stochastic fluctuations (tremors/LFEs) produce large-scale continuous deformation (SSEs). Assuming that a cluster of tremor/LFE represents a small SSE (Wech et al., 2010; Hawthorne et al., 2016; Gombert et al., 2016; Bletery et al., 2017; Aiken and Obara, 2020), we may define almost all size of slow earthquakes with different time constant, or duration T , from 0.1 s to years. The compilation of recent catalogs of slow earthquakes shows that the maximum seismic moment M_o at a given duration T is proportional to T , i.e., $M_o \leq cT$ ($c \sim 10^{12}$ Nm/s, Ide and Beroza, 2022), which is the updated interpretation of the scaling relation of Ide et al. (2007).

For fast earthquakes, both the maximum and minimum of seismic moment at a given duration are strictly limited by the duration, as $M_o \propto T^3$. Rupture process of earthquakes are almost self-similar, with scale invariant stress drop and scaled energy (e.g., Kanamori and Anderson, 1976; Ide and Beroza, 2001). The self-similarity continues from the very beginning of the rupture initiation, and it is almost impossible to predict the final size of an earthquake at the initial stage of rupture (Iio, 1995; Ellsworth and Beroza, 1995; Uchide et al., 2010; Meier et al., 2016). Despite complexity in each rupture process, the dynamic rupture is controlled by some structural heterogeneity, and the isolated heterogeneity produces repeating or imperfectly repeating earthquakes (Uchida et al., 2007; Ide, 2019). Therefore, the dynamic rupture process of fast earthquakes can be modeled by multiscale patch model with fractal fracture energy distribution (Ide and Aochi, 2005). In such a model, rupture continue to propagate for wide scale range, at changing propagation speed, which is of significant fraction ($\sim 70\%$) of shear wave speed. Rupture cannot propagate slowly, for example at 10% of shear wave speed, because the dynamic rupture is a coupled process between seismic wave propagation and fracture.

The most fundamental difference between fast and slow earthquakes is the governing equation coupled with friction/fracture equation: wave equation and diffusion equation, respectively. Diffusional mechanisms are various, and dependent on regional environmental conditions. Therefore, slow earthquakes appear diverse. On the other hand, fast earthquakes are rather unique, a special type of deformation mode.

Off-fault Plasticity Controls the Spectrum of Fault Slip: From Slow to Fast and From Small to Large

Ahmed Elbanna¹, Md Shumon Mia¹, and Mohamed Abdelmeguid¹

¹Dept. CEE, Univ. Illinois Urbana Champaign, Urbana, IL, USA

Earthquakes are among nature's deadliest and costliest hazards. Physics-based simulations are essential to complement the lack of data and elucidating the complex patterns of earthquakes. While significant progress has been made in understanding earthquake source processes in linear elastic domains, the response of the rocks near the fault is complex and likely to be inelastic due to the extreme stresses and deformations associated with fault slip. The effect of this more realistic fault zone response on seismic and aseismic fault slip is poorly understood. Here, using a hybrid finite element-spectral boundary integral scheme (FEBE), we simulate sequence of earthquakes and aseismic slip of a rate-and-state fault embedded in an elastoplastic bulk subject to slow tectonic loading. We show that off-fault plasticity significantly influences the source characteristics. Specifically, off-fault plasticity may lead to partial ruptures and emergence of spatial segmentation as well as temporal seismic clustering. Seismicity pattern changes from simple periodic to complex depending on the bulk yield strength and viscosity. We also observe small repeating earthquakes and slow slip for lower yield strength. When yield strength is further reduced, the fault remains locked and off-fault plastic deformation compensates for the slip deficit. Simulating a simple spring-slider model, we observe analogous features of different sliding pattern ranging stick-slip, slow slip, and locked depending on the stiffness and yield strength of the spring. These results highlight the implications of plasticity on frictional sliding and indicate the importance of characterizing the fault zone mechanical response beyond their elastic properties to better inform seismic hazard models.

Fault frictional heterogeneities can explain the observations of slow earthquake transiting to fast rupture

Yoshihiro Kaneko¹, Nealey Sims², Carl Tape², Ryo Ito¹, Andrea Perez³

¹ Kyoto University, ² University of Alaska – Fairbanks, ³ Victoria University of Wellington

While most earthquakes start abruptly, with no evidence for a nucleation process, accelerating foreshock sequences within or in the vicinity of the eventual mainshock rupture zone for some moderate to large crustal earthquakes have been documented previously. In particular, Tape et al. (2018) reported unique observations of nucleation signals of crustal earthquakes in the Minto Flats fault zone in central Alaska, manifested by ~20 seconds of simultaneous high-frequency foreshocks and a very low-frequency earthquake. One potential explanation for such observations is a slow slip front propagating over the fault and triggering these foreshocks as it transitions into the mainshock rupture (e.g., Tape et al., 2018). Another explanation may be that accelerating foreshocks represent cascading sequences of fault ruptures due to static and/or dynamic stress changes, without underlying slow slip, as known as a cascading hypothesis (e.g., Ellsworth and Bulut, 2018). Here we show that a numerical fault model incorporating full inertial dynamics and rate-and-state friction laws with frictional heterogeneities reproduces ~20 seconds long, accelerating foreshock sequence that led to a mainshock as observed in the Minto Flats fault zone. We find that the time scale of accelerating foreshock sequence depends on the degree and size of frictional heterogeneities and tectonic loading rate. In the models, a foreshock triggers another foreshock mainly via the propagation of afterslip in the neighboring rate-strengthening patches. Accelerating afterslip due to numerous foreshocks eventually triggers the nucleation of the mainshock, and hence slow deformation plays an important role in the generation of accelerating foreshocks. Furthermore, an accelerating foreshock sequence occurs in only a transitional regime between an earthquake swarm regime and the regime of mainshocks with no foreshocks. This may explain why the observations of accelerating foreshock sequences are relatively rare.

The influence of heterogeneity on the strength and stability of faults

D.R. Faulkner¹, J. Bedford², N. Lapusta³ and V. Lambert⁴

¹Rock Deformation Laboratory, University of Liverpool, UK, ²Japan Agency for Marine-Earth Science Technology, Kochi, Japan, ³Seismological Laboratory, California Institute of Technology, USA, ⁴Earth and Planetary Sciences, University of California Santa Cruz, USA

Heterogeneity of fault zones is seen at all scales in nature. It may manifest itself in terms of both the variability of material property distribution over the fault, and by stress heterogeneity brought about by the history of previous earthquake ruptures. In this contribution, we consider the effect on the strength and stability of faults of small-scale heterogeneity in laboratory experiments, and large-scale heterogeneity from numerical dynamic rupture modeling. In model laboratory faults at slow slip rates (0.3 and 3 microns/s), the area occupied by rate-weakening gouge (quartz) versus rate-strengthening gouge (clay) was systematically varied and the results compared with homogenized mixtures of the two gouges. We found that the heterogeneous experimental faults were weaker and less stable than their homogenized counterparts implying that earthquake nucleation might be promoted by fault zone heterogeneity. In elasto-dynamic numerical models based on rate and state friction but with enhanced dynamic weakening (EDW) through pore fluid pressurization, uniform material properties on the fault plane are assumed, and heterogeneity is provided by stress variations along the fault. In these 1D models, once nucleated, larger ruptures that result in greater degrees of EDW are more able to propagate through areas of low shear stress that may arrest smaller events. This leads to a relationship between rupture size and the average shear stress over the rupture plane before the earthquake occurs. Faults that host larger events may overall appear to be driven by lower average shear stress and hence appear 'weaker'. It is clear that apparent fault strength and stability is difficult to predict from either simple homogeneous gouge experiments, or from scaling up of these results. Heterogeneity at all scales will affect the slip behaviour of faults.

Earthquake scaling from dynamic rupture simulations

Hideo Aochi^{1,2} and Sergio Ruiz³

¹Laboratoire de Géologie, ENS/CNRS, PSL Research University, France, ²BRGM, France,

³Univesidad de Chile, Chile

Among various scaling relations in earthquakes, the fracture energy scaling was proposed explicitly from the measurements in Ohnaka (JGR, 2003), but had been theoretically expected earlier, for example, in Andrews (JGR, 1976) or Shibazaki and Matsu'ura (GRL, 1992). This is necessary for a non-dimensional rupture process, namely, a constant rupture velocity and constant slip rate at all the scales. Regardless of the resolution problem, there have been many attempts to estimate the fracture energy of earthquakes through dynamic rupture simulations by fitting the ground motions. Aochi and Twardzik (Pageoph, 2020) listed 14 earthquakes (Mw from 6.0 to 7.8) from the 1979 Mw6.5 Imperial Valley (US) earthquake to 2017 Mw 6.9 Valparaiso (Chile) earthquake from 19 studies. They vary in their approaches. Ones minimize the number of parameters by introducing an elliptical description of asperity (main slip area) in dynamic rupture simulations. The others construct more heterogeneous model, inspired from the kinematic inversion results. Thus, it is not easy to compare one after another even for the same earthquake. However, Aochi and Twardzik (2020) demonstrated the scaling relation between the fracture energy integrated over the rupture area and effective radius.

The inversion by ellipse is handy but sometimes oversimplify the rupture process. In principal, the method is able to provide one biggest ellipse corresponding to the magnitude of earthquake. Two ellipses are difficult to obtain, as the second one may not be unique. It is only possible when two asperities are geometrically separated and ruptured by a time shift. Aochi and Ruiz (2021) analyzed the 2015 Illapel (Chile) earthquake, and obtained one small elliptical patch at the beginning (~Mw6.9) and another later biggest one (~Mw8.1). The latter can add an estimation (8.5×10^{16} J for a radius of 60 km) as shown in the below figure confirming the scaling relations of dynamic rupture simulations catalogued by Aochi and Twardzik (2020).

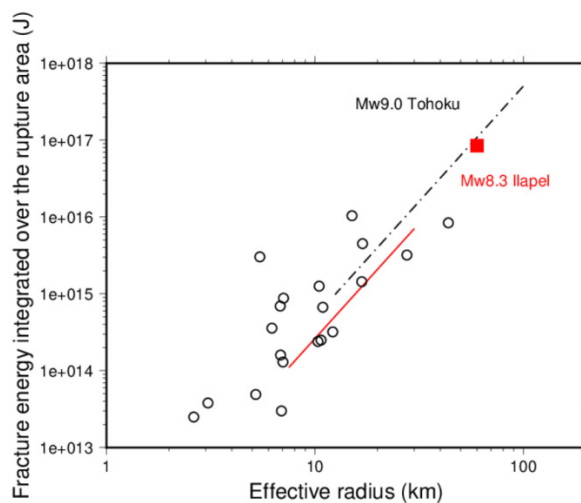


Figure: Scaling relation between effective radius and fracture energy integrated over the rupture area (modified after Aochi and Twardzik, 2020). The black circles represent the dynamic rupture simulations of the earthquakes catalogued by Aochi and Twardzik (2020). The broken line corresponds to the one assumed in Ide and Aochi (Tectonophys., 2013) for the 2011 Mw9.0 Tohoku earthquake. The red solid line and square show the simulation for the 2015 Mw8.3 Illapel earthquake (Aochi and Ruiz, 2021).

Slow fault slip dynamics reproduced by subdaily low-frequency earthquake activity

Caroline Mouchon¹, William Frank¹, Mathilde Radiguet², Piero Poli², Nathalie Cotte²

¹Department of EAPS, MIT, USA, ²ISTerre, Univ. Grenoble Alpes, France

Abstract:

Slow earthquakes play a major role in the earthquake cycle but their typical observational constraints lack the resolution to image their rupture dynamics in detail. While slow slip events were discovered and are still mostly observed using GNSS surface motion, geodetic measurements only capture their long spatial- and temporal-wavelength behavior. Low-frequency earthquakes, small repeating earthquakes on the plate boundary, are often spatiotemporally correlated with slow slip, giving us the opportunity to explore slow slip dynamics at shorter time scales. We realize a multi-disciplinary analysis of a 2.5-year period that includes multiple phases of a major slow slip cycle in Guerrero (Mexico). We use the low-frequency earthquake (LFE) activity to reproduce geodetic fault slip at both daily and subdaily time scales. We define a simple model of fault slip on the plate interface that represents the competition between long-term loading due to the plate convergence and intermittent slow slip release, as estimated from the fault-slip time history of LFEs. We show that our LFE models only fit well the geodetic estimates of fault slip, at both daily and subdaily sampling, with long-term loading rates on the order of plate convergence, implying 100% coupling on the plate interface at short time scales. We also highlight that a model with a non-linear relationship between seismic and aseismic fault slip is preferred. As the studied period includes a Mw7.5 SSE, seven smaller Mw6.4 events, and Mw<5.5 daily slow transients, all of which are interspersed with intermittent periods of tectonic loading, a power-law scaling between seismic and aseismic fault slip is necessary for our model to fit the data. We observe that this power law must vary during different phases of this slow slip cycle, suggesting that LFEs are a powerful monitor of slow fault slip until their source region gets saturated by the growing aseismic rupture.

Shallow tectonic tremor activity near the Japan Trench from 2016 to 2022: development of fully automated monitoring system and its application to the Off Sanriku and the Off Fukushima tremor clusters

Shukei Ohyanagi¹, Kazuaki Ohta², Yoshihiro Ito³, and Ryota Hino⁴

¹Kyoto University, Graduate School of Science, ²National Research Institute for Earth Science and Disaster Resilience, ³Kyoto University, Disaster Prevention Research Institute, ⁴Tohoku University

After a discovery of slow earthquake phenomena in the early 2000s, a long-term slow earthquake catalog now become an essential tool to track the spatiotemporal evolution of seismological properties at subduction plate interfaces. In the Japan Trench subduction zone, various offshore shallow slow earthquake activities have been reported [VLFE: Baba et al., 2020, Matsuzawa et al., 2015; tectonic tremor: Nishikawa et al., 2019; Ohta et al., 2019; Tanaka et al., 2019; SSE: Honsho et al., 2019, Ito et al., 2013]. Especially, the deployment of the S-net [Aoi et al., 2020], a cabled network of ocean bottom seismometers (OBSs) makes continuous monitoring of the offshore shallow tremor activity feasible. However, none of the publicly-available researches reported the shallow tremor activity occurring after August 2018. Thus, despite of continuous ocean bottom observation, shallow tremor activity for the last 4 years remains unknown.

To understand up-to-date activity in the Japan Trench subduction zone, we developed a fully automated monitoring system of the shallow tremor. The system is composed of 3 steps; tremor candidate detection, false detection removal, and spatiotemporal clustering. The tremor candidates are detected and located by an envelope correlation method [Mizuno and Ide, 2019]. Contaminating non-tremor detections, such as earthquakes are removed using Earthquake Transformer [Mousavi et al., 2020], and the air-gun pulses associated with active-source seismic surveys are removed based on identification of spectral feature [Ohta, 2021 SSJ]. Finally, after performing spatiotemporal clustering, we eliminate the short-duration events to finalize the tremor catalog. Fusion of multiple processes other than spatiotemporal clustering enable efficient monitoring of tectonic tremor in the region near the seismically active area such as the Japan Trench subduction zone.

The developed system is applied to S-net cabled OBSs located in Off Sanriku and Off Fukushima, which are regions neighboring to the large coseismic rupture region of the Mw 9.0 Tohoku-Oki earthquake [Iinuma et al., 2012]. We construct a tremor catalog spanning from August 2016 to July 2022. The tremor activity revealed by the new catalog is characterized by long-term decay throughout the period of analysis, which observed in both of the targeted regions. During 2016–2017, Off Sanriku has 11 hours of monthly tremor duration on average, but decreased to 7 hours as of 2021–2022. The mean monthly duration also becomes a half in Off Fukushima in the corresponding time window. Decline in the tremor activity may indicate deceleration of the afterslip of the Tohoku-Oki earthquake in the targeted regions.

Interdisciplinary earthquake science on the late-interseismic Alpine Fault and opportunities for generalizable hypothesis-testing

John Townend¹, Emily Warren-Smith², Calum J. Chamberlain¹, Caroline Holden^{1,3},
Carolyn J. Boulton¹, Jamie Howarth¹, Konstantinos Michailos⁴

¹School of Geog., Env. & Earth Sciences, Victoria Univ. of Wellington, New Zealand,

²GNS Science, New Zealand, ³SeismoCity Ltd., New Zealand, ⁴University of Lausanne, Switzerland

The Alpine Fault is late in its $M \sim 8$ seismic cycle, offering an unparalleled opportunity to test hypotheses about interactions between slow, late-interseismic deformation, earthquake nucleation and rupture propagation, and the relationships between complex coseismic slip and regional strong ground motion.

Extensive paleoseismological research along the Alpine Fault using on- and off-fault indicators has yielded one of the most spatially and temporally extensive paleoearthquake records of any fault worldwide and indicates that the Alpine Fault produces major to great earthquakes on recurrence intervals of 249 ± 58 years on its 250 km-long central section (Howarth et al., 2021, *Nature Geosci.*). Although the timings of successive earthquakes are remarkably consistent, their inferred magnitudes vary depending on which combinations of the geometrically distinct southern, central, and northern segments of the fault rupture simultaneously. More than 300 years have passed since the last major earthquake, in 1717 CE, and the Alpine Fault is thus recognized as being late in the typical interseismic phase of its earthquake cycle, with the likelihood of a $M_w > 7$ earthquake occurring in the coming 50 years estimated to be 75% (29–99%; 95% confidence interval).

The Alpine Fault is also anomalously hot, at least along the central section where exhumation rates and slip rates are highest. Scientific drilling conducted during the Deep Fault Drilling Project (DFDP) and subsequent seismological and thermochronological studies reveal the central portion of the Alpine Fault to have an extremely high geothermal gradient ($\sim 120^\circ\text{C}/\text{km}$), reflecting the combined effects of rapid orogenic exhumation and active groundwater flow (Sutherland et al., 2017, *Nature*). The geotherm diminishes laterally along strike, accounting for marked variations in contemporary microseismicity cutoff depths along the central section of the fault (Michailos et al., 2020, *Geochem., Geosys., Geophys.*). The thermal regime at either end of the fault is less well understood and what time-varying factors (e.g., temperature, fluid pressure, or stress) or intrinsic geological factors (e.g., fault geometry or rheology) account for the mode-switching behavior of section boundaries are the subject of active research. The locations and focal mechanisms of low-frequency earthquakes observed at depths of 17–42 km suggest that some deeper portions of the fault are slipping. However, how

any late-interseismic deep slip and along-strike variations in seismogenic thickness may affect the distribution of future coseismic slip has yet to be investigated in detail.

A key challenge in quantifying the seismic hazard posed by any large fault is to reliably and efficiently compute the ground motions produced by a broad range of plausible but as-yet unobserved rupture scenarios represented by a complex distribution of source terms. In this presentation, we review the opportunities afforded by the Alpine Fault to constrain parameters likely to affect the nucleation and evolution of rupture in the next large earthquake. We focus on new findings regarding the properties and effects on rupture propagation of key section boundaries that should inform dynamic rupture models, and on ambient-noise-based (“virtual earthquake”) investigations of regional ground shaking effects now underway using the 450 km-long Southern Alps Long Skinny Array (SALSA).

The paleoseismological, geological, and seismological observations made along the length of the Alpine Fault in recent years provide a rare (time-limited?!) opportunity for the global earthquake science community to pose generalizable hypotheses about large earthquake phenomena that will likely be tested within years or decades rather than centuries or millennia.

Seismogenesis in the Guerrero Seismic Gap: A Slow and Fast Slip Swaying

Víctor M. Cruz-Atienza¹, Josué Tago², Sara Franco¹, Jorge Real¹, Carlos Villafuerte³, Vladimir Kostoglodov¹, Yoshihiro Ito⁴, Darío Solano², Ekaterina Kazachkina¹, Arturo Ronquillo⁵, Anne Becel⁶, Takuya Nishimura⁴, Luis A. Domínguez¹ and Ana Rocher¹.

¹Instituto de Geofísica, UNAM, Mexico, ²Facultad de Ingeniería, UNAM, Mexico, ³Laboratoire de Géologie, ENS, Paris, France, ⁴DPRI, Kyoto University, Japan, ⁵Instituto de Ciencias del Mar, UNAM, Mexico, ⁶LDEO, Columbia University, USA

On September 8, 2021, a Mw7.0 thrust earthquake took place beneath Acapulco, Mexico, causing significant local damage and triggering the public early warning system in Mexico City, which is located 280 km north of the epicenter. The earthquake occurred in the heart of the Guerrero seismic gap and is a repetition of the event of May 11, 1962 (Mw7.1), where a doublet took place nine days later (Mw7.0) next to the great rupture of 1957 (Mw7.7) that toppled the Angel of Independence, an emblematic historical monument of the country's capital, and gave birth to the earthquake engineering in Mexico.

Four months earlier, on May 2021, a slow slip event was initiating in Oaxaca, southeast of the Acapulco earthquake rupture area, and propagated to the state of Guerrero along the deep part of the plate interface (i.e., between 25 and 50 km depth). Based on a dense GPS network and unprecedented seafloor geodetic observations, we show that a year before the earthquake, from September 2020, another Mw6.6 shallow slow slip earthquake initiated at the oceanic trench of the seismic gap and propagated downdip towards the earthquake hypocentral region close to the shoreline. This aseismic event as well as the mainshock were recorded offshore either by hydrostatic pressure sensors (vertical sea bottom displacement) and/or collocated tiltmeters (sea bottom rotations). The earthquake and its postseismic relaxation produced the development of a Mw7.3 long-term slow slip event deep in Guerrero (between October 2021 and April 2022) significantly increasing the seismicity of the region and particularly in the 1957 rupture zone, where most of the aftershocks are concentrated. Earthquake clustering offshore and continuous geodetic observations, last acquired at sea in June 2022, strongly suggest that a new short-term shallow slow slip event (0-15 km depth) is taking place offshore Acapulco (preliminary Mw6.5) starting around January 2022 where seismicity rate remains high. All these observations and the corresponding inverse modeling suggest that the genesis of potentially devastating earthquakes in the Guerrero seismic gap is controlled by the sway of slow transient events interacting from the trench to 50 km depth, which has large dynamic implications for the origin of subduction earthquakes.

Do Slow Slip Events on the La Venta-Chacalapa fault system (Mexico) conform the RSF law?

Vladimir Kostoglodov¹, Ekaterina Kazachkina¹, Victor Cruz-Atienza¹, and Allen Husker²

¹ Institute of Geophysics, National Autonomous University of Mexico, Mexico

² California Institute of Technology, Seismological Laboratory, Pasadena, CA, USA

The La Venta-Chacalapa creeping fault system (LVC) is a boundary separating the North America tectonic plate (NA) and adjacent to it the Xolapa sliver in the South of Guerrero and Oaxaca states of Mexico. CMT solutions and long-term GPS observations reveal a contemporary tectonic activity of the LVC (Kazachkina et al., 2019, 2020). The Xolapa sliver is slowly moving to SE with respect to (wrt) the NA with an average rate of ~ 5 mm/year as a consequence of the oblique subduction between Cocos and NA plates. New observations unveil transient episodes of crustal slow slip events (cSSE) on the LVC. These cSSE are incited by large subduction thrust slow slip events (tSSE) developing on the interface between the Cocos and NA. Periodically happening tSSE gradually reduces the normal stress and the friction on a certain segment of LVC, so that this leads it to the cSSE. Only a few crustal, Mw ~ 5 left-lateral strike-slip earthquakes were recorded close to the geologic trace of LVC, but their slip was not aligned with the LVC main strike. The along trench, SE component of Xolapa displacement during the cSSE consistently develops with a clear time lag wrt the trench normal displacement component. This observation is in favor of the ‘Rate and State Friction’ behavior of the LVC akin to the laboratory experiments of Boettcher and Marone (2004).

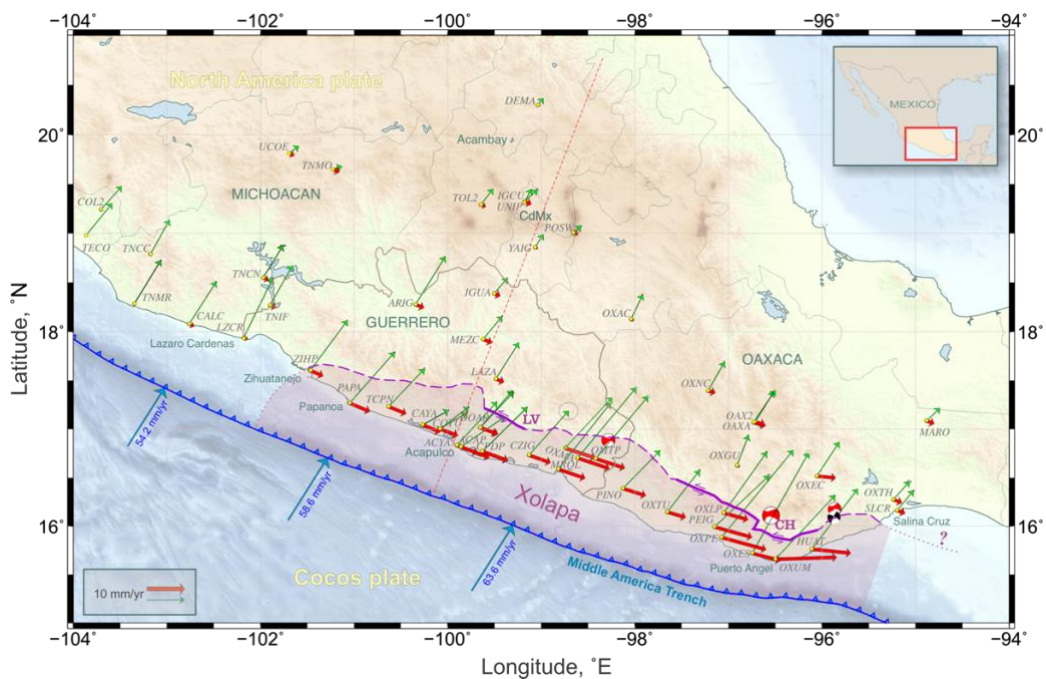


Figure 1. (Modified from Kazachkina et al., 2020). The study area (Inset) and location of permanent GPS stations (small yellow circles). Secular GPS velocities (wrt the fixed North America plate, mm/year) are shown as green vectors, and red vectors are their oblique components (parallel to the Middle America trench, MAT). The solid-dashed purple line delineates a trace of the La

Venta-Chacalapa (LVC) fault zone (according to geological data). LV - La Venta segment, and CH - Chacalapa segment of the LVC. An abrupt decrease of the secular oblique velocity is noticeable across the LV fault zone, which is roughly the northern border of the Xolapa allochthonous terrain (XOLAPA, shaded area located between the MAT and the LV-CH). Blue vectors are the Cocos - North America PVEL convergence velocities (DeMets et al., 2010) at the MAT. Red beach-balls are the CMT of crustal, Mw~5 left-lateral strike-slip earthquakes (www.globalcmt.org), and black one is the focal mechanism estimated by the National Seismological Service (SSN) for the M5.5, May 25, 2022 earthquake.

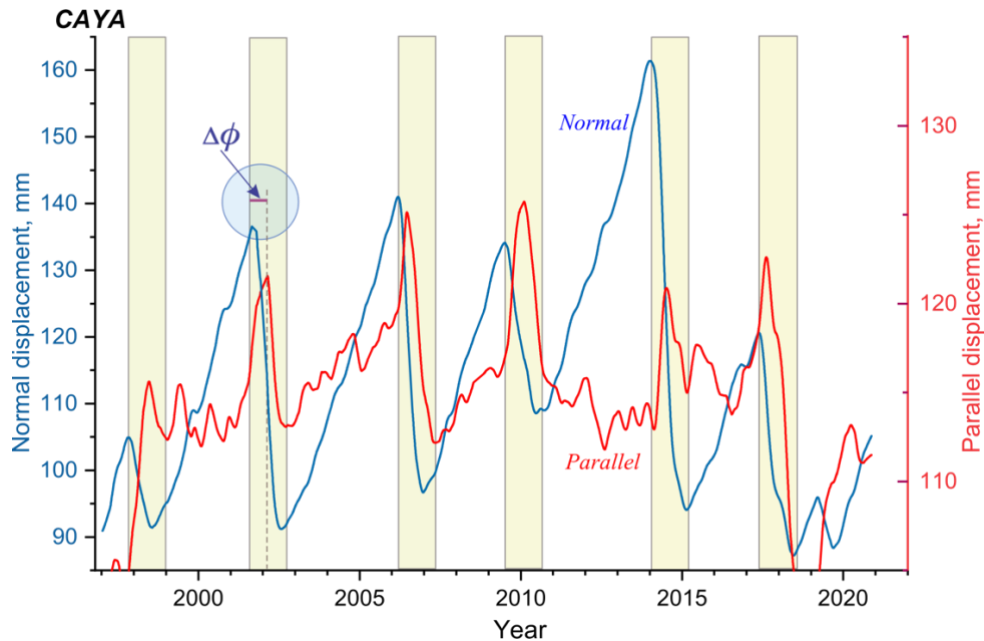


Figure 2. Smoothed and detrended time series at CAYA GPS station. Phase lag ($\Delta\phi$) is between the normal and parallel to the MAT displacement components during the cSSE. The $\Delta\phi$ delays are similar to the phase lags (time difference between the peaks of the normal and shear stresses) observed in normal stress vibration laboratory experiments by Boettcher and Maron, (2014).

References:

- Boettcher, M.S., and Marone, C., 2004. Effects of normal stress variation on the strength and stability of creeping faults, *Journal of Geophysical Research: Solid Earth*, 109. doi: 10.1029/2003JB002824.
- DeMets, C., Gordon, R.G., and Argus, D.F., 2010. Geologically current plate motions, *Geophysical Journal International*, 181, 1-80. doi.org/10.1111/j.1365-246X.2009.04491.x
- Kazachkina, E., V. Kostoglodov, A. Husker, and N. Cotte (2019), Activity of crustal faults and the Xolapa sliver motion in Guerrero–Oaxaca forearc of Mexico, from seismic data, *Earth, Planets and Space*, 71(1), 104, doi:10.1186/s40623-019-1084-9.
- Kazachkina, E., Kostoglodov, V., Cotte, N., Walpersdorf, A., Ramirez-Herrera, M.T., Gaidzik, K., Husker, A., and Santiago, J.A., 2020. Active 650-km Long Fault System and Xolapa Sliver in Southern Mexico, *Frontiers in Earth Science*, 8, 155. doi: 10.3389/feart.2020.00155.

The break of rupture asperities as resolved by distributed acoustic sensing

Zhongwen Zhan¹, Jiakuan Li¹, Taeho Kim¹, Nadia Lapusta¹, Ettore Biondi¹

¹Seismological Laboratory, Division of Geological and Planetary Sciences, California Institute of Technology, Pasadena, CA, USA

Imaging of megathrust earthquakes reveals frequency-dependent rupture signatures, but the role of high-frequency radiators remains unclear. While many moderate-sized crustal earthquakes could provide critical constraints, similar observations are rare without ultra-dense local arrays. Here, we push the resolution limit of back-projection imaging for moderate-sized earthquakes by converting two pre-existing dark fibers into an ultra-dense seismic array. With about 9,000 channels spanning a total distance of around 90 kilometers, we apply a 3D back-projection imaging and tracked the high-resolution rupture process for the July 8th, 2021, Mw6.0 earthquake in the Antelope Valley, eastern California. We resolve four high-frequency energetic subevents in a 3 km-by-5 km area. We verify their location and origin time by timing their S-wave arrival on several nearby strong-motion stations. By comparing with the moment rate function determined from long-period waveforms, we find that their timings mark the onset of high moment release. We suggest that the high-frequency subevents are related to the initiation/breaking of individual rupture asperities that substantially modulate the overall rupture dynamics. To verify this hypothesis, we perform dynamic rupture simulations by considering a homogeneous planar seismogenic zone containing high-normal-stress patches with locations based on the imaged subevents. Our rupture simulation reproduces several key observations: the moment magnitude, the relatively long rupture duration, the significant rupture slow down before the last and largest subevent, the two local peaks of the moment rate function (with a larger second peak), the time of subevents/breaking of asperities, and the elliptical shape of final slip distribution. The simulation shows both rupture delay and promotion by asperities depending on their properties and stress levels. Since there are numerous other moderate-sized crustal earthquakes showing complex moment-release patterns, such modulation of rupture behavior by local fault heterogeneities may be ubiquitous. Combining the DAS-enabled high-frequency imaging of moderate-sized earthquakes and dynamic rupture simulations, we could form a unique insight into the role of geometrical, stress, and material heterogeneities in earthquake ruptures.

Development on seafloor fiber optic sensing to capture slow process in the Nankai Trough megathrust.

Eiichiro Araki¹, Takashi Yokobiki¹, Hiroyuki Matsumoto¹, Satoru Baba¹, Shuhei Tsuji¹,
Shuhei Nishida¹, Yuya Machida¹, and Yoshiyuki Tanaka²

¹JAMSTEC, ²Dept. EPS, Univ. Tokyo,

In the Nankai Trough, slow earthquakes occur in the shallow part of the Philippine Sea Plate subduction. From the recent borehole observation, these shallow slow earthquakes are associated with slow slip in the background repeatedly occur in the subduction plate interface. The mechanism of slip in the shallow plate interface has many unresolved questions, such as its relationship with the structure of the plate boundary and the mutual relationship with distant slip patches, including ones to cause large megathrust earthquakes. Long-term broadband and high dynamic range observations in the seafloor are necessary to clarify these questions.

Optical fiber sensing is a technology that can observe strain distribution in optical fibers. We consider the distributed fiber sensing technology applied to submarine seafloor cable has good potentials in monitoring slow processes in the subducting plate interface in wide area. Therefore, we plan to apply the technology to submarine fiber optic cables in the Nankai Trough aiming to observe slow events in the Nankai Trough plate interface as well as coming large earthquakes in the vicinity of these sources. We have begun observations using the Muroto-oki submarine cable of JAMSTEC to verify applicability of fiber optic sensing technologies for our purposes.

Currently, distributed acoustic sensing (DAS) is widely used among fiber optic sensing technologies, suitable for detecting small earthquakes, although in low-frequency seismic band, the observation noise of commercially available DAS is not matching the expected signal strength from very low frequency earthquakes (VLFs) which occurrence is observable with broadband seismometer in the nearby seafloor observation network (DONET).

The wavelength stability of the laser source used in the DAS is directly related to the background noise of the observed data, so we decided to improve low frequency observation noise of AP Sensing's DAS N5225b by feeding it a very stable laser with high wavelength stability. We modified the AP Sensing's DAS N5225b to be able to run on external laser source, and we feed the DAS with a cavity-locked laser (Stable Laser Systems SLS-INT-1550-200-1) and performed observation with the Muroto seafloor fiber optic cable in the Nankai Trough.

Our initial results show a significant improvement in long-period noise compared to what has been obtained with DAS to date. This means that the DAS can be expected to observe the VLFE in the vicinity of these sources. With the achieved low frequency observation noise floor, infragravity wave is easily observed with sufficient signal to noise ratio. This means that we can also expect to observe Tsunamis by the DAS through seafloor deformation from Tsunami pressure loading.

We are also aiming to detect slow slip events with much longer period than VLFE and crustal deformation of the seafloor by fiber optic sensing. For this purpose, it is important not only to be able to make stable measurements over very long periods, but also to prevent dynamic strain

changes caused by earthquakes occurring during these periods, resulting failures in phase tracking, which is difficult with DAS. Therefore, we have developed a fiber optic sensing instrument (TW-COTDR) based on the principle of measuring the Rayleigh scattered light wavelength shift due to strain changes in optical fibers by evaluating the Rayleigh scattered light intensity of optical fibers at many wavelengths. We also started observations using the TW-COTDR technology with the Muroto seafloor fiber optic cable.

In TW-COTDR, we calibrate the wavelength of the Rayleigh scattering evaluation with high precision, so it is possible to evaluate strain changes in the same optical fiber as a difference from long past measurements. It is therefore considered to be very effective in evaluating seafloor crustal deformation for many years.

From our measurements with TW-COTDR technology in Muroto cable, there were some areas where the daily strain change is close to 10 μ strain. It is considered that there are water temperature changes exceeding 1°C. However, in most sections of the Muroto cable, the daily changes are small and within 1 μ strain. The daily changes are also well correlated with seafloor water pressure. Therefore, by correcting for the effects of water temperature changes and ocean tides pressure changes, it is highly possible to detect seafloor strain fluctuations associated with slow slips and other events of less than 1 μ strain. In the past, such measurement of seafloor crustal deformation is only possible with intermittent and infrequent GNSS/A surveys. With the ability to observe the seafloor strain changes in real time with high spatio-temporal density, such fiber optic sensing technologies will revolutionize the way we observe crustal deformation of the seafloor.

Source parameter estimations using DAS and comparison with seismic stations

Xiaowei Chen¹, Jiuxun Yin², Qimin Wu³, Zhongwen Zhan²

¹Department of Geology and Geophysics, Texas A&M, ²Seismological Laboratory, Caltech, ³Lettis Consultants International, Inc.

Distributed Acoustic Sensing (DAS) has been used for passive seismic monitoring, including earthquake detections and tomographic imaging. However, there have not been many applications of DAS to earthquake source parameters. In this study, different DAS arrays are used to study earthquake source parameters, and the results are compared with those obtained from seismic stations.

Using the Brady Hot Springs array in Nevada, two $M > 4$ regional earthquakes located at 150 km are analyzed using spectral ratio method, in which smaller earthquakes within 5 km are selected as empirical Green's function (EGF) events. Spectra are calculated using 5-second window following S-wave arrival for the collocated geophone arrays (geometric mean of two horizontal channels) and DAS channels. For each target-EGF pair, stacked spectral ratio is obtained using stations with good signal-to-noise ratio (SNR). Comparison between DAS and geophone results suggests similar shape of spectral ratios and corner frequencies.

The Ridgecrest array is located at about 30-50 km away from the Ridgecrest aftershock sequence, and three earthquakes from the Stress-Drop-Validation project are selected for analyses. Events that are within 1 km lateral and 1 km depth difference, at least 0.75 magnitude unit smaller are selected as EGF events. The spectral ratio from stacked DAS channels with good SNR resembles nearby seismic stations from regional network.

Current efforts are focused on testing the influence of window length, source complexity, and EGF selection on spectral ratio analysis, as well as testing relative source time function algorithm on DAS data. Updated results will be presented at the workshop.

Towards the automatic detection of slow slip events using machine learning

Bertrand Rouet-Leduc¹, Sylvain Michel², Romain Jolivet², Claudia Hulbert³, Manon Dalaison²

¹DPRI, Kyoto University, ²Dept. Geosciences, PSL University, France, ³Geolabe, USA

Faults can accommodate stress in a variety of slip modes, from dynamic rupture to slow slip events and aseismic slip. Among these slip modes, slow slip events and often-accompanying tremor remain among the most elusive and poorly understood.

Unraveling the interactions between slip modes is at stake: while laboratory experiments point to aseismic nucleation generally preceding dynamic rupture, observations in the field are far from systematic, and more the exception than the rule.

However, the difficulty in detecting transient slow slip events, either seismically or geodetically, points to a possible observational gap that may explain the relative rarity of slow deformation detected prior to dynamic earthquakes.

In this presentation, the use of machine learning to improve the detection of slow slip events and accompanying tectonic tremor will be explored, as a tool to fill this observational gap, both in seismic data and in geodetic data.

Following a general introduction on the interaction between slip modes from the laboratory to the field, the development of deep learning methods for the detection of slow slip events both in seismic and in geodetic data will be detailed in a first part. In a second part, it will be showed that the automatic detection of slow slip events using machine learning reveals interplay between transient aseismic deformation and small to moderate earthquakes on the San Andreas Fault.

Segmentation characteristics of tectonic tremors in Shikoku, Japan, using machine learning approaches

Hao-Yu Chiu¹, Kate Huihsuan Chen², Kazushige Obara³

¹Department of Geosciences, National Taiwan University, ²Department of Earth Sciences, National Taiwan Normal University, ³Earthquake Research Institute, the University of Tokyo

The Shikoku of the western Nankai Trough showcases the along-strike segmentation of slow earthquake behavior. Whether the spatial variation of tremor behavior reflects the regional differences in structure and source property, and how much such difference can be recognized by the seismic signals itself? Through advanced methods in recognizing and classifying signals using machine learning approaches, we attempt to answer these questions by conducting experiments of signal classification in Shikoku, Japan.

In this study, we first demonstrate the regional characteristics using tremors catalog by [Annoura et al. \(2016\)](#). During the study period from 1 June 2014 to 31 March 2015, the number of tremors in four different areas (A to D, from east to west) reaches 15000, 31000, 10000, and 16000, respectively. Tremors at four areas are treated as different classes and here, the tremors in the catalogs were segmented into 60-s-long signals as the labeled data. Each class of tremor events is split into training (70%) and testing data (30%) sets. The supervised k -NN classifier is trained to distinguish tremors from four different areas of Shikoku. In order to obtain the efficient features that better represent the properties of tremors in each area, we adopt the binary classification with a set of experiments. When the k -NN classifier is applied on 29 seismic features, the classification performance reaches $> 90\%$ classification rate at all 12 stations.

We further design a triangle test to select the features that can better represent the difference in source properties between areas. We found that the efficient features are associated with (1) the number of peaks in temporal evolution of Discrete Fourier Transform (DFTs) and (2) the energy distribution in the autocorrelation function (ACF). In order to meet the different behavior revealed by ACF, the size of tremor zone that mainly controls how long the seismic energy lasted in a tremor episode, is found to be largest in Area B and smallest in Area C. Whereas the heterogeneity of asperities in the tremor zone that may control how spiky the tremor signals evolve in time, is found to be strong in Areas B and C. Together with the previously documented variation in slow earthquake behavior in the same area, we finally propose a conceptual model that provides a better understanding of regional difference in tremor sources of Shikoku, Japan.

Slow slip event detection from GNSS data using deep learning in the Cascadia subduction zone

Giuseppe Costantino¹, Anne Socquet¹, Sophie Giffard-Roisin¹, Mauro Dalla Mura^{2,3}, David Marsan¹, Mathilde Radiguet¹

¹Univ. Grenoble Alpes, Univ. Savoie Mont Blanc, CNRS, IRD, Univ. Gustave Eiffel, ISTerre, 38000 Grenoble, France, ²Univ. Grenoble Alpes, CNRS, Grenoble INP, GIPSA-lab, 38000 Grenoble, France, ³Institut Universitaire de France (IUF), France

Detecting small Slow Slip Events (SSEs) is still an open challenge and a crucial issue for the characterization of the slip spectrum and for the understanding of the mechanics of active faults. The difficulty in revealing low magnitude events is related to their detection in the geodetic data, notably in subduction zones where tremors cannot serve as a proxy for the slow slip detection. It is therefore necessary to provide new observations by employing more powerful equipment or to develop novel methods to perceive potential bursts of slow slip.

Unlike seismic data, geodetic observations provide the sole direct access to slow slip deformation, which need to be analyzed within a large time span (weeks to years). Moreover, they contain spatiotemporal information, which needs to be leveraged to consistently constrain the slip evolution. However, the detection of small potential events is still debated and hard to automatize. Traditionally employed methods rely on the visual inspection of the data and dedicated modelling methods with a fine-tuning of the parameters (e.g. Ozawa et al., 2001; Hirose & Obara, 2005; Wallace & Beavan, 2010; Radiguet et al., 2011; Ozawa et al., 2013; Radiguet et al., 2016; Socquet et al., 2017; Wallace et al., 2016; Wallace, 2020; Bletery & Nocquet, 2020; Itoh et al., 2022). Here we develop a method based on deep learning for the systematic detection of SSEs. We focus our analysis on the Cascadia subduction zone, where a link between slow slip and bursts of tremor activity has been established (Rogers & Dragert, 2003). In this direction, tremor catalogues can be used to validate potential SSEs detections against the spatiotemporal distribution of tremors. Moreover, a catalogue of SSEs has been recently assessed by (Michel et al., 2019), providing an additional benchmark to our analyses. Nevertheless, the number of available labelled events is still scarce and does not allow for an adequate training of deep learning models. Therefore, we make use of synthetic data by generating synthetic slow slip events obtained from synthetic dislocations (Okada, 1985) and by means of the slab2 model (Hayes et al., 2018). Each SSE template, assumed as a sigmoidal-shaped transient, is further added to a window of noise obtained from real GNSS data.

We develop a method based on deep learning, using a Convolutional Neural Network (CNN), followed by a Transformer model, to detect small slow slip events in GNSS data. The CNN extracts features from the input GNSS time series by learning optimal convolution filters, while the Transformer focuses on specific parts of the input window thanks to a self-attention mechanism. We test our method both on synthetic and real position time series from Nevada Geodetic Laboratory (NGL). Results on synthetics are consistent and show a detection trade-off between the SSEs location, magnitude and the density of the GNSS network. The spatio-temporal information is thus taken into account, showing that our model is able to correctly learn the network geometry and exploit the temporal dependencies in the data. Results on real GNSS positional time series show a good agreement between our detections and existing catalogues (cf. Michel et al., 2019). Moreover, new detections have been carried out, which correlate well with the temporal distribution of tremors, suggesting that those events could be

new SSE detections, which will be further validated by assessing their spatio-temporal consistency.

The spatiotemporal distribution of aseismic and seismic slip at Nankai and Cascadia inferred from geodetic observations

Elizabeth M. Sherrill¹, Kaj M. Johnson¹, and Noel M. Bartlow²

¹Indiana University, ²University of Kansas

A spectrum of aseismic and seismic slip behaviors is observed at subduction zones including earthquakes, afterslip, slow slip, and creep. Growing evidence suggests that some large earthquakes at subduction zones begin with slow slip events (SSEs) near or within the fully coupled (or locked) zone and numerical models indicate that SSEs are capable of loading the locked zone and evolving into dynamic rupture. Understanding the spatiotemporal relationship of the various slip zones is critical for estimating seismic hazard at subduction zones. Additionally, recent interseismic locking inversions infer a gap between the bottom of the locked zone and the top of the slow slip, or episodic tremor and slip (ETS) zone at Cascadia, which may imply that the ETS zone is not significantly stressing the locked zone at Cascadia. We present here results of two different inversions that help to provide more information about the spatiotemporal distribution of aseismic and seismic slip behaviors at subduction zones: an iterative least squares inversion of vertical surface displacement data for coseismic slip during and postseismic slip following the 1944 & 1946 Nankai earthquakes and a probabilistic inversion of surface velocities and baseline rate changes for the boundaries of the locked zone and the upper and lower transition zones at Nankai and Cascadia subduction zones.

For Nankai, we conducted iterative inversions for a suite of elastic subducting slab and overriding plate geometries and mantle viscosities. The inversions all infer 30 years of sustained afterslip following the 1944/46 earthquakes within the ETS zone and regions in and around the area of high coseismic slip (Figure 1). We sum the cumulative coseismic slip and afterslip estimates from our inversion with previous estimates of cumulative slip during the interseismic period, including SSEs. We find that the slip budget beneath eastern Shikoku island has nearly all been met for a 150-year interseismic cycle, whereas beneath western Shikoku there is a slip deficit of roughly half the budget (4 out of 8.25 meters) above 20 km depth on the subduction interface.

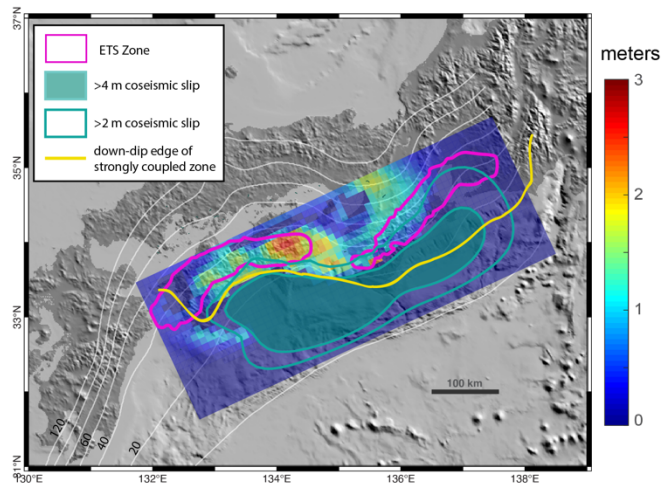


Figure 1 (from Sherrill & Johnson, 2021). Cumulative total afterslip distribution relative to the ETS zone (Obara et al., 2010), the best-fitting coseismic slip model (>4 m and >2 m), and the downdip edge of the strongly coupled zone (Yokota et al., 2016). White contour lines represent slab depth at Nankai in 20 km intervals (Hayes et al., 2012).

For Nankai and Cascadia, we use a Markov chain Monte Carlo inversion of interseismic deformation to obtain posterior probability distributions of the locked and transitional creep zone boundaries. The backslip rate is equal to the plate (i.e., fully coupled) in the locked zone,

approximated as an upward-propagating creep front following Bruhat and Segall (2017) in the transitional creep zone below the locked zone, and computed using a boundary element calculation that assumes no stress accumulation in the transitional creep zone above the locked zone. Our homogeneous elastic halfspace inversion infers that the ETS zones at Nankai and Cascadia are fully contained within the lower transition zones. While there is minimal separation between the bottom of the locked zone and the top of the lower transition zone at Nankai (Figure 2), there appears to be a gap between the locked zone and lower transition zone at Cascadia. We are currently working to explore the impact of elastic heterogeneity and viscoelastic cycle deformation on the coupling models. We will also perform a similar probabilistic inversion of long-term average slow slip velocities at Nankai and Cascadia and compare the boundaries of the inverted ETS zone to boundaries of the locked zone.

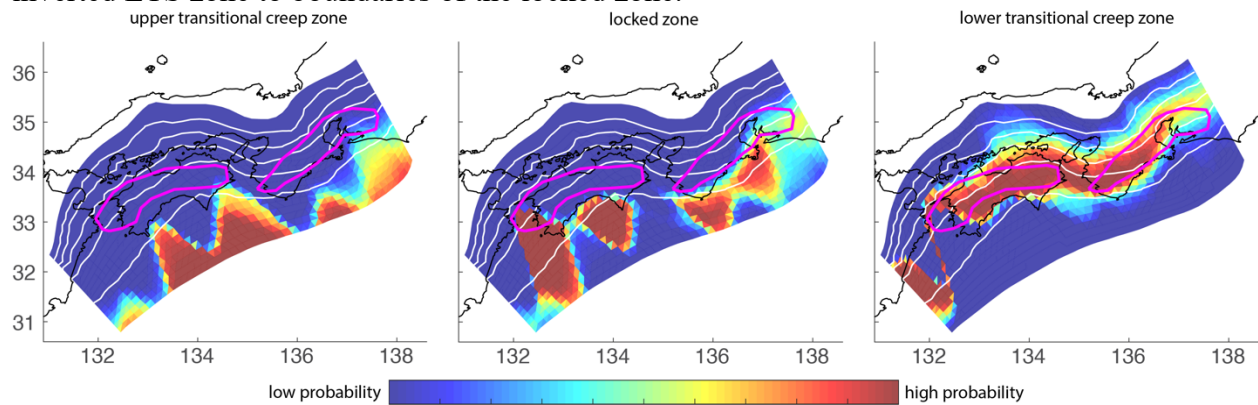


Figure 2. Probability that a patch is in the upper transitional creep zone (left), the locked zone (middle), and the lower transitional creep zone (right) at Nankai subduction zone. Rough outlines of the ETS zone (Obara et al., 2010) are shown in pink. White contour lines represent slab depth at Nankai in 20 km intervals (Hayes et al., 2012).

Energy-based scenarios for Nankai trough earthquakes: The impacts of aseismic slip events on strain energy accumulation

Akemi Noda¹, Tatsuhiko Saito²

¹MRI, JMA, ²NIED

Dense and precise GNSS observations enable us to estimate the spatiotemporal changes of interplate coupling, leading to future megathrust earthquakes. It is expected to model future earthquakes by combining such geophysical observations with a physical model in addition to the empirical information on historical earthquakes. There have been two approaches to creating possible earthquake scenarios: (1) kinematic modeling in which a coseismic slip is obtained by multiplying the slip deficit rate by the accumulation time, and (2) dynamic modeling in which source models are obtained via dynamic rupture simulations. A new energy-based method to model earthquake scenarios was proposed to bridge these two approaches and overcome their disadvantages (Noda et al., 2021). Based on the stress accumulation model calculated from the slip deficit rates, the method constructs multiple scenarios as static-slip distributions with a lower computational load than dynamic modeling. It subsequently examines whether each scenario follows the mechanics of faulting from the perspective of the energy balance of fault rupture, which is lacking in kinematic modeling.

We applied the method to the interplate earthquakes along the Nankai trough and obtained ten scenarios with different source regions (Figure 1). For evaluating the energy balance of each scenario, the energy-based method introduces “residual energy,” which is defined as the difference between the strain energy released by the coseismic slip and the energy dissipated on the fault. Since positive residual energy is a necessary condition for earthquake generation in terms of the law of conservation of energy, we can select scenarios with positive residual energy as realistic rupture scenarios. The residual energy is usually negative immediately after a seismic event, but then gradually increases due to the accumulation of strain energy caused by interplate coupling and eventually reaches a positive value. Thus, we quantified the increase in earthquake potential with elapsed time since the previous earthquake by using the residual energy.

Next, we considered the effects of aseismic slip events occurring outside the seismogenic zone, such as afterslip, slow slip event, and preseismic slip acceleration, on the earthquake scenarios. Assuming the total amount of aseismic slip during an interseismic period consistent with the slip budget within the seismic cycle, we computed stress loading on the seismogenic zone due to the aseismic slip. The earthquake scenarios considering the stress loading due to aseismic slip had a slip amount and seismic moment approximately twice as large as those of the scenarios without considering the effect of aseismic slip. The residual energy also increased accordingly. These results suggest that the aseismic slips have considerable impacts on the potential of anticipated earthquakes. Aseismic slip events including slow earthquakes have been considered to promote the occurrence of large earthquakes in adjacent areas, but it was difficult to quantify their impacts on the earthquake potential. The energy-based method makes this possible in terms of the accumulation of strain energy required to generate an earthquake.

To demonstrate the validity of our method, we generated source models of historical

earthquakes, the 1854 Tokai, 1854 Nankai, 1944 Tonankai, and 1946 Nankai earthquakes, by applying the energy-based method with the stress loading due to aseismic slips to the earthquake history in the Nankai trough subduction zone (Figure 2). The estimated moment magnitude of the source models was compatible with that of the actual earthquakes based on historical and seismic records.

Reference:

Noda et al. (2021). *JGR: Solid Earth*, <https://doi.org/10.1029/2020JB020417>

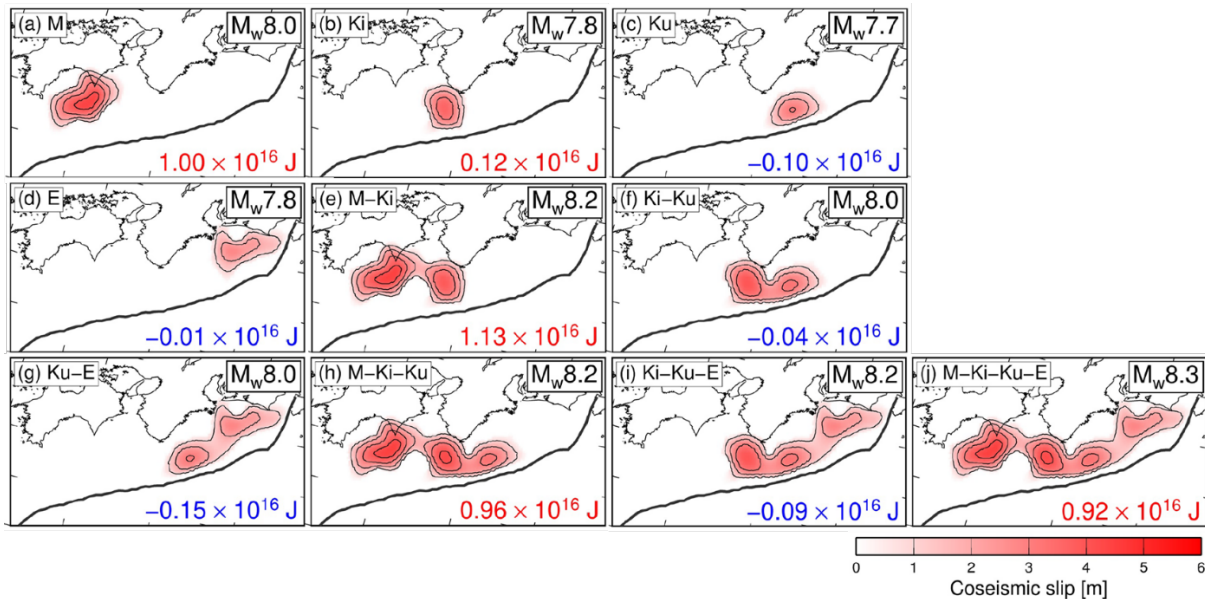


Figure 1. Ten earthquake scenarios assuming an accumulation time of 150 years (Noda et al. 2021). The moment magnitude and residual energy are shown in the upper right and lower right of each panel, respectively.

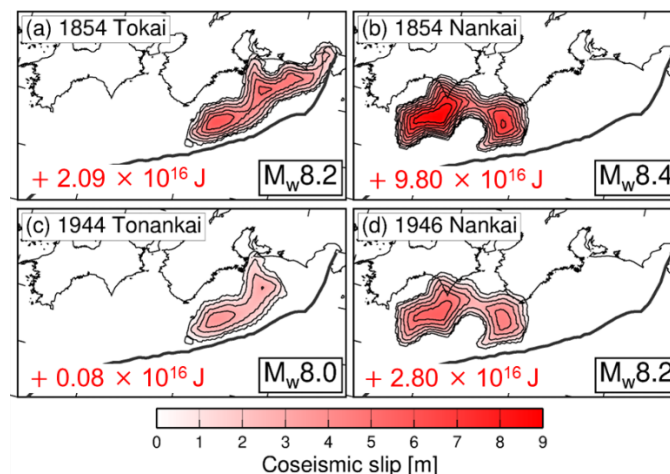


Figure 2. Source models of (a) the 1854 Tokai, (b) 1854 Nankai, (c) 1944 Tonankai, and (d) 1946 Nankai earthquakes considering the stress loading due to aseismic slip events. The moment magnitude and residual energy are shown in the lower right and lower left of each panel, respectively.

Geological features from trench to tectonic backstop controlling slip behaviors in the Nankai Trough

Takeshi Tsuji¹

¹Univ. Tokyo

We show the geological features that control the earthquake slip behaviors in the Nankai Trough, Japan. We used multi-channel seismic data and advanced techniques, and investigated 3D fault geometry and other geological features over the transition from the partially coupled to the fully coupled plate interface.

At the outer wedge (from trench to outer ridge) where slow slip events have been observed, we identified thick shear zone around the plate interface (Tsuji et al., 2014). The shear zone can be identified from its low seismic velocity and low reflection amplitude, which may signify the presence of high pore pressure. A detailed comparison of the mapped shear zone and the distribution of tectonic tremor (Hendriyana and Tsuji, 2021; Fahrudin et al., 2022) demonstrate that tremor tended to occur in the thick part of the shear zone, where high pore fluid pressure may weaken faults and thereby facilitate slow earthquakes. Furthermore, the tremors align on the oblique strike-slip faults that caused variation of the shear zone thickness as well as fluctuation of stress and pore pressure.

At the transition from outer to inner wedge (i.e., outer ridge), the underthrust sequence is thinner than that in the outer wedge. The overburden to the plate interface (or underthrust sequence) may increase at the landward of the outer ridge (i.e., inner wedge), because the higher density of the inner wedge overlays the plate interface. Therefore, large amounts of fluid might be expelled from underthrust sediments around the outer ridge, causing increasing pore pressure there. As a results, the tremors mostly occurred at the high pore pressure area at the outer wedge area, and a smaller number of tremors can be observed at the inner wedge area.

At the inner wedge, we found that a gently dipping plate boundary décollement extends beneath the entire Kumano forearc basin on several seismic profiles (Tsuji et al., 2017). The 1 April 2016 Off-Mie earthquake (Mw6.0) and its aftershocks occurred, where the plate boundary décollement steps down close to the oceanic crust surface. This location also lies beneath the trenchward edge of an older accretionary prism (~14 Ma) developed along the coast of the Kii peninsula (Tsuji et al., 2015). Thus, the fault planes of the 2016 earthquake and its aftershocks were influenced by the geometry of the plate interface. The 2016 earthquake occurred within the rupture area of large interplate earthquakes such as the 1944 Tonankai earthquake (Mw8.1), although the 2016 rupture area was much smaller than that of the 1944 event. Whereas the hypocenter of the 2016 earthquake was around the underthrust sequence beneath the younger accretionary prism (~6 Ma), the 1944 great earthquake hypocenter was close to oceanic crust surface beneath the older accretionary prism. The variation of fault geometry and lithology may influence the degree of coupling along the plate interface, and such coupling variation could hinder slip propagation toward the deeper plate interface in the 2016 event.

This study demonstrates that the fault geometry and geological formation largely influence upon the slip behaviors. Therefore, if such geological features can be obtained via seismic or other geophysical approaches, we could infer the spatial variation of slip behavior in the Nankai Trough area.

References

- Fahrudin, Chhun, C., Tsuji, T., 2022. Influence of shear zone thickness and strike-slip faulting on tectonic tremor in the Nankai Trough, southwest Japan, *Tectonophysics*, 838, 229519. <https://doi.org/10.1016/j.tecto.2022.229519>
- Hendriyana, A., Tsuji, T., 2021. Influence of structure and pore pressure of plate interface on tectonic tremor in the Nankai subduction zone, Japan. *Earth Planet. Sci. Lett.* 558, 116742. <https://doi.org/10.1016/j.epsl.2021.116742>
- Tsuji, T., Kamei, R., Pratt, R.G., 2014. Pore pressure distribution of a mega-splay fault system in the Nankai trough subduction zone: Insight into up-dip extent of the seismogenic zone. *Earth Planet. Sci. Lett.* 396, 165–178. <https://doi.org/10.1016/j.epsl.2014.04.011>
- Tsuji, T., Ashi, J., Strasser, M., Kimura, G., 2015. Identification of the static backstop and its influence on the evolution of the accretionary prism in the Nankai Trough. *Earth Planet. Sci. Lett.* 431, 15–25. <https://doi.org/10.1016/j.epsl.2015.09.011>
- Tsuji, T., Minato, S., Kamei, R., Tsuru, T., Kimura, G., 2017. 3D geometry of a plate boundary fault related to the 2016 Off-Mie earthquake in the Nankai subduction zone, Japan, *Earth Planet. Sci. Lett.* 478, 234-244. <https://doi.org/10.1016/j.epsl.2017.08.041>

Crustal structure of the Nankai subduction zone revealed by two decades of onshore-offshore and ocean-bottom seismic data

Dan Bassett¹, Adrien Arnulf², Shuichi Kodaira³, Ayako Nakanishi³, Alistair Harding⁴, Gregory Moore⁵

¹GNS Science, ²University of Texas at Austin, ³JAMSTEC, ⁴Scripps Institution of Oceanography.,

⁵Department of Earth Sciences, University of Hawaii

Some subduction zones produce the largest earthquakes and tsunami on Earth, while others slip aseismically. To understand what factors impact subduction zone slip behavior, we have integrated two-decades of onshore-offshore, ocean-bottom seismometer, and passive-source data in SW Japan to construct the first high-resolution, 3-D image of an entire subduction zone. This image reveals large variability in the offshore extent of dense, rigid crustal rocks and suggests the position of this crustal backstop may influence the shallow transition from aseismic to seismic slip along the Nankai megathrust. The landward extent of seismic slip is also spatially variable and appears to be predominantly controlled by trajectory of the subducting plate. Collectively, along trench variability in the position of the crustal backstop (up-dip transition) and the geometry of the subducting slab (down-dip transition) combine to produce large variability in the width of the seismogenic zone. Earthquake magnitude is proportional to rupture area and pinching of the seismogenic due to the convergence of shallow and deep frictional transitions may explain the smaller magnitude of earthquakes offshore Kyushu. Our results suggest crustal-scale architecture is a key driver of profound along-strike transitions on the location of frictional transition zones, and the width and slip behavior of the intervening seismogenic zone at Nankai Trough.

Rock record constraints on the structures, materials and environment of deep-seated slow slip and tremor

Whitney Behr¹

¹Geological Institute, Dept. of Earth Sciences, ETH Zurich, Switzerland

Deep-seated slow slip and tremor (SST), including slow slip events, episodic tremor and slip, and low-frequency earthquakes, occur down-dip of the seismogenic zone of numerous subduction megathrusts and plate boundary strike-slip faults. These events represent a fascinating and perplexing mode of fault failure that has greatly broadened our view of earthquake dynamics. In this talk I will review constraints on SST deformation processes from geological observations of exhumed field analogues, and draw comparisons to the geophysical record in modern subduction zones. I describe the materials, deformation mechanisms, and metamorphic and fluid pressure conditions that characterize exhumed rocks from SST source depths. Both the geophysical and geological records strongly suggest the importance of a fluid-rich and high fluid pressure habitat for the SST source region. Observations of vein networks from exhumed rocks can provide key information on fluid-flow pathways and permeability and may relate to SST timescales. Additionally, transient deformation features preserved in the rock record, involving combined frictional-viscous shear in regions of mixed lithology and near-lithostatic fluid pressures, may scale with the tremor component of SST. While several open questions remain, it is clear that improved constraints on the materials, environment, structure, and conditions of the plate interface from geophysical imaging and geologic observations will enhance model representations of the boundary conditions and geometry of the SST deformation process.

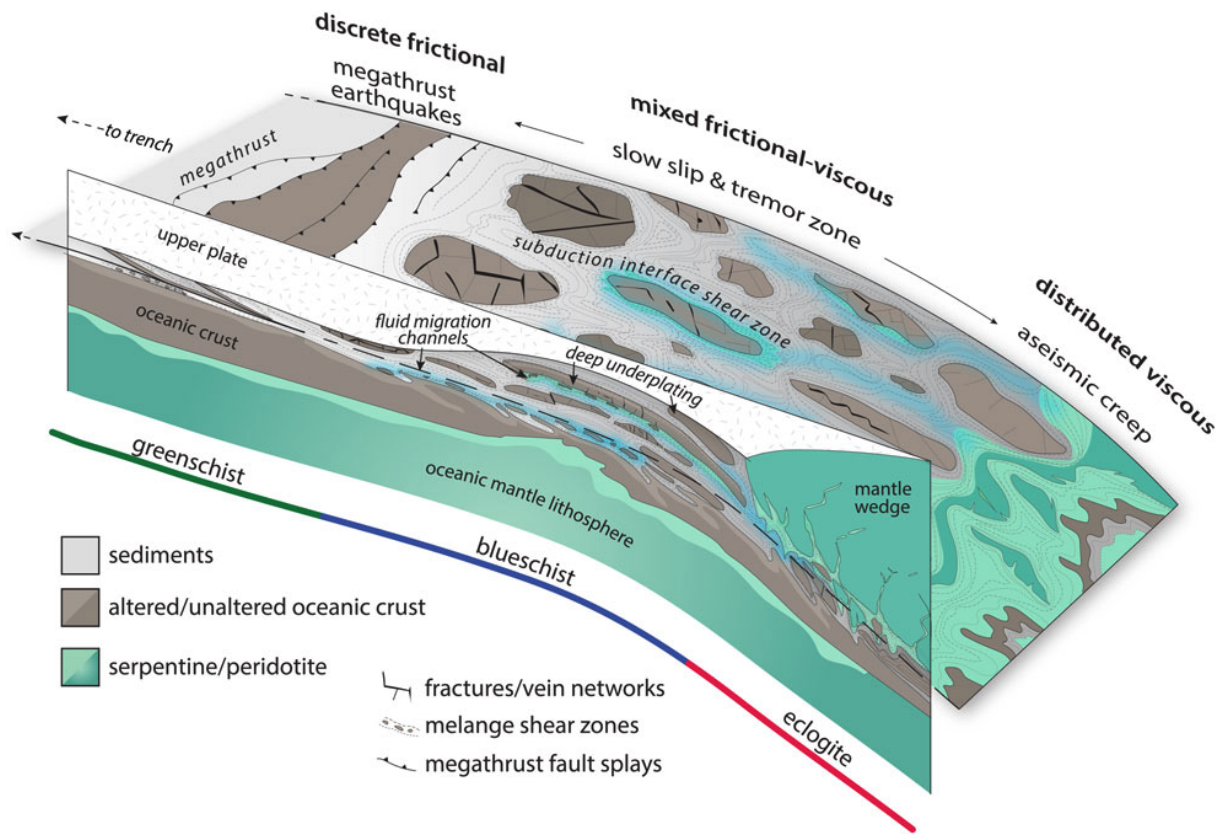


Figure 1. Summary schematic view of the subduction plate interface as inferred from the exhumed geological record. From Behr & Bürgmann, *Phil. Trans. Roy. Soc. A* 379.

Estimation of shear strength and fluid pressure in world subduction zones based on the earthquake energy budget

Nelson Pulido¹

¹National Research Institute for Earth Science and Disaster Resilience (NIED)

I estimated fault shear strength of global subduction zones based on calculations of the seismic energy budget during large earthquakes. Estimates of shear strength are based on the calculation of the total energy released during earthquake rupture, which is partitioned into radiated energy, fracture energy (G) and frictional (heat) energy. Radiated energy can be readily obtained from radiated seismic waveforms or using information of the source time function of earthquakes. Accurate estimates of fracture energy are more difficult to obtain, and for this purpose I use the Finite Width Slip Pulse dynamic rupture model that accounts for the contribution of mixed anti-plane and in-plane rupture modes, combined with information of the heterogeneous fault rupture process of large earthquakes (208 fault rupture models of the NEIC finite fault slip database, from 1990 to 2022, and $M_w > 7$). Estimates of G are largely influenced by the heterogeneous distribution of fault rupture velocity, rise time and slip of earthquakes across the fault plane. In a previous study I showed that fracture energy is underestimated by a factor of 5 when estimations do not account for the heterogeneity in fault rupture process of large earthquakes, as typically assumed by the calculations based on the difference between average stress drop and the apparent stress of earthquakes (known as G'). Furthermore, recent studies also suggest that megathrust earthquakes experience an almost complete strength drop during fault rupture (i.e. 2011 Tohoku). If a strong dynamic weakening typically takes place during fault rupture of large earthquakes (substantial stress undershoot) then frictional energy can be neglected, and therefore average shear stress and shear strength (by adding half the stress drop) can be obtained. Based on this assumption I calculated lower bound estimates of shear strength across subduction regions and oceanic lithosphere worldwide. My results indicate a severe fault strength weakening during all megathrust earthquake ruptures (with a global average around 4 MPa), notably tsunami earthquakes belonging to the weakest faults (around 1 MPa), implying that fluids are extremely over-pressured across the majority of subduction regions worldwide. By using my shear strength results, I obtained a global average of λ (the fluid pore pressure to lithostatic pressure ratio) of 0.98, for subduction megathrusts. In contrast, I showed that oceanic lithosphere at ridges, transform faults and fracture zones is 5 to 10 times stronger. This considerable difference indicates that fluid pressure plays a major role in controlling strength of earth's lithosphere. Furthermore, my estimations of average shear stress during fault rupture also enable the calculation of seismic efficiency. I obtained that average seismic efficiency for megathrust subduction earthquakes, is smaller than the average value for earthquakes in oceanic lithosphere.

Development of geochemical machine-learning models to quantify silica transport in metamorphic rocks

Masaoki Uno¹

¹GSES, Tohoku Univ.

Fault-sealing by silica precipitation is considered as one of the major processes controlling fluid pressure in subduction zones. Recent geophysical observations suggest that the time-scales of silica precipitation may control the reoccurrence of the slow and fast earthquakes (e.g., Audet and Burgman, 2014). Geological observations revealed that repeated fault-sealing by silica and fracturing do occur at the slow-to-fast seismogenic zones (e.g., Ujiie et al., 2018). However, the amount of silica transport at the slow-to-fast seismogenic zones has not been quantified in a unified manner, and the distribution of silica precipitation and their effects on the fault-sealing processes are largely unknown.

Here we present a geochemical machine-learning approach to quantify silica transport in metamorphic rocks. Silica transport in metamorphic rocks is generally quantified by comparing the composition of metamorphosed rocks with the composition prior to the metamorphism (i.e., protoliths). However, in many cases, the exact protoliths of metamorphic rocks is not accessible. Recently, based on global geochemical datasets of basalt, we have developed a machine-learning approach to quantify the protolith composition and mass transfer history of metabasalt (Matsuno et al., 2022 *Scientific Reports*). Following the approach of Matsuno et al. (2022), we have developed a new machine-learning model to quantify silica transport in metapelitic rocks.

Global compositional datasets of marine sediments, including mudstones, sandstones, and siliciclastic rocks are compiled for SiO₂, TiO₂, Al₂O₃, Nb, Zr, Y, and Th (5442 samples). The models were designed to estimate SiO₂, TiO₂, Al₂O₃, Nb, Zr, Y and Th concentrations from only the ratios of 6 elements (TiO₂/Zr, Al₂O₃/Zr, Nb/Zr, Y/Zr and Th/Zr). The compositional correlation between the input elemental ratios and output elements were calibrated with gauss process (GP), a machine-learning algorithm with predictive uncertainty estimation.

The modeling results show that SiO₂ concentrations can be estimated with the reproducibility of $\pm 5\text{wt}\%$ (1σ). The absolute concentrations of TiO₂, Nb, Y, Th, Zr were reproduced with $\pm 25\%$ (1σ), showing that mass transfer in metapelitic rocks can be analyzed for the reproducibility of $\sim 25\%$. The developed model was applied to the silica-metasomatized rocks reported by Ague et al. (2011), where metapelitic rocks were altered along quartz-kyanite veins. The model could successfully reproduce the protolith compositions of the altered rocks and their host rocks. These results show that using 5 elemental ratios (TiO₂/Zr, Al₂O₃/Zr, Nb/Zr, Y/Zr and Th/Zr) that are typically immobile during metamorphism, silica transport can be quantified from arbitrary metapelitic rocks. We will further extend these models to the metapelitic and metaigneous rocks in high-pressure metamorphic belts and accretionary prisms, and reveal the amount of silica transport in the slow-to-fast seismogenic zones.

Audet and Bürgmann (2014) *Nature*, 509, 389–392.

Ague (2011) *American Mineralogist*, 96, 333–352.

Matsuno et al. (2022) *Scientific Reports*, 12: 1385.

Ujiie et al. (2018) *GRL*, 45, 5371–5379.

Geologic and petrologic constraints on fluid sources, pressures, and consequences for deep slow earthquakes in subduction zones

Cailey B. Condit¹, Melodie E. French², Victor E. Guevara³, William F. Hoover¹, Peter C. Lindquist¹, Jonathan R. Delph⁴,

¹Dept. ESS, University of Washington, ²Dept. EEPS, Rice University, ³Geology Dept. Amherst College, ⁴Dept. EAPS, Purdue University.

In a subset of subduction zones, episodic tremor and slip (ETS) events along the plate interface between depths of 25 and 65 km have been identified by coupled geodetic and seismic observations. These ETS events comprise non-volcanic tremor and slow earthquakes, where energy is released slowly over weeks to months, often equaling a Mw 6-7.5 earthquake. These slow earthquakes slip at rates much slower than seismic events, but several orders of magnitude faster than tectonic creeping, and occur episodically ever few months to years. Geologic studies of exhumed terranes representative of the source area of ETS suggest that the region is a lithologically heterogeneous, fluid-rich tabular shear zone experiencing relatively low differential stresses (≤ 10 s MPa) with thicknesses on the order of 100s of meters. Geophysical observations of low shear wave velocities (V_s) coupled with tidal triggering (on the order of several kPas) of slow slip events together have lead to the interpretation that this region has (intermittent) near lithostatic pore fluid pressures. Rheological requirements for slow earthquakes include (1) stress perturbations of 10s kPa resulting in strain rate increases of several orders of magnitude and (2) deformation accommodated at low differential stresses. Given these constraints, a range of hypothesized mechanisms for these slow earthquakes include mixed brittle-viscous flow or slip hosted by frictional deformation activated by elevated pore fluid pressures. However, we lack a mechanistic understanding ETS, including the lithologies that host slow earthquakes and the potential role and sources of fluids in this region.

Here, we present petrologic and rheological modeling coupled with microstructural and geologic observations from exhumed subduction terranes to examine the fluid environment of slow earthquakes and the mechanisms that produce these events. We begin by investigating the source of fluids along the plate interface at ETS conditions using thermodynamic modeling of typical subduction lithologies along pressure-temperature (P-T) paths of several tremorgenic margins (Cascadia, Shikoku and Kii, and Mexico). This analysis reveals that punctuated dehydration from mafic rocks (the subducting slab crust) releases ample aqueous fluids at the depths of ETS due to the breakdown of lawsonite, chlorite, and/or Na-amphibole and growth of epidote and Ca-amphibole. We then show geologic evidence that documents \sim lithostatic pore fluid pressures during subduction at \sim 30 km paleodepths using arrays of crack-seal quartz veins. Finally, we combine structural and microstructural observations from the exhumed rock record from a range of lithologies with rheological modeling using laboratory derived constitutive relations to demonstrate that during periods of high pore fluid pressure, slow slip can readily be hosted within metasomatic lithologies such as talc-schist by frictional deformation. Together, these results suggest that (1) fluids at the depths of ETS in subduction zones are sourced from *in situ* metamorphic devolatilization reactions from the subduing slab, (2) geologic evidence corroborates geophysical modeling of intermittent \sim lithostatic pore fluid pressures, and (3) metasomatic lithologies including talc-schists may host slow earthquakes through frictional deformation during periods of elevated pore fluid pressures.

Mineral dehydrations at subduction zones conditions: experimental evidence of non volcanic tremors and high Vp/Vs ratio

Alexandre Schubnel¹, Arefeh Moarefvand¹, Julien Gasc¹, Damien Deldicque¹, Loïc Labrousse², Sandra Babinski³, Timm John³ and Jörn Kummerow⁶

¹LG-ENS, PSL University, Paris France; ²ISTEP, Sorbonne University, Paris France;

³Freie Universitat Berlin, Germany

Non-volcanic tremors (NVTs) have been extensively documented in deep subduction environments, often in relation with zones where large Vp/Vs ratios have been observed. However, up to this day and to our knowledge, neither have yet been reproduced in the laboratory at subduction zones P–T conditions, in such way that the origin of both, as well as their first order controlling mechanisms, remains enigmatic.

First, we investigate NVTs by performing dehydration-deformation experiments combined with detailed investigations of mineral reactions and acoustic emissions. All experiments have been carried out on dehydrating chlorite peridotites (Balmuccia peridotite with synthetically added chlorite, minerals representative of subduction zones lithologies) following a subduction zone geothermal gradient using a high-pressure apparatus (Griggs-type). The experiments were conducted from room conditions to maximum conditions of pressures of 1.5-3.0 GPa and temperatures of 750- 800 °C. Experiments were conducted both under hydrostatic and deviatoric stress conditions. An array of transducers was employed to monitor, detect, and analyze the micro seismic events. Dehydration of the sample material containing 10 vol.% of chlorite suffices to trigger acoustic emissions, which display wave forms similar to those of non-volcanic tremors. Microstructural observations demonstrate that an almost isochemical dehydration of the chlorite took place. Accordingly, the appearance of the tremor-like acoustic emissions after crossing a temperature of 600 °C can be linked to a dehydration process linked with the chlorite breakdown in the sample. Interestingly, experiments under deviatoric stress produced no tremor-like acoustic emission suggesting that the deformation suppressed the development of the processes that lead to acoustic emissions. Therefore, we conclude that the fluid release during dehydration is the cause of non-volcanic tremors, whereas shear movement seem to counteract their development with no occurrence of tremors at high-rates of deformation. In consequence, the triggering mechanism of NVTs can be tentatively interpreted as a fluid propagation front, traveling as a resonance wave resulting in the vibration of grains.

Second, using the same apparatus, we performed antigorite dehydration experiments during which we monitored the evolution of P-wave velocities at pressure and temperature conditions representative of subduction zones (1 to 2.5 GPa). Velocities were measured at constant pressure conditions of 1, 1.5, 2 and 2.5 GPa while heating the sample beyond dehydration temperatures. In all our experiments, P-wave velocity decreased dramatically at the onset of dehydration. This important drop in elastic properties is related to the fracturing and porous space generated by water release. At 700 °C, velocity drops occurred over a shorter time interval, and were more pronounced compared to experiments performed at 650 °C, which we correlate to more advanced and hence faster dehydration reaction. The velocity drop also decreases in amplitude with increasing pressure, but remains noticeable, even at 2.5 GPa, a pressure at which the reaction volume change is expected to be negative. In the

absence of fluid overpressure, this implies that the reaction is accompanied by an important amount of microcracking/softening. Recovered samples were then analyzed using EDS and BSE imaging. With these textural data, the final reaction progress was estimated, and we show a good agreement with reaction progress values retrieved from in situ measurements of p-wave velocity, which therefore represents a good proxy for reaction progress and kinetics, provided some assumptions are made on the geometry of cracks. Finally, combining our experimental data and thermodynamic databases, we compute the elastic properties of dehydrating mineral assemblages, and their frequency dependence, using effective medium theory modeling. We predict that, at subduction zone conditions, mineral dehydration signature is indeed that of low V_p , but large V_p/V_s ratios, which is compatible with seismological observations.

What causes the local increase in pore-fluid pressure around the source region of shallow slow earthquakes?

Shunya Kaneki¹ and Hiroyuki Noda¹

¹DPRI, Kyoto Univ.

Rock strength increases with increasing effective stress σ_e (normal stress σ minus pore-fluid pressure p) in the brittle regime. Particularly in plate subduction zones, the relationship between local increase in p and the occurrence of slow earthquakes has been discussed based on the seismological and geodetic observations. Rice (1992) realized constant σ_e at depth (i.e., gradients of σ and p are equivalent at depth) by modeling an upward flow of fluid with constant properties along a vertical strike-slip fault zone whose permeability is a rapidly decreasing function of σ_e . The development of similar models for subduction zones enables us to quantitatively evaluate the local increase in p in subduction zones, which deepens our understandings of the generation of slow earthquakes.

In order to quantitatively examine the causes of the local increase in p in the shallow section of a subduction zone, we performed hydraulic modeling that incorporated mechanisms characteristic to subduction zones. We focused on the Kumano Transect in the Nankai Trough as a representative subduction zone, and referred to the experimental results using the core samples to determine the physical properties for the model calculations. Our basic model considers the effect of smectite dehydration and the mechanical effect (e.g., compaction) of subduction on the sediments, as well as realistic fluid property as a function of temperature and pressure. As in Rice (1992), physically sound solutions of the model show that the gradient of σ_e remarkably decreases with increasing depth, whereas the realistic fluid properties rule out the nearly constant σ_e at depth. We obtained a monotonic increase in σ_e with increasing depth, and failed to generate a locally high p even with fluid release due to smectite dehydration. It was also absent, despite considering fluid leakage through a splay fault. In the case with a local decrease in permeability, possibly owing to silica cementation or pressure solution-precipitation process, locally high p is realized around the low-permeability region. Therefore, the local decrease in permeability is a possible candidate for the occurrence of shallow slow earthquakes. The water release caused by the dehydration reaction of smectite is not likely to be the dominant factor on p , although smectite dehydration releases silica and can promote its precipitation.

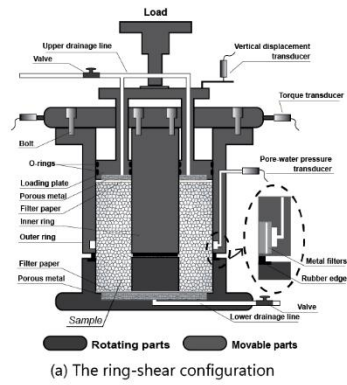
Constitutive Properties and Frictional Behavior of Simulated Fault Zone of Halite Developed in Granular Medium

Chengrui Chang¹, Hiroyuki Noda², Gonghui Wang², Tetsuo Yamaguchi¹

¹Department of Biomaterial Sciences, The University of Tokyo, ²Disaster Prevention Research Institute, Kyoto University

Tectonic faults and landslides exhibit an extensive spectrum of velocities. A key motivation of this study is to better understand the physical processes that dictate the slow-to-fast transition of frictional behavior in earthquakes and landslides by combining the friction measurements and microscopic analysis of the experimental fault zone. We simplify the questions as (1) the effect of the comminution rate and segregation of granular material in determining the friction coefficient; (2) the connection between the frictional parameters and the development of shear fabric with the increasing displacement of shear.

We employ a unique ring-shear configuration that has a large shear box (18.0 cm in outer diameter, 12.0 cm in inner diameter, and 10.9 cm of available sample height) to contain a larger volume of granular particles than that of conventional rotary or direct shear configurations for fault mechanics. It could produce experimental shear zones of large dimensions at significantly great shear displacements (Figs. a-c). The ring-shear apparatus is in Kyoto University and has been used in studies of landslide behavior. It should be emphasized that a shear zone is developed within the granular medium. In the most of the previous friction experiments, a simulated shear zone of a millimeter scale is defined by the amount of gouge sandwiched between hard host rocks and cannot grow to be thicker. We vary the total normal stress from 0.2 to 1.0 MPa and the slip rate from about 0.001 cm/s to 10 cm/s for velocity-step tests. We use analog granular materials with two initial size distributions, i.e., coarse and fine halite particles with size distributions of 2-5 mm and 0.25-2 mm, respectively, to examine the constitutive properties and frictional behavior. We begin with a run-in process for materials to reach steady state of friction, and a substantial weakening ($\mu \approx 0.4$) is observed at a low slip rate (0.05 cm/s) (Fig. d). We stop and hold the tests for about 1,000 seconds and the fine halite weakens rapidly once the shear is resumed. We then perform velocity-step tests and reproduce unstable stick-slip and stable sliding behaviors at relatively low and high slip rates, respectively (Fig. e). The experimental shear zone is observed after the shear test (Figs. b-c). The thickness of the shear zone is from several millimeters to tens of millimeters and it is larger in coarse granular media. A spring-slider model is used to fit the stable velocity-step tests to obtain the frictional properties in a rate- and state-dependent friction law. Finally, we combine the measurements of frictional parameters, observation of shear zone development, and comminution and packing of particles to dissect the key issue that how they interact and regulate the slow and fast motion.



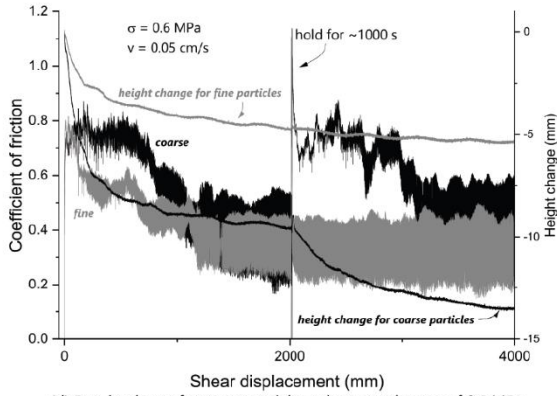
(a) The ring-shear configuration



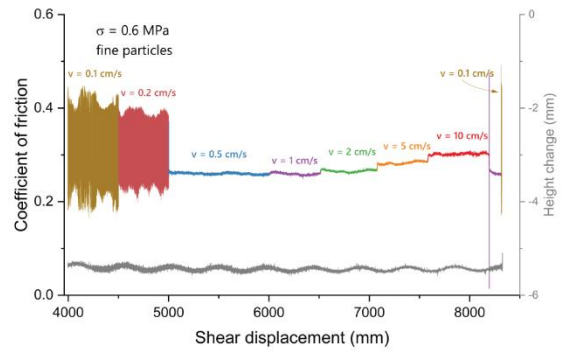
(b) A photo of an experimental shear zone in coarse halite particles (thick)



(c) A photo of an experimental shear zone in fine halite particles (thin)



(d) Run-in phases for two materials under normal stress of 0.6 MPa. We stop and hold the tests for ~1000 s and the fine material shows rapid weakening when the shear is resumed



(e) Results of velocity-step tests on fine particles under normal stress of 0.6 MPa, showing unstable stick-slip and stable sliding

A forward/inverse modeling framework for earthquake deformation problems

Simone Puel^{1,2}, Thorsten W. Becker^{1,2,3}, Umberto Villa³, Omar Ghattas^{1,3,4}, and Dunyu Liu²

¹Dept. Geological Sciences, Univ. Texas at Austin, ²Institute for Geophysics, Univ. Texas at Austin,

³Oden Institute for Computational Engineering and Sciences, Univ. Texas at Austin, ⁴Walker Dept.

Mechanical Engineering, Univ. Texas at Austin

Analysis of coseismic and postseismic surface displacements can help constrain Earth structure and the physics of deformation mechanisms occurring at depth. Here, we propose a new finite-element (FE) based computational framework to solve forward and inverse elastic deformation problems for earthquake faulting including adjoint optimization methods. Based on two advanced open-source computational libraries, FEniCS and hippylib for the forward and inverse problems, respectively, this framework is flexible, transparent, and easily extensible. We represent a fault discontinuity through a stress-accurate implementation in a mixed FE elastic formulation, which exposes the prescribed slip explicitly in the variational form without using conventional split node and decomposition discrete approaches. To demonstrate the potential of this new computational framework, two examples are shown. Synthetic geodetic data are used to infer the coseismic slip distribution during megathrust earthquakes (linear inversion) and the crust and mantle Poisson's ratio (non-linear). While the estimation of the fault slip is crucial to understand seismic source processes and mitigate seismic and tsunamigenic hazards, the Poisson's ratio has been used as a proxy of presence of fluids and postseismic poroelastic effects. For the linear inversion, we compare our results with the standard linear approach where fault slip is inferred using elastic Green's functions. Inherent limitations may be overcome by adjoint-based optimization methods, which efficiently minimize the gradient of the cost functional. In this case, the computational time is independent of the number of model parameters. We compare eigenvalues and eigenfunctions of both approaches to gain insights on performance for the linear problem, and then explore the non-linear problem. Our inversion represents a novel technique to infer the spatial distribution of material properties such as Poisson's ratio, often used as a proxy for fluid flow, in the crust and mantle wedge. Lastly, we combine the two inversion schemes to jointly infer both model parameters, fault slip and the material properties distribution. Our approach has promise to explore more general inverse questions, such as to the best constitutive behaviour, and might be helpful in future optimal experimental design and parametric sensitivity studies.

Diffusional shear slip as the common mechanism for tectonic low-frequency earthquakes and volcanic deep-long-period earthquakes

Naofumi Aso¹

¹Tokyo Tech

Deep long-period earthquakes (DLPs) or low-frequency earthquakes (LFEs) are deep earthquakes around the Moho that radiate long-period (low-frequency) seismic waves despite their small magnitude. Tectonic LFEs on plate interfaces and volcanic DLPs widely observed in volcanic regions are unique slow deformation processes that exist in nature. While tectonic LFEs are known to be slip events driven by tectonic motion, the physical mechanism of volcanic DLPs is unclear yet.

Although their geographic distribution around active volcanoes implies the importance of fluids in their genesis, the mechanical effect of fluids in the occurrence of DLPs is debated: either deformation driven by fluid flow or shear slips enabled by high pore-fluid pressure. While fluid flow is controlled by fluid diffusion, slow shear slip is also known to be diffusive. To capture any fluid-related diffusive phenomena, we translate the swarm-like nature of DLPs into a diffusive one. For this purpose, we modify the epidemic-type aftershock sequence (ETAS) model, a standard tool for evaluating seismicity.

First, I detect DLPs in Eastern Shimane, Japan, using the matched-filter technique to the seismograms at permanent networks and my campaign network. Then, I model the swarm-like seismicity using the ETAS model. Here, I consider an additional term explaining the diffusional decaying characteristics. The new ETAS model successfully explains the seismicity much better than the classic ETAS model. The characteristic decay time is ~ 8 s. Considering that the diffusion scale is more expansive than each source size of ~ 50 m but smaller than the source cluster size of ~ 2 km, the diffusion coefficient is estimated to be 10^3 – 10^5 m²/s.

Since the diffusivity is much larger than the estimates for shallow volcanic events (10^0 – 10^1 m²/s) but close to those of tectonic tremors (10^4 – 10^5 m²/s), the principal mechanical process of the DLPs is likely shear slip. The diffusional migration rate may not be as high as the typical rupture velocity of ordinary earthquakes, but this is still sufficient to cause seismic radiation at a lower frequency range.

While the areal extent of aseismic slips is greater on the plate interface than in a less-mature system at volcanic roots, tectonic low-frequency earthquakes tend to be smaller than volcanic DLPs. The following scenario can explain this paradox. First, we consider shear slip to expand diffusional with similar diffusivities in both cases. Then, the larger the diffusion scale is, the slower the characteristic shear rate becomes. As a result, earthquakes triggered at seismic patches at an extensive plate interface (tectonic LFEs) get smaller than those at a small system (volcanic DLPs).

Temporal gravity anomalies in long-term slow slip areas along the Nankai Trough and Cascadia

Yoshiyuki Tanaka¹, Hiromu Sakaue¹, and Yuichi Hiramatsu¹

¹Dept. EPS, Univ. Tokyo

The water in Earth's mantle is closely related with plate subduction and volcanism. Recent studies revealed that the mantle wedge corner at approximately 30 km depth holds high-pressure water, where slow earthquakes occur. To quantify how such water behaves during slow earthquakes helps understand the mechanisms of slow earthquakes and (eventually) a part of the long-term water cycle between the interior and surface of the Earth. However, evidences suggesting transient flows of such water are still limited. In a previous study, we reported anomalous gravity anomalies during two long-term slow slip events in the Tokai area in Japan, which were detected by absolute gravity measurements over 20 years. We presented a poroelastic fluid flow model assuming a localized deformation within the fault fracture zone. The model could reproduce the gravity change with a permeability range between those suggested by laboratory experiments and numerical simulations of slow earthquakes. Similar observations using absolute gravimeters were carried out in the Bungo Channel, the Hyuganada and Cascadia. In this presentation, we show that temporal variations in the gravity anomaly on the order of 1 microGal are observed at these sites. Based on the result, we will discuss what kind of constraint the gravity data could give on transient fluid flow.

Transient fluid infiltration in the shallow mantle wedge recorded in the Oman Ophiolite

Kazuki Yoshida¹, Ryosuke Oyanagi², Masao Kimura³, Oliver Plümer⁴, Mayuko Fukuyama⁵,
and Atsushi Okamoto¹

¹Tohoku Univ., ²Kokushikan Univ., ³High Energy Accelerator Research Organization (KEK),

⁴Utrecht Univ., ⁵Akita Univ.

Fluid flow in subduction zones is one of the essential factors in seismic activity in subduction zones. However, the timescale of fluid flow and its flux in the supra-subduction setting is unclear. In this study, we report the novel texture of the antigorite veins with a brucite-rich reaction zone in dunite in the crust-mantle transition zone of the Oman ophiolite, and investigated the timescale and fluid flow velocity during the vein formation.

In this study, we observed samples in the lower crust to upper mantle section obtained from the Oman Drilling Project CM1 site (Kelemen et al., 2020). The crust-mantle transition zone is mainly composed of completely serpentinized dunite. The matrix of the dunite is mainly composed of lizardite and brucite, and cut by antigorite-chrysotile (Atg-Ctl) vein network. Trace element analysis using LA-ICP-MS revealed that the Atg-Ctl vein is enriched in As and Sb compared to the matrix. These results suggest that the Atg-Ctl veins were formed by fluids interacting with subducting sediments. Some of the Atg-Ctl veins are accompanied by brucite-rich reaction zones. The brucite-rich reaction zone was developed at both sides of the antigorite veins with a thickness of 0.5 – 4 mm. Mass balance calculations and thermodynamic considerations of the reaction zone and host rock suggest that the formation of the reaction zone was caused by the removal of silica from the host rock during the precipitation of antigorite in the veins.

Based on a diffusion model, we find that the fluid activity is short-lived (2.2×10^{-1} to 6.6×10^0 yr), and the fluid flow velocity of 4.4×10^{-3} to 4.5×10^{-2} m s⁻¹, which is much faster than those observed for the intact mantle and crustal rocks. This fluid flow velocity along the fractures within the mantle wedge is similar to the values obtained from tremor migration (e.g., $\sim 10^{-2} - 10^{-1}$ m s⁻¹; Rogers & Dragert, 2003). These results suggest that although the dehydration of subducting slab is continuous, the drainage of fluid into the overlying plate occurs as episodic pulses as observed as the migration of seismicity in the present subduction zones.

References

Kelemen, P. B. et al., Proceedings of the Oman Drilling Project.
Rogers, G. & Dragert, H. Science 300, 1942–1943 (2003).

Dynamic simulations of coseismic slickenlines on non-planar and rough faults: Towards inferring the rupture directions of paleoearthquakes

Takumi Aoki¹, Yoshihiro Kaneko¹, Jesse Kearsse²

¹Graduate School of Science, Kyoto Univ., ²Victoria Univ. of Wellington

Knowing the directions of rupture propagation of paleoearthquakes is a challenging, yet important task for our understanding of earthquake physics and seismic hazard, as the rupture direction significantly influences the distribution of strong ground motion. Recent studies proposed a relationship between the direction of rupture propagation and curvature of slickenlines formed during seismic slip (Kaneko and Kearsse, 2020). The relationship was established using a global catalogue of historic surface-rupturing earthquakes and dynamic models of idealized, planar faults. At the same time, some slickenlines previously documented on geometrically complex fault segments show their convexity opposite from the simple model prediction, which we refer to as 'abnormal convexity'. To explain such observations, we perform simulations of spontaneous earthquake ruptures on non-planar and rough faults. We find that a non-planar fault model can lead to abnormal convexity of slickenlines in places where the fault dip angle changes abruptly from the average dip of the fault. In the case of strike-slip faults, abnormal convexity of slickenlines is produced when the initial along-dip stresses are larger than, and are opposite in direction to, the dynamic stresses imparted by the mixed-mode rupture. Such results are also confirmed in our rupture simulations with a rough fault. Our results also show that the parameter space for which abnormal convexity of slickenlines occurs near Earth's surface is narrow, especially when the fault strength and initial shear stresses increase with depth. Nevertheless, slickenlines on geometrically complex faults need to be carefully interpreted and investigation of rupture direction using curved slickenlines should focus on structurally simple parts of faults.

Forearc mylonite formed along a plate boundary of high temperature conditions related to Cretaceous ridge subduction

Asuka Yamaguchi¹, and Ipppei Yamamoto¹

¹AORI, Univ. Tokyo

Mylonite, a plastically deformed fault rock, has been found in many faults within granitic continental crusts, but has rarely been reported in subduction zones. An epidote-amphibolite-facies mylonite within an ancient accretionary complex was found in the Kerama Formation, the Ryukyu Arc, Japan. Here we report occurrence and formation condition of the mylonite and discuss implications for rheology of subduction plate interface.

The Kerama Formation is located at the southwestern end of the Shimanto Belt. It consists of mafic rocks, sandstone, and pelitic phyllite. Raman spectroscopy of carbonaceous material in sandstone and pelitic phyllite shows maximum temperatures of 470-530°C, whereas Ti-Amphibole thermometer (Liao et al., 2021) for mafic rock shows temperatures of ~514°C. The pressure condition estimated by the Phengite barometer (Massonne and Schreyer, 1987) ranges 0.6-1 GPa. Sedimentary and metamorphic ages are estimated to be ~100 and ~90 Ma, respectively, based on youngest U-Pb age of detrital zircon and K-Ar age of muscovite. Presence of greenstones intruded into the clastic rocks is considered to record ridge subduction along the paleo-Ryukyu Arc.

In the Kerama Formation, foliations of mafic rock, sandstone, and pelitic phyllite are almost parallel to bedding plane and dips SW in general. Stretching mineral lineations and fibers of layer-parallel quartz veins on the foliation exhibit NW-SE. Axes of asymmetric folds observed in pelitic phyllite show NE-SW trend, suggesting top-to-SE thrusting shear. High-angle normal faults branching from low-angle normal fault are found in pelitic phyllite. These deformation features are classified into three deformation stages: D1 (underthrusting), D2 (underplating) and D3 (exhumation), respectively.

Strongly deformed mylonite of D2 stage originated from conglomeratic sandstone occurs in the Kerama Formation. The mylonite is characterized by shear bands of fine-grained quartz. Most of the crystallographic preferred orientation of recrystallized quartz show random fabric, but some shows a type II crossed girdle fabric. The deformation temperature was estimated as 530°C according to the thermometer of Faleiros et al. (2017), and differential stress was estimated to be 27 MPa by the piezometer of Cross et al. (2016). These values are consistent with flow law of quartz (Hirth et al., 2001).

In the Shimanto Belt in Kyushu, Palazzin et al. (2016) reported that plastic deformation of quartz begins at about 300°C. The maximum strength of the subduction plate boundary would be primarily controlled by plastic deformation of quartz at temperatures of ~300-530°C, and thus a plate boundary with extremely high temperature setting, such as ridge subduction, could only possess weak and thin seismogenic layer.

A systematic detection of intermediate-depth earthquakes within the Bucaramanga earthquake nest, Colombia

Ayako Tsuchiyama¹, William B. Frank¹, Germán A. Prieto²

¹Dept. EAPS, MIT, ²Dept. Geociencias, Univ. Nacional de Colombia

Intermediate-depth earthquakes (70-300 km depth) are generated in a deeper portion of subduction slabs where the extremely high pressures and temperatures make frictional slip unlikely. Seismicity in the deep Earth can provide essential information on the physical processes that control fluid distribution within the mantle, yet the mechanism of intermediate-depth earthquakes is still enigmatic. Under extreme conditions with high pressure and temperature in the subduction zones, three plausible models might explain the rupture process of intermediate-depth earthquakes; (1) dehydration of minerals in the subducting slab along pre-existing faults where dehydrated fluids can easily concentrate (2) dehydration-driven stress transfer where fluid overpressures are unlikely, (3) thermal shear instabilities that account for high-stress drops and repeating earthquakes. Both models essentially depend on the local fluid distribution likely sourced from the subducting slab that controls the kinematic properties and rupture process of the fault and seismicity. The Bucaramanga earthquake nest in Colombia, where intermediate-depth earthquakes are significantly concentrated in both time and space (with a magnitude up to 6). A high-resolution catalog of Bucaramanga seismicity will likely yield key information on the rupture process of intermediate-depth earthquakes.

Here we systematically explore the seismicity within the Bucaramanga earthquake nest with matched-filtering to construct a high-resolution earthquake catalog. We use continuous-waveform data from 2015 to 2020 recorded on more than 20 seismic stations operated by the Servicio Geológico Colombiano (SGC). In our method, we choose a template waveform in the original event catalog determined by SGC, then detect earthquakes through each template by matched-filter detection. Using all catalog events as templates, we will significantly update the total number of events including smaller earthquakes. Our dense, detailed catalog will provide precise intermediate-depth source information such as magnitude, clustering of events into families, and correlation coefficients, that will allow us to estimate earthquake relocations, earthquake source properties via spectral analysis, and seismic tomography to understand the mechanism of the intermediate-depth earthquakes and conditions of the source region.

On The Seismic Hazard in the Western Himalayas Using PSHA Methodology

D. Shanker¹ and D. Kushwah²

¹Dept. of Earthquake Engineering IIT, Roorkee, India, d.shanker@eq.iitr.ac.in,

²Dept. of Earthquake Engineering IIT, Roorkee, India

Western Himalaya (Latitude 32.30-36.30 N and Longitude 73.50-80.50 E), which include part of the North-West India and parts of eastern Pakistan and Afghanistan is highly earthquake-prone due to the presence of many active faults. This region faced two highest magnitude earthquakes one in Kangra Valley on the 4th of April, 1905, of Mw 7.8 and other in Muzaffarabad, Pakistan of Mw 7.6. Study uses the Gumbel Extreme Value method to estimate the Gumbel parameters as well as the expected frequency of events, return period and probability of occurrence for different time periods. A homogenous, complete and region-specific Earthquake catalogue from 1900 to 2021 with $M_w \geq 4.0$ has been prepared. For the seismic hazards we have used probabilistic seismic hazard analysis (PSHA) methodology by Crisis 2015 software. The study area has been divided into the Karakorum, Kishtwar, and mantle fault zones based on the seismo-tectonic and geomorphic setup. The G-R constants, $a = 4.72$ & $b = 0.923$ values are estimated, which is comparable to computed Gumbel's estimates 3.195 and 0.7, respectively. The peak ground accelerations (PGA) are estimated for periods of 225yrs, 475yrs, and 2475yrs at 20%, 10%, and 2% probabilities of exceedance for 22 cities of the considered region. As per this study, the lower PGA values in eastern part indicating lesser levels of seismic hazard whereas, the state of Jammu & Kashmir and the Union territory of Ladakh is found to be a highly seismically active region.

Temporal evolution of fluid flow along fractures in high-grade metamorphic rocks related to seismic events in the middle crust.

Diana Mindaleva¹, Masaaki Uno¹, and Noriyoshi Tsuchiya¹

¹Grad. School of Environmental Studies, Tohoku Univ.

Fluid flow in the crust modifies rock transporting properties and controls the triggering of earthquakes. However, there are limited numerical constraints on the fluid volumes with the available duration of fluid infiltration. There is also a gap in our knowledge of time-integrated fluid fluxes estimated from geological samples and their influence on controlling seismic/aseismic activity. Merging the timescales of fluid infiltration with the transport properties estimated from the geological samples such as metamorphic reaction zones is essential to understanding the fluid flux during crustal fracturing and its influence on controlling some characteristics of seismic/aseismic events.

This study focuses on fluid flow through a single fracture and the fluid-rock reaction zones and applies its results to low-magnitude fracturing events, such as tremors and low-frequency earthquakes. Understanding fluid flow provides an opportunity to calculate the seismic moment and cumulative magnitude of the possibly triggered seismic/aseismic event.

Particularly, to approximate the duration of fluid infiltration and time-integrated fluid fluxes we analyse amphibolite-facies fluid-rock reaction zones and then combines with estimates of possible associated seismicity and concludes that flow along a single fracture is compatible with seismicity of non-volcanic tremor and low frequency earthquakes. This study is based on evidence of rapid fluid infiltration (~ 10 h) caused by crustal fracturing and permeability evolution from low- to highly-permeable rocks ($\sim 10^{-9}$ – 10^{-8} m²).

Perpendicular time-integrated fluid fluxes to a given fracture and fluid flux through the overall reaction zone were estimated. Coupled methodology, including reactive-transport modeling and thermodynamic analyses, based on Si alteration processes within reaction zones is used to estimate fluid volumes involved in triggering seismic activity. Time-integrated fluid flux through the fracture results in 10^{3-6} m³/m². The lower range is similar to the fluxes through the upper crustal fracture zones ($\sim 10^{3-4}$ m³/m²), while the almost whole range is comparable to the contact metamorphism zone ($\sim 10^{2-5}$ m³/m²).

In this study, we follow McGarr, 1976 and use fluid volumes and shear modulus to estimate cumulative seismic moment. We also constrain magnitude using single fracture geometry and compare two independent methods.

Fluid volumes transported through the fracture were compared with fluid injection experiments results. We also compare durations of fluid infiltration to the durations of the slow slip events. There is no universal theory of slow slip phenomena in perspectives of geological and geophysical properties. Theoretically, high-grade metamorphic rocks can be related to the slow slip events. Our finding reveals that the transportation of voluminous fluid volumes through a fracture may be related to short seismic/aseismic events such as tremors and LFEs, as suggested from duration (~ 10 h) and cumulative magnitude, representing the maximum values as 2.0–3.8, the lower limit of the magnitude for a single fluid-driven seismic event as -0.6 to 0.2 . Single fractures described in this study remain possible to transfer voluminous fluid flow. They could be an essential control on the generation of seismic activity above the tremor and slow slip events source regions in the lower–middle crust.

Slip behavior, strain, and deformation mechanisms in a fossil earthquake fault in an exhumed accretionary complex

Yoshitaka Hashimoto¹, Mako Kawaji¹, Jinpei Mitani¹, and Taizo Uchida¹

¹Dept. Global Environment and Disaster Prevention, Kochi University

Geological constraints on slip rates for fossil faults lead to understandings of rock mechanics for variable fault-slip rate from geophysical observations. Because spatial resolution is much higher in geology than in geophysics, the geological constraints on fault-slip rates would reveal the spatial relationships between faults with variable slip rate, which could provide clues to discuss interactions between slow and fast slips.

In this study, we conducted 1) a constraint on slip rate from temperature distribution across the fault, 2) strain analysis by anisotropic magnetic susceptibility (AMS) and 3) detection of a thermal event using magnetic experiments. Finally, we discuss about slip behavior with combinations between slip rate, strain and deformation mechanisms.

We focused on a fossil seismogenic fault in an exhumed accretionary complex, the Yokonami mélangé, the Cretaceous Shimanto Belt, SW Japan. The fault contains 1 mm thick of fault with pseudotachylyte (PS) within 20 cm thick of cataclastic zone. Dynamic recrystallized grains are observed in the quartz blocks. Temperature close to the PS is estimated from the grain size of the grains indicating about 324°C. Vitirinite reflectance adjacent to the outside of cataclasite indicates decreasing trend with distance from the PS. Using the temperature distribution assumed by frictional heating, we constrained thermal generation rate (Q) and slip duration (Tr) which are comparable with those for slow earthquakes in a scaling law from geophysical observations.

AMS analysis indicates oblate strain in host rocks overprinted by prolate strain in the fault zone. Medium overprinting of prolate strain shows ductile deformation, but random oriented strain axes are observed in larger amount of overprinting of prolate strain, suggesting ductile deformation was recorded in the early stage of shear deformation, but brittle deformation could be expected in the end.

Thermal event at 300-350°C in cataclasite was also detected from magnetic analysis. The result is consistent with the temperature as described above. Magnetic analysis also provided rotations of the magnetic direction, which indicate anticlockwise rotation from NW to SW. Because this is a preliminary result, we need to examine amount of strain also from the rotation of magnetic direction in the future.

Numerical experiments using a friction law both for rapid and slow sliding

Takane Hori¹, and Hideo Aochi²

¹JAMSTEC, ²BRGM

To realize various fault slip behavior as regular and slow earthquakes, I assume a simple friction law. In the friction law, the frictional strength decreases due to fault slip and recovers with time. These two processes along the fault, slip-weakening and healing are the intrinsic ones to model regular and slow earthquake sequences. Here, an evolution equation of the frictional strength proposed by Nielsen et al. (2000) is used. In this equation, there are two frictional parameters, d_c and t_c , which represent a characteristic displacement for slip-weakening and a characteristic time for healing, respectively. The balance of these two parameters controls how frictional strength evolves depending on the fault slip history. To examine fault slip behavior with the evolution equation, a single degree of freedom elastic system, composed of a block and a spring with constant loading is introduced. The block starts to slip following the strength evolution equation when the shear stress acting on the contact surface of the block reaches the strength. On the other hand, the block is in stationary contact if the shear stress is less than the strength. Note that this is a classical constitutive law without direct effect in a rate- and state-dependent friction law (Nakatani, 2001). To examine the slip behavior depending on the above system, I modified a simulation code used in Aochi and Matsu'ura (2002), which introduces more complex evolution equation of fault strength. Some preliminary results show that both rapid and slow fault slip sequences can be demonstrated depending on the two frictional parameters. These slip behaviors are similar with regular and slow earthquakes. One interesting behavior in slow fault slip sequences here is that both the stress drop and the recurrence time interval are much smaller than those of the rapid fault slip sequences but the peak strength is identical. Furthermore, the slow slip behavior is similar with that found at Izu-Bonin Trench (Fukao et al., 2021).

Estimation of 3D S-wave velocity model in the western Niigata area using surface wave analysis of microtremors

Minoru Ideno¹, Takeshi Tsuji¹, Hiro Nimiya², Tastunori Ikeda³

¹Univ. Tokyo, ²AIST, ³Kyushu Univ.

Knowledge of the geological structure and its composition makes it possible to predict the seismic intensity of earthquakes, estimate geological formations that can store carbon dioxide in CCS, and explore for oil, natural gas, and other resources. Recently, many seismometers have been installed throughout Japanese Island, and microtremors acquired at these stations have been available. A method based on the seismic interferometry for extracting seismic waves propagating between seismometers has been widely used to estimate the subsurface.

In this study, our target was western part of Niigata where seismogenic faults are distributed. In this field, large amount of data (946 seismometers) can be used. The SPAC and zero-crossing methods were used to obtain dispersion curves at many positions within the study area. In the SPAC method, we can estimate a dispersion curve by fitting a Bessel function based on the cross-correlation function (Fig. 1). On the other hand, the zero-crossing method is a way for estimating a dispersion curve based only on zero-crossing points of the function, and not affected by the form of the cross-correlation function. Finally, three-dimensional S-wave velocity structure in this field was obtained by tomography based on the estimated dispersion curve.

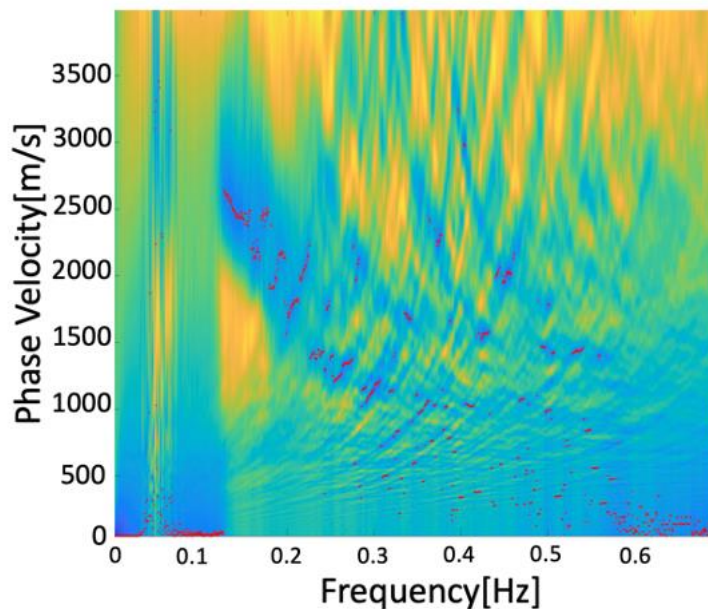


Fig. 1 Dispersion curve obtained from SPAC method.

Insights into the occurrence and relationship between seismicity and a relief of plate interface near the trench at the western part of Guerrero seismic gap from a recent seafloor experiment

Yoshihiro Ito¹, Shukei Ohyanagi², Raymundo Omar Plata Martinez³, Emmanuel Soliman Garcia¹

¹DPRI, Kyoto Univ., ²JAMSTEC

Capturing the spatial and temporal distribution of slow and fast earthquakes offshore at subduction zones becomes fundamental tasks in seismology. Almost all large fast earthquakes and slow earthquake around them are below the sea which still causes difficulty in monitoring them. Ocean bottom seismometers (OBSs), especially the autonomous type, are useful to measure activities of both fast and slow earthquakes at the ocean bottom away from coastline, simply and with portability. We deployed 9~10 OBSs at the western part of the Guerrero seismic gap, off Mexico in two observation periods lasting one year each from 2017 to 2018 and again from 2018 to 2019, to capture both fast and slow earthquakes. Detection of fast earthquakes and their P&S arrivals picking are performed with the Earthquake Transformer (Mousavi et al., 2020), which is AI-based earthquake signal detector using a deep neural networks. The Earthquake Transformer is applied to continuous trace of OBS records to create a bank of P&S arrivals at each station. After applying phase association for all of the picked phases using the REAL algorithm (Zhang et al., 2019), we invert their hypocenters with the Hypomh (Hirata and Matsu'ura, 1987) assuming horizontal layered seismic structure. Slow earthquakes, especially tectonic tremors, are detected with a modified envelope correlation method (Mizuno and Ide, 2019); the detection was done using a 300 s time window with 150 s time shifts (Plata-Martinez et al., 2021). We have proposed a silent zone, absent of fast and slow seismicity, located at the western part of the Guerrero seismic gap, where we also identified a negative anomaly on residual gravity and bathymetry, which we interpret as related to variations in the geometry of the subducting plate surface (Plata-Martinez et al., 2021). One of the major aims of reanalysing with the AI-based detector on OBS data is to test the hypothesis that the geometry of the plate interface exerts a control on the occurrence of slow-to-fast earthquakes.

Nearly 2500 events in the 2017-2018 period were detected with Earthquake Transformer although approximately 500 earthquakes had been detected in the manual picking of the first arrivals. Many events are distributed near the coastline, while they are rarely distributed within the Guerrero seismic gap. The low seismicity zone is well consistent with the negative anomaly in both residual gravity and bathymetry; it may correspond to a velocity-strengthening domain and low possibility of a large earthquake nucleating (Plata-Martinez et al., 2021). The landward edge of the silent zone is also still clearly identified; the hypocenters of repeating earthquakes, as well as those of microseismicity, are located in the silent zone. We compare both catalogs in terms of the differences in hypocenter locations. Almost all relocation vector lengths at both locations show less than a 5 km difference horizontally, suggesting that the silent zone is possibly a zone of low seismicity, including microseismicity detected by the machine learning technique.

Monitoring of seismic velocity change surrounding area of Mt. Fuji using ambient noise

Yusuke Kakiuchi¹, Takeshi Tsuji¹, Hiro Nimiya², Tatsunori Ikeda³

¹Univ. Tokyo, ²AIST, ³Kyushu Univ.

Various factors such as earthquakes and volcanic eruptions cause seismic velocity change. Previous research demonstrated that seismic velocity depends on pore pressure (Christensen and Wang, 1985) and stress (Toksöz et al., 1976). Thus, monitoring seismic velocity change is crucial to estimate the crustal stress state and to predict volcanic eruptions (Brenguier et al., 2008) and earthquakes (Whitcomb, 1973). Here we used the ambient seismic noise recorded over 8 months to show the seismic velocity change around Mt. Fuji before and after 2011 Tohoku earthquake (Mw 9.0). We applied cross-correlation analysis to extract Rayleigh waves from ambient seismic noise in the frequency range of 0.1-0.9 Hz. Then, we estimated seismic velocity change by using stretching interpolation technique (Sens-Schönfelder & Wegler 2006) to 21 stations (Fig.1). The velocity near Mt. Fuji decreased during the 2011 earthquake (Fig.2), likely caused by pressurization of volcanic fluids. Such fluid pressurization could influence upon volcanic activity. Furthermore, variation of velocity change is decreasing in accordance with the increase of distance from Mt. Fuji. In this study, we focused on the volcano monitoring. However, we will apply similar approach to the seismogenic faults in order to identify the dynamic behavior of the faults associated with slow and fast earthquakes.

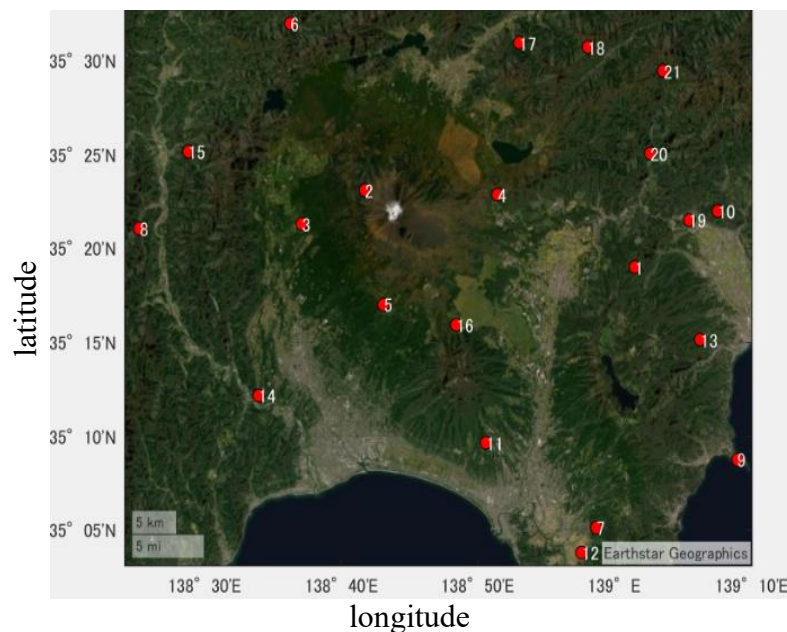


Fig.1 Distribution of seismic stations used in this study (red dots).

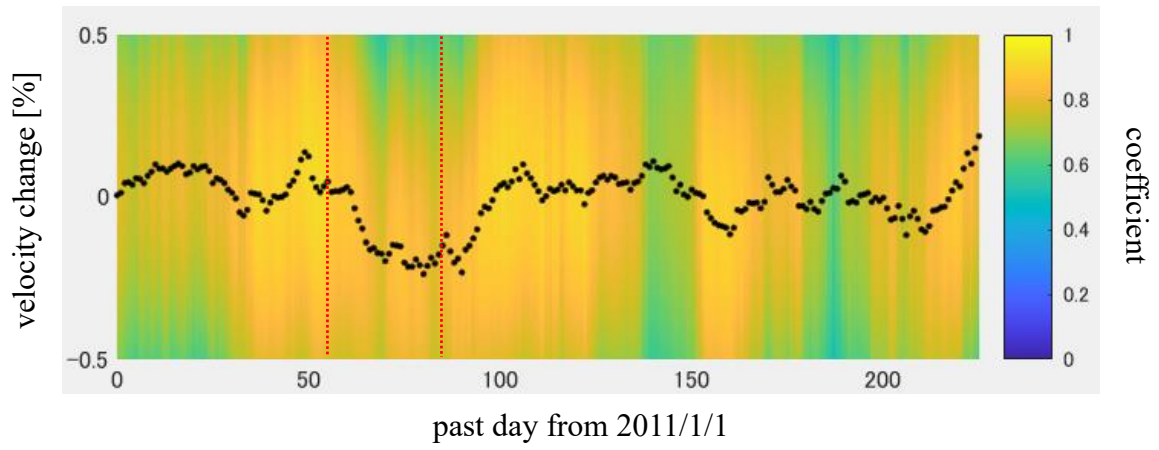


Fig.2 Seismic velocity change between station 4 and 16

Chemical composition of subduction-zone fluids

Tatsuhiko Kawamoto¹

¹Dept of Geosciences, Faculty of Science, Shizuoka University, Shizuoka 422-8529, Japan

Deep tectonic tremors occur along plate boundary in the Nankai subduction zone. The foci of the tremors make a belt-like zone along the subducting Philippine sea slab. The tremors occur along the isothermal line of 450°C that crosses the isodepth lines at 30-60 km (Yoshioka and Murakami 2007). The tremors can be caused under high pore-fluid pressure conditions by aqueous fluids released under at around 450°C, which corresponds to dehydration reactions of blueschist facies in oceanic crust to form eclogite facies. Such fluids can be reserved in the deep-seated rocks as form of fluid inclusions (Figure 1, Kawamoto et al., 2013).

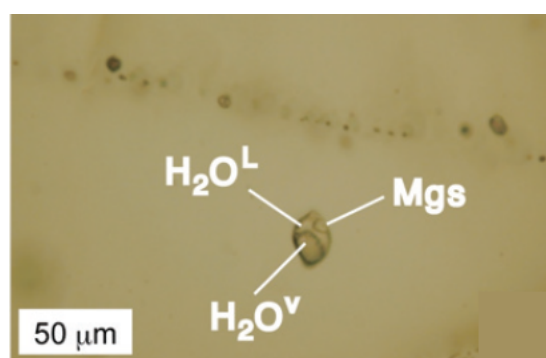


Figure 1 Fluid inclusion composed of saline solution ($\text{H}_2\text{O}^{\text{L}}$), vapor ($\text{H}_2\text{O}^{\text{V}}$), and magnesite (MgCO_3 , Mgs) in an olivine from a mantle xenolith collected from the Mount Pinatubo (Philippines) (Kawamoto et al., 2013).

Raman microscopy tells species of the fluids and microthermometry using cooling-heating stage allows to estimate salinity based on depression of melting temperature of ice as a function of wt.% NaCl equivalent. Up to the present fluid inclusions observed in mantle xenoliths and high-pressure metamorphic rocks have indicated the presence of saline fluids with or without carbon in the mantle wedge and plate boundaries, respectively (Figure 2, Joachim-Mrosko et al., 2022). Their averaged salinity is similar to and a little higher than that of seawater (3.5 wt.% NaCl), suggesting seawater cycling from oceanic hydration to dehydration during plate subduction. The salinity of aqueous fluids can be increased due to incompatibility of Cl to anhydrous minerals during “seawater cycling”. Saline fluids with or without carbon are supplied to the plate boundaries and hydrate minerals at the base of the mantle wedge. Pore-fluids can exist in fully-hydrated mantle rocks, serpentinite stable in <650°C, 1–2 GPa, and transported to the surface as Arima-type hot springs or preserved in fluid inclusions beneath the fore-arc region (Figure 2).

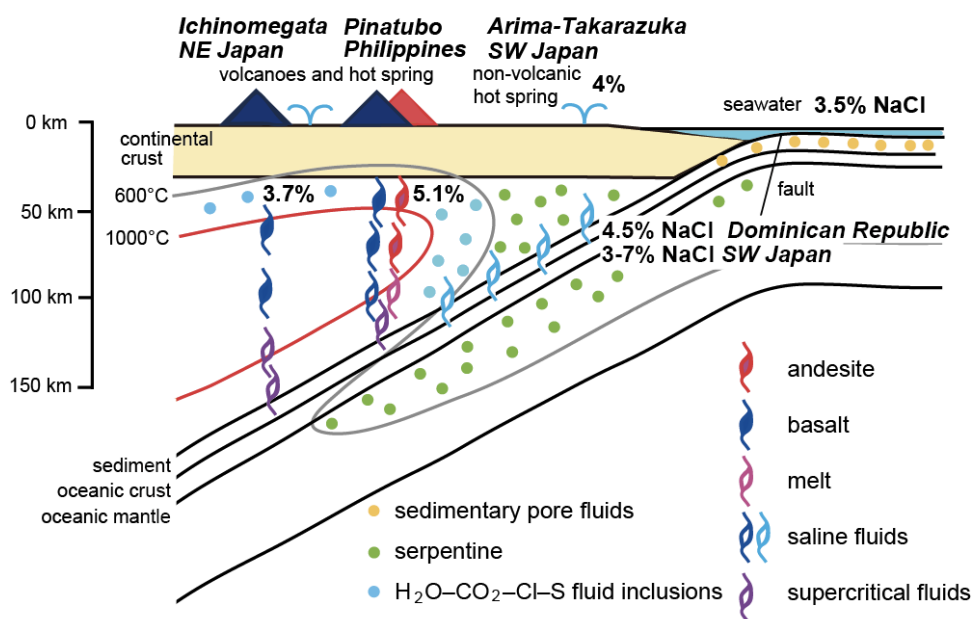


Figure 2 Salinity map of subduction-zone fluids (Joachim-Mrosko et al., 2022). Saline fluid inclusions in the mantle wedge peridotite are observed with carbonate or CO₂ (Kawamoto et al. 2013; Kumagai et al., 2014). Aqueous fluids with 4.5 % NaCl and 3–7 % NaCl without carbon are observed in plate-boundary rocks (Kawamoto et al., 2018; Shinji et al., 2019), respectively. Arima–Takarazuka (Japan) is a hot spring in the forearc region and is characterized by high ³He/⁴He ratios suggesting its deep mantle origin (Kusuda et al., 2014).

Joachim-Mrosko, B, Kawamoto, T, Bureau, H (2022) Experimental and observational constraints on halogen behavior at depth, *Elements*, 19.

Kawamoto T, Yoshikawa M, Kumagai Y, Hannah M, Mirabueno T, Okuno M, Kobayashi T (2013) Mantle wedge infiltrated with saline fluids from dehydration and decarbonation of subducting slab. *Proceedings of the National Academy of Sciences of the United States of America* 110: 9663-9668.

Kawamoto T, Hertwig A, Schertl H-P, Maresch WV (2018) Fluid inclusions in jadeitite and jadeite-rich rock from serpentinite mélanges in northern Hispaniola: Trapped ambient fluids in a cold subduction channel. *Lithos* 308-309: 227-241.

Kumagai Y, Kawamoto T, Yamamoto J (2014) Evolution of carbon dioxide-bearing saline fluids in the mantle wedge beneath the Northeast Japan arc. *Contributions to Mineralogy and Petrology* 168: 1-13.

Kusuda C, Iwamori H, Nakamura H, Kazahaya K, Morikawa N (2014) Arima hot spring waters as a deep-seated brine from subducting slab. *Earth Planets Space* 66:119.

Shinji Y, Tsujimori T, Kawamoto T (2019) Two groups of fluid inclusions in the Yunotani eclogite from the Hida-Gaien Belt: Implications for changes of fluid salinity during exhumation. *Journal of Mineralogical and Petrological Sciences*, 114: 302–307.

Yoshioka, S, Murakami, K (2007) Temperature distribution of the upper surface of the subducted Philippine Sea Plate along the Nankai Trough, southwest Japan, from a three-dimensional subduction model: relation to large interplate and low-frequency earthquakes, *Geophysical Journal International*, 171: 302–315.

Incorporation of Experimental Data of Fault Material derived from Nankai Trough into Simulation of Dynamic Rupture Propagation

Kenichi Tsuda¹, Saruul Dorjaparam², and Tetsuro Hirono³

¹Institute of Technology, Shimizu Corporation, ²Ohsaki Research Institute,

³ Department of Geosciences, Osaka Metropolitan University

In order to model the coseismic rupture propagation, some reasonable initial conditions including stress conditions, such as frictional property, fault geometry etc. are necessary. However, such information is usually poorly constrained because of its scarcity of the data. To solve such problems, especially to investigate the frictional conditions, the experiment studies using fault materials directly grubbed from plate boundary have been conducted (e.g., Ujiie *et al.*, 2013, Hirono *et al.*, 2016). Based on such experiments focusing on the Nankai Trough, which is thought to be the source of the historical large tsunamis in the Tonankai region, Tsuda and Hirono (2022) have investigated the influences of levels of friction and pore-fluid pressure on the rupture propagation along the fault. They have quantitatively evaluated the potential for slip along the fault by integrating a dynamic rupture simulation in 2D model based on the friction data obtained from actual fault rocks by using different results of experimental data from various conditions. The sensitivity of the frictional properties might be attributed to the diversity and complexity of the style and the amount of fault slip during an earthquake.

In this study, we have extended such results from 2D simulation into 3D problem to investigate the rupture propagation along a fault based on a realistic fault rock dataset incorporating dynamic rupture simulation. We have assumed the simple planar fault shape with 10° dipping based on Spectral Element Method (Galvez *et al.*, 2014). We have set the asperity with rectangle shape referring to the size of asperity area of 1944 Tonankai earthquake (e.g., Ichinose *et al.*, 2003) with stress drop 3MPa. The results from experimental results have been incorporated into the initial conditions up on the area above the asperity. We have set the dynamic frictional coefficient 0.01 including the effects of thermal pressurization based on experimental results (Tsuda and Hirono, 2022). We also assumed the 0.8 of pore-pressure ratio (Tsuji *et al.*, 2014). The critical distance (D_c) for that area is also set based on such results. The maximum slip was around 20m and resultant seismic moment was 8.02×10^{21} [Nm] (M_w 8.5). We have estimated radiated energy scaled to the seismic moment showing 1.21×10^{-5} , which is compatible to the values for the inter-plate earthquake (e.g., Ye *et al.*, 2015). We further do the parameter studies with changing simulation conditions, such as the dipping angle to investigate the effects of vertical displacements on the surface, the material property to investigate the effects of soft sediment layers corresponding to the accretionary wedge on rupture propagation and generation of ground motions, and the asperity geometry (e.g., Park *et al.*, 2015). Such integrated approach incorporating the frictional behaviour based on fault rock analysis from plate boundary might bring better assessments of tsunamigenic potential of megathrust earthquake and can contribute to a better understanding of megaquake physics.

Crustal structures and spatial correlation with seismic activities in the western Nankai Trough

Kazuya Shiraishi¹, Yasuyuki Nakamura¹, Ryuta Arai¹, Gou Fujie¹, Shuichi Kodaira¹,
Yohei Hamada¹, Seiichi Miura¹, Ryo Miura¹, Fujio Yamamoto¹, Yanxue Ma²,
Masataka Kinoshita², Yoshitaka Hashimoto³, Rie Kamei², and Kimihiro Mochizuki²

¹JAMSTEC, ²ERI, Univ. Tokyo, ³Kochi Univ.

To better understand the relationship between crustal structures and seismic activities in the Nankai subduction zone, we have conducted intensive seismic surveys for elucidating detailed geological structures in the Nankai Trough. We newly collected 2D multichannel seismic (MCS) survey data from off Kochi to the Hyuga-nada during the cruises KM20-05 and KM21-07 with R/V Kaimei in 2020 and 2021. The 2D MCS survey lines were arranged in the area of a boundary of the megathrust rupture of 1940s earthquakes (e.g., Sagiya and Thatcher et al., 1999) and the active area of slow earthquakes near the subducting Kyushu-Palau Ridge in the Hyuga-nada. The occurrence of tectonic tremors and very low-frequency earthquakes (VLFs) in the Hyuga-nada were revealed by recent ocean-floor seismic observations (e.g., Yamashita et al., 2015, 2021; Tonegawa et al., 2020).

We interpreted several characteristic features on seismic reflection profiles from the newly acquired MCS data and the legacy MCS data before 2018 in the same region. We generated the smoothed surfaces from the interpretation of two key reflection boundaries. The oceanic crust surface is deepening gradually to the north in the area off Shikoku and steeply to the northwest directions in the western part of the Hyuga-nada and off Ashizuri. We identified continuous clear reflectors at the deep in the accretionary prism off Ashizuri, which are continued from the basal décollement at the frontal imbricated thrust zone. The geological unit sandwiched by the deep reflector and the top of the oceanic crust is likely an underthrust sequence with lateral thickness variation beneath the accreted sediments. The interpreted most thickened part of 0.7-1.0 s in two-way time with approximately 30 km × 30 km area is located between the 1940s rupture area and the active slow earthquake region. Furthermore, cone-shaped structures are identified within the accretionary prism and the sediment layers in the Shikoku basin on the Philippine Sea plate. A prominent cone-shaped structure with the height of approximately 2 s in two-way time (a few kilometers) is located on the underthrust sequence at the middle of a cluster of VLFs located by Tonegawa et al. (2020). The regional interpretation results from dense seismic reflection profiles implies good spatial correlation between the structural features and the seismic activities in the western Nankai Trough.

Relation between geological structure caused by seamount collisions and slow-earthquake insight from numerical geodynamic modeling.

Ayumu Miyakawa¹

¹Geological Survey of Japan, AIST

Seamount subductions cause characteristic geological structures such as collapse of slopes, and uplift of accretionary wedges and enhanced sediment subduction. The enhanced sediment subduction, which can locally elevate pore pressures, or result in km-scale spatial variations in composition along plate boundary faults that can produce a mix of different types of slip behavior (e.g., Saffer and Wallace 2015). Therefore, the geological structure caused by the seamount subduction can be a clue to understand the slow earthquakes in subduction zones.

We proposed a conceptual geological model for the collision of multiple seamounts with a forearc accretionary wedge (Miyakawa et al., 2022). We conducted numerical simulations using the discrete element method to examine the effects of three seamount collisions with forearcs. Multiple seamount collisions create a cycle of formation of seamount collisional structures. At a low horizontal compressive stress, a “shadow zone” is formed behind (i.e., seaward of) the seamount. When the next seamount collides, the horizontal compressive stress increases and tectonic compaction progresses, which reduce the porosity in the underthrust sediments. The strong horizontal compressive stresses associated with the current seamount collision has increased the pore pressure within the underthrust sediments associated with previous seamounts. The location of the high-pore pressure zones corresponds to the location of the very-low-frequency earthquakes in shallow portion of the Nankai Trough off Kumano, Japan. This conceptual geological model can explain the occurrence of the high-pore pressure causing very-low-frequency earthquakes in shallow portion of the Nankai Trough off Kumano, Japan.

Turning to deep slow earthquakes, tremors are distributed over a wide area, whereas slow slips are patchy and localized. These patchy and localized slow slips event This patchy and localized occurrence of slow slip suggest of local causes such as seamounts. However, geological structures in such a deep situation are still unknown. In this case, numerical modeling can be a powerful tool to investigate the geological structure and geodynamics in deeper portion of subduction zones. We will provide a preliminary result of the numerical geodynamic modeling targeting into deep subducting seamount.

Saffer, Demian M., and Laura M. Wallace. "The frictional, hydrologic, metamorphic and thermal habitat of shallow slow earthquakes." *Nature Geoscience* 8.8 (2015): 594-600.

Miyakawa, Ayumu, Atsushi Noda, and Hiroaki Koge. "Evolution of the geological structure and mechanical properties due to the collision of multiple basement topographic highs in a forearc accretionary wedge: insights from numerical simulations." *Progress in Earth and Planetary Science* 9.1 (2022): 1-13.

Temporal changes in pore fluid overpressure during slow earthquake cycle estimated from foliation-parallel extension veins

Makoto Otsubo¹, Kohtaro Ujiie², Ayumu Miyakawa¹

¹Geological survey of Japan/AIST, ²University of Tsukuba

Pore fluid pressure (P_f) is of great importance to understand slow earthquake mechanics. In this study, we estimated the pore fluid pressure during the formation of foliation-parallel quartz veins filling mode I cracks. The foliation-parallel extension cracks can function as the fluid pathway in the *mélange*. In outcrops, multiple mineral veins can be observed in parallel. In the poro-elastic model, the distance (D) between parallel mineral vein groups is known to depend on the size of the pore fluid overpressure ($\Delta P_f = P_f - \sigma_3 - T_s$; T_s : tensile strength) in the fracture, Young's modulus (E), and the aperture width (W) of the mineral veins (Price and Cosgrove, 1990). The formation of mineral veins requires elastic shortening of the host rock side by the thickness of the mineral vein precipitated in the fracture (Price and Cosgrove, 1990). Therefore, in the 2D poro-elastic model, the relationship between the spacing (D) between parallel mineral veins, the pore fluid overpressure ΔP_f in the fracture, the Young's modulus E of the host rock, and the aperture width (W) of the mineral veins is

$$\Delta P_f = E \left(\frac{W}{D} \right).$$

In this study, we estimated the pore fluid overpressure during the formation of foliation-parallel quartz veins filling mode I cracks in the Makimine *mélange* of Late Cretaceous Shimanto accretionary complex of SW Japan (temperature = 300–350°C, Palazzin et al., 2016). The *mélange* preserves quartz-filled shear veins, foliation-parallel extension veins and subvertical extension tension vein arrays. The coexistence of the crack-seal veins and viscously sheared veins (aperture width of a quartz vein: a few tens of microns) may represent episodic tremor and slow slip (Ujiie et al., 2018). W and D of foliation-parallel quartz veins measured in the Makimine *mélange* are $\sim 14\text{--}78 \mu\text{m}$ and $\sim 1\text{--}5 \text{m}$, respectively (W : Ujiie et al., 2018). Estimated ΔP_f in the case of the Makimine *mélange* are $\sim 8\text{--}200 \text{kPa}$ (assuming depth = 10 km, tensile strength = 1 MPa and Young's modulus = 3 GPa; Gholami and Rasouli, 2014). The ΔP_f are concordant with stress drop of a slow earthquake (about 0.01 to 1.0 MPa; e.g., Gao et al., 2012).

Our results mean that as the pore fluid overpressure changes, the mineral vein spacing changes, i.e., the spacing of fractures through which fluid paths (the width of the fracture zone) changes. If mineral veins are related to slow earthquakes, the mineral vein spacing may provide information on the temporal variation of the excess pore fluid pressure within a slow earthquake cycle, in which case the pore fluid overpressure (pore fluid pressure greater than σ_3) may provide a clue to the size of the slow earthquake (shear zone width, etc.).

Reference: Gao (2012) Bulletin of the Seismological Society of America, 102, 352–360; Gholami and Rasouli (2014) Rock Mechanics and Rock Engineering, 47, 1763–1773; Gudmundsson (1999) Geophys. Res. Lett., 26, 115–118; Palazzin et al. (2016) Tectonophysics, 687, 28–43; Price and Cosgrove (1990) Analysis of Geological Structures. Cambridge University Press, Cambridge, 502 p; Ujiie et al. (2018) Geophys. Res. Lett., 45, 5371–5379.

Along-Strike Forearc and Subducted Upper Slab Structure beneath subduction regions of Alaska and Chile : Implications towards the occurrence of Slow Slip

Pousali Mukherjee¹, Yoshihiro Ito¹, Kajaljyoti Borah², Admore Phindani Mpuang¹, Emmanuel Soliman Garcia¹, Raymundo Plata-Martinez³

¹Kyoto University, ²Indian Institute of Science Education and Research Kolkata, ³Japan Agency for Marine Earth Science and Technology

Slow slip ranging from intermediate depth (30-40 km) to very deep (>70 km), has been documented in the Chilean and Alaskan regions in the last twenty years. The Iquique, Atacama, and Valparaiso areas of northern Chile have experienced slow slip (Ruiz et al., 2014; Socquet et al., 2017; Klein et al., 2018; Ruiz et al., 2017). In Alaska, the slow slip is primarily concentrated in the Lower and Upper Cook Inlet regions of the state (Ohta et al., 2006; Fu et al. 2015; Li et al. 2016; Wei et al. 2012). Along-strike and along-dip structural control, spatial variation, and segmentation in areas, particularly of seismically slow ruptures, are still debated and unanswered research questions. We have investigated the lithospheric structure in the forearc of the Chile and Alaska subduction regions respectively, that include the clusters slow slip event region using receiver function and inversion. It is important to investigate the nature of the region close to plate interface, especially the oceanic crust, the oceanic upper mantle and the forearc mantle in slow slip regions, especially in deeper part. This would enable us to understand if there is any structural control on slow slip regions, along with investigating structural properties.

We estimated the forearc and the subducted upper slab structure beneath North Chile from 19°S - 33°S using teleseismic receiver function and inversion method. The structural control of slow slip in North Chile was investigated. Backazimuth variation estimates showed the difference in the structure in the North West and South East segment beneath the study region, specially depth and velocities of major interfaces. Crustal thickness was found to range from ~19 km to ~60 km, increasing inland; slab top range from ~30 to ~90 km; oceanic crustal thickness ~5 to ~10 km; depth of oceanic Moho 40 km to ~90 km; oceanic crust velocities < 4 km/s; mantle velocities 4.2 to 4.9 km/s. Some of the fluctuating crustal velocities could be attributed to presence of partial melts, sediments beneath the region. As slow slip occurs close to the plate interface, representative velocities at the plate interface region such as the shear wave velocities at the bottom of wedge mantle, the top of the oceanic crust and the top of oceanic mantle were investigated closely, all along trench-strike. Consistent high velocities at the top of oceanic crust and lower wedge mantle velocities were recorded toward south of Iquique zone, where there is no evidence of slow slip. The wedge mantle velocities were

relatively low near the Iquique slow slip zone. The velocity profiles beneath many stations have been obtained first time. We suggest the possibility that the incoming ridges and seamount subduction could play a vital role in the architectural properties of the lithosphere around the plate interface region, and could be a potential candidate for controlling the S-wave velocities around the plate interface region, especially around bottom of wedge mantle, oceanic crust and top of subducted oceanic mantle. This in turn could control the occurrence of slip and rupture in the region, including slow slip in Iquique. The structural control of Chilean slow slip, in especially Iquique could be a combined effect from lower wedge mantle, oceanic crust and top of subducting mantle, along with subducting ridge and seamount influence.

In a similar manner, we characterized the property of the upper lithosphere in the Alaska subduction region in and around the slow slip region and further away from the slip region along the subduction forearc, by estimating velocity models beneath the stations near and away from slow slip. The depth variation of velocities incorporating backazimuth effect, estimating and comparing the distinct velocities around the plate interface region (in lower wedge mantle, upper oceanic crust and top of oceanic mantle), the depths of the deeper oceanic Moho were estimated first time in the literature. The depth of the oceanic Moho varies from ~29 km to ~82 km in this region, deepening more inland, showing backazimuth variation. This could be related to the dip of the subducting plate. We estimated the velocities around the plate interface, near and further away from the slow slip areas. The velocities in the lower wedge mantle vary from ~4.2 - 4.8 km/s, in the top of subducted oceanic crust from ~3 – 3.9 km/s and in the upper part of subducted oceanic mantle from ~4 – 4.7 km/s. In the plate interface region, the velocities of top of oceanic mantle dominated the lower range. This could be related to subduction of the two oceanic crusts, the Pacific plate and the Yakutat terrane. The velocities at the top of the oceanic crust were heterogeneous, but high velocities were present along with low velocities in and around the Cook Inlet region. This is also the region of the slow slip in south Alaska.

Fast 3D fully-dynamic earthquake cycle simulations on non-planar fault.

Pierre Romanet¹, Tatsuhiko Saito¹ and Eiichi Fukuyama^{1,2}

¹NIED, ²Kyoto University

Understanding the influence of fault geometry on earthquake behavior is one of the fundamental questions in seismology. It is widely recognized that faults are rough, at every scale and that the geometry of fault (including roughness, seamount, bends...) has an influence on earthquake initiation and arrest. Recent studies tend to prove that it also has a significant influence on the segmentation of slow-earthquakes.

However, because of time consumption of running such simulations of earthquakes, many assumptions have been made to study the influence of geometry of faults on earthquake dynamics. Among them, the most frequently employed simplifications are probably (1) the quasi-dynamic approximation, which simplifies the wave field by introducing the radiation damping term instead of the inertial term, and (2) using a 1D fault approximation. Removing these approximations may be of importance because non-planar geometry has an influence of the emitted waves and that a rupture on a 1D-fault is forced to go through a geometrical asperity. On the contrary, on a 2D-fault, the rupture can avoid and encompass the geometrical asperity.

To overcome these issues, we have developed a 2D-fault spectral boundary element method that incorporates non-planar geometry by using the small slope approximation. Using this method, we are able to perform fully-dynamic 2D-fault simulations in a reasonable time on a personal computer: ~3days for 10 cycles, using 262,144 elements on a 4-core machine.

We have used this method on a 3D rough fault quasi-dynamic earthquake cycle, where it can be seen that as expected, the rupture sometimes avoids geometrical complexity and encompasses it to finally rupture it. We also have tried to compare the difference between a planar fault and a fault with a seamount. Finally, we have applied our method to the SCEC benchmark for 2D-fault fully dynamic earthquake cycle modeling.

In near future, this will open the way for more parameter studies that were previously out of reach because of the limited computer resources.

Links between mud volcanoes, upper-plate fluid conduits and shallow slow earthquakes in the Hyuga-nada subduction zone

Ryuta Arai¹, Seiichi Miura¹, Yasuyuki Nakamura¹, Kazuya Shiraishi¹, Gou Fujie¹, Shuichi Kodaira¹, Tsutomu Takahashi¹, Ayako Nakanishi¹, Yuka Kaiho¹, Yohei Hamada¹, Yanxue Ma², Kimihiro Mochizuki², Rie Nakata², Masataka Kinoshita², Yoshitaka Hashimoto³

¹JAMSTEC, ²ERI, Univ. Tokyo ³Kochi Univ.

The Hyuga-nada subduction zone located in the westernmost part of the Nankai Trough hosts a variety of slow earthquake activities, such as tectonic tremor and very low-frequency earthquakes (e.g., Yamashita et al., 2015, 2021; Tonegawa et al., 2020), and thus offers an ideal location to link our understanding of structural and hydrogeologic properties at subduction faults to slip behavior. The study area is also known to generate abundant mud volcanoes on the seafloor (Ujiie, 2000). Although the both phenomena are closely related to fluids at depth, the origin, distribution and transfer system of the fluids remain enigmatic.

To better understand the subsurface hydrological system and its relation to mud volcanoes and slow earthquake activity in the Hyuga-nada area, we performed dense seismic refraction experiments using ocean bottom seismographs (OBS) and multi-channel seismic (MCS) reflection surveys in 2020 and 2021. For constructing a high-resolution seismic velocity model, we applied a full waveform inversion analysis to the OBS refraction data. The P-wave velocity (V_p) model along the seismic line of HYU01, which is aligned parallel to the regional trend of the Nankai Trough in the southwest-northeast direction and crosses the source area of the low-frequency tremor distributed between the shallow and deep subducting seamounts, reveals ~10-km-wide, near-vertical columns with significantly lower P-wave velocities ($V_p=2.0-4.0$ km/s) in the upper plate on the western side of the tremor region (east off Kagoshima prefecture). The low-velocity anomalies extend from near seafloor down to the plate boundary at 10-13 km depths and probably represent high-porosity damage zones that accommodate vertical conduits which facilitate fluid migration leading up to seafloor mud volcanoes. The distribution of the upper-plate fluid conduits is negatively correlated with the seismic reflectivity at the plate boundary and the population of slow earthquakes. These structural features we found are consistent with the drainage system at the source regions of deep tremor proposed by Nakajima and Hasegawa (2016) and suggests that the upper-plate drainage system plays a key role in controlling the fluid pressure and occurrence of slow earthquakes at the shallow plate boundary as well as at the deep plate boundary.

On the eastern side of the tremor area (south off Shikoku), on the other hand, we discovered a high-velocity body ($V_p=3.0-5.0$ km/s) in the upper plate, which is in a contrast with the aforementioned low-velocity fluid conduits on the western side. These results suggest that the source areas of shallow slow earthquakes can be delimited by various factors associated with upper-plate structural heterogeneities.

Synthetic tests of joint CMT analysis using translation and strain data

Suguru Yabe¹ and Kazutoshi Imanishi¹

¹Geological Survey of Japan, AIST

Non-double couple (NDC) components of seismic moment tensor is important to interpret seismic source process. Recent advances in slow earthquakes and induced seismicity pointed out importance of pore fluids in earthquake genesis. Such seismic source would have NDC components of seismic moment tensor, though its estimation uncertainties may not be small enough to discuss possibilities of NDC components in such earthquakes. In this study, we developed a method using strain data in addition to translation data for Centroid Moment Tensor (CMT) analysis and conducted synthetic tests to investigate estimation uncertainties of estimated moment tensors. In the southwest Japan, where we focused, translation data of F-net is usually used for CMT analysis. We also used seismic data from strain observatories constructed by Geological Survey of Japan in this region. We mainly tested effects of observation noises and uncertainties in subsurface structure used for Green's function calculation to uncertainties in estimated moment tensors. As a result of synthetic tests, we confirmed that uncertainties in estimated moment tensors are reduced by joint CMT analysis compared with CMT analysis with single data type.

Mechanical coupling on plate interfaces: Rupture scenarios of megathrust earthquakes and aseismic slips

Tatsuhiko Saito¹ and Akemi Noda²

¹NIED, ²MRI, JMA

Slip deficit distributions have been widely used to assess the potentials of megathrust earthquakes in various subduction zones. However, the conventional studies have some points to improve for a more reliable and useful assessment. One of the points is that the slip deficit estimated from onshore geodetic observations is inevitably poor in the resolution of offshore coupling distributions. Another point is that the afterslip scenarios were not fully examined based on the plate coupling distributions. We develop an inversion method to estimate the stress rate distribution as mechanically coupled areas. Numerical experiments show that the inversion of the stress rate on the plate boundary can estimate offshore plate coupling better than conventional slip-deficit rate analysis. It is because we use a model of mechanical coupling along the subducting plate as a kind of prior information to restrict offshore slip-deficit distributions although onshore data itself generally do not contain enough information to resolve offshore slip-deficit distributions. We apply our inversion method to the Nankai trough subduction zone in southwestern Japan to detect mechanically coupled areas. Some of the estimated coupled areas correspond to the rupture areas of historical earthquakes. We then construct a possible rupture scenario based on the estimated mechanically coupled areas. We consider scenarios of an earthquake sequence in which a foreshock, an afterslip, and a mainshock occur (Figure 1).

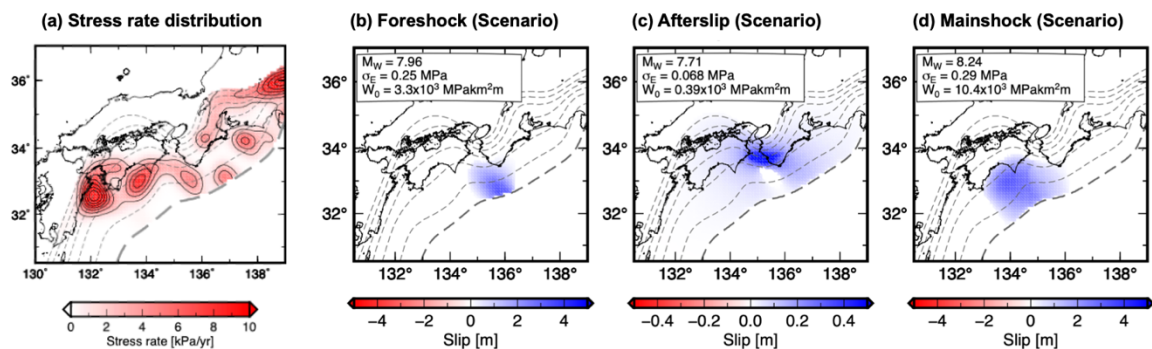


Figure 1. (a) Estimated shear stress rate at the plate interface as mechanically coupled areas. Contour lines are plotted at 2 kPa/year intervals. Slip distributions of possible rupture scenarios: (b) a foreshock, (c) its afterslip, and (d) a mainshock. It is assumed that the afterslip is not allowed in the region where the local stress drop is high in the foreshock rupture.

Saito, T. & Noda, A. (2022). Mechanically Coupled Areas on the Plate Interface in the Nankai Trough, Japan and a Possible Seismic and Aseismic Rupture Scenario for Megathrust Earthquakes. *Journal of Geophysical Research: Solid Earth*, 127(8). <https://doi.org/10.1029/2022JB023992>

Resolving slip directions in the finite fault with the radiation-corrected empirical Green's function

Ritsuya Shibata¹, Naofumi Aso¹

¹Dept. EPS, Sch. Sci., Tokyo Institute of Technology

The waveform inversion is a useful method to estimate a spatio-temporal slip distribution, which is important for understanding the earthquake mechanics or the background stress field. This method requires Green's functions to reproduce observed waveforms, and the empirical Green's function (EGF) is a kind of way to provide them (e.g. Hartzell, 1978, GRL). Although the EGF is superior to the theoretical Green's functions with its applicability in the relatively high-frequency range higher than 1 Hz, there are some limitations; the suitable earthquake to utilize for EGF has to exist and the slip directions different from the EGF event are not resolvable.

To reduce these limitations, we have developed a waveform inversion method with the radiation-corrected EGF, whose amplitude is corrected by considering the difference in the theoretical radiation patterns (Shibata et al., 2022, GJI). Since the radiation correction allows us to synthesize the EGF waveform for any focal mechanisms, we can resolve multiple slip directions at each subfault (Fig. 1). At the process of solving the inverse problem, we assign the EGF radiation pattern as the weighting factor, which stabilizes the estimates of spatio-temporal slip distribution including slip directions.

In this study, we applied this new waveform inversion method to multiple M6-class inland earthquakes in Japan to investigate its applicability. As a result, we confirmed the effectiveness of this method in estimating slip directions using the relatively high-frequency range. We also investigated the rupture mode preferences by focusing on the relationship between the slip directions and rupture propagation directions based on the obtained slip distributions.

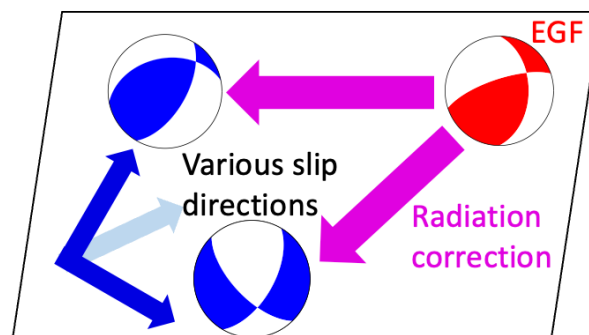


Figure 1. The concept of the radiation correction in the finite fault inversion. We synthesized the radiation-corrected EGF waveforms for multiple focal mechanisms at each subfault.

Fluid flow and silica transport along the subduction interface: example from the Franciscan metamorphic belt, USA

Simon R. Wallis¹, Shogo Soejima¹

¹Dept. EPS, Univ. Tokyo

The development of slow earthquakes in subduction zones is thought to be closely associated with the movement of water-rich fluids. The flow of such fluids will result in the transport of other elements which may allow them to be identified in the rock record. Subducted siliciclastic sediments contain abundant SiO₂ in the form of quartz. SiO₂ is highly soluble in subduction fluids and their flow is likely to be associated with significant transport of SiO₂. Audet & Burgmann (Nature, 2014) propose that the transport and deposition of silica accommodated by the movement of water-rich fluids may be important in controlling the time scales of deep slow earthquakes and suggest the recurrence period of deep slow earthquakes is controlled the amounts of silica accreted to the lower forearc crust with estimated amounts of 5–15 vol.%. The high solubility of SiO₂ compared to other common phases in subducted rocks implies the amount of silica accreted in the crust of the hangingwall domain of subduction zones should closely correspond to an equivalent volume increase. This implies that estimates of the volume increase in metamorphic rocks that have been exhumed from equivalent parts of the subduction system can be used to estimate silica precipitation in these domains. If the physical conditions associated with precipitation are known, the amount of precipitated silica can also be used to estimate the time-integrated water flux responsible for its transportation.

Estimates of volume change associated with fluid flow are normally approached by measuring bulk chemistry of rocks and comparing the results to some known or assumed original composition. In addition, some immobile element or elements have to be assumed. The results are subject to large uncertainties particularly where the original undeformed rock cannot be sampled. Geometric methods based on analysis of geological structures can also be used to estimate volume change. However, these are generally on the grain scale and cannot incorporate sliding along grain boundaries which is likely to be an important auxiliary process in rocks undergoing deformation by solution transfer. As part of this study we developed a method based on analysis of deformed vein sets that can be used to assess appropriate uncertainties and incorporate grain scale deformation. Application of this method to metagreywacke in Del Puerto Canyon in the Franciscan belt allows a quantitative estimate of volume change to be made. The Del Puerto metagreywacke represents a unit accreted to the hangingwall of the Franciscan accretionary complex and our results yield a volume increase of 7–21 vol.%, in good agreement with estimates by Audet & Burgmann (2014). The volume of quartz precipitated in the lower forearc crust estimated in this study can be related to the time-integrated flux of water moving upward from the subducted plate and overlying sediments. Assuming that water percolated vertically, the time-integrated fluid flux is estimated to be 1.0×10^6 – 1.9×10^7 (m³/m²). This result is tens of times higher than the fluid fluxes estimated by combining results of thermal models of subduction zones, the distribution of hydrous minerals in subducting rocks and the stability of hydrous minerals. Such large discrepancies are difficult to explain by uncertainties in the models of fluid flow or estimates of *P-T* conditions which control the concentration of SiO₂ in the subduction fluids. We suggest that our results are best explained by the channeling of subduction fluids along the plate boundary. Such a model is compatible with the known permeability anisotropy of foliated serpentinite that is likely to form the upper boundary of subduction zones in the domain of deep slow earthquakes.

Nankai Forearc Structural and Seismogenic Segmentation caused by a Magmatic Intrusion off the Kii Peninsula

G. Kimura¹, Y. Nakamura¹, K. Shiraishi¹, G. Fujie¹, S. Kodaira¹, T. Tsuji², R. Fukuchi³, and A. Yamaguchi⁴

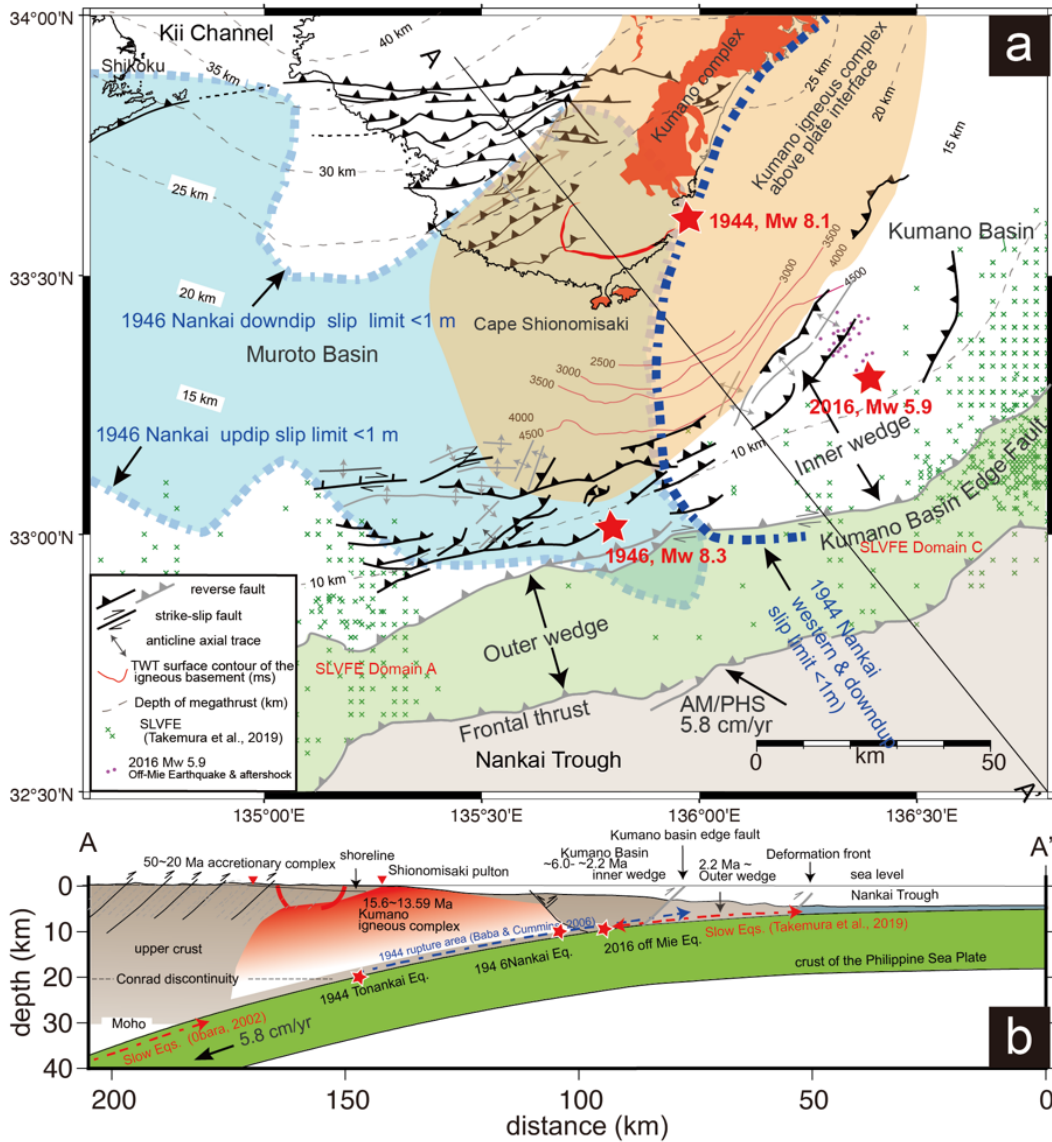
¹Research Institute for Marine Geodynamics, Japan Agency for Marine Earth Science and Technology, 3173-25, Showa-machi, Kanazawa-ku, Yokohama-city, Kanagawa 236-0001, Japan.

²Department of Systems Innovation, School of Engineering, The University of Tokyo 7-3-1 Hongo, Bunkyo-ku, Tokyo 113-8656, JAPAN

³Naruto University of Education, 748, Nakajima, Takashima, Naruto-cho, Naruto-shi, 772-8502 Japan

⁴Department of Ocean Floor Geoscience, Atmosphere and Ocean Research Institute, The University of Tokyo, 5-1-5 Kashiwanoha, Kashiwa-shi, Chiba 277-8564, Japan.

The causes for forearc basin and megathrust rupture zone segmentation are controversial. The Nankai forearc, Japan, is separated into five domains based on topography: Enshu, Kumano, Muroto, Tosa, and Hyuga. The boundaries of these domains correspond to the rupture limits of large earthquakes. We examined the geologic structure of the boundary region between the Kumano and Muroto domains off the Kii Peninsula using multichannel seismic reflection data to evaluate the role of upper plate composition in controlling segmentation. The results suggests that thick cover sediments and underlying accretionary prism are obliquely thrust landward over the igneous basement complex rock in the region of offshore of Cape Shionomisaki and separate the forearc basin. The igneous basement complex rocks directly overly the plate interface in the hypocentral regions of 1944 Tonankai and 1946 Nankai earthquakes. The 1944 earthquake originated at the base of the complex, and the rupture extent slipped past its basement boundary, whereas the 1946 event nucleated at the updip boundary of the basement complex. The dense igneous rocks might have worked as a heavily loaded barrier on the seismogenic megathrust and separated the rupture area of both the earthquakes. Upper plate geology may be an important factor in controlling seismogenesis in the Nankai Trough and may serve as an example for understanding the controls on megathrust slip in other subduction zones.



A tectonics synthesis map (a), and a profile (b) of the inner wedge surrounding Cape Shionomisaki, Kii Peninsula. Note that the Kumano igneous complex is situated on the seismogenic plate boundary megathrust. Hypocenters of 1944 Tonankai, 1946 Nankai, and 2016 off-Mie Earthquakes are projected on the profile. (Kimura et al., 2022 G-cubed)

A Slow Earthquake Gap on the Smoothened Decollement off the Kii Peninsula, Nankai Trough

K. Shiraishi¹, Y. Nakamura¹, **G. Kimura**¹, G. Fujie¹, S. Kodaira¹, T. No¹, Y. Kaiho¹, and S. Miura¹

¹Japan Agency for Marine-Earth Science and Technology, 3173-25 Showa-machi, Kanazawa10ku, Yokohama, Kanagawa, 236-0001, Japan

Very-low frequency earthquakes (VLFs), low-frequency tremors (LFTs), and slow slip events (SSEs) have been detected based on both land and marine long-term observations in the Nankai Trough located southwest of Japan. In contrast to the frequent occurrence of VLFs in the areas off Kumano and off Muroto, the VLFE activity is lower to the south of the Kii Peninsula, we call the area as a slow earthquake gap in this paper. The slip behaviors of the plate interface in subduction zones have been linked to the topography of the incoming seafloor; especially for slow earthquakes, topographic variations in the oceanic crust are considered one of the fundamental factors affecting their occurrence. In the off-Kumano region, Toh et al. (2018) investigated the effect of subducting ridges on VLFE occurrence in the Tonankai region of the Nankai Trough. Shiraishi et al. (2020) and Hashimoto et al. (2021) clarified the local relationship between oceanic crust topography and VLFE occurrence based on 3D seismic data. Nakamura et al. (2022) analyzed seismic reflection profiles in the off-Muroto region and revealed the correlation of the rough topography and the tremors and VLFs distribution. In contrast to active VLFE region, Qin et al. (2021) suggested that a smooth topography of the subducting plate surface may be a reason for the lower activity of VLFs south of the Kii Peninsula compared with the Kumano and other regions. To reveal the detailed topography of the oceanic crust, plate boundary decollement and frontal part of the accretionary wedge, we conducted a dense 2D seismic survey in an offshore area southwest of the Kii Peninsula. This survey area covers both the active and less active regions of VLFE distribution and the structure of plate boundary decollement with overriding wedge. The survey has resulted in the following new findings; The rough surface of the oceanic plate contacts directly with the decollement in the region of the slow earthquakes, whereas smoothened decollement within underthrust sediments is developed in the region of the quiet seismicity.

References: Hashimoto et al. (2021): Scientific Rept., Kimura et al. (2022): G-cube, Shiraishi et al. (2020): EPS, Toh et al. (2018): GRL, Qin et al. (2021): GRL

Numerical modeling of SSEs in the Nankai region

-Segments of short-term SSEs-

Takanori Matsuzawa¹, and Bunichiro Shibazaki²

¹NIED, ²BRI

Slow earthquakes have been intensively studied, since the discovery of deep tectonic tremor in the Nankai region (Obara, 2002). It is observed that active tremor episodes are accompanied by short-term slow slip events (SSEs). Such phenomena are sometimes called as episodic tremor and slip (ETS). Tremor is thought as an indicator of slip or stress state at the plate boundary (Obara and Kato, 2016). In the Nankai region, long-term catalogs of slow earthquakes are available (e.g., Kano et al., 2018), as the monitoring of slow earthquakes continues for two decades. In this presentation, we discuss the numerically reproduced segments of short-term SSEs in the Nankai region, based on the numerical result in the time scale of seismic cycles. We also compare the result with the actually observed segments of ETS.

Our numerical model is similar to Matsuzawa et al. (2013). Our modeled region is spanned from the Tokai to the Hyuganada region. The plate interface of the subducting Philippine Sea plate is expressed by about 170,000 of triangular elements. To simulate the frictional stress at the plate interface, we adopt a rate- and state-dependent frictional law (RS-law) with a cut-off velocity. Elastic response of semi-infinite homogeneous medium is assumed as the interaction of each element. In our model, short-term SSE region, where (a-b) in RS-law is negative, is based on the actual distribution of tremor.

To extract SSEs, we defined short-term SSEs as the period in which the slip velocity exceeds ten times of the loading velocity (i.e., subduction velocity) at each element below the depth of 28 km. In addition, if elements within 5km satisfy this condition at the same time, they are considered as the same SSE. This process is iterated until no more SSEs are related as the same event. We discuss the segments of short-term SSEs which are greater than Mw4.5, using the result of two seismic cycles (~216 years). Several local peaks are found in the spatial distribution of edges of short-term SSE segments in the strike direction. This suggests that the segments of short-term SSEs have characteristic boundaries. These boundaries seem to locate around the discontinuity of tremor distribution (e.g., Ise Bay) or the region where width of short-term SSE region in the dip direction (W) largely changes in the strike direction. This suggests that the segments of short-term SSEs are characterized by the spatial distribution of W.

We compare the obtained result with the tremor catalog by the NIED (Maeda and Obara, 2009; Obara et al., 2010). Actual segments of ETS may be controlled not only by W, but also by other complexities, as the actual segments are sometimes shorter than the numerically reproduced ones (e.g., northern and central Kii region). Reproduced segments of short-term SSEs are almost similar during seismic cycles. This implies that the segments are strongly characterized by W, and not largely affected by the stress changes during the seismic cycle.

Serpentine deformation mechanism in depths of deep slow earthquakes of the shallow wedge

Takayoshi Nagaya¹, Simon R. Wallis¹, Ryosuke Ando¹

¹Dept. EPS, Univ. Tokyo,

Two distinct models have been proposed for the deformation mechanism associated with the generation of slow earthquakes: model 1) a fault with mechanical heterogeneity consisting of brittle patches in a ductile background and the ductile deformation associated with a stress exponent, n , of ~ 1 , and model 2) a creeping fault consistent with the rate and state friction law. Neither of these models is consistent with deformation by dislocation creep with $n \geq 3$. Hydrated forearc mantle along the subduction boundary is thought to consist dominantly of antigorite-rich serpentinite at the depths at which deep slow earthquakes occur in subduction zones. Experimental studies of antigorite serpentinite have been carried out but there is no good consensus about the dominant deformation processes: both dislocation creep and semi-brittle deformation have been proposed for deformation conditions appropriate for the subduction boundary. Examination of naturally deformed antigorite rocks can provide more information to help clarify the deformation mechanism of antigorite under natural strain rates. In this study we performed microstructural and chemical analyses of two samples of shear zone domains within natural antigorite-rich serpentinite from the Besshi and Shiraga regions of the Sanbagawa metamorphic belt, central Shikoku, SW Japan using electron backscattered diffraction (EBSD) and electron probe micro analyzer.

The antigorite grain boundaries were defined using EBSD and this revealed that shear zones are defined by the shape preferred orientation of antigorite grains, which increases towards the center of the shear zones. In addition, only very limited misorientation within individual grains was observed even within the highest strain domains. This implies that there was no significant formation of subgrains or distortion associated with the presence of dislocations and dislocation creep was not the dominant deformation mechanism. There were also only minor changes in grain size and grain aspect ratio with increasing strain implying a lack of grain size reduction that is normally associated with dislocation creep. In addition, micro-talc mixing within the antigorite grains in the shear zone from the Besshi sample and the micro-cracking of antigorite grains in the shear zones from the Besshi and Shiraga samples were observed. These features imply that antigorite grains of shear zones deformed due to the grain boundary sliding accommodated by micro-cracking and solution transfer creep (such as the dissolution-precipitation creep).

The constitutive law and associated stress exponent of the serpentinite in this study strongly depend on the accommodated mechanisms. Dissolution-precipitation creep is associated with $n = 1$ and the presence of a talc component within antigorite grains supports the idea that this is an important accommodation mechanism for the antigorite grain boundary sliding inferred in the present study. Deformation of antigorite schist that is controlled by the dissolution-precipitation accommodation mechanism is consistent with the ductile background deformation required for model 1). The brittle patches in model 1) may be explained by the presence of rigid olivine-rich patches within serpentinite bodies. Deformation of antigorite schist that is controlled by microcracking with sliding along the microcracks is expected to be distinct. Frictional deformation experiments on sheet silicates that are frictionally weak including antigorite, have shown they exhibit a friction rate strengthening dependence. The

contribution of dissolution-precipitation creep within the fault zone can also promote the friction rate strengthening dependence. Therefore, the deformation mechanism of antigorite grain boundary sliding accommodated by mainly microcracking is consistent with the fault creep with the rate-dependent friction of model 2). In this case, the required effective normal stress in model 2) is lower compared with that of the case of the friction rate weakening dependence such as olivine.

Deformation of antigorite serpentinite by grain boundary sliding associated with dissolution-precipitation and microcracking accommodation mechanisms suggested by this study is consistent with previous studies of deformation mechanisms in deep slow earthquakes generated domains in the shallow wedge and this combination of deformation mechanisms is likely to be important in controlling deformation along the slab-mantle boundary in subduction zones.

Analytical understanding of condition of slow and fast earthquakes based on the BK model and the interaction among heat, fluid pressure and porosity

Takehito Suzuki¹, and Hiroshi Matsukawa¹

¹Dept. Phys. Sci., AGU

For natural faults, slow earthquakes sometimes repeat and change to fast earthquakes. When the transition from the slow to fast earthquakes occurs is now a controversial problem. Additionally, after the repetition of slow earthquake and succeeding fast earthquake, whether the slow earthquakes again occur or not is not clarified. The systematic understanding of time series of slow and fast earthquakes should be performed with a single framework.

We consider the Burridge-Knopoff (BK) model and the interaction among heat, fluid pressure and porosity, to treat both the slow and fast earthquakes in a single framework. The fault rocks are considered as poroelastic media, including pores inside them. We consider the BK model with the poroelastic block and substrate. The BK model generates the stick-slip behavior, and the slip is interpreted as the dynamic deformation within a region around the contact area in the current model. The region has a finite width and is called the slip zone. During the slip, the pore generation (PG) [frictional heating (FH)] reduces [raises] the fluid pressure in the slip zone, inducing the increase [reduction] in the friction stress acting on the slip zone and the reduction [increase] in the slip velocity. Therefore, slow and fast earthquakes are dominated by PG and FH, respectively. Notably, we also consider pore-healing (PH) during the interval of the dynamic slips, which reduces the porosity.

Considering the energy balance before and after the slip, the function governing the system behavior, $F(u_f)$, was found, where u_f describes the slip distance for each earthquake. Though the condition of the energy balance, $F(u_f) = 0$, has several positive solutions, the smallest solution is realized for each earthquake, and such a solution is shown in the current study. The solution indicates that the larger p_0 and smaller ϕ_0 tend to generate slow earthquakes, where p_0 and ϕ_0 are the values of the fluid pressure and porosity in the slip zone at the onset of each dynamic slip, respectively. The values of p_0 and ϕ_0 are determined by many physical processes, and among them, we focus on PH here. The PH effect is controlled by the parameter α_1 , and larger α_1 generates faster PH. We first assume the negligible α_1 , and found that after the slow earthquakes repeat several times, the fast earthquakes occur repeatedly. The slow earthquakes will not occur once the fast earthquake occurs in this case. We interpret this behavior as the slow-fast transition. On the other hand, if we raise the value of α_1 , the slow earthquakes again occur after the first fast earthquake. This case is understood as the slow-fast-slow transition. We suggest that the critical value exists for α_1 , which categorizes the transitions.

The indirect triggering of a normal faulting earthquake sequence in the Ibaraki-Fukushima prefectural border, Japan by M_w 9.0 Tohoku-Oki megathrust: the elusive role of low-angle normal fault slow-slip

Yohai Magen^{1,2}, Asaf Inbal¹, Alon Ziv¹, Gidon Baer², Roland Burgmann³, Axel Periollat⁴, and Takeshi Sagiya⁵

¹Department of Geophysics, Tel-Aviv University, Tel Aviv, Israel, ²Geological Survey of Israel, Jerusalem, Israel, ³Department of Earth and Planetary Science, University of California Berkeley, Berkeley, CA, USA, ⁴Univ. Grenoble Alpes, Univ. Savoie Mont Blanc, CNRS, IRD, Univ. Gustave Eiffel, ISTerre, 38000 Grenoble, France, ⁵Disaster Mitigation Research Center, Nagoya University, Nagoya, Japan

Although deep-seated blind normal faults are common in subduction environments, their rheology, kinematics and interaction with the upper crust are poorly constrained. A month-long shallow normal faulting sequence in the Ibaraki-Fukushima prefectural border (IFPB), northeast Japan, which followed the M_w 9.0 Tohoku-Oki earthquake (TOE) and culminated in the M_w 6.7 Iwaki earthquake, provides a window into megathrust-to-normal fault interaction. Stress change calculations clearly indicate that the IFPB earthquake sequence cannot be explained in terms of direct triggering by the TOE co- and post-seismic slip. In quest for an alternative triggering mechanism, we analyzed post-TOE GNSS data from eastern IFPB. A key step in this analysis is the removal of the large-scale post TOE displacement field, after which a distinct highly-localized strain along the coastline becomes apparent. The accumulation of this strain was mostly aseismic and migrated with time prior to the Iwaki earthquake in a manner that correlates well with post-TOE local seismicity. We attribute the pre-Iwaki earthquake strain accumulation to aseismic slip along low-angle seaward dipping blind normal fault, activated by the TOE. Stresses transferred by this slip episode accelerated the failure along the IFPB shallow normal faults. This indirect triggering of the Iwaki earthquake sequence by the TOE highlights the complexity of stress transfers in subduction environments.

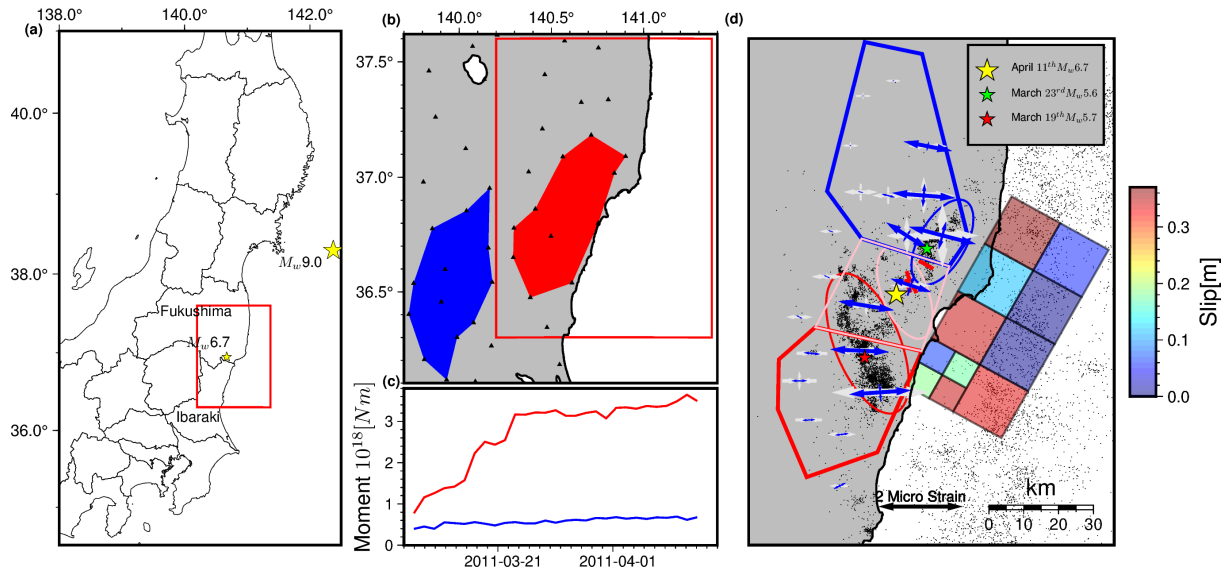


Figure 1

(a) present location map of northeast Japan with the hypocenter location of the M_w 9.0 TOE and the M_w 6.7 Iwaki earthquakes. The Red rectangle shows the inset location of the IFPB study area to the right. (b-c) Comparison of geodetic moment time series within the IFPB region (red polygon) and a reference region (blue polygon) in the month following the TOE. The significant differences between the two regions indicate that there is an increased geodetic moment and strain localization within the IFPB area. (d) The IFPB observed (white arrow) and models (blue arrow) strain field, alongside the seismicity in the month following the TOE. The month-long cumulative slip distribution along the low angle normal fault surface projection is shown with colored black rectangles. The slip propagates at a minimum speed of 8 km/day from southeast to northwest with the equivalent moment magnitude equal to M_w 6.7.

Propagation of Slow Slip Events on Rough Faults

Yudong Sun¹, Camilla Cattania¹

¹Dept. of Earth, Atmospheric, and Planetary Sciences, Massachusetts Institute of Technology

Seismic and geodetic observations show that slow slip events (SSEs) in subduction zones can happen at all temporal and spatial scales and propagate at a wide range of velocities. Observation of rapid tremor reversals (RTRs) indicates back-propagating fronts traveling at least ten times faster than the main rupture front. Heterogeneity of fault properties, such as fault roughness, is often invoked to explain this complex behavior, but how roughness affects SSEs is not well understood. Here we use quasi-dynamic seismic cycle simulations to model SSEs on a rough fault. Roughness induces heterogeneity in normal stress σ and causes locked asperities where σ is high. We find that more SSEs tend to rupture like a pulse rather than a crack when the sinusoidal σ perturbation amplitude is larger and the wavelength is smaller. In simulations, pulse-like ruptures are clusters of small subevents propagating slowly, while crack-like ones are single extensive events and propagate faster. Using a continuum model and treating asperities as spring-sliders rupturing in sequence, we derive two analytical expressions for the forward propagation velocity of crack-like ruptures, which is mainly controlled by σ of asperities. We identify a delayed stress drop caused by fluctuations in slip velocity when rupture passes the low- σ regions, which induces secondary back propagation. The back and forward propagation velocity ratio increases with higher σ perturbation amplitude. On rough faults with fractal elevation profiles, the transition from pulse to crack can also lead to the re-rupture of SSEs. Our study provides a possible mechanism for the complex evolution of SSEs from geophysical observations.

Detailed seismic structure along the plate interface and its implication for the interplate seismic coupling in Nankai Trough off Cape Muroto

Gou Fujie, Ryuta Arai, Kazuya Shiraishi, Yasuyuki Nakamura, Shuuichi Kodaira, Gaku Kimura, Yuka Kaiho, Koichiro Obana, Seiichi Miura

JAMSTEC

Along the boundary between the overriding plate and the subducting oceanic plate in the plate subduction zone, various slip behaviors with a variety of slip speed, such as normal earthquakes with a fast slip and a wide-range of slow earthquakes, are observed. Generally, slow earthquakes are predominant at the shallowest portion of the plate boundary, whereas normal earthquakes including megathrust tend to occur at the deeper portion of the plate boundary than the shallow slow earthquake area. The boundary between the area where slow earthquakes are predominant and the area where megathrusts occur is considered to correspond to a boundary of the interplate seismic coupling. The interplate seismic coupling is affected by various factors such as pressure-temperature condition, pore-fluid pressure, materials along the plate interface, and the geometry of the plate interface. To reveal these potential factors controlling the interplate seismic coupling and in turn the interplate slip behaviors, detailed seismic structure at around the depth of the plate boundary is critically important.

Nankai Trough is one of the most investigated seismogenic subduction zones in the world. Especially in the central part of the Nankai Trough, seismic activities are constantly monitored using a seafloor seismic observatory system (DONET) and detailed distribution of the shallow very low frequency earthquakes (sVLFE), a kind of slow earthquakes, are well constrained. The downdip limit of sVLFE approximately corresponds to the updip limit of the strong interplate coupling area suggested by geodetic studies and past megathrust earthquakes in this subduction zone. However, the factor determining this boundary between the strong and weak coupling areas are poorly understood.

In 2019, we conducted a wide-angle seismic reflection and refraction survey off the Cape Muroto where detailed sVLFE activities are well constrained by DONET monitoring. The downdip limit of the sVLFE is located around a prominent seafloor valley called Tosa-bae basin. We deployed Ocean Bottom Seismometers (OBSs) every 2 km to reveal the detailed seismic structure up to a depth of the subducting oceanic crust across the Tosa-bae basin. In order to discuss the factor controlling the transition point of the interplate seismic coupling. First, we developed a long-wavelength P-wave velocity (V_p) model by the first arrival tomography. Next, using the V_p model derived by the first arrival tomography as the starting model, we applied Full-Waveform Inversion (FWI) to the wide-angle seismic data to reveal detailed V_p model. To investigate the spatial resolution of the obtained model, we applied the checkerboard resolution tests (CRT) and confirmed that the spatial resolution at around the depth of the plate interface is 1km (horizontal) x 0.5km (vertical). As expected, our V_p model shows intriguing differences between the shallower and deeper sides of Tosa-bae basin at around the depth of the plate interface. The V_p at the bottom of the overriding plate is significantly lower in the shallower area of the Tosa-bae basin than that in the deeper area of the Tosa-bae basin. In addition, a thin low velocity layer (a velocity reversal layer), possibly

corresponding to the decollement, exists only the shallower side of the Tosa-bae basin. These observations suggests that the nature of the plate boundary, especially the materials/physical conditions at the bottom of the overriding plate, is the first order control on the interplate seismic coupling and the slow-to-fast earthquakes.

Effects of long-term slow slip events on in-slab stresses and seismicity in Bungo Channel, Southwestern, Japan

Saeko Kita^{1,2}, Heidi Houston³, Roland Burgmann⁴, Suguru Yabe⁵,
Youichi Asano⁶ and Takeshi Kimura⁶

¹Building Research Institute, ²GRIPS, ³University of California, Berkeley,
⁴University of Southern California, ⁵Japanese Geological Survey, AIST, ⁶NIED

Kita et al. [2021, Nature Communications] reported that short-term slow slip events (SSEs) on the plate interface in Kii peninsula can change the stress field and seismicity within the subducting Philippine Sea plate, examining data before and after 40 SSEs for 17 years. They indicated that it is possible to indirectly monitor the reduction of locking on the plate boundary by using time-space variations of in-slab seismicity. In the present study, we examine the relationship between in-slab events and shallow SSEs in the Bungo channel, where there are in-slab earthquakes and long-term SSEs (L-SSEs) with recurrence time of ~ 7 years and ~ 1 year duration. We applied a stress-tensor inversion method to focal mechanisms of in-slab events for 19 years and examined temporal changes of stress axes relative to the duration time of the three L-SSEs. In general, the Sigma-3 axes of inversion results strike in the east-west direction, whereas the Sigma-1 axes are close to vertical (~ 70 degrees) and parallel to the direction of plate motion of the subducting plate. During the period of one year preceding the L-SSEs, the strike of the Sigma-1 of in-slab events rotates ~ 30 degrees in a clockwise direction and the plunge rotates ~ 10 degrees becoming less vertical. After the initiation of the two L-SSEs, the plunge of Sigma 1 rotates several degrees becoming much less vertical and the strike rotates back to the direction of plate motion of the subducting plate. During the period of one year after the end of the L-SSEs, the plunges of Sigma 1 rotate back to the initial position. The b-values of the in-slab events tend to decrease in the period of the L-SSEs. The stress ratio R is generally ~ 0.5 , but it becomes ~ 0.3 during the period of one year just after the end of the L-SSEs and returns back to ~ 0.5 by 1.5 years after the L-SSEs. The stress-axis rotation in the southern portion of the fault plane of the L-SSEs is generally larger than that in the northern portion of the fault plane. The stress ratio R before and after the L-SSEs is respectively ~ 0.8 and ~ 0.15 in the southern portion, whereas the ratio in the northern portion remains almost constant (~ 0.5). This suggests there is less friction in the northern portion of the fault plane of the L-SSEs. These results suggest the promise of our methodology, using in-slab events to infer the timing of L-SSEs and to monitor ongoing changes in locking of the plate boundary by aseismic slip.

Precise monitoring of slow earthquakes around Nankai Trough toward early detecting crustal deformation

Keisuke Ariyoshi^{1*}, Toshinori Kimura¹, Yasumasa Miyazawa¹, Sergey Varlamov¹, Takeshi Iinuma¹, Akira Nagano¹, Joan Gomberg^{2,3}, Eiichiro Araki¹, Toru Miyama¹, Kentaro Sueki¹, Shuichiro Yada¹, Takane Hori¹, Narumi Takahashi⁴, Shuichi Kodaira¹

¹ JAMSTEC, ² USGS, ³ Univ. of Washington, ⁴ NIED

In our recent study (Ariyoshi et al., 2021a, 2021b), we detected the pore pressure change due to the slow slip event (SSE) in March 2020 at the two borehole stations (C0002 and C0010), where the other borehole (C0006) close to the Nankai Trough seems not because of instrumental drift for the reference pressure on the seafloor to remove non-crustal deformation such as tidal and oceanic fluctuations. To overcome this problem, we use the seafloor pressure gauges of cabled network (DONET) stations nearby boreholes instead of the reference by introducing time lag between them. We confirm that the time lag is explained from superposition of theoretical tide modes. By applying this method to the pore pressure during the SSE, we find pore pressure change at C0006 about 0.6 hPa. We also investigate the impact of seafloor pressure due to ocean fluctuation on the basis of ocean modeling, which suggests that the decrease of effective normal stress from the onset to the termination of the SSE is explained by Kuroshio meander and may promote updip slip migration, and that the increase of effective normal stress for the short-term ocean fluctuation may terminate the SSE as observed in the Hikurangi subduction zone. Recently, we have applied an ocean state nowcast/forecast system (JCOPE-T DA: Miyazawa et al., 2021) to JAMSTEC's monitoring system of slow slip events along Nankai trough.

References

- Ariyoshi, K., Iinuma, T., Nakano, M., Kimura, T., Araki, E., Machida, Y., Sueki, K., Yada, S., Nishiyama, T., Suzuki, K., Hori, T., Takahashi, N., Kodaira, S. (2021a). Characteristics of Slow Slip Event in March 2020 Revealed from Borehole and DONET Observatories. *Front. Earth Sci.* 8, 600793. doi: 10.3389/feart.2020.600793
- Ariyoshi, K., Kimura, T., Miyazawa, Y., Varlamov, S., Iinuma, T., Nagano, A., Gomberg, J., Araki, E., Miyama, T., Sueki, K., Yada, S., Hori, T., Takahashi, N., Kodaira, S. (2021b) Precise Monitoring of Pore Pressure at Boreholes Around Nankai Trough Toward Early Detecting Crustal Deformation. *Front. Earth Sci.* 9:717696. doi: 10.3389/feart.2021.717696
- Miyazawa, Y., Varlamov, S. M., Miyama, T., Kurihara, Y., Murakami, H., Kachi, M. (2021). A Nowcast/Forecast System for Japan's Coasts Using Daily Assimilation of Remote Sensing and In Situ Data. *Remote Sensing*, 13, 2431. doi:10.3390/rs13132431

Slip deficit and its correlation with slow and fast earthquakes at the Nankai subduction zone.

Raymundo Plata-Martinez¹, Takeshi Iinuma¹, Fumiaki Tomita², Takuya Nishimura³,
Ryoichiro Agata¹, Takane Hori¹.

¹Japan Agency for Marine-Earth Science and Technology, ²International Research Institute of Disaster Science, Tohoku University, ³ Disaster Prevention Research Institute, Kyoto University

Interplate slow and fast earthquakes both possess very different styles of slip, commonly thought to be regulated by frictional characteristics mostly driven by an accumulation of interplate slip. We can explore this more deeply by correlating precise slip deficit rate observations with seismic activity to understand how, fast and slow earthquakes interact. The Nankai subduction zone, located where the Philippine Sea plate subducts under the Amur plate at the southwest of Japan, is a good study region to continue studying this. The Nankai region has presence of large interplate earthquakes and multiple observations of slow earthquakes, as well as exceptional resources for geodetic observations. To estimate a precise plate interface slip deficit rate distribution, we inverted data from GNSS stations from the dense inland GEONET array as well as 20 offshore GNSS-Acoustic stations, from time intervals contained between 2002 to 2016 (Nishimura et al. 2018). Co-seismic and post-seismic displacements had been previously removed from the data (Nishimura et al. 2018). We used Green functions estimated from a three-dimensional heterogeneous structure to achieve more realistic results. Inversion was done using a trans-dimensional reversible-jump Markov chain Monte Carlo inversion method (Tomita et al. 2021), which allows the number of model parameters to be automatically adjusted based on the spatial resolution of data. We accomplished an updated model of slip deficit rate for the Nankai subduction zone that matches prior models. Location of slow earthquakes agrees with intermediate values of slip deficit rate where we can see the transition between a locked and unlocked plate interface.

Shallow VLFE activity at the Japan–Kuril trench junction region revealed from a broadband OBS array and F-net observation

Ryosuke Azuma¹, Ryota Takagi¹, Satoru Baba², Ryota Hino¹, Masanao Shinohara³

¹Grad. Sch. Sci., Tohoku Univ., ²JAMSTEC, ³ERI, Univ. Tokyo

Along the Japan and Kuril trench subduction zones, high shallow VLFE activities are usually observed in the junctional region of these trenches by F-net (e.g., Baba et al., 2019). Recent seafloor observations have also discovered the high tectonic tremor activity, forming the belt-like distribution, near the VLFE area (S-net: Nishikawa et al., 2019; temporal OBS: Kawakubo et al., 2021). However, the spatial comparison of tremor and VLFE activities is difficult because of the difference in the precision of offshore hypocenter determination between on-land and seafloor observatories. On the other hand, a subducting seamount also exists nearby the junctional slow earthquake region and may relate to the occurrence of shallow slow earthquakes. From these viewpoints, to understand the spatial relationship, VLFEs, tectonic tremors the subducting seamount, the precise hypocenter distribution of VLFEs is firstly important so that a broadband OBS observation above the VLFE area is essential.

We have installed an OBS array on the junctional VLFE area from Jul 2019 to Oct 2020. The array is composed of one broadband and four 1 Hz OBSs (Fig a). During the observation, large tectonic tremor activities in the belt zone have been detected two times by S-net data analysis (Azuma et al., 2021). Because an intense activation of VLFE at each tremor activity is routinely observed by F-net (hereafter the Baba catalog, self-communication with Dr. Baba), we can investigate the signal of cataloged VLFEs on the OBS record.

We preliminarily confirmed that the broadband OBS sufficiently recorded VLFE signals with 0.02–0.05 Hz band, provided that an epicentral distance is less than 60 km, though 1 Hz sites are always hard to recognize. Hence, the epicenter of VLFE in the Baba catalog means the synthetic source location and the detected event signal has a high cross-correlation coefficient with the synthetic seismogram at that source (Baba et al., 2019). Thus, we compared observed and synthetic seismograms sharing a hypocenter by aligning at the origin time for each site. As a result, the onset of observed signals at the broadband OBS seems to be more fluctuated than at F-net sites, while waveform is relatively similar between the synthetic and observation. The found feature possibly implies more spread distribution of epicenters surrounding the synthetic source location. To investigate the precise distribution of VLFEs, we will examine a hypocenter determination by a moment tensor solution (Zhu and Ben-Zin, 2013).

We used F-net broadband seismograms (<http://www.fnet.bosai.go.jp>), National Research Institute for Earth and Disaster Resilience (2020). We used the synthetic waveform calculation code (FK: Zhu and Ben-Zin, 2013).

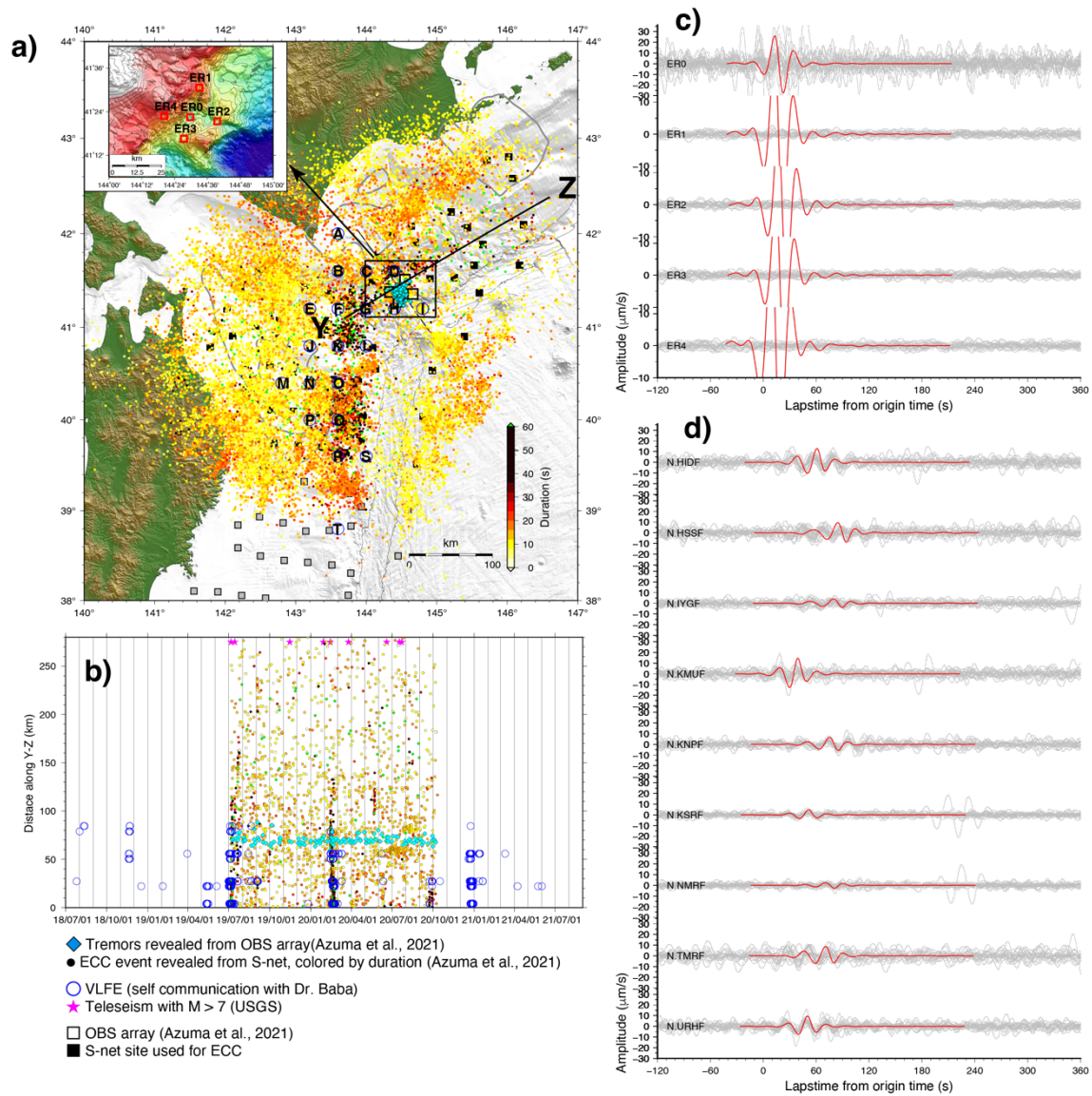


Fig. a) Map view of epicenters. Circle plots colored in duration include regular earthquakes and tectonic tremors detected by S-net. Cyan diamonds are tectonic tremors detected by the OBS array. Blue circles represent VLFs. b) Space-time plots of events along the Y-Z profile. c,d) Observed (gray) and synthetic (red) seismicogram of events at synthetic source C in the map.

Complexities in Earthquake Source Spectra Revealed by the Multiple Spectral Ratio Analyses

Takahiko Uchide¹

¹Geological Survey of Japan, AIST

Individual earthquakes have their own characteristics, which is often presented by earthquake source spectra. The stress drops inferred from the corner frequencies of source spectra and circular crack models have been well studied for investigating the self-similarity of earthquakes (e.g., Abercrombie, 1995; Ide and Beroza, 2001; Cocco et al., 2016) and the fault properties (e.g., Hardebeck and Aron, 2009; Uchide et al., 2014). The standard model for source spectra is the omega-square model (Aki, 1967; Brune, 1970; Boatwright, 1978). Recently, based on the development of the data analysis methods and seismic observation, the deviation of source spectra from the omega-square model has been evident (Denolle and Shearer, 2016; Uchide and Imanishi, 2016; Wu et al., 2019; Ji and Archuleta, 2020, 2022).

Earthquake source spectral studies (and also other seismological data analyses for earthquake source studies in general) try to mute the seismic propagation (path) and site effects on seismograms and extract the source effects. The spectral ratio method (e.g., Berckhemer, 1962) is one of the ways. Taking the spectral ratio of seismograms from nearby earthquakes, we cancel the path and site effects and obtain the ratio of source spectra of the earthquakes. Uchide and Imanishi (2016) proposed the multiple spectral ratio method in which multiple events (EGF events) near a target event are used to reduce the uncertainties. They fitted the spectral ratios of the target event to individual EGF events and stacked the residual spectra. They interpreted that the stacked residual spectrum indicates the deviation from the omega-square model. They applied their method to M3 – 4 earthquakes in the northern Ibaraki prefecture and Fukushima-Hamadori area and found both the cases with and without clear deviations from the omega-square model.

In this study, I quantified the source complexities by applying the method of Uchide and Imanishi (2016) to the M3 – M4 earthquake in the entire Japan. I used the seismogram from Hi-net stations maintained by NIED. The target events are shallower than 20 km around the Japanese Islands, extracted from the NIED F-net Moment Tensor Catalog. I used five or more EGF events within 1 km from the target events.

I found the stacked residual spectra with various amplitudes. The histograms of the amplitudes for various areas show some variation, but the differences are not significant. The histogram is also similar to those for earthquakes in the Ridgecrest sequence in California. This suggests that the variation in the source complexities is not from an areal scale (~ 10 – 100 km) but from a smaller scale (~ km or even smaller), such as the complexities in the fault structure. The cause of the source complexities is still under investigation.

Acknowledgment

We used Hi-net data and F-net Moment Tensor Catalog from NIED. This research was supported by JSPS KAKENHI Grant Number JP21H05205 in Grant-in-Aid for Transformative Research Areas (A) “Science of Slow-to-Fast Earthquakes.”

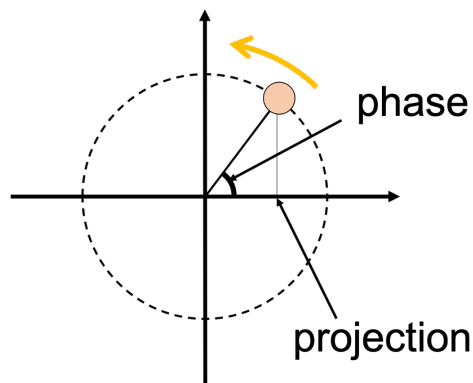
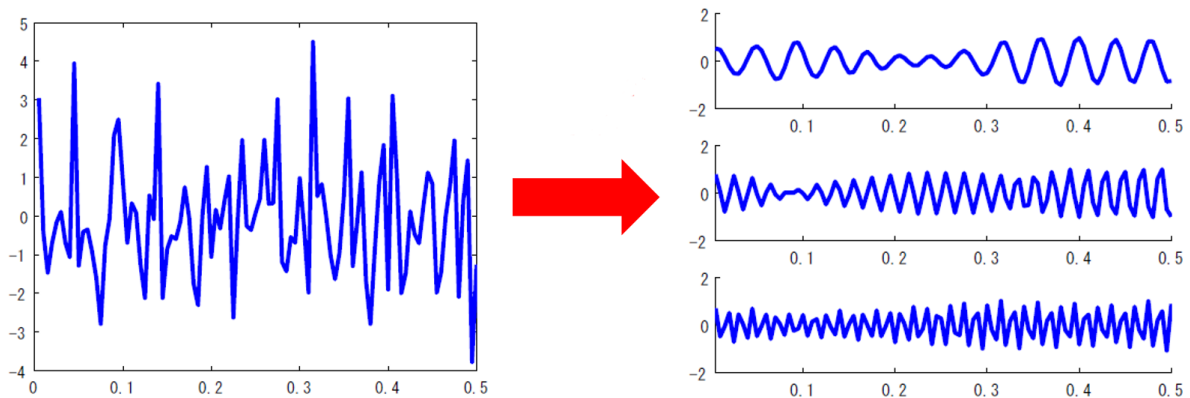
Data-driven decomposition of slow-to-fast earthquakes

Takeru Matsuda

RIKEN Center for Brain Science, Japan

Oscillator decomposition (OSC-DECOMP) is a Bayesian statistical method for extracting oscillators from time series data [1,2]. This method determines the number, frequencies and powers of oscillators in a data-driven manner and does not require arbitrary selection of band-pass filters. It is based on a Gaussian linear state space model that describes several oscillators underlying time series data. Time series decomposition is obtained by using empirical Bayes method with Kalman smoother, and the number of oscillators is determined by minimizing Akaike Bayes Information Criterion (ABIC).

We will present some preliminary results on application of OSC-DECOMP for data-driven decomposition of slow-to-fast earthquakes.



References

- [1] T. Matsuda and F. Komaki. Time series decomposition into oscillation components and phase estimation. *Neural Computation*, 29, 332--367, 2017.
- [2] T. Matsuda and F. Komaki. Multivariate time series decomposition into oscillation components. *Neural Computation*, 29, 2055--2075, 2017.

Cluster formation of particles found in mixtures of viscoelastic fluids and particles under shear stress as an analog experiment for the spatio-temporal distribution of slow earthquakes and melange formation.

Rinya MIYAKAWA, Kota KAMIJO and Yutaka SUMINO

Department of Applied Physics, Tokyo University of Science, Japan

Slow earthquakes are thought to occur in a marginal region of the subducting plate between an aseismic steady sliding zone and a rigidly fixed seismogenic zone. In this marginal region, plastic flow and localized brittle fracture should be spatially coupled and exhibit dynamic self-organization. Such a dynamic pattern should have a significant impact on the dynamics of slow earthquakes. Indeed, many studies try to infer dynamics at a plate boundary by analyzing the created patterns in minerals and rocks. Unfortunately, in situ observation of such dynamics is difficult not only because of their large temporal and spatial scales but also because the location to occur is deep underground. Therefore, this study aims to reproduce rocks near slow-slip events using a mixture of rigid unreformable particles and a ductile viscoelastic fluid. With an analog experiment, we aim to reveal the spatio-temporal patterns observed during slow earthquakes.

Viscoelastic fluids with transient networks are known to behave as Maxwell fluids with a single relaxation time [1]. A sample with a single relaxation time shows a steep change in a response from viscous to elastic when the shear rate exceeds the inverse of the viscoelastic relaxation time. Dispersing particles in such a sample would be expected to produce a difference in the local viscoelastic response, and the various spatio-temporal pattern would emerge. In fact, previous studies have shown that the particles align in a linear fashion when a sample of spherical particles dispersed in a viscoelastic fluid is subjected to reciprocal shear [2]. However, the mechanism has not been clarified. In this study, we constructed a system in which particles are dispersed in a viscoelastic fluid, and shear is applied continuously at a constant rate, aiming to reproduce the linear alignment and clarify the mechanism.

In the experiment, we used a viscoelastic fluid made of oil-in-water microemulsions cross-linked with a telechelic polymer were used. The relaxation time of the viscoelastic fluid used was $\tau = 5.1 \times 10^{-2}$ s. The sample consists of the viscoelastic fluid mixed with zircon beads of diameter $\phi = 0.7$ mm with a volume ratio of 6:1. The experimental setup is shown in Fig. 1, where the distance between the two disks is set to $h = 1$ mm, the 7 mL of sample is introduced into the gap, and the lower disk is rotated at a constant angular velocity Ω . If the distance from the center of rotation is R , the shear rate given to the sample is $\dot{\gamma} = R\Omega/h$. On the other hand, since the particles mixed in the sample are not deformed, the gap between the disks is effectively small in the vicinity of the particles. As a result, the effective shear rate near the particles is $\dot{\gamma} = R\Omega/(h - \phi)$. The differences in viscoelastic response are defined by the dimensionless quantity Weissenberg number $Wi (= \tau\dot{\gamma})$, with $Wi < 1$ indicating viscous behavior and $Wi > 1$ indicating elastic behavior. In this

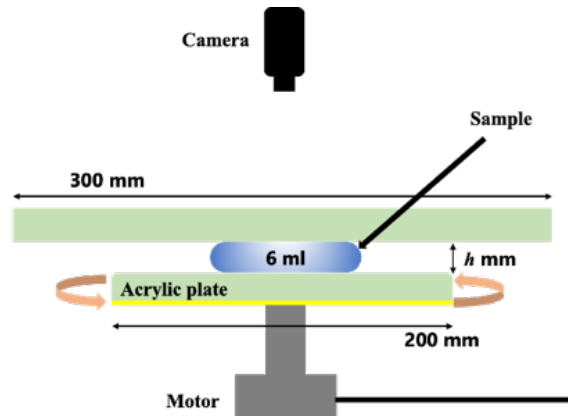


Fig. 1: Schematics of experimental system

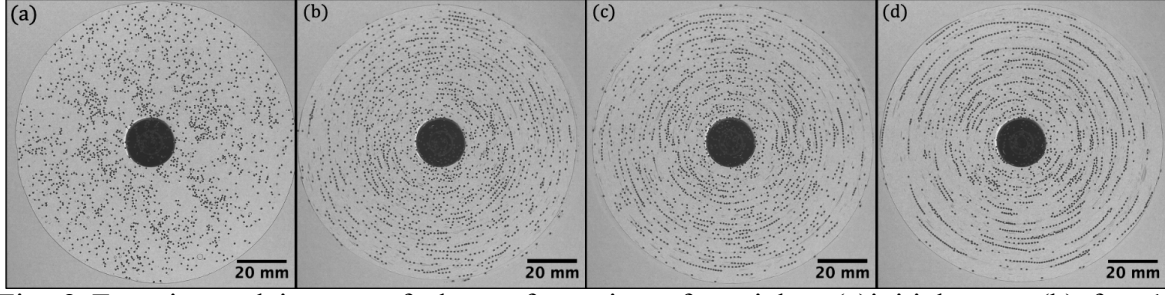


Fig. 2 Experimental images of cluster formation of particles. (a)initial state, (b)after 1 rotation. (c)after 2 rotations. (d)after 5 rotations Scale bars represent 20 mm.

experiment, the rotational angular velocity of the disk, Ω , was used as the control parameter.

Fig. 2 shows the results at $\Omega = \pi/15$ rad/s. Cluster formation was observed, in which randomly dispersed particles in the sample were aligned in the shear direction with rotation. Experiments at different rotation speeds confirmed that cluster formation was observed only under conditions where $Wi = R\omega\tau/h < 1$ in the absence of particles and $Wi = R\omega\tau/(h - \phi) > 1$ in the vicinity of particles.

To elucidate the mechanism of cluster formation, we measured the angular velocity of each particle ω while the number of the particle was reduced so as to observe independent particles without interaction between them (Fig. 3). In the measurement at low rotational speeds ($\Omega = \pi/30$ rad/s), where no cluster formation is observed, the dispersion of the angular velocity of each particle was found to be small, and the particles were found to move at a rotational speed of approximately Ω of the lower plate. On the other hand, at the rotational speed at which cluster formation occurs ($\Omega = \pi/15$ rad/s), the average angular velocity is about half of the rotational speed of the lower plate, Ω , and the angular velocity dispersion is large. In the region where the angular velocity dispersion is large, the velocity of the particles oscillates between the two states with high and low angular velocity.

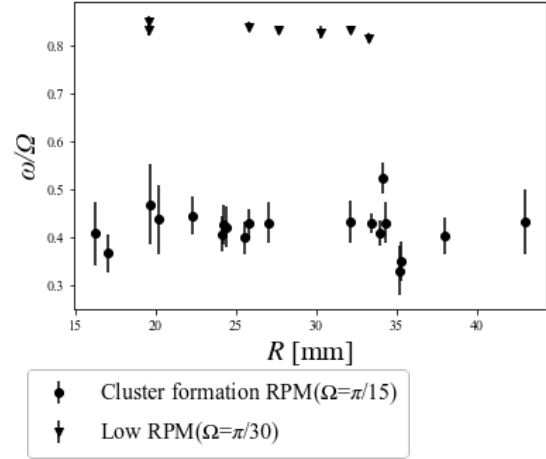


Fig. 3 Normalized angular velocity ω/Ω and its radial position R for each particle. Symbols \circ and ∇ corresponds data obtained from $\Omega = \pi/15$ rad/s and, $\Omega = \pi/30$ rad/s respectively. Error bars represent \pm standard deviation.

References

- [1] Michel, E. et al., *Langmuir*, **16**, 8702-8711 (2000).
- [2] Won, D. and Kim, C., *J. Non-Newtonian Fluid Mech.* **117**, 141–146 (2004).
- [3] Filali, M. et al., *J. Phys. B*, **103**, 7293-7301 (1999).

Analog experiment of slow to fast earthquakes using viscoelastic fluid: fractures promoted by external shear strain

Yuki Shinohara, Hiroki Maeda, Yutaka Sumino

Dept. Applied Physics., Tokyo University Science

In this study, we try to create an analog experimental system in which external shear strain promotes the fracture formation of injected fluid. We paid special attention to having the analog system sustain repeating fracture formation to allow ones to peruse statistical analysis. Indeed, such a system would lead to analyzing the transition of slow to fast earthquakes in terms of the viscoelastic nature of subducting plates [1].

In similar analog experiments, there is a previous study in which shear is applied to a gel with a single relaxation time that undergoes brittle fracture as an experimental system that imitates the subduction zone [2]. This experiment focused on the shear-induced change in the slip behavior. Another study observed viscoelastic fracturing by injecting low-viscosity fluid into a Hele-Shaw cell filled with viscoelastic fluid [3]. When the injection rate is small, finger-like patterns known as viscous fingering are observed due to Saffman-Taylor instability [4]. In the case of the high injection rate, viscoelastic fracturing is observed. In this study, we tried to observe the transition from viscous fingering to viscoelastic fracturing by applying external shear strain. In addition, we tried to find the conditions where the fracturing is observed repeating manner.

We use a sample made of oil in water microemulsions cross-linked by telechelic polymers as a viscoelastic fluid [5]. The viscoelastic character is described by the Maxwell model with a single relaxation time, τ . Also, this sample shows brittle fracture when the applied shear rate exceeds $\dot{\gamma}_c = 1/\tau$.

Fig. 1 shows dynamic viscoelastic measurement of the sample used in this experiment. We get viscoelastic relaxation time $\tau = 3.97 \times 10^{-2}$ s by this result. In addition, the stress measurement under the steady shear rate (Fig. 2) shows steep decrease of shear stress which indicates brittle fracture when the shear rate exceeds $\dot{\gamma} = 1/\tau$.

The experimental system is composed of two parallel plates whose gap is 1 mm (Fig. 3). Here, the upper plate is fixed while the bottom one is connected to a motor to rotate. After a sample was introduced between the plates, we rotated the bottom plate with a fixed angular velocity ω . The sample is sheared with the shear rate $\dot{\gamma} = R\omega/h$, which depends on the radial position R from the center of the rotating disk. Thus, the

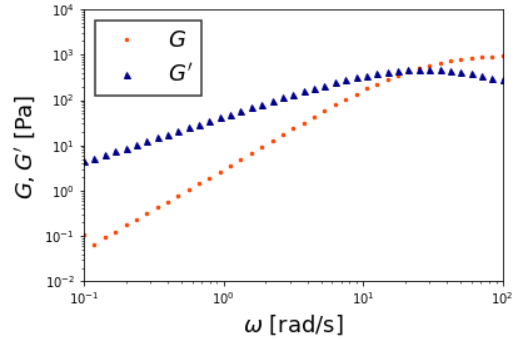


Fig. 1 Dynamic viscoelastic measurement of G' and G'' .

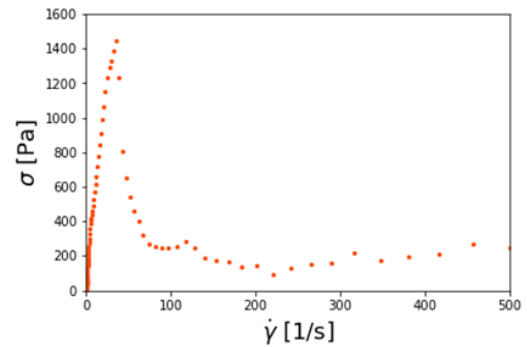


Fig. 2 Stress measurement under the steady shear rate.

Weissenberg number Wi depends on the distance from the central part of the parallel plates. In this experiment, we fixed angular velocity $\omega=20, 30, 40$ rpm to observe the area of fluidness transition. We then injected air at a fixed rate 100 mL/min from the central part of the fixed upper plate to promote fracturing. This air injection speed does not exceed the critical value to have viscoelastic fracturing in the absence of the external shear. We measured injected air pressure while the movies are taken.

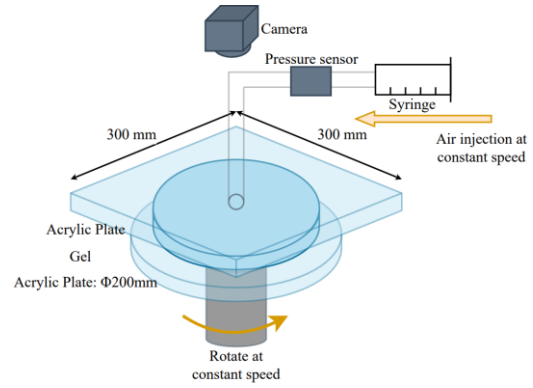


Fig. 3 Experimental setup.

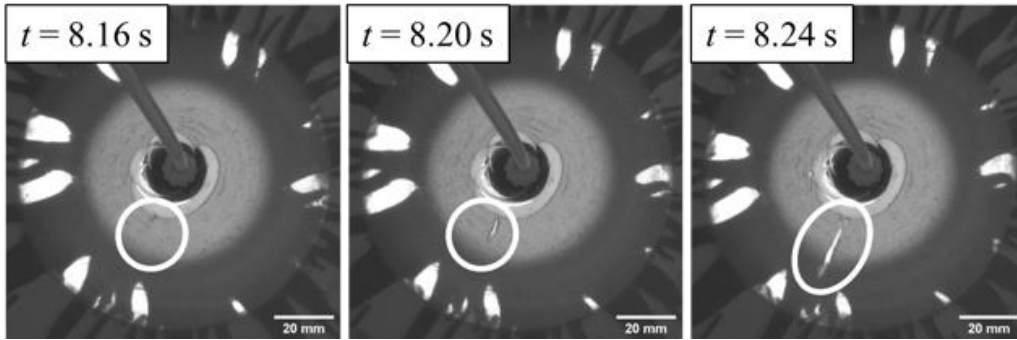


Fig. 4 Snapshots of crack propagation promoted by external shear strain. Crack is indicated by white circles.

Fig. 4 shows the typical result ($\omega=40$ rpm). The sample behaves like a viscous fluid near the air injection hole because the shear rate with small R is lower than $\dot{\gamma}_c$. Therefore, air spreads isotropically. However, the sample showed fracture formation by air where the shear rate exceeded $\dot{\gamma}_c$, indicated by white circles in Fig. 3. Interestingly, a crack was sealed due to the fluid nature of the sample. Therefore, we could observe the situation of crack propagation repeatedly.

Fig. 5 shows the injected air pressure P in the situation of repeated crack propagation. When the air spreads at the central part, the pressure gradually increases while the pressure decreases rapidly when a crack propagates.

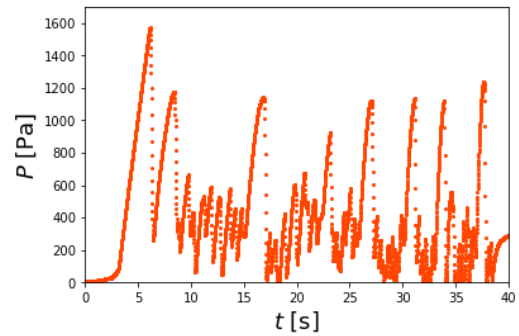


Fig. 5 Temporal change in injected air pressure.

References

- [1] K. Obara and A. Kato, Science 353, 253-257(2016).
- [2] A. Namiki et al., J. Geophys. Res. 119, 3169-3181(2014).
- [3] E. Lemaire et al., Phys. Rev. Lett. 67, 2009-2012(1991).
- [4] G. M. Homsy, Annu. Rev. Fluid Mech. 19, 271-311(1987).
- [5] M. Filali et al., J. Phys. Chem. B 103, 7293-7301(1999).

Pattern formation during fluid injection into highly water absorbent granular media

Kojiro Otoguro¹, Kiwamu Yoshii², and Yutaka Sumino¹

¹Dept. of Appl. Phys., Tokyo Univ. of Sci., ²Grad. Sch. of Eng. Sci., Osaka Univ.

Water in the subducting plate influences the occurrence of slow earthquakes. In the shallow subduction zone, water is supplied by the chemical dehydration of plates at the deeper region. Such supplied water triggers slip due to reduced friction by lubrication and the reduced effective normal stress by enhanced pore fluid pressure. The migration of water is thus an essential process for slow slip events. A previous study reveals that water permeability in quartz gouge, an analog of the plate boundary, decreases with time while water penetrates [1]. This fact suggests that water flow can create complex spatial patterns induced by the permeability reduction of the medium. To illustrate such a possibility, here we conducted an analog experiment where a fluid is injected into a porous medium whose permeability decreases as it contacts with the injected fluid.

As a porous medium with variation in permeability, we used the water-absorbent ionic gel particles composed of sodium polyacrylate whose medium particle size is 350 μm . These gel particles can swell 1000 times in volume when immersed in pure water. The swelling capability of ionic gel particles is derived from the osmotic pressure caused by the ionic concentration difference between the interior and exterior of the particles immersed in an aqueous phase. Thus, the swelling rate can be reduced by adding ionic salt to an aqueous phase [2]. We measured the swelling rate of the particles immersed in the sodium chloride solution whose concentration C was varied from 0 wt.% to 20 wt.%. The swelling rate of the particles where $C = 0$ wt.% increased 20 times as that where $C = 20$ wt.%.

We used a thin 2-dimensional cell that is constructed with acrylic plates whose gap is 1 mm Fig.1(a). The gel particles were introduced into the cell and densely packed by tapping the cell a dozen times. We placed glass beads near the inlet to avoid clogging before the injection process started. Then, sodium chloride solution was injected into the cell at a constant injection rate from the syringe pump. During the injection, we captured images of the fluid front and measured the injection pressure. A schematic illustration of the experimental setup is shown in Fig.1(b). We changed the injection rate I and concentration of injected fluid C , and obtained

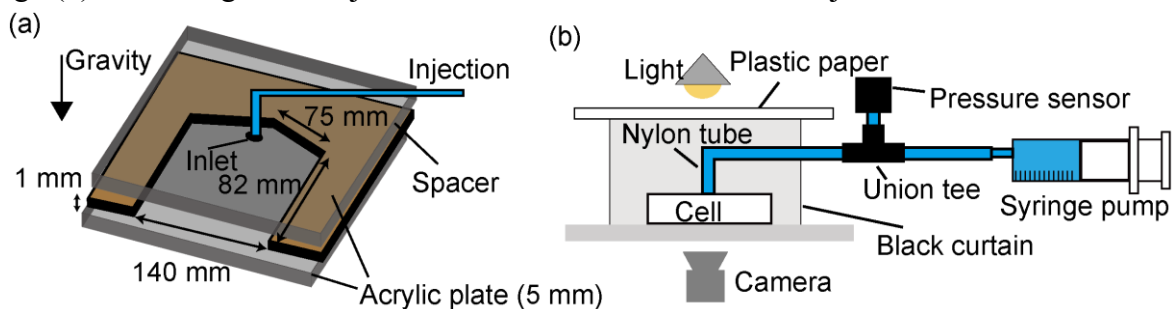


Fig.1 (a)Setup of a thin 2-dimensional cell whose gap was set on 1 mm. (b)Schematic illustration of experimental setup. The inner fluid was injected with syringe pump.

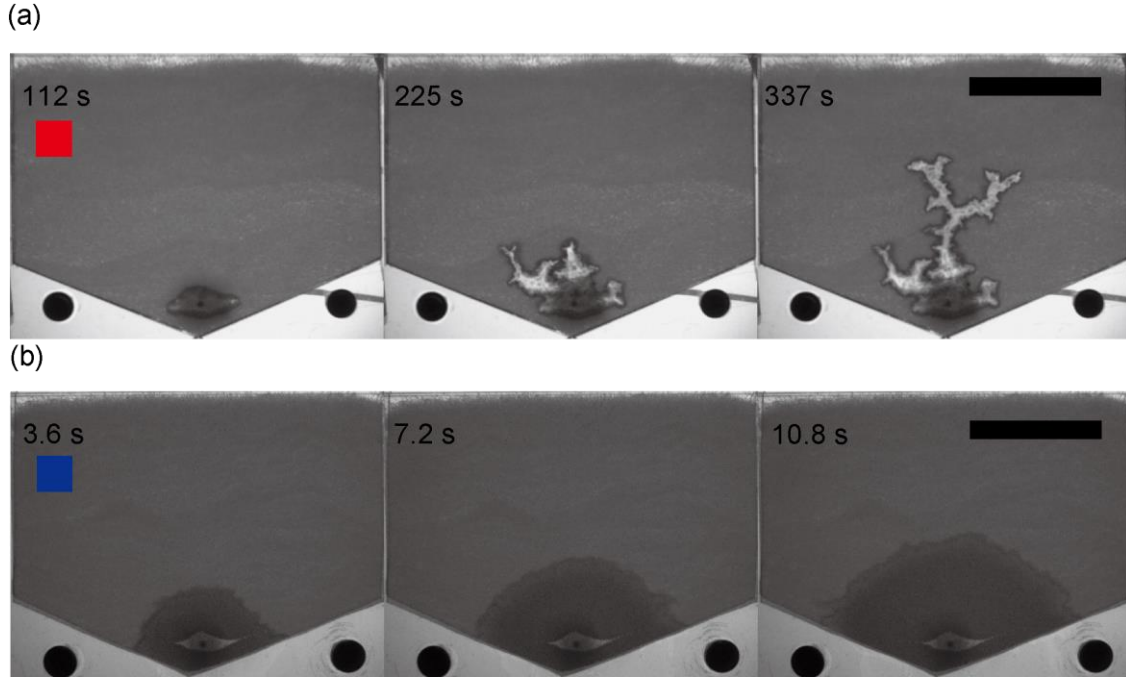


Fig.2 (a) Snapshot of branch pattern growth where $C = 0$ wt.%, $I = 0.32$ mL/min. (b) Snapshot of penetration pattern growth where $C = 20$ wt.%, $I = 10$ mL/min. Scale bars indicate 50 mm.

two typical propagation patterns of the injection front. I was varied from 0.1 to 32 mL/min. and C was varied from 0 wt.% to 20 wt.%.

We show the results of the injection up to 1.8 mL where $C = 0$ wt.%, $I = 0.32$ mL/min. and $C = 20$ wt.%, $I = 10$ mL/min. in Fig.2(a) and (b) respectively. In the dark areas of the images, only dry particles exist. The darker and brighter areas of the images are the areas immersed with the fluid. In the bright areas, immersed particles were well swollen and became transparent. For low I and C , the fluid flow was interrupted by swollen particles and injection front branched (shown in Fig.2(a)). For high I and C , the injected fluid penetrated isotropically (shown in Fig.2(b)). We discovered that the transition of fluid propagation pattern depends on the ratio of the characteristic timescale of swelling and flow. Temporal variation in pressure characterizes these different injection behaviors. For the branching pattern, injection pressure increased initially and then decreased as a general trend with repeating small oscillation (Fig. 3(a)). The sealing of the flow path due to swelling of particles and crack formation in the particle bed causes these small oscillations. For the penetration pattern (Fig. 3(b)), injection pressure was small and a steady increase was noted during the measurement.

In the poster presentation, we would discuss the more detailed comparison of pressure data.

[1] S. B. Giger, et al., *J. Geophys. Res.* **111**, (2006).

[2] I. Ohmine and T. Tanaka, *J. Chem. Phys.* **77**, 5725-5729 (1982).

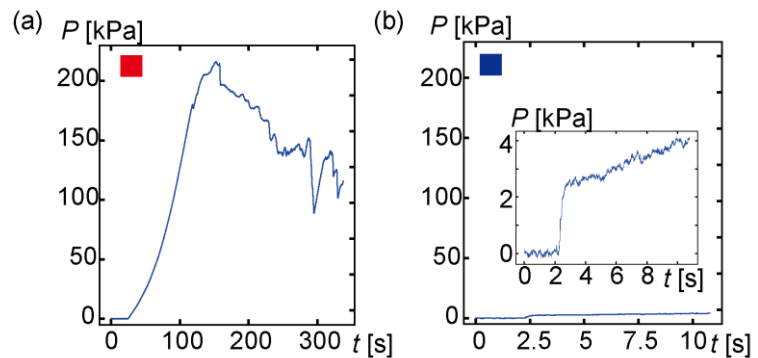


Fig.3 (a) and (b) show pressure evolution as a function of time, corresponding to Fig.2(a) and Fig.2(b) respectively. Inset of (b) is enlarged graph.

Adjoint tomography of an accretionary wedge and shallow slow-slip regions in the North Island of New Zealand

Shun Adachi¹, Bryant Chow², Yoshihiro Kaneko¹

¹Kyoto University, ²University of Alaska Fairbanks

The Hikurangi subduction zone in the North Island of New Zealand hosts repeating slow-slip events, a thick accretionary wedge, subducted seamounts, and a fully-locked plate interface that is capable of generating megathrust earthquakes. Recently, Chow et al. (2022a,b) undertook the first application of earthquake-based adjoint tomography of the Hikurangi subduction zone and imaged two high-velocity anomalies below the East Coast of the North Island, which have been interpreted as previously unidentified, deeply subducted seamounts. The presence of these seamounts is supported by independent evidence including seafloor bathymetry data and the presence of nearby geophysical anomalies. They are also linked with spatial variations in slip behavior observed along the Hikurangi subduction margin. In this tomographic study, we extend the domain of Chow et al. (2022a,b) 400 km to the northeast to include the 2017-2018 IODP (International Ocean Discovery Program) drill sites (Barnes et al., 2020), the 2021 M7.3 East Cape earthquake (Okuwaki et al., 2021), offshore seamounts identified by active source seismics (Bell et al., 2010) and a thick low-velocity wedge in the northern margin (Kaneko et al., 2019). Using 60 geographically well-distributed events recorded by 88 permanent and temporary broadband stations, we perform iterative model updates using spectral element and adjoint simulations to fit waveforms with periods ranging from 6 – 30 s. We present ongoing efforts towards imaging and understanding the accretionary wedge of the Hikurangi subduction zone and its link to spatial variations in megathrust slip behavior.

Development of classification methods for tectonic tremor, earthquake and noise using deep learning

Amane Sugii¹, Yoshihiro Hiramatsu¹, Takahiko Uchide², Kazutoshi Imanishi²,

¹Kanazawa Univ., ²AIST

Tectonic tremors (hereinafter referred to as tremors), which have a dominant frequency of 1 to 10 Hz and a duration of several minutes to several hours, have been observed in subduction zones around the world and occur at depths of approximately 30 to 40 km in the Philippine Sea plate subducting from the Nankai Trough. The envelope correlation method (Obara, 2002) and semblance analysis (Neidell and Taner, 1971) are known as automatic detection methods for tremors. However, these methods often detect not only tremors but also earthquakes and noises, requiring visual inspection.

To avoid misdetection of tremors, Nakano et al. (2019) developed a classification method between tremors, earthquakes, and noises using deep learning from DONET seismic waveform data, showing that each event could be classified with high accuracy for their test data. Takahashi et al. (2021) proposed a neural network model similar to Nakano et al. (2019), trained it using S-net data, and succeeded in the classification. However, it is not clear which parameters in the deep learning model play an important role in the classification. In other words, it is more difficult to know the criteria of the classification by deep learning than conventional methods such as the envelope correlation method. Furthermore, Nakano et al. (2019) found that teleseismic earthquakes are possibly misclassified as tremors. Therefore, this study aims to develop a deep learning model to classify tremors, earthquakes (including teleseismic earthquakes), and noises, and to clarify the reason why the networks make specific decisions.

We used waveform data recorded by the array observation network installed by AIST in the northern Kii Peninsula, Japan. We made spectrogram images from waveform data with two minutes duration and used those as input data. Each spectrogram image was created with a window width of 5 seconds, an overlap of 80%, and a linear frequency axis. The model consists of two convolutional layers and three fully connected layers, and the convolutional and fully connected layers are coupled by the Global Average Pooling layer. Takahashi et al. (2021) reported that training on data with high noise levels reduced the accuracy of the detection of tremor. Therefore, we screened the data based on the noise level and used 37800 images as training data. As a result of training, 99.3 % accuracy was confirmed for 3150 test images with clear features of each event. Setting a lower limit for the velocity spectra on the images improved the accuracy. Furthermore, ScoreCam (Wang et al. 2019) was applied to show what contributed to the model's decision, indicating that the trained model captured the features of each event, such as the frequency range of tremors, P- and S-waves of earthquakes, and sparse spectral value of noises. This result indicates that this model is suitable as a classification method between noises, tremors, and earthquakes. Applying the model to non-screened data, the accuracy of the classification reaches 85.2 % for earthquakes and 78.6 % for tremors. For earthquakes, we recognize that a lack of high-frequency components causes misclassification. Therefore, we could not correctly classified teleseismic events as earthquakes. In this presentation, we will also report the results of a case that includes teleseismic earthquakes in the category of regular earthquakes and a case that integrates three-component images as one image.

A thermal event detected in a cataclastic seismogenic fault using paleomagnetic methods.

Taizo Uchida¹, Yoshitaka Hashimoto¹

¹Kochi University

Paleomagnetism on fault zones will provide evidence to discuss deformations using paleomagnetic orientations and thermal events, such as frictional heating, using thermoremanent magnetization. We examined deformation history and thermal event on a fossil seismogenic fault zone in an exhumed accretionary complex, the Yokonami mélange in the Cretaceous Shimanto Belt, Southwest Japan. The fault zone is located at the northern end of the Yokonami mélange close to a coherent unit in the North. The rocks around the fault zone were classified into three; host rock mélange, cataclasite with pseudotachylyte, and sandstone in a coherent unit adjacent to the Yokonami mélange. Based on vitrinite reflectance, the paleo-maximum temperature was reported around 250 ± 30 °C. We have performed thermal and alternating field demagnetization experiments on these rocks.

Blocking temperatures obtained from the thermal demagnetization experiments is expected to indicate the maximum temperature at a re-heating event if there is in a case. In the results of experiments, the blocking temperature, which could be related to a re-heating event, of 300-350°C higher than 250 ± 30 °C was identified only in cataclasite. At the temperature, the direction of remanent magnetization changed from NE to SW with a counterclockwise rotation. The paleo-maximum temperature within the cataclasite was estimated to be about 324°C using grain size of a dynamic recrystallization in a previous study. This is also higher than the paleo-maximum temperature from Vitrinite reflectance. And our results from the thermal demagnetization experiments are also consistent with the higher temperature in the cataclasite. Accordingly, we interpret that the cataclasite have a thermoremanent magnetization with change in paleomagnetic direction when this seismic fault activated, which suggests the high temperature was caused by a frictional heating.

Normally magnetic direction is useful to discuss about a regional tectonic rotation with age. It is, however, challenging to use the magnetic direction in the strongly deformed mélange zone and cataclastic seismogenic fault. We will carefully examine the magnetic direction with considerations both regional tectonic history and local deformations.

Geological constraints on dynamic changes of fluid pressure in seismic cycles

Takahiro Hosokawa¹, Yoshitaka Hashimoto¹

¹Dept. Global Environment and Disaster Prevention, Kochi University

Fluid pressure along faults plays a significant role in fault behaviors in seismic cycles in subduction zones. When a thermal pressurization event occurs, the fluid pressure rises; conversely, when a fault-valve behavior event occurs, the fluid pressure falls. The two models have different time scales and may coexist in an event. Therefore, the purpose of this study is to quantify the change in fluid pressure from a natural fault zone, focusing on the underplating thrust zone accompanied with extension veins in the Mugi *mélange*, the Cretaceous Shimanto Belt, SW Japan.

Mugi *mélange* is a underplating accretionary prism. The faults in this study are fault zones consisting mainly of basalt rocks that steeply slope south or north in an east-northeast strike and are thought to be related to underplating. In the *mélange* just above the fault zone, the extension veins cutting the *mélange* structures show a network texture. The network veins cut each other, suggesting that the development of the mineral veins was repeated in multiple stages.

The dike method was applied to the mineral veins to estimate paleo-stress state and driving fluid pressure ratio (P^*). P^* is defined as the maximum fluid overpressure normalized by differential stress. The results of stress analysis and outcrop observation indicated that the mineral veins recorded stress exchanges with seismic cycles between reverse to normal fault stress regimes.

We constrained the tensile strength and depth to be 6.94-9.38 MPa and 5.14-5.33 km, using P^* and the fluid pressure from fluid inclusions from previous study. We also constrained the dynamic fluid pressure increase from the minimum fluid pressure predicted from the rock failure theory to be 6.7-9.0 MPa and 8.3-11.3 MPa in reverse and normal fault stress regimes. In the cases, fluid pressure ratio for each regime is equivalent to 1.1 and 0.9, respectively. The fluid pressure increase in the reverse fault stress regime could be a dynamic phenomenon because the estimated fluid pressure exceeds over lithostatic pressure, which cannot be a stable condition. The fluid pressure decreased in the normal fault stress regime. The changes in fluid pressure were described with the stress regimes related to seismic cycles.

We constrained the dynamic change in fluid pressure quantitatively in seismic cycles. To fully evaluate fluid pressure fluctuations in the fault zones, investigations on shear veins and hybrid extensional shear veins are needed to be conducted.

Observation of slow earthquakes by distributed acoustic sensing off Cape Muroto, southwest Japan

Satoru Baba¹, Eiichiro Araki¹, Yojiro Yamamoto¹, Yasuyuki Nakamura¹, Gou Fujie¹, Takane Hori¹, Hiroyuki Matsumoto¹, Shuhei Nishida¹, and Takashi Yokobiki¹

¹JAMSTEC

We first observed tectonic tremors, a type of slow earthquake, by distributed acoustic sensing (DAS) observation, which uses a fiber-optic cable as a strain sensor. The DAS observation allows us more spatially high-density observation than seismometers; therefore, DAS is widely used for seismic observations recently. Off Cape Muroto, a part of the coseismic slip area of the 1946 Nankai earthquake ($M_w \sim 8$), a real-time DAS observation is conducted by AP Sensing with a fiber length of ~ 55 km from January 2022. In this area, shallow slow earthquakes are observed in the updip of the coseismic slip area. Because the relationship between slow and megathrust earthquakes is pointed out, locating slow earthquakes with a high resolution is required to investigate the tectonic environment of slow earthquake activity. In this study, we observed and located tectonic tremors off Cape Muroto by using DAS and the Dense Oceanfloor Network system for Earthquake and Tsunami (DONET) data.

Approximately 30 tremors were observed by the DAS observation in a frequency range of 2–8 Hz from January 30, 2022, to February 8, 2022. The signals of these tremors were widely observed in broadband seismograms of DONET stations. The duration of tremor signals observed in the DAS channels (40–60 s) is longer than that observed in DONET stations (~ 30 s). In detail, tremor signals observed in the DAS channel are composed of several phases with a variable apparent velocity. These phases are coherent within a distance of 50–100 m.

We located tremors observed by DAS channels by using the envelope waveforms of DAS channels and broadband seismograms of DONET stations in a frequency range of 2–8 Hz. We manually picked the onset of the tremor signals and located the events at the point where the residual between synthetic and observed arrival times is the least by the grid search. Most of the tremors were located around 134.7°E , 32.8°N , northeast of the G-node of DONET. This area is south of the Tosa-bae basin and corresponds to the updip of the subducted seamount peak (Nakamura et al., 2022). As indicated in previous studies (e.g., Toh et al., 2020; Sun et al., 2020), the spatial relationship between slow earthquakes and a seamount is suggested in this region. In a frequency range of 0.02–0.05 Hz of broadband seismograms of DONET stations, the signals of very low frequency earthquakes (VLFs) are found at the time of detected tremors by DAS. In this presentation, we discuss the spatiotemporal correlation of tremors and VLFs in this region.

Quality of S-net seafloor pressure data in geodetic frequency band

Ryota Hino¹, Tatsuya Kubota², Naotaka Y. Chikasada², Yusaku Ohta¹, Hideto Otsuka¹

¹Tohoku Univ., ²NIED

Long-term continuous observation of seafloor pressure is effective for detecting seafloor vertical deformations associated with transient tectonic phenomena such as slow slip events. A series of seafloor motions before and after the 2011 Tohoku earthquake were detected by seafloor pressure observations and played significant roles in constraining the distributions of slow to fast fault motions preceded the M-9 mainshock. In this paper, we inspect the quality of seafloor pressure data obtained by Seafloor observation network for earthquakes and tsunamis along the Japan Trench (S-net) in view of seafloor geodesy. The characteristics of continuous seafloor pressure records at all the 150 stations were examined by comparing the records obtained by more than 100 deployments of autonomous ocean bottom pressure recorders (OBPRs) along the Japan Trench. It turns out that most of the S-net records are much noisier than the OBPR records in a period range of longer than 50 hours.

There are two main types of noise found in S-net station records. One is fluctuation in the period range of more than 1000 hours, but its behavior varies from one station to another, and it is difficult to identify the cause and invent an idea to reduce it. This long-term instability of unknown reasons hinders detection of long-term slow slip events. The other type of noise is caused by the strong correlation of pressure data with temperature. This temperature noise occurs over a wide periodic range. When the temperature-dependent fluctuation component was estimated by adaptive filtering and removed from the original data, a significant reduction in noise level was observed at many stations. After removing the temperature noise, the S-net pressure data showed common mode noise of a few hPa in amplitude, caused by non-tidal oceanic fluctuations. The common mode noise can be reduced by applying principal component analysis.

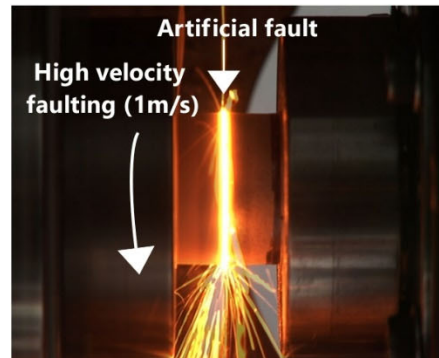
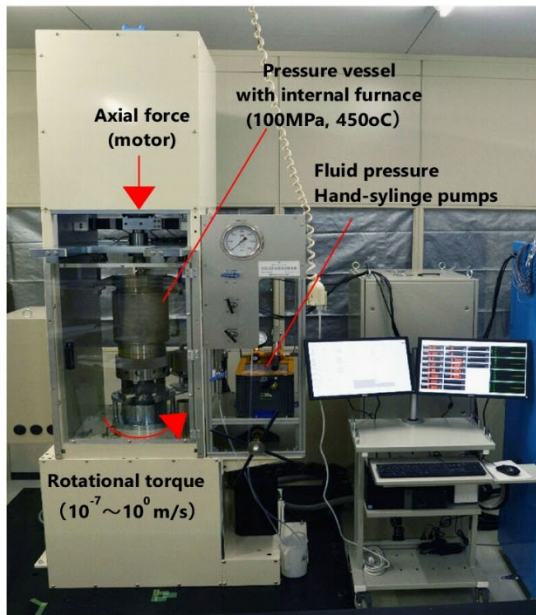
As a result of these noise reduction procedures, we were able to obtain continuous seafloor pressure records at ~ 50 stations with noise levels two to three times larger than those by the OBPR, in periods shorter than 1000 hours. According to previous studies, the discrimination threshold for slow slip events on the shallow part of the plate boundary, based on the OBPR observations in the Japan Trench, is M~6. Considering the higher noise level, S-net seafloor pressure observation can seafloor vertical displacement when there is a short-term slip event larger than M~6.3 in the immediate vicinity of the observation nodes. We have not detected any significant seafloor pressure changes that can be interpreted as being caused by tectonic transients, on the processed S-net pressure records so far.

Hydrothermal rotary-shearing apparatus in Kochi/JAMSTEC toward understanding slow to fast faulting processes

Takehiro Hirose¹, Wataru Tanikawa¹, Yohei Hamada¹, John Bedford¹, and Keishi Okazeki^{1,2}

¹JAMSTEC, ²Hiroshima Univ.,

Earthquakes involve a wide range of slip rates, from slow/aseismic to fast/seismic slip along faults. Thus, frictional properties of faults over wide slip rates (nm/s to m/s), in particular under hydrothermal conditions similar to those expected in seismogenic zones, are essential for a unified understanding of all earthquake events. A hydrothermal, low- to high-speed rotary-shearing apparatus has been installed at Kochi/JAMSTEC (see below), in order to study the fault constitutive properties at slow to fast slip rates and the physicochemical mechanisms underlying mechanical responses. The apparatus is currently capable of applying slip rates from 100 nm/s to 2 m/s, normal stress up to 55 MPa, fluid pressure up to 100 MPa and temperature up to 450°C with infinite displacement. We have been improving the apparatus to work as we intended. In pilot tests, we used quartz powder (~0.1 mm in size) as a starting material that is a major component of the Earth's crust. We will present our initial results, current problems and future research plans along with the basic design of the apparatus.



Reproduction of fast faulting in laboratory. Significant frictional heat inevitably generates at fast slip rates, leading to dynamic fault weakening.

Hydrothermal rotary-shearing apparatus in JAMSTEC. Slow to fast faulting processes can be reproduced under super-critical water conditions in the pressure vessel.

Periodic changes in activity pattern of short-term slow slip events in the northern Kii Peninsula, Japan

Hitoshi Hirose^{1,2,3}, Naoya Chujo^{2,†}, Takeshi Kimura³

¹RCUSS, Kobe Univ., ²Dept. Planetology, Kobe Univ., ³NIED, [†]Now at Takamatsu High Sch.

In the southwest Japan subduction zone, short-term slow slip events (S-SSEs) accompanying nonvolcanic tremor have repeatedly been observed. Because the S-SSEs occur on the deeper extension of the anticipated megathrust earthquakes source area, it is important to monitor the S-SSE activity for understanding the process of strain accumulation and release around the plate interface and the stress transfer to the megathrust area.

Long-term moment release history due to the S-SSEs has been discussed (e.g., Sekine et al., 2010; Nishimura et al., 2013), but it is difficult to know the difference in moment release history in local scale because many of these studies assume a rectangular source fault with uniform slip for an S-SSE. Hirose and Kimura (2020) estimated a number of slip distributions for S-SSEs in Shikoku based on National Research Institute for Earth Science and Disaster Resilience (NIED) Hi-net high-sensitivity accelerometer (tiltmeter) data for 18 years (2001-2019). They found the local scale segmentation in the S-SSE slip area in Shikoku and the activity is affected by nearby long-term SSEs. However, these difference of the S-SSE activity in local scale is unknown in the other areas than the Shikoku area.

Here we applied the inversion method of Hirose and Kimura (2020) to the tiltmeter data in the northern Kii Peninsula area to estimate slip distributions of the S-SSEs for 18 years (2002-2021) in order to discuss the difference in the S-SSE recurrence behavior in local scale. We also discuss the moment release history and a moving-averaged slip rate history at points on the plate interface.

We detected and analyzed 80 episode of the S-SSEs in the northern Kii Peninsula for the 18 years. The moment magnitude of the S-SSEs ranges from 5.3 to 6.3. We identified two segments of the activity, one is around Ise Bay and the other is around the Shima Peninsula. This means that a slip distribution of a particular S-SSE is localized on a single segment for most of the S-SSEs although there are some exceptions whose slip area extends to multiple segments.

The cumulative seismic moment versus time plot for all of the segments shows a large increase in the moment rate (a slope of the plot) around 2016-2018. This increase may be caused by a long-term SSE around the Shima Peninsula (Kobayashi and Tsuyuki, 2019). We identified at least four time periods that last for about a year with larger SSEs with longer recurrence interval. This long-term fluctuation in the moment release history can also be seen in the seismic

moment versus time plot and in the averaged slip rate history time-series. These time periods are characterized by an increase in the averaged slip rate and SSEs with larger seismic moment. This may indicate an intrinsic periodic nature of interplate slip observed along the Japan Trench (Uchida et al., 2016).

Acknowledgments

We are grateful to Sawako Teshiba for her valuable comments. Meteorological observation data were provided by Japan Meteorological Agency. Tremor catalog was provided by the NIED Hi-net group. This research was supported by JSPS KAKENHI Grant Number JP16H06474, JP21K03702, JP21H05206, and the MEXT Earthquake and Volcano Hazards Observation and Research Program.

We investigate temporal changes of seismic attenuation structure around an area where slow-slip events occur. Along the upper boundary of the subducting Philippine Sea plate in the southwestern part of Ibaraki Prefecture, slow-slip events occur periodically, and the rates of slow slip are estimated from activity of repeating earthquakes (for example, Uchida et al., 2016). Nakajima and Uchida (2018) proposed a model that drainage from the plate boundary to the overlying continental plate repeatedly occurs during each slow-slip event by temporal correlation between seismic activity and changes of P-wave attenuation. However, what is going on in the subducting plate prior to each slow-slip event is poorly understood. Therefore, we carried out following analyses. The first analysis is to estimate Q_{s-1} in the overlying plate, which was not estimated in Nakajima and Uchida (2018) and to compare quantitatively the temporal changes of Q_{p-1} and Q_{s-1} . The second analysis is the estimation of the temporal changes of seismic attenuation in the subducting slab immediately below low-slip events, which will provide a clue to understand a coupled, fluid-related process in the slab, plate interface, and overlying plate.

We investigated Q_{p-1} and Q_{s-1} in frequency ranges of 20-45Hz using spectral ratios for pairs of earthquakes that occurred in a period of 2009~2021. Waveforms of these earthquakes were recorded by eight seismometers of MeSO-net whose sampling frequencies are 200Hz. The dataset of hypocenters is taken from the earthquake catalog of the Japan Meteorological Agency and the repeater catalog of Igarashi (2020). We obtained three main results. The first result confirms that the annual temporal change between Q_{p-1} in the overlying plate and the occurrences of slow-slip event continues at least until 2019, which extended the result of Nakajima and Uchida (2018) by 4 years. The second result is a clear temporal change of Q_{s-1} in the overlying plate, where we observed an annual temporal of Q_{s-1} but attenuation is apparently lower than Q_{p-1} . This result may provide a strong constraint for better understanding of attenuation mechanism related to a fluid-induced process. The third result is the temporal changes of Q_{p-1} in the subducting slab, and it may represent a process of fluid accumulation in the slab by dehydration reactions prior to the occurrence of SSE along the plate interface.

Why do Gutenberg-Richter b-values decrease with time prior to large earthquakes? Insights from rate-and-state earthquake cycle simulations with frictional heterogeneities

Ryo Ito¹, Yoshihiro Kaneko¹

¹Graduate School of Science, Kyoto University, Japan

Understanding the mechanism of foreshock generation is an important issue for earthquake forecasting as well as our fundamental understanding of earthquake physics. Observations of seismicity prior to large earthquakes show that a slope of Gutenberg-Richter magnitude-frequency relations, known as a b-value, often decreases with time before the occurrence of a large earthquake. For example, Nanjo et al. (2012) reported that b-values in the hypocentral region of the 2011 Mw9.0 Tohoku-Oki earthquake had decreased prior to the mainshock. Yet, interpreting observed temporal changes of b-values remains challenging. Here we use numerical simulations of earthquake cycles with frictional heterogeneities and attempt to simulate the temporal variations of b-value. We first identify a parameter regime in which the model gives rise to an accelerating foreshock behavior prior to the mainshock. We then focus on the spatio-temporal pattern of foreshocks. We find that, like in observations, a complex pattern of migrating foreshocks can be seen in this model. Next, we analyze the resulting foreshock statistics and find that the b-values decrease with time prior to the mainshock. In this case, increased shear stresses within the creeping (or velocity-strengthening) patches due to numerous foreshocks makes these patches more susceptible to future co-seismic slip, increasing the likelihood of large ruptures and resulting in smaller b-values with time. Interestingly, our model shows that the average shear stresses over the entire fault are nearly constant with time during the accelerating foreshocks. From this result, we conclude that a potential physical explanation for a temporal decrease in b-values is an increasing level of shear stresses in stably-slipping regions that make the regions more susceptible to co-seismic slip, leading to larger foreshocks.

Experimental evidence for rapid fault healing after seismic slip

John D. Bedford^{1*}, Takehiro Hirose¹ and Yohei Hamada¹

¹JAMSTEC (Kochi Institute for Core Sample Research)

Fault strength recovery (healing) following an earthquake is a key process in controlling the recurrence of future events; however, the rates and mechanisms of fault healing are poorly constrained. Here, by performing high-velocity friction experiments, we show that granite and gabbro fault gouges recover their strength rapidly after experiencing dynamic weakening during shearing at seismic slip velocities. The healing rates are two orders of magnitude faster than those observed in typical frictional healing experiments performed at micrometer-per-second slip velocities. Analysis of the sheared gouges using Raman spectroscopy suggests that enhanced healing after seismic slip is associated with thermally activated chemical bonding at frictional contacts in the gouge. Our experimental results support geophysical evidence of faults regaining their strength early during interseismic periods following large earthquakes, indicating that earthquake recurrence may be more strongly controlled by other processes, such as far-field tectonic loading or frictional stability transitions during the seismic cycle.

Heterogeneous interseismic coupling and aseismic slip event along the Peruvian subduction zone

Villegas-Lanza Juan¹, Chlieh Mohamed², Nocquet Jean², Tavera Hernando¹, Pulido Nelson³.

¹Geophysical Institute of Peru (IGP), ²Institut de Recherche pour le Developpement (IRD),

³National Research Institute for Earth Science and Disaster Resilience (NIED).

The rapid subduction of the oceanic Nazca plate beneath the continental South American plate results typically in elastic stress accumulation along the plate interface that produces moderate to large earthquakes, and permanent deformation of the overriding plate. The 2200 km-long Peruvian subduction margin (Lat. 3°S to 19°S), shows a diverse behavior. The earthquake history for this area that dates back to the XVI century (Dorbath, et al., 1990; Nishenko, 1991), shows that in southern and central Peru (Lat. 10°S to 19°S) large earthquakes ($M \geq 8.0$) occurred with an approximate recurrence interval of 150 to 200 years (Dorbath et al., 1990). In contrast, in the northern Peru subduction segment no large earthquake ($M \geq 8$) has been reported so far. The northern segment is characterized by hosting moderate magnitude tsunami-earthquakes (≤ 7.6), such as the 1960 near Piura and the 1996 near Chimbote events (Pelayo and Weins, 1990, Ihmle et al., 1998). Geodetic GPS measurements of crustal deformation made during the past decade in the Peruvian subduction margin show a heterogeneous deformation velocity field. In south and central Peru, the deformation rates along the coast vary between 12 to 21 mm/yr in the direction of the convergence, showing lateral variations and systematic decreasing inland. In contrast in north Peru, GPS velocities show a systematic 5 mm/yr displacement in a southeast direction with little internal deformation; this behavior is consistent with the hypothesis of rigid movement of a tectonic block that involve the forearc including the trench up to the western cordillera extending southward to the Altiplano. The inversion of the static GPS velocities allowed obtaining models of interseismic coupling (ISC), that reflect three areas with strong ISC. These areas are located in: (1) the central Peru subduction zone, extending from Barranca to Pisco (>400 km long along strike); (2) offshore the Nazca city (~ 150 km); and, (3) the southern Peru subduction zone, from Moquegua to northern Chile (>150 km). In the subduction of northern Peru, we observe a completely different behavior, the model shows a weak to null ISC, with small and sparse weakly coupled asperities. Nevertheless, in 2009 a seismicity swarm accompanied by an aseismic slip near Lat. 5°S were detected; this event lasted around 7 months allowing to relax equivalent seismic moment to an earthquake of 6.7 Mw. These results are consistent with the earthquake history of the Peruvian subduction margin. The southern areas have not experienced a major earthquake since about 100 to 150 years. Similarly, in the central Peru area no megathrust earthquakes occurred since 1746 ($M 8.8$), therefore, currently there is a high seismic potential to produce larges earthquakes. Here we present a current GPS velocity field and the interseismic coupling model for the subduction plate interface in Peru, including a case of a mixed seismic and aseismic slip in northern Peru. Finally, we introduce an approach to construct physically based fault rupture scenarios for future megathrust earthquakes in the subduction zone of Peru.

Single-station detection of seismic slow earthquakes using their broadband characteristics

Koki Masuda¹, Satoshi Ide¹

¹Department of Earth and Planetary Science, The University of Tokyo

Slow earthquakes radiate tiny signals and are observed only in some limited frequency bands with low noise. Those observed in 1-10 Hz are called tectonic tremors or low-frequency earthquakes and those observed in 0.01-0.05 Hz are called very-low-frequency earthquakes (VLFE). These seismic slow earthquakes are spatiotemporally correlated, and the seismic-moment rate calculated from VLFE is almost always proportional to the seismic-energy rate calculated in the tremor frequency band (Ide et al., 2008). Brownian motion-type models (e.g., Ide, 2008) can explain this relationship and also have predicted the radiation of broadband signals through 0.01-10 Hz. In fact, broadband detections of seismic slow earthquakes including microseism frequency of 0.05-1 Hz support the idea (e.g., Kaneko et al., 2018; Masuda et al., 2020). In this study, we utilize this characteristic of slow earthquakes to design a method to monitor slow-earthquake activities even from a single-station data.

From a broadband seismogram recorded at a single station, we measure seismic energy rate as the squared-velocity waveform in 2-8 Hz and, and seismic moment rate as the displacement waveform in 0.02-0.05 Hz. Then we calculate the correlation coefficient between the seismic energy rate and seismic moment rate, every 10 s in a time window of 100 s, and take a moving average of 10000 s. We regard the timing when this value exceeds a certain threshold is “detection”.

The first application of this method is to the continuous records of F-net, a broadband seismic network of 75 stations in Japan for 18 years. The stations with many detections were lined up along a band of tectonic tremors in the Nankai subduction zone. This spatial correlation verifies the effectiveness of the new method. However, some stations near the tremor band have only small number of detections, and some stations far from slow-earthquake activities have many detections. Such false behavior of the method can be explained by the effect of the radiation pattern and the environmental noise mainly due to the weather. Therefore, with a certain caution, this method can also be applied to other regions, especially to less instrumented regions.

Extraction of tremor migrations beneath Shikoku, southwest Japan, and their characteristics

Kodai Sagae¹, Takahiko Uchide¹, Takanori Matsuzawa²

¹ Geological Survey of Japan, AIST, ²NIED

One of the significant characteristics of tectonic tremors is tremor migration, which is a phenomenon that source locations migrate in various timescales. Tremor episodes with durations ranging from several hours to several days migrate along the strike direction of a subducting plate at a speed of approximately 10 km/day (e.g., Obara, 2010; Houston et al., 2011). This is referred to as the main front in this study. In the timescales of several hours, tremors migrate in the reverse direction of the main front, which is called rapid tremor reversal (RTR) (Houston et al., 2011). It is difficult to identify each of the numerous tremor migrations visually due to the complex migration pattern not only in the along-strike direction but also in the along-dip direction. In this study, we objectively extract tremor migrations beneath Shikoku, southwest Japan, using a space-time Hough transform (Sagae et al., 2021, JpGU) and investigate spatiotemporal characteristics of tremor migrations.

The space-time Hough transform is a method for extracting tremor migrations in space-time (longitude, latitude, occurrence time). This method enables us to extract locations, durations, propagating directions, and speeds of tremor migrations. We express the straight line in space-time by using four parameters (ρ , θ , ϕ , ψ), where ρ is the distance from an origin to the straight line, θ is the zenith angle, ϕ is the azimuth, and ψ is the rotation angle. In particular, $\tan \theta$ represents the speed of the tremor migration. By considering the straight line with spatial spread (cylinder), we extract the straight line in consideration of tremor uncertainties. We search for the cylinder that contains the largest number of tremor events and regard it as a tremor migration.

We use a tremor catalog (NIED catalog) determined by NIED using the hybrid method (Maeda and Obara, 2009) from January 2010 to December 2019. The temporal resolution is one minute, and the location uncertainties are 5 km on average. Thus, we set a radius of a cylinder to 5 km. We prepare four parameters (ρ , θ , ϕ , ψ) to extract tremor migrations by the space-time Hough transform. ρ is set at an interval of 0.25 km in a range of 0–120 km, ϕ and ψ are set at an interval of 10° in a range of 0–350°, and θ ($\tan \theta$) is set at an interval of 1 km/hr in a range of 0.125–60 km/hr. Firstly, we prepare time windows with lengths of 1, 2, 3, 4, 6, 8, 12, and 24 hours and move the time windows from the beginning of the catalog without overlapping. Secondly, we apply the space-time Hough transform to data in time windows with ten or more

tremor events. We extract tremor migrations that contain eight or more tremor events. After removing the tremor events included in the previously detected tremor migration, we find other tremor migrations in the same way. This processing is iterated until there are less than ten tremor events in the time window or less than eight tremor events are contained in all cylinders. Finally, we create a catalog of tremor migrations after removing overlapping tremor migrations which are extracted from multiple time windows.

As a result, we succeed in extracting 6,712 tremor migrations beneath Shikoku. We investigate the spatial distribution of propagating directions, durations, and speeds of tremor migrations. In the areas where the median duration is relatively long (approximately six hours), the median speed is relatively slow (24 km/day). This characteristic is consistent with the main front. When we focus on tremor migrations with high speeds (10 km/hr or more), the tremor migrations tend to propagate in the opposite directions of the main front. These results suggest the existence of areas where the main front and RTR repeatedly occur. By comparing the spatiotemporal characteristics of tremor migrations with the spatial distribution of tremor energies, we discuss a relation between behaviors of tremor migrations and heterogeneity on the plate interface.

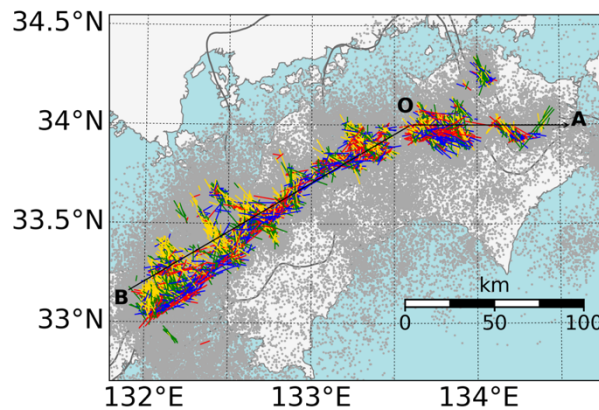


Figure 1. Spatial distribution of tremor migration beneath Shikoku, southwest Japan. Grey dots show tremor locations in the tremor catalog (NIED catalog). Colored lines show tremor migrations extracted in this study. Colors show propagating directions, where red is east direction along the strike (B–O–A), blue is west direction along the strike, yellow is up-dip direction, and green is down-dip direction.

Swarms of microearthquakes associated with tectonic tremor bursts in the northern Japan Trench

Kazuma Matsumoto¹, Ryota Hino¹, Hidenobu Takahashi², Masanao Shinohara³

¹Graduate School of Science, Tohoku University, ²Central Research Institute of Electric Power Industry, ³ Earthquake Research Institute, University of Tokyo

In the Japan Trench subduction zone, tectonic tremors, a type of slow earthquakes, and ordinary earthquakes are distributed in the same depth range and in close proximity. It is expected that the detailed characterization of the spatio-temporal relationship between tremors and ordinary earthquakes will provide a clue for a comprehensive understanding of the mechanisms of slow and fast earthquakes generation. In this study, we investigate the details of the spatio-temporal distribution of ordinary earthquakes that were associated with tremor episodes in the northern Japan Trench in 2007 and 2008 [Takahashi et al., in prep.]. We used P and S arrival times to relocate hypocenters of the earthquakes, identified as events with a duration shorter than 20 s by an envelope correlation method by Takahashi et al. [in prep.]. The number of relocated earthquakes was 3909 and the smallest event size was $M -0.4$. It turns out that most of the tremor episodes were followed by evident rises of activity of ordinary earthquakes in their vicinities. The temporal variation of event sizes during the seismicity suggests that the activities are more like a swarm type than a mainshock-aftershock type. In the tremor episodes with the largest spatial scale, ordinary earthquakes, including small ($M 0.8 \sim 1.0$) repeating earthquakes, became active after the initial tremor burst. The epicenters of tremors and ordinary earthquakes migrated along the strike of the subduction zone with a speed of ~ 4 km/day. The migration pattern of other smaller episodes can also be explained by the same speed. Obana et al. [2021] reported that ordinary earthquakes occurred in the wake of the tremor migrations in the southern Japan Trench. Their observations showed a couple of similarities to ours: Tremors tend to precede activations of ordinary earthquakes, and tremors and earthquakes share a common migration. Based on the observed relationships between tremors and ordinary earthquakes, we suggest that an aseismic slip event triggers ruptures of tremor and ordinary earthquake patches in close proximity. The similarities in swarm-earthquake activities in the northern and southern regions in the Japan Trench may indicate a prevalence of the aseismic slip events driving tremors and small ordinary earthquakes over a wide area along the subduction zone.

Calibration of AE sensors using ARX model used for estimating source properties of foreshocks during large-scale rock friction experiments

Kurama Okubo¹, Futoshi Yamashita¹, Eiichi Fukuyama^{2, 1}

¹NIED, ² Graduate School of Engineering, Kyoto University

During the stick-slip experiments using meter-scale biaxial friction apparatus, the emergence of foreshocks has been observed (e.g. Yamashita et al. 2021). While its source mechanisms have been investigated to understand the relationship to the nucleation process of dynamic ruptures, the estimated source properties by the measurements of AE sensors have been limited in frequency bands due to the uncertainty of the sensor response. The previous studies also pointed out the importance of sensor calibration to evaluate the source properties associated with the foreshocks and/or the failures of the rock sample in laboratory experiments (e.g. McLaskey et al., 2014; Yoshimitsu et al., 2014; Kwiatek et al., 2014; Marty et al., 2021, Naoi et al., 2022). While we have calibrated the gain factor of AE sensors using the ball-drop sources to convert from the output voltage to the velocity (Okubo et al., 2021AGU), the frequency response remains to be corrected due to the limitation in the frequency contents of the signal radiated from the ball-drop source that has the corner frequency of $\sim 100\text{kHz}$. The correction of phase also plays an important role in identifying the source properties, including the slip directions as well as the magnitude and the source duration. Thus, this study aims to estimate the frequency response including the phase shift associated with the AE sensors, which is used to remove the instrumental response from the observed waveforms of foreshocks during the stick-slip experiments.

We individually measured waveforms radiated from the electrically excited transducer using the Laser Doppler Vibrometer (LDV; Denshigiken, Melectro V100) and the AE sensor (Olympus, V103-RM) following the previous studies (e.g. Naoi et al., 2022). We used a stainless steel block of 100mm x 100mm x 127mm. The piezoelectric transducer with a diameter of 10mm for excitation was installed at the center of the side surface of the block as the source. We then fixed three measurement points to conduct the case studies associated with the robustness of the response model: at the center (50mm, 63.5mm) and the top (50mm, 85mm) on the opposite surface, and at the center on the orthogonal surface. At each point, we assume that the signals recorded by LDV are considered as "true" motion and treated as the input to the system. The signals recorded by AE sensor are the output from the system in the context of system identification. The AE sensor is attached using silicone grease. We stacked both measurements (10,000 and 2,000 stacks for the LDV and the AE sensors, respectively) to improve the S/N ratio enough to identify the frequency response.

Ideally, the instrumental response can be estimated by dividing the Fourier spectrum of the output measured using the AE sensor by that of the input with the LDV. However, the response is usually oscillated and needs to be smoothed to stably extract the ground motion by removing the instrumental response with its deconvolution. Therefore, we modeled the response using the autoregressive with exogenous input (ARX) model following McLaskey and Glaser (2012), which is a linear transfer function represented with the poles and zeros. The smoothness of the frequency response is reasonably controlled by the order of the model, and the coefficients of poles and zeros are used to remove the instrumental response in the same framework with the

seismometers. The signal of the AE sensor is amplified with the preamplifier (Mistras Group, 2/4/6C), whose response is convolved with the response of the AE sensor. In this study, we included the response of the preamplifier in the instrumental response. We removed the instrumental response from the output of AE sensors with the procedure widely applied to the seismic dataset (e.g. pre-filtering, water level) as implemented in the obspy (Krischer et al., 2015).

To evaluate the robustness of the response model, we chose the test dataset associated with one of three measurement points with which we evaluated the poles and zeros of the model, and applied the model to the rest of the datasets as a blind test to investigate if the input (measured with the LDV) can be estimated from the output of AE sensors. We obtained the poles and zeros using the least square method (e.g. Kay and Marple, 1981). We determined the number of poles and zeros based on the AIC with each case. We evaluated the misfit between the simulated waveform and the input, regarded as the true signal, using the normalized mean square error (NMSE, Baise et al., 2001).

For the cases with the measurement point either at the center or the top of the opposite side from the source, the input is fairly reconstructed with the response model for the cases with both the test and the validation datasets in the frequency range of between 60k and 200kHz. The error increases above the frequency range due to the contributions of the aperture effect, similar to that reported by McLaskey and Glaser (2012). For the case with the measurement point on the orthogonal side from the source, the response model poorly worked on both the test and the validations. This could be caused due to the complicated motions at the measurement point in horizontal and vertical directions, both of which would be reflected in the output of AE sensors. If so, it does not fit the measurement of vertical motion using the LDV.

This analysis shows the potential of estimating the instrumental response to convert from the output of the AE sensor to the time domain motion on the surface of the medium. The response model will be used to correct the waveforms associated with foreshocks to identify its source properties by minimizing the bias that comes from the instrumental response, which would help reveal the accurate mechanisms of foreshocks and its role in the nucleation of dynamic ruptures.

Nature of the plate boundary domain at the depth of deep slow earthquakes: evidence from the Sanbagawa belt

Yukinojo Koyama, Simon R Wallis, Takayoshi Nagaya

Dept. EPS, Univ. Tokyo

The Sanbagawa belt, SW Japan provides a window into regions deformed at depths and conditions in subduction zones that are similar to where ETS is common in modern SW Japan and is a good area to study possible connections between natural rock structures and observed ETS.

Proposals for geological structures that may be related to the formation of ETS include *mélange* block-in-matrix; quartz-filled crack seal shear veins; and shear folds with pressure solution, expressed through the development of crenulation cleavage. The formation of both quartz-filled shear cracks and crenulation cleavage involves a brittle fracturing stage with dilation followed by an inflow of fluid and deposition of quartz. Both styles of deformation are promoted by high fluid pressure making them good candidate structures for the origin of ETS. However, no good evidence for shear cracks was observed in the study area. Serpentine blocks are present scattered throughout the area, but these blocks are absent in the low-grade region and other lithologies show good continuity implying the mechanical characteristics of *mélange* do not play an important part in controlling how this region deformed. In contrast, crenulation cleavage and related folds on various scales are widely observed in low-grade areas. Geological studies suggest the low-grade domain has a kilometer-scale width during peak metamorphism.

In this study, a compilation of deformation temperatures estimated from quartz c-axis crystallographic orientation patterns and peak metamorphic temperatures from Raman carbonaceous material thermometry shows good agreement between the two methods suggesting the main deformation occurred close to peak metamorphic conditions. The stress can be estimated using paleopiezometers based on the recrystallized grain size of quartz. Combining this information with flow laws for dislocation creep and known plate subduction rates allows the thickness of the subduction channel to be estimated.

Our results suggest the channel width was several kilometers at relatively high P-T (520°C, 0.9 GPa, estimated depth: 25-30km), which is consistent with the channel width implied by construction of geological cross sections. However, unrealistically large widths are estimated at lower P-T (300-440°C, 0.6 GPa, estimated depth: 15-25km), possibly indicating that other deformation processes were dominant. Quartz pressure-solution creep and phyllosilicate slip are one possibility as witnessed by the widely observed development of crenulation cleavage and dissolution selvages. It is also suggested that strain rate of these deformation mechanisms can be much larger than that of quartz dislocation creep.

Our estimates of the width of the subduction boundary channel imply the plate boundary was not a plane but a zone of penetrative deformation with dominant deformation mechanisms that changed with depth. Furthermore, our results suggest that models for the origin of ETS should consider deformation in a broad subduction channel of several kilometers width. The development of trains of folds forming at various scales including crenulation cleavage can account for the main features of ETS and is compatible with our observations.

Various waveform characteristics of deep low-frequency earthquake in volcanic regions

Ryo Kurihara

Hot Springs Research Institute of Kanagawa Prefecture

Regular earthquakes and slow earthquakes are classified according to their time scale and waveform characteristics. Furthermore, slow earthquakes are classified as tremors, low-frequency earthquakes, or very low-frequency earthquakes and so on, based on their waveform characteristics. This classification is not only applied for earthquakes occurring at plate boundaries, but also earthquakes occurring in volcanic regions. The fact that slow earthquakes can be divided into multiple types with different time-scale is being investigated through observational, experimental, and simulation studies to elucidate their physical mechanisms. However, with the exception such as volcanic tremor with monochromatic waveforms, the mechanisms of the radiation of the low-frequency waveform remain unclear. In this study, we examine why volcanic deep low-frequency earthquakes have predominant waveforms in the 1-8 Hz band based on the observation in Kirishima, Hakone, and Fuji volcanoes.

First, one possible candidate for the low-frequency waveform is that these earthquakes occur at relatively deep depths in volcanic regions with strong attenuation, so that high-frequency seismic waves are attenuated, and consequently only low-frequency earthquakes are observed. However, this theory is difficult to explain because both earthquakes with a large low-frequency component and a large high-frequency component have been observed within a short period of time from the same epicenter in some areas, for example, Fuji Volcano. Another possible candidate mechanism is due to fluid. At the period of the 2011 eruptions of the Kirishima volcano, Kyushu, Japan, deep low-frequency earthquakes were activated with a clearly lower dominant frequency waveform than that of deep low-frequency earthquakes at other times. No such waveform was observed during the 2018 eruption, and the activation of deep low-frequency earthquakes was small. Therefore, it is likely that these lower-frequency earthquakes occur when fluid is supplied around the source region of deep low-frequency earthquakes. Thus, the waveform characteristics of deep low-frequency earthquakes in volcanic regions are thought to be deeply related to the fluid in the deep volcanic zone.

The downdip limit of the megathrust seismogenic zone: comparing thermal and lithological controls on frictional and viscous deformation

Liam Moser^{1,2} and Camilla Cattania¹

¹Dept. of Earth, Atmospheric and Planetary Sciences, Massachusetts Institute of Technology, ²Dept. of Geology and Geophysics, Woods Hole Oceanographic Institution

The depth limit of the subduction seismogenic zone controls landward ground motion intensity and megathrust nucleation conditions. What controls this maximum depth? One model relies on rock yield strength constrained by the frictional and viscous flow failure envelopes. A second hypothesis is that a temperature-controlled transition (~350-500 °C) from rate-state velocity-weakening to velocity-strengthening friction prevents earthquake nucleation past a certain depth. Another combined approach posits that seismogenic zone extent is thermally controlled in 'hot' subductions zone and limited by the overriding plate Moho in 'cold' subduction zones. We revisit these models by combining published thermal modeling and observational data for 17 subduction zones. Our analysis suggests that the depth limit of inter-plate subduction earthquakes does not appear to be solely temperature-controlled either by rate-state friction or by the onset of viscous flow. In ongoing work, we investigate the effect of grain size, and its temperature and depth dependence, on viscous strength.

Precise evaluation of element transfer in metabasalt with sample-based predictive uncertainty estimation using machine-learning

Satoshi Matsuno¹, Masaaki Uno¹, Atsushi Okamoto¹

¹Graduate School of Environmental Studies Tohoku University

Seismic events in subduction zones are linked to the presence and transfer of dehydrated water from subducted oceanic crust, whose fluid flow might control the slow earthquakes (Audet et al. 2014). The traces of fluid flow are directly recorded in metamorphic rock as fluid-rock reactions, and we can interpret fluid flow from the element transfer associated with the reactions. However, element transfer in metamorphic rocks is not always evaluable, due to the lack of information of pre-metamorphic rock or "protolith" composition. Matsuno et al. (2022) have presented Protolith Reconstruction Models (PRM), a machine learning based approach to reconstructing protolith composition from metabasalt composition and enables us to calculate element transfer for each sample of metamorphic rock. However, the predictive uncertainty for individual elements and individual samples was not available in the current machine learning algorithm; it is still ambiguous whether the estimated element transfer from field samples is reliable.

In the present study, we introduced a new machine learning algorithm to the PRMs and enabled PRMs to estimate element transfer with predictive uncertainty. Following Matsuno et al. 2022, the models were constructed by learning the global compositional dataset of basalt (Ocean Island basalt, Mid-ocean ridge basalt, and Island arc basalt) containing Rb, Ba, U, K, La, Ce, Pb, Sr, Nd, Y, Yb, Lu, Zr, Th, Ti, and Nb, and designed to estimate trace element compositions from limited numbers of input trace element concentrations (i.e., 2–9 elements). We chose Zr, Th, Ti, and Nb as the input elements, one of the best combinations for analyzing metamorphic rocks discussed in Matsuno et al. 2022. The output elements are as below: Rb, Ba, U, K, La, Ce, Pb, Sr, Nd, Y, Yb, and Lu. To evaluate the predictive uncertainty, NGBoost was adopted as the machine-learning algorithm, a supervised machine-learning method based on gradient decision trees, a type of decision tree. The advantage of using NGBoost is that it enables predictive uncertainty estimation through probabilistic predictions (Duan et al., 2020). Because of computational cost, we evaluated only the above-chosen combination models and compared the result of test data with Matsuno et al. 2022.

In most cases, the accuracy of NGBoost models was equal to or better than the previous models trained by LightGBM. Overall, the Root Mean Squared Error in log space for constructed models is slightly improved for most elements compared to previous LightGBM models, which might depend on the parameter tuning with Bayesian optimization and the natural gradient method adopted in NGBoost's algorithms. In addition, each model for estimating element had fine estimation (e.g., under 20% error) and provided under 20% uncertainty, the uncertainty's averages are better than the error means for all elements, and each sample's uncertainty can provide correct evaluation for estimated value: which proved that NGBoost's uncertainty works correctly and can infer the confidence level of its estimates. Compared to the accuracy between predicted concentration and raw concentrations, there are almost the same trends that occurred in the LightGBM models: In low concentrations for Rb, K, and Pb, there were noticeable errors in the test data above 100%, which might be caused by analytical detection limit. For these large error samples, NGBoost models provide significant uncertainty (e.g., up to 100% for Rb); on the other hand, almost other samples were fine

estimation (e.g., under 30% error for Rb) and provided little uncertainty (e.g., around 35% for Rb). Consequently, the NGBoost models proved beneficial for their better estimation with predictive uncertainty.

The new NGBoost-based PRMs will enable us to evaluate element transfer with predictive uncertainty (i.e., around 30% for Rb, K, and Pb; around 10 to 20% for other elements). When applied to the field, the NGBoost-based PRMs will strongly support the estimated element transfer and make its evaluation more accurate.

References

- Audet, Pascal, and Roland Bürgmann. 2014. "Possible Control of Subduction Zone Slow-Earthquake Periodicity by Silica Enrichment." *Nature* 510 (7505): 389–92.
- Matsuno, Satoshi, Masaaki Uno, Atsushi Okamoto, and Noriyoshi Tsuchiya. 2022. "Machine-Learning Techniques for Quantifying the Protolith Composition and Mass Transfer History of Metabasalt." *Scientific Reports* 12 (1): 1385.
- Duan, Tony, Anand Avati, Daisy Yi Ding, Khanh K. Thai, Sanjay Basu, Andrew Ng, and Alejandro Schuler. 2020. "NGBoost: Natural Gradient Boosting for Probabilistic Prediction." *37th International Conference on Machine Learning, ICML 2020 Part F16814*: 2670–80.

Investigation of earthquake source scaling laws using dynamic rupture simulations with a hierarchical patch structure

Kazuki Masuda¹, Yoshihiro Kaneko¹

¹Graduate School of Science, Univ. Kyoto

Understanding the earthquake rupture growth processes and the resulting seismic radiation is important for earthquake physics and seismic hazard. To constrain the physical processes of earthquake rupture growth, scaling laws of source parameters are often studied. However, it has not been understood whether scaling laws result from the heterogeneities of physical properties in the fault zone or the characteristics of a scale-dependent friction law. Here we test a hypothesis that models of spontaneous dynamic ruptures on faults characterized by hierarchical patches of fracture energy G_c in the framework of a slip-weakening friction law can explain several, well-known scaling relations for earthquake source parameters. Our modeling approach is based on a spectral element method and incorporates a renormalization procedure proposed by Aochi and Ide (2003). We simulate earthquakes with a wide range of magnitudes (M2 to M6) on a fault characterized by hierarchical patches of fracture energy G_c . We then quantify and examine various scaling laws for simulated source parameters, such as seismic moment versus source duration, magnitude-frequency relations, moment growth versus time, and fracture energy versus coseismic slip. We analyze how these scaling laws change as the model parameters are varied. Among the model parameters tested, the so-called seismic ratio (S ratio) has the largest influence on the trend of scaling laws, which suggests that the scaling laws may be used to constrain the underlying model parameters. We will report our efforts on identifying key model parameters on the resulting scaling laws and implementing our model procedure to two-dimensional faults.

Seismic structures and shallow tremor distributions in Hyuga-nada

Yanxue Ma¹, Rie Nakata¹, Kimihiro Mochizuki¹, Yoshitaka Hashimoto², Yohei Hamada³

¹ ERI, Univ. Tokyo, ² Kochi Univ., ³ JAMSTEC.

In recent years, many shallow slow earthquakes, including tectonic tremors, have been detected by broadband ocean bottom seismometers in Hyuga-nada, Japan (Yamashita et al., 2015, 2021). Hyuga-nada is located off the eastern shore of Kyushu Island and at the western end of the Nankai Trough. Many controlled-source seismic surveys were conducted to better understand the relationships between seismicity and structures in Hyuga-nada. The Kyushu Palau Ridge (KPR) is a remnant of the Izu-Bonin island arc system. The northern end of the KPR is located in Hyuga-nada. The KPR is regarded as a crucial geological feature that may influence the occurrence of slow earthquakes. A reflection seismic survey line, KR0114-8, crosses the Ryukyu Trench, the KPR, and the Nankai Trough. The resolution of the existing seismic reflection image of the line (Park et al., 2009) is insufficient to understand shallow structures in detail. In this study, we reprocessed the KR0114-8 line. We applied Kirchhoff prestack depth migration and migration velocity analysis to obtain a high-resolution seismic image. Based on the image, we interpreted complex subsurface features, including bottom-simulating reflectors, faults, accretionary prisms, décollement, splay faults, and the top of the oceanic crust (Figure 1b).

We separate the survey line into three distinct areas (Figure 1s); the Ryukyu Trench, the KPR, Nankai Trough sides, and discuss the relationships between the distribution of tremors and the structures. Based on the tremor catalog in Yamashita et al. (2021), we calculated the probabilities of each tremor at a 1 km interval along the line by taking into account errors in their epicenter estimation. Then we plotted the expected values of tremor counts by taking the sum of the probabilities at each point along the line (Figure 1a). On the Ryukyu Trench side, high tremor activity (Yamashita et al., 2015) may be correlated to a compression regime on the down-dip of a subducted seamount. Few tremors occurred above the seamount of the KPR. We suggest that there is a stress shadow above the seamount. Many tremors were observed on the Nankai Trough side. The expected values of the tremor counts are smaller in the western part than in the eastern part of the Nankai Trough side (Figure 2b). In the seismic image, the sediments between the décollement and the top of the oceanic plate are thinner in the west than in the east (Figure 2c). We observe a prominent contrast of reflection amplitudes along the décollement between the west and the east (Figure 2a). These suggest that the Nankai Trough side consists of two distinct areas in terms of structures, seismic properties, and tremor activities. Our next step is to study their relationships, which will contribute to understanding the mechanisms of tremor generation.

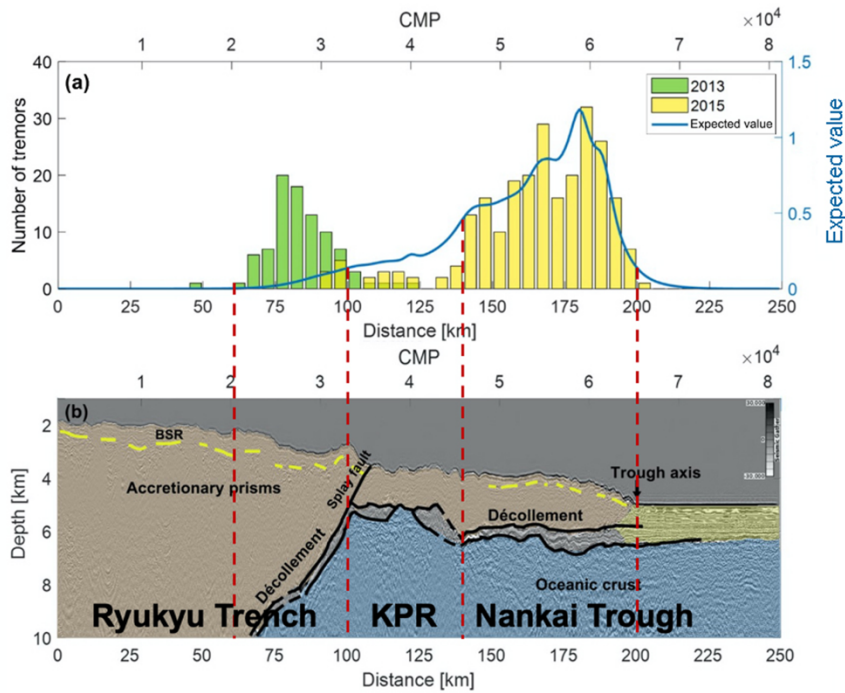


Figure 1. Seismic image of the KR0114-8 line compared with the tremor distributions. (a) Tremor distribution (Yamashita et al., 2015; 2021). (b) Seismic image with interpretations.

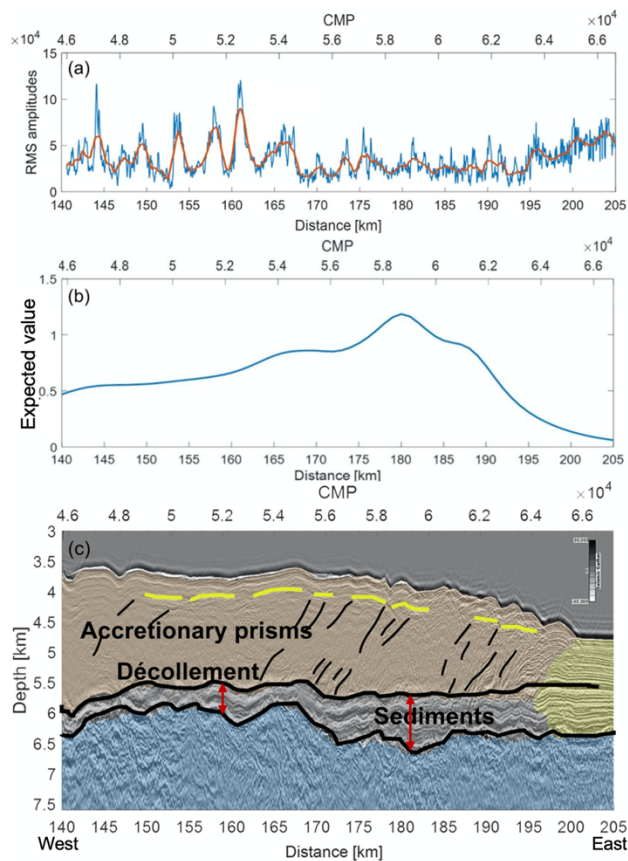


Figure 2. Seismic image compared with RMS amplitudes and tremor distributions on the Nankai Trough side. (a) RMS amplitudes of the décollement. The red line indicates values by applying a smoothing moving average. (b) Expected values of tremors. (c) Seismic image with interpretations.

Deformation mechanisms and rheology of a *mélange* shear zone associated with seamount subduction

Madison Frank¹, Kohtaro Ujiie¹, Ginta Motohashi¹, Takayoshi Nagaya², Takashi Sano³

¹Dept. Life & Env. Sci., Univ. Tsukuba, ²Dept. EPS, Univ. Tokyo, ³Dept. Geol & Palaeo., Kahaku

Subduction zone rocks exhumed from slow earthquake source regions provide critical evidence of the lithology, P-T conditions, and deformation mechanisms at slow earthquake temperatures. At Asanzaki, Amami-Oshima Island, the lithology of an exhumed sequence from the Southern Chichibu accretionary complex consists of a *mélange* dominated by argillaceous mudstone and seamount-derived micritic limestone and basalt blocks. Peak metamorphic temperature from Raman spectra analysis is ~285 °C. Experimentally derived constitutive equations modeling deformation in quartz, microcrystalline calcite, and chlorite have been compared to microstructures preserved in the mudstone, limestone, and basaltic sediments to identify the dominant rheology under past P-T conditions at various shear velocities. Microstructures in the mudstone record evidence of dislocation creep in quartz and pressure solution and frictional sliding of phyllosilicates at aseismic velocities under hydrostatic fluid pressure or pressure solution and frictional sliding of phyllosilicates at all sub-seismic velocities under elevated fluid pressures. Foliation parallel quartz veins with crack-seal texture exist within the mudstone indicating cyclical periods of near-lithostatic fluid pressure. Microstructures in the mixed micritic limestone and basalt blocks indicate rheology was controlled by frictional sliding of chlorite over plastic deformation of microcrystalline calcite, corresponding to slow earthquake shear velocities.

Tectono-sedimentary history of the Wharton Basin and its roles of subduction input at the northern Sunda Trench

Mari Hamahashi¹

¹Faculty of Global and Science Studies, Yamaguchi University, Japan

The Sunda Trench where the Indo-Australian Plate subducts beneath the Sunda and Burma Plate, is an active seismogenic zone which generated the 2004 Mw 9.2 mega-earthquake and devastating tsunami offshore Northern Sumatra, characterized by a large shallow slip near the trench (Chlieh et al., 2007; Rhie et al., 2007; Fujii & Satake, 2007), and an extremely thick (>4 km) incoming section at the deformation front (Dean et al., 2010; McNeill & Henstock, 2014). To investigate the nature and impact of the incoming section on seismogenic processes, the International Ocean Discovery Program (IODP) Expedition 362 drilled into the Indo-Australian Plate ~225 km distance from the trench at 2 primary sites (1480, 1481) offshore Northern Sumatra (McNeill et al., 2017).

Seaward of the Sunda Trench, the incoming plate is composed of the Wharton Basin, which is shaped by N-S oriented fracture zones that formed during Cretaceous to Eocene spreading along the fossil Wharton Ridge (Jacob et al., 2014). The basin here is filled by thick sedimentary covers consisting of the Bengal-Nicobar Fan system, which are terrigenous input that began in the Early Miocene, primarily sourced from the Himalaya. The full sedimentary succession from the seafloor to 1415.35 mbsf was recovered by Expedition 362 east of the Ninety-East Ridge (McNeill et al. 2017; Pickering et al. 2020). They consist of predominantly siliciclastic sediments interpreted to be the Nicobar Fan (Lithologic Units I–II), underlain by mixed tuffaceous and pelagic sediment (Unit III) and thin intervals of intercalated pelagic and igneous material overlying oceanic crust (Units IV and V).

Major transitions in lithology, age, and physical properties mark the boundary between the unlithified Nicobar fan sediments and lithified pre-fan pelagic sediments, which is a horizon traceable throughout the Wharton Basin, and is one of the potential pre-decollement horizons at the subduction zone offshore Sumatra (Dean et al., 2010; McNeill & Henstock, 2014; Bradley et al., 2019). In this study, to investigate the internal architecture of the Early Miocene/Paleocene pelagic section (Units III and V), three-dimensional microstructural observation was conducted using a micro-focus X-ray CT scanner and optical microscopy on thin sections. To examine the particle shape and mineral occurrence, textural/element analysis was made using FE-SEM.

A distinct concentration of normal faults is observed in the pelagic units, characterized by thin anastomosing faults which randomly cross-cut each other. Sand dikes and diagenetic spots also occur in the sediments, and the normal faults generally cut through the sand dikes but generally leave the diagenetic spots uncut. The flattened geometry of the diagenetic spots overprinting the normal faults and the high conjugate angle and wavy geometry of the faults may imply that the normal faulting occurred before significant compaction. The concentrated deformation in the pelagic section may have occurred in an active ridge environment at that time and thermal subsidence followed by rapid sedimentation of the Nicobar Fan.

The geometry of sedimentary structures, small faults, and major particles were documented in further detail from the microstructural analysis in the vertical and horizontal direction in Units III and V. General bedding (0.3-0.4 mm thickness) dips 5-15 degrees, whereas multiple foliations of relatively low to high angle (to bedding) are observed. The low-angle structures

are generally cut by the high-angle structures. Among the sediments, high density circular-shaped particles of ~0.3 mm is often observed, inferred to be heavy minerals. These particles are generally compacted in the vertical direction compared to the horizontal direction. Circular clast or wavy foliation (not consecutive) of 0.9 mm thickness is observed to have relatively lower density than these particles (yet higher density than the surrounding), and the circular clasts are compacted in the vertical direction (aspect ratio: 0.3-0.4). In the horizontal direction, circular shaped nanofossils and forams (of ~1.3mm) are sparsely distributed. Dike structures are observed to exist in relatively high angle (30-70 degrees), and exist in step forms. These clasts are likely to be tuffaceous sandstone clasts (high density due to diagenesis or recrystallization) and nanofossils, as observed in smear slides, whereas wavy foliations are likely to be sand dikes. In contrast, the more consecutive foliations that dip at higher angle (~20 degrees) with similarly high density are distinguished to be faults. Occasionally these high-angle faults have lower density. The low angle faults (~10 degrees) are distinguished by difference in dips from the surrounding. Since the composition of the sediments are relatively consistent, CT values can be converted to rock density (e.g. Conin et al. 2014). For quantitative analysis on the internal structure, the evaluation of weak planes, potential fluid paths and preferred deformation are discussed by converting CT values to density, porosity and P-wave velocity values. To compare the CT values, density contrast and major foliations, X-ray CT scan was also conducted on representative samples from Units I-V.

Pre-existing fault zones and areas of major physical property contrasts on the incoming plate can be a candidate for localized deformation and decollement formation at the trench. This study aims to address the following questions:

What is the nature of the physical property contrast (e.g. high V_p) across the pelagic sediments and the relation with internal structure?

The pelagic sediments are well consolidated as inferred from the geometry of compacted clasts and buried faults and distribution of high-density clasts. Varying dip angles in the pelagic sediments may also contribute to significant physical property anisotropy.

What are the roles of pelagic sediments on subduction inputs and potential pre-decollement horizons?

Small faults in the pelagic section often exhibit wavy geometry in complex cross-cutting relationship. Network of high- and low-density foliations/faults in the pelagic sediments provide insights into the geometry of fluid paths and weak/strong planes for deformation.

References:

- Chlieh et al. 2007. *Bulletin of the Seismological Society of America*, 97, 1A, S152-S173.
Rhie et al. 2007. *Bulletin of the Seismological Society of America*, 97, 1A, S115-S127.
Fujii & Satake, 2007, *Bulletin of the Seismological Society of America*, 97, 1A, S192-S207.
Jacob et al. 2014. *Journal of Geophysical Research*, 119, 169-190.
Pickering et al. 2020. *Sedimentology*, 67, 2248-2281.
McNeill et al. 2017. *Proceedings of the IODP*, Vol. 362
Dean et al. 2010. *Science*, 329 (5988), 207-210.
McNeill & Henstock, 2014. *Tectonics*, 33, 112-134.
Bradley et al. 2019. *Geochemistry, Geophysics, Geosystems*, 20, 1646-1664.
Conin et al. 2014. *Tectonophysics*, 611, 181-191.

Comparison between deep learning, Kalman filtering, and classical methods for evaluating (quasi-)periodic signals

Yuta Mitsui¹

¹Dept. Geosci., Shizuoka Univ.

Geophysical time-series data frequently include (quasi-)periodic variations originating from tides, groundwater, and meteorological effects. It is elementary to evaluate these (quasi-)periodic variations when a sophisticated physical model is constructed such as for tides, or when the period of variation is fixed. However, there are cases where the period of variation fluctuates, or where the period of variation is not clear due to large noises. Although many methods have been applied to the evaluation of (quasi-)periodic signals, we introduce a multi-layer neural network (deep learning) and evaluate (quasi-)periodic variations. Similar to previous studies (e.g., Yamaga and Mitsui, 2019), we use a recurrent neural network (RNN) suitable for learning time-series data.

In RNN, the data in a certain time window is used as input, and the following data is used as output. As the time window is shifted, the parameters of the intermediate layer between the input and output are estimated, and the relation between the input and output is learned. After that, the data in the time range not used for learning is input again, and the output is obtained as the forecasted value. In the intermediate layer, we place four LSTM units (Hochreiter and Schmidhuber, 1997) that can store long-term information to enable deep learning.

We tried numerical tests on artificial data with random noise added to periodic variations. For the artificial data of five sine periods, we performed deep learning of LSTM by shifting the time window by two periods. After that, the forecasts for three periods were output and checked for consistency with the artificial data. The results of this deep learning were compared with the results of Kalman filtering and some classical methods (based on seasonal decomposition or regression analysis), in terms of the value of the absolute sum of residuals. As a result, when the amplitude of the random noise was a few tens of percent of the amplitude of the sine function, the deep learning showed better forecast performance than the other methods. On the other hand, when the noise amplitude became even larger, the forecast performance of deep learning decreased significantly. Conversely, even when the noise amplitude was smaller, the forecast performance of deep learning did not exceed that of simple regression analysis. Thus, deep learning can be a powerful tool for noise removal, but it requires certain conditions to be met to achieve high performance.

Discriminating seismic events using 1D and 2D CNNs: applications to tectonic tremor and volcanic events

Masaaru Nakano¹ and Daisuke Sugiyama¹

¹JAMSTEC

Detecting seismic events, discriminating between different event types, and picking P- and S-wave arrival times are fundamental but laborious tasks in seismology. In response to the ever-increasing volume of seismic observational data, machine learning (ML) methods have been applied to try to resolve these issues. Although it is straightforward to input standard (time-domain) seismic waveforms into ML models, many studies have used time–frequency-domain representations because the frequency components may be effective for discriminating events. However, detailed comparisons of the performances of these two methods are lacking. In this study, we compared the performances of 1D and 2D convolutional neural networks (CNNs) in discriminating events in datasets from two different tectonic settings: tectonic tremor and ordinary earthquakes observed at the Nankai trough, and eruption signals and other volcanic earthquakes at Sakurajima volcano. We found that the 1D and 2D CNNs performed similarly in these applications. Half of the misclassified events were misassigned the same labels in both CNNs, implying that the CNNs learned similar features inherent to the input signals and thus misclassified them similarly. Because the first convolutional layer of a 1D CNN applies a set of finite impulse response (FIR) filters to the input seismograms, these filters are thought to extract signals effective for discriminating events in the first step. Therefore, because our application was the discrimination of signals dominated by low- and high-frequency components, we tested which frequency components were effective for signal discriminations based on the filter responses alone. We found that the FIR filters comprised high-pass and low-pass filters with cutoff frequencies around 7–9 Hz, frequencies at which the magnitude relations of the input signal classes change. This difference in the power of high- and low-frequency components proved essential for correct signal classifications in our dataset.

Shallow slow earthquake activity from December 2020 southeast off the Kii Peninsula inferred from dense ocean bottom seismometer array

Motoki NEGISHI¹, Kazushige OBARA¹, Shunsuke TAKEMURA¹, Takeshi AKUHARA¹,
Yusuke YAMASHITA², Hiroko SUGIOKA³, Masano SHINOHARA¹

1.ERI, Univ. of Tokyo, 2.DPRI, Kyoto Univ., 3.Kobe Univ.

Shallow slow earthquakes actively occurred from December 2020 to January 2021 in the shallow part of the plate boundary near the Nankai Trough off the southeast coast of the Kii Peninsula, Japan. Tremors and very low-frequency earthquakes (VLFs) have been observed by permanent seismic networks of F-net and DONET, and their activity patterns and source parameters have been studied (e.g., Ogiso & Tamaribuchi, 2022; Takemura et al., 2022). In this study, we investigated the characteristics of slow earthquake waveforms observed by a dense ocean bottom seismometer array to understand the state of this shallow slow earthquake episode in detail.

The dense ocean bottom seismometer array used in the study consisted of 15 three-component seismometers with a natural frequency of 1 Hz, installed in the region between DONET1 and DONET2 during the period September 20, 2019, to June 1, 2021. It includes two sets of cross-shaped arrays of five seismometers with a station spacing of approximately 1 km. We analyzed filtered vertical-component seismograms from December 1, 2020, to January 31, 2021. According to Tonegawa et al. (2020), we employed band-pass filters with 0.05-0.10 Hz and 0.10-0.15 Hz for VLFE. To obtain tremor signals, we also applied a band-pass filter of 2-8 Hz. We focused on seismograms on December 12, 2020.

As a result, about 120 tremor signals were identified in the high-frequency band. We also confirmed that about 20% of these signals were synchronized with VLFE signals in the 0.10-0.15 Hz band, and another half of them were also synchronized in the 0.05-0.10 Hz band. These temporal synchronizations suggest that tremors and VLFs occurred synchronously during the episode.

Toward constructing a statistical model for slow earthquakes

Tomoaki Nishikawa¹

¹DPRI, Kyoto Univ.

Episodic slow fault slips (slow earthquakes) are closely related to the occurrence processes of fast, regular earthquakes in subduction zones (Obara & Kato, 2016). Slow earthquakes sometimes trigger great earthquakes and swarms of fast earthquakes (Ozawa et al., 2003; Radiguet et al., 2016). Furthermore, numerical simulations of megathrust earthquake cycles (e.g., Matsuzawa et al., 2010) suggest that the activity of slow earthquakes may change before great earthquakes. Therefore, understanding and forecasting the activity of slow earthquakes are thought to lead to an improved forecast of fast earthquakes. However, there is currently no standard model to describe and forecast activity of slow earthquakes. Therefore, it is currently difficult to forecast future slow-earthquake activity, and there is no standard method to quantify its characteristics and objectively detect its anomalies. With this background, I aim to construct a new statistical model to forecast and quantify slow-earthquake activity by utilizing seismological and geodetic observation records of slow earthquakes accumulated in the Nankai Trough over the past 20 years.

This presentation presents my plan to construct a new statistical model and my preliminary results. The outline of this study is as follows. This study addresses the construction of a new statistical model for slow earthquakes, especially for low-frequency earthquakes. Comprehensive detection of low-frequency earthquakes has been conducted in the Nankai Trough, and sufficient observation records have already been accumulated (Kato & Nakagawa, 2020). I use these observation records for statistical modeling. The Nankai Trough, the study area of this study, is a subduction zone with the most advanced slow-earthquake research in the world, and the spatial distribution of a wide variety of slow earthquakes, their occurrence patterns, and the relationships and interactions between them have been investigated in detail (e.g., Ide, 2010; Obara, 2020). I utilize the findings of these previous studies to formulate a statistical model of low-frequency earthquakes.

I construct a statistical model to forecast the occurrence times of low-frequency earthquakes with reference to the epidemic-type aftershock-sequence model (Ogata, 1988), which is a standard statistical model for fast earthquakes. I divide the Nankai Trough into a number of subregions, and we conduct modeling for each subregion. On the basis of the findings of past slow-earthquake studies (e.g., Ide, 2010; Obara, 2020), I consider the following formulation. The occurrence rate of low-frequency earthquakes is determined by (1) the effect of random occurrence at a constant rate, (2) the effect of slow-slip events triggering low-frequency earthquakes, (3) the effect of fast earthquakes triggering low-frequency earthquakes, (4) the effect of low-frequency earthquakes triggering another, and (5) the effect of periodic external forces, such as tidal forces, triggering low-frequency earthquakes. In (2), I consider a functional form in which the power of the moment rate of slow-slip events is proportional to the occurrence rate of low-frequency earthquakes. In (3) and (4), we consider functional forms in which the occurrence rate of low-frequency earthquakes shows a power-law decay from a triggering event. The magnitudes of triggering effects (3) and (4) are varied with magnitudes of fast and low-frequency earthquakes.

I apply the model formulated above to a catalog of low-frequency earthquakes in the Nankai Trough from 2004 to 2015 (Kato & Nakagawa, 2020). For triggering effect (2), I use a catalog of slow-slip events along the Nankai Trough from 1997 to 2019 (Okada et al., 2022). I estimate model parameters via the maximum likelihood method. Furthermore, on the basis of my new model, I quantitatively evaluate the magnitudes of triggering effects (1) to (5). This evaluation clarifies which effects significantly contribute to the occurrence of low-frequency earthquakes and help elucidate the occurrence mechanism of low-frequency earthquakes.

Earthquake swarm and transient crustal deformation in the Noto Peninsula, central Japan: Implication from combined analysis of multiple GNSS networks

Takuya Nishimura¹, Yoshihiro Hiramatsu², and Yusaku Ohta³

¹ DPRI, Kyoto Univ., ²Kanazawa Univ., ³Tohoku Univ.

Earthquake swarms are generally interpreted as phenomena related to external stress perturbation including slow slip events and magma intrusion or weakening of fault strength due to pore pressure increase. An extensive seismic swarm, as well as anomalous transient deformation, started in December 2020 at the northern tip of the Noto Peninsula, central Japan, which is a non-volcanic/geothermal area far from the major plate boundaries. We present crustal deformation clarified from a combined analysis of multiple GNSS networks, seismicity, and their interpretation. The swarm activity started with several episodic earthquake bursts in the first several months and turned to be a continuous activity. The number of $M \geq 1$ earthquakes has continued at ≥ 100 per week since July 2021, as of July 2022. The focal depth ranges mostly between 10-20 km. We analyzed data at 30 continuous GNSS stations operated by SoftBank Corp., the Geospatial Information Authority of Japan, and universities within ~ 50 km from the epicentral region of earthquake swarms. The total displacement pattern for one and a half years from the start of the earthquake swarm shows horizontal inflation and uplift up to 65 mm around the source of the earthquake swarm. Assuming a tensile crack source, we estimated a volumetric increase of $\sim 3.9 \times 10^7 \text{ m}^3$ at a depth of ~ 14 km. We speculate that the volumetric increase is caused by deep upwelling fluid. The distribution of earthquakes except for a southern earthquake cluster locates in the region of the Coulomb stress increases predicted by the estimated source explains. The seismicity rate in 2020-2021 is also roughly explained by the stress perturbation deduced from the geodetic model and the model based on rate and state-dependent friction law (Dietrich, 1994). However, they cannot reproduce the seismicity rate in 2022. It may suggest that fault weakening due to pore fluid migration into the fault zone is a more dominant mechanism for triggering earthquakes in 2022.

Acknowledgments: We are grateful to SoftBank Corp. and ALES Corp. for providing us with the original GNSS network data. We thank the Geospatial Information Authority of Japan (GSI) and the Japan Meteorological Agency (JMA) for providing GNSS and earthquake catalog data, respectively. We also thank the Suzu City Government and the Noto Town Government for permitting the installation of new GNSS stations.

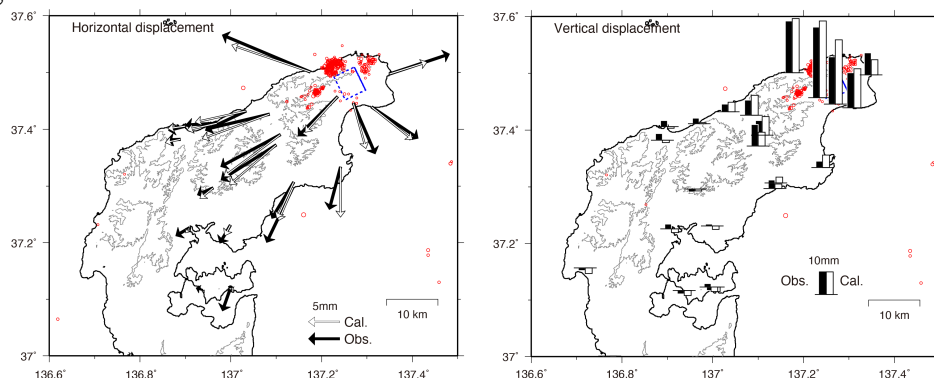


Figure 1 Transient displacements observed from February 2021 to February 2022 at continuous GNSS stations. A blue rectangle indicates the estimated tensile crack.

Evolution of normal stress heterogeneity due to frictional heating and thermo-elastic effect: Implication for size effect in friction experiments

Hiroyuki Noda¹

¹DPRI, Kyoto Univ.

Yamashita et al. (2015) compared friction experiments for a large, meter-scale sample and a small, centimeter-scale sample, and reported that the later shows significant weakening at slip rate V of about 0.1 m/s, while the former shows similar weakening at about 0.01 m/s. They argued that the difference is caused by heterogeneity and concentration of normal stress and thus frictional power, which leads to activation of dynamic weakening (Di Toro et al., 2011). The normal stress heterogeneity conceivably affects macroscopic frictional property of a fault, and its evolution may be a key to understand the scale effect of friction. In the present study, the evolution of the normal stress heterogeneity due to frictional heating and thermoelastic effect is analyzed.

For simplicity, an in-plane problem for an infinite uncoupled thermoelastic medium (thermal conductivity: β , pressure change per temperature change under fixed displacement: α) is considered. If a fault is idealized as a planer heat source, the normal stress perturbation on it can be expressed as spatio-temporal convolution of previous frictional power density and a Green's function. For the Green's function, an analytic solution by Xiao et al. (2021) for a concentrated line heat source is used. Fourier transform in the direction parallel to the fault and assumption of constant slip rate V and friction coefficient f lead to an expression of a Fourier mode amplitude of the normal stress perturbation $\Delta\sigma$ of an angular wavenumber k in terms of temporal convolution of its previous history and an integration kernel. It is found that the integral equation has a steady-state solution $\Delta\sigma_{ss} = \sigma_0 V / (V_{cr} - V)$, where σ_0 is the initial amplitude of the perturbation under uniform temperature, $V_{cr} = \gamma\beta|k|/\alpha f$, and γ is a function of the Poisson's ratio ν , $\gamma = 4(1 - \nu)/(1 - 2\nu)$. At low slip rate $V < V_{cr}$, the steady-state solution has the same sign with the initial value. Otherwise, the steady-state solution contradicts with the intuition that a region of higher normal stress thermally expands more significantly.

This system has been integrated (Figure 1) using a standard boundary integral equation method and a memory variable method (Noda, 2022), which turned out to be much more efficient than the standard method. $\Delta\sigma$ approaches asymptotically to $\Delta\sigma_{ss}$ at low slip rates $V < V_{cr}$. In this regime, the $\Delta\sigma$ does not exceed $\sigma_0 V / (V_{cr} - V)$ and thus careful preparation of the sliding surface to reduces σ_0 help us suppress the effect due to heterogeneous normal stress during experiments. On the other hand, $\Delta\sigma$ increases almost linearly with time at $V = V_{cr}$ and increases exponentially at high slip rates $V > V_{cr}$. Importantly at $V/V_{cr} = \alpha f V / \gamma\beta|k| \geq 1$, at relatively high slip rate and low wavenumber, $\Delta\sigma$ grows indefinitely and fails to approach the steady state solution. Under such circumstances, the evolution of the heterogenous normal stress should ultimately cause severe effects on the frictional property due to concentration of frictional

power and associated activation of dynamic weakening.

With physical properties for gabbro (Schön, 1996), $V_{cr} = 4.0 \times 10^{-2}$ m/s for $k = 2\pi/(10^{-2}$ m), and $V_{cr} = 4.0 \times 10^{-4}$ m/s for $k = 2\pi/(1$ m). These critical slip rates are within the range of typical laboratory friction experiments. Therefore, the thermos-elastic effect may have played an important role in previous experiments for samples of different sizes. A sample cannot host perturbation of a longer wavelength than its own length. For example, in experiments at $V = 10^{-3}$ m/s, the thermos-elastic effect is modest for centimeter-size samples, but can be significant for a meter-scale sample. It is probably important to measure distribution of temperature change and correction of stress measurement with strain gauges for the effect of thermal expansion during large-scale friction experiments. In application to the natural fault, which can host perturbation of a much longer wave length, effect of spatio-temporally variable slip rate and coupling with inertial effect should be taken into account.

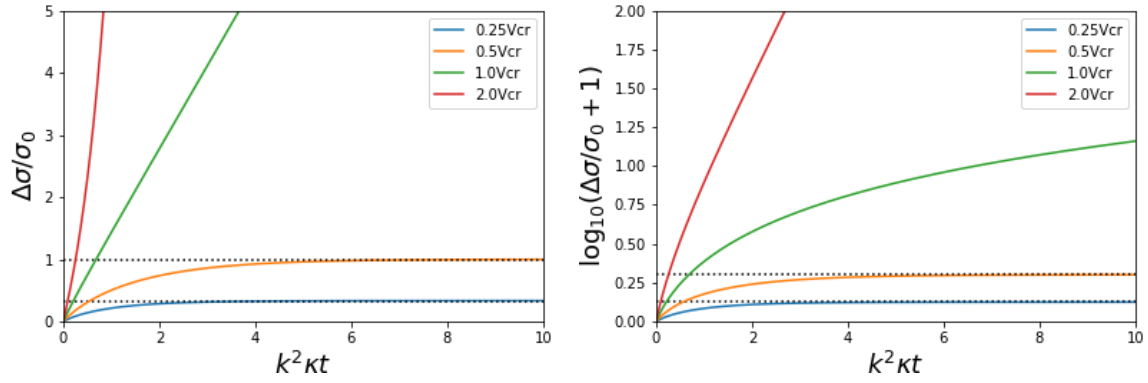


Figure 1. Evolution of $\Delta\sigma$ as a function of nondimensional time for various slip rates in a linear scale (left) and a logarithmic scale (right). t is time after onset of frictional sliding, and κ is the diffusion coefficient of temperature. Horizontal dashed lines show steady-state solution for $V < V_{cr}$.

References

- Di Toro et al., 2011. Fault lubrication during earthquakes. *Nature* 471, 494–498. doi:10.1038/nature09838
- Noda, H., 2022. Dynamic earthquake sequence simulation with an SBIEM accounting for interseismic poroelastic rebound. *Earth, Planets and Space* 74, 89. doi:10.1186/s40623-022-01649-8
- Xiao, W.-Y., et al., 2021. 2D Quasi-Static Accurate Solutions for Isotropic Thermoelastic Materials with Applications. *Mathematical Problems in Engineering* 2021, e8825226. doi:10.1155/2021/8825226
- Yamashita, F., et al., 2015. Scale dependence of rock friction at high work rate. *Nature* 528, 254–257. doi:10.1038/nature16138

Deep low frequency earthquakes evolve similarly to ordinary fast earthquakes

Genki Oikawa¹ and Naofumi Aso¹

¹Tokyo Institute of Technology

To understand the rupture process of slow earthquakes, it is an important issue whether slow earthquakes have similar evolutions to ordinary fast earthquakes. Ide et al. (2007) has proposed different scaling relationship from ordinary earthquakes by compiling various slow-deformation phenomena at different time scales. However, the evolutions of individual slow earthquake phenomena such as low frequency earthquakes (LFEs) do not necessarily follow the same scaling. Therefore, we investigated the relationship between duration and seismic moment for tectonic LFEs occurring on the plate boundary as well as volcanic LFEs.

To estimate the duration and the seismic moment of LFEs, we developed a new method based on the envelope fitting with the following three procedures. We calculated envelope waveforms of transverse component after applying 1-20 Hz band-pass filter. At first, we estimated the duration and amplitude by fitting boxcar functions to the envelope waveforms. We also considered exponential decay to characterize coda attenuation in boxcar functions. Then, we obtained empirical functions to relate the estimated duration and amplitude to the source duration and seismic moment based on same analysis for synthetic waveforms. Finally, applying these empirical functions to the parameters estimated in the first step, we obtained the source duration and seismic moment. Our suggested new method with calibration processes has advantage in evaluating and reducing the influence of limited bandwidth of the seismograms and the uncertainties in Green's functions.

We performed this analysis to volcanic LFEs beneath Zao volcano and tectonic LFEs in western Ehime. For both types, the obtained relationship between duration and seismic moment is close to that of ordinary fast earthquakes, which indicates that LFEs has similar rupture evolution process to ordinary earthquakes. In addition, the obtained seismic moments are about two orders of magnitude smaller than ordinary earthquakes with similar durations. Assuming that rupture velocity is same for LFEs and ordinary events, stress drops of LFEs are interpreted to be smaller than those of ordinary events by two orders of magnitudes as well.

Systematic detection of short-term slow slip events along the Japan and Kuril Trenches

Yutaro Okada¹ and Takuya Nishimura²

¹Graduate School of Science, Kyoto University

²Disaster Prevention Research Institute, Kyoto University

Recently, aseismic transient fault slips called slow slip events (SSEs) are observed all over the world by using both land and seafloor geodetic measurements. SSEs are kinds of slow earthquakes and they sometimes synchronize with other slow earthquakes including tectonic tremors and very low-frequency earthquakes (VLFs) (Ito et al., 2007; Rogers & Dragert, 2003). In the past two decades, huge fast earthquakes and active slow earthquakes have been reported along the Japan and Kuril Trenches where the Pacific plate subducts beneath the Okhotsk plate (e.g., Baba et al., 2020; Nishikawa et al., 2019). Although short-term SSEs (S-SSEs) lasting several days to weeks have also been observed along the Japan Trench (Ito et al., 2013; Nishimura, 2021), their activity in the entire Japan-Kuril Trenches region is still unclear. Here, we investigate the S-SSE activity, that is, their source parameters and spatio-temporal distribution, by applying the systematic detection method.

We used the daily coordinates of 529 GNSS stations operated by the Geospatial Information Authority of Japan, Japan Coast Guard, and International GNSS Service. The coordinates were estimated using GipsyX with a strategy of precise point processing and those in the period from December 1996 to November 2021 were used for the detection. We removed the artificial offsets, displacements relating to fast earthquakes, seasonal oscillation, and common-mode errors as preprocesses (Cleveland et al., 1990; Tobita, 2016; Wdowinski et al., 1997). We applied the S-SSE systematic detection method (Okada & Nishimura, in prep.; Okada et al., 2022) to the preprocessed GNSS data. Firstly, we applied the geodetic matched filter analysis (Rousset et al., 2017) to extract the candidate events of S-SSEs. Then, we estimated the rectangular fault model and duration of the candidate events (Matsu'ura & Hasegawa, 1987; Miyaoka & Yokota, 2012; Rousset et al., 2017) and categorized the candidates into class 1, and 2 SSEs based on the estimation results. In our classification, class 1 includes the events probably to be SSEs and class 2 includes less reliable events than class 1. In addition, we applied further categorization to distinguish between SSEs and the events relating to fast earthquakes.

In the preliminary result, we detected 114 S-SSEs during the 25-year analysis period. Most of the detected events stand in the southmost part of the Japan Trench, where the active S-SSEs have been previously reported (e.g., Nishimura, 2021) (Figure 1). Their bi-modal distribution is consistent with that in Nishimura (2021) (Figure 1b). We also found the S-SSE synchronizing with tectonic tremors offshore Choshi, which was reported by Nishikawa et al. (2019). In addition to the southern part, we also detected minor S-SSE clusters in offshore Miyagi and offshore Tokachi (Figure 1). We found that a few S-SSEs in offshore Tokachi synchronized with VLFs. We stacked 121-day GNSS time series based on 14 VLFE bursts assuming that offshore Tokachi SSEs certainly synchronize with VLFE bursts (Frank et al., 2015; Kano et al., 2019). The average displacement field calculated from the stacked time series shows coherent southeastward displacements around Cape Erimo. We also estimated a rectangular fault model using the average displacements and the fault stands at the up-dip extension of the source area

of the 2003 Mw 8.0 Tokachi-oki earthquake (Yamanaka & Kikuchi, 2003).

Although our results reveal many probable S-SSEs along the Japan and Kuril Trenches, our detected events still include some false ones whose displacement pattern is scattered. Some coseismic and/or postseismic signals of large fast earthquakes were miscategorized into S-SSEs despite our effort for removing earthquake-related signals from the GNSS time series and categorizing them into the events relating to fast earthquakes. Improvement of the criteria to distinguish between S-SSEs and non-SSE events is the next challenge to enhance our detection capability.

Acknowledgments

We used RINEX data provided by the Geospatial Information Authority of Japan, the Japan Coast Guard, and the International GNSS Service. The plate models by Iwasaki et al. (2015) were constructed from topography and bathymetry data by the Geospatial Information Authority of Japan (250-m digital map), Japan Oceanographic Data Center (500m mesh bathymetry data, J-EGG500, http://www.jodc.go.jp/jodcweb/JDOSS/infoJEGG_j.html) and Geographic Information Network of Alaska, University of Alaska (Lindquist et al., 2004).

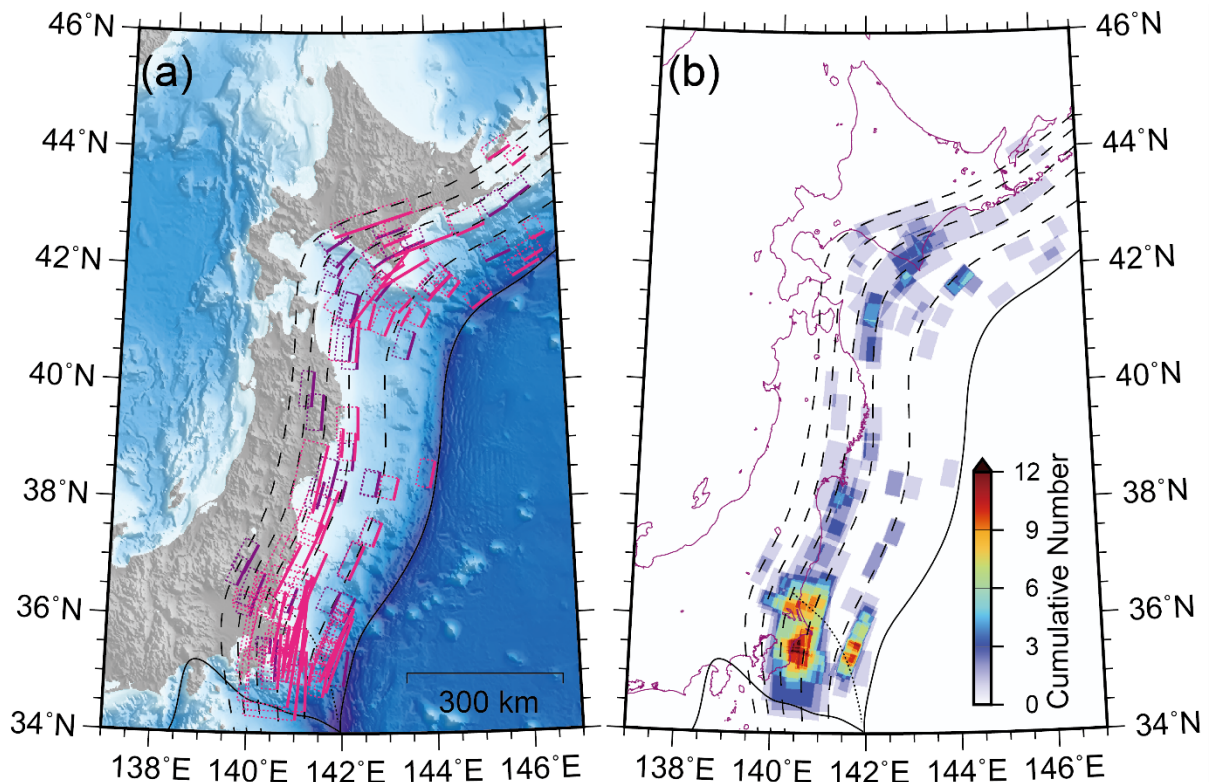


Figure 1. Spatial distribution of the detected S-SSEs. Black solid and dashed lines represent the Trench axis and the 20 km interval iso-depth contours of the Pacific plate (Iwasaki et al., 2015). **(a)** Fault model distribution of the detected events. Pink and purple rectangles show the fault models of class 1 and 2 SSEs, respectively. **(b)** Cumulative number of the detected events in the period from December 1996 to November 2021.

Role of smectite-illite transition in the onset of seismogenic zone in subduction zones from experimental viewpoints

Hanaya Okuda¹, Manami Kitamura², Miki Takahashi², Asuka Yamaguchi¹

¹AORI, Univ. Tokyo, ²GSJ, AIST

Seismogenic zone depth in subduction zones has been considered to be caused by the transition in frictional behavior of subducting sediment from stable sliding to potentially unstable sliding. Smectite-illite transition occurring at the temperature of $\sim 150^{\circ}\text{C}$ is one of the hypotheses for the control of transition in frictional behavior (e.g., Oleskevich et al., 1999). To clarify the role of smectite-illite transition in the onset of seismogenic zone, friction experiments on smectite-illite mixture have been conducted under room temperature (Saffer & Marone, 2003; Saffer et al., 2012; Tembe et al., 2010), showing little correlation between smectite-illite transition and transition in frictional behavior. However, the elevated temperature conditions critically change frictional behavior of various materials (e.g., den Hartog et al., 2012, Blanpied et al., 1995) and the effect of temperature on the frictional behavior of subducting sediment is rarely investigated. To evaluate the role of smectite-illite transition in the seismogenesis at the plate boundary fault (décollement) where temperature increases with depth, we used gas-medium high-temperature-high-pressure triaxial deformation apparatus in GSJ, AIST (Masuda et al., 2002), and conducted friction experiments on gouges with simulated sediment (quartz-albite-orthoclase-smectite-illite mixture) under *in-situ* pressure and temperature conditions in the Nankai Trough. Amount of smectite and illite in the gouge was varied based on locations along the décollement calculated by the kinetic expression of smectite-illite transition (Pytte & Reynolds, 1989) and the thermal structure in the Nankai Trough (Sugihara et al., 2014).

Preliminary, we did not see a transition from stable to potentially unstable sliding as illite content increased even at the temperature condition of the updip depth of seismogenic zone ($\sim 150^{\circ}\text{C}$), whereas friction coefficient of the gouge shows a positive relation with illite content. This result suggests that the décollement becomes frictionally strong with depth, but its seismic potential may not increase by the smectite-illite transition. Therefore, the onset of seismogenic zone would be contributed by factors other than the smectite-illite transition, such as frictional behavior of illite at high temperature (den Hartog et al., 2012), of consolidated sediment (Ikari & Hüpers, 2021), or of altered oceanic crust (Okuda et al., under review).

References:

- Blanpied, M.L., Lockner, D.A., & Byerlee, J.D. (1995). Frictional slip of granite at hydrothermal conditions. *Journal of Geophysical Research*.
- den Hartog, S.A.M., Niemeijer, A.R., & Spiers, C.J. (2012). New constraints on megathrust slip stability under subduction zone P – T conditions. *Earth and Planetary Science Letters*.

- Ikari, M.J., & Hüpers, A. (2021). Velocity-weakening friction induced by laboratory-controlled lithification. *Earth and Planetary Science Letters*.
- Masuda, K., Fujimoto, K., & Arai, T. (2002). A new gas-medium, high-pressure and high-temperature deformation apparatus at AIST, Japan. *Earth, Planets and Space*.
- Okuda, H., Niemeijer, A.R., Takahashi, M., Yamaguchi, A., & Spiers, C.J. (under review). Hydrothermal friction experiments on simulated basaltic fault gouge and implications for megathrust earthquakes. *Under review in Journal of Geophysical Research: Solid Earth*.
- Oleskevich, D.A., Hyndman, R.D., & Wang, K. (1999). The updip and downdip limits to great subduction earthquakes: Thermal and structural models of Cascadia, south Alaska, SW Japan, and Chile. *Journal of Geophysical Research*.
- Pytte, A.M., & Reynolds, R.C. (1989). The thermal transformation of smectite to illite. *Thermal History of Sedimentary Basins*.
- Saffer, D.M., Lockner, D.A., & McKiernan, A. (2012). Effects of smectite to illite transformation on the frictional strength and sliding stability of intact marine mudstones. *Geophysical Research Letters*.
- Saffer, D.M., & Marone, C. (2003). Comparison of smectite- and illite-rich gouge frictional properties: application to the updip limit of the seismogenic zone along subduction megathrusts. *Earth and Planetary Science Letters*.
- Sugihara, T., Kinoshita, M., Araki, E., Kimura, T., Kyo, M., Namba, Y., Kido, Y., Sanada, Y., & Thu, M.K. (2014). Re-evaluation of temperature at the updip limit of locked portion of Nankai megaspray inferred from IODP Site C0002 temperature observatory. *Earth, Planets and Space*.
- Tembe, S., Lockner, D.A., & Wong T.-F. (2010). Effect of clay content and mineralogy on frictional sliding behavior of simulated gouges: Binary and ternary mixtures of quartz, illite, and montmorillonite. *Journal of Geophysical Research*.

What makes low-frequency earthquakes low frequency?

Qing-Yu Wang^{1,2}, William Frank¹, Rachel Abercrombie³, Kazushige Obara², and Aitaro Kato²

1.Dept. EAPS, MIT. 2. ERI, Univ. Tokyo. 3. Boston Univ.

The Nankai Trough (Japan) hosts many slow earthquakes that could potentially precede, and even, trigger a large subduction zone earthquake. Constraints on the physical mechanisms responsible for slow earthquakes are essential to understand this potential interaction. Tiny repetitive earthquakes with a characteristic low-frequency signature, called low-frequency earthquakes, occur in conjunction with slow slip events. Learning the source properties of low-frequency earthquakes and the source region have essential implications for understanding the physical mechanisms responsible for slow earthquakes and the broad spectrum of faulting modes.

We isolate two 10 km-radius depth columns, one where low-frequency earthquakes periodically occur and one where they do not. Taking the collocated regular earthquakes below and above the subducting plate interface, we develop a three-step cluster-based approach to correct for local site effects, extract the accurate Empirical Attenuation functions, and apply them to the correction of Low-frequency earthquakes. The falloff of corrected displacement spectra inversely obeys the ω -square hypothesis with a maximum possible corner frequency of f_c at $\sim 2 - 3\text{Hz}$. The local 1-D vertical structure inverted from earthquake travel times suggests strong heterogeneities within the expected depths of the plate interface in both depth columns and a distinct difference in the ratios of seismic attenuation and velocity. The column with low-frequency earthquakes shows a quick change in the attenuation ratio at $\sim 42 - 45\text{km}$, where the intraslab seismogenic zone begins. The zone of low-frequency earthquakes is outlined by a relatively higher ratio of Q_p/Q_s larger than one and a ratio of V_p/V_s at depths of $\sim 25 - 45\text{km}$. Assuming seismic waves go through similar paths within depth column, the local attenuation is insufficient to generate specific low-frequency spectral content that differs from fast earthquakes. Instead, our results support a relative contrast of Q over depth with a higher Q at shallow depth above the zone of low-frequency earthquakes. This high Q layer may serve as an impermeable layer and produce an environment with enhanced pore-fluid pressure and heterogeneous frictional characteristics different from the zone with regular earthquakes. This particular condition favors low-frequency earthquakes and generates distinct nucleation procedures or/and rupture processes of low-frequency earthquakes from regular earthquakes.

Subsurface structural variations imaged by seismic reflection data along the Japan trench between 36–37.8°N: the overlapping of slow earthquake swarm and the rupture damping zone of 2011 Tohoku earthquake

Yanfang Qin¹, Yasuyuki Nakamura¹, Shuichi Kodaira¹, Gou Fujie¹

¹Japan Agency for Marine-Earth Science and Technology,
3173-25 Showa, Kanazawa, Yokohama, Japan 236-0001

The coseismic slip during the 2011 Tohoku earthquake has been revealed to reach the Japan trench axis, but the detailed slip behaviors in different zones along the trench remain an unsolved problem. To investigate the along-trench structures that directly affect the coseismic activities, we collected densely distributed seismic reflection data south of the major coseismic slip zone in the region of 36–37.8°N. The southern boundary of the 2011 event large coseismic rupture zone at ~37°N, has been indicated by previous studies that it correlates to an area in which slow earthquakes frequently occurred (Nishikawa et al., 2019), and can be defined by a density contrast (Bassett et al., 2016), which is also consistent with high velocity anomalies within the upper plate (e.g., Hua et al., 2020). Based on our dataset, this transition zone appears to correlate with the landward extension of a subducting channel in the deep places, and it has a coincidence with the slow earthquakes rupture zone. The shallow deformation of buried trench thrusts and folds rooted on the décollement are not well imaged in our profiles, probably they have not yet well developed as those in the main rupture zone (Nakamura et al., 2013, Kodaira et al., 2012). In addition, our seismic data document numerous local structural variations along different segments of the study zone: varying thicknesses of incoming sediments; diverse internal structures of the wedge front and morphologies of the subducting plate, with distinct physical properties above the plate interface and influencing, in turn, shallow megathrust slip and tsunami genesis.

Deformation of the seismogenic zone in the northeastern part of the Izu Peninsula, Japan, inferred from GNSS observations

Ryosuke Doke¹

¹Hot Springs Research Institute of Kanagawa Prefecture

The Izu collision zone, which is characterized by the collision between the Izu-Bonin arc and the Honshu arc, is located in the northernmost part of the Philippine Sea Plate. Particularly in the northeastern margin of the zone, numerous large earthquakes have occurred throughout history. To clarify the convergent tectonics of this zone related to the occurrence of these large earthquakes, in this study, we collected and analyzed GNSS observation data from the Izu collision zone. Our analysis provided the following results:

- 1) The GNSS velocity vectors in the eastern and western parts of the Kita-Izu Fault Zone are different; in particular, the sites located farther east have larger northward velocities in the area between the fault zone and the Ashigara Plain. That is, there is a shear deformation zone in the area extending from the northeastern part of the Izu Peninsula to the south of the Tanzawa Mountains, with maximum shear directions that agree with the left-lateral slip direction of the Kita-Izu Fault Zone (Figs. 1 and 2).
- 2) Seismic activities in the Tanzawa Mountains and the northeastern part of the Izu Peninsula were correlated. This might suggest that both areas are affected by temporal changes in stress accumulation due to the subduction of the Philippine Sea Plate.
- 3) The deformation rate obtained by GNSS data is almost the same as or twice the geologically determined deformation rate. This fact is important when considering the relationship between the accumulation process of deformation in the shear zone and the occurrence of large earthquakes at the West Sagami Bay Fracture or the Sagami Trough.
- 4) The shear zone can be regarded as the transition zone between plate collision and subduction zones: that is, the northeastern part of the Izu Peninsula is being dragged by the relative motion between the separated Izu Peninsula and the North American Plate, which is coupled to the rigid portion of the Philippine Sea Plate (Figs. 3a, b and d).
- 5) We assumed a weakly coupled detachment zone beneath the shear deformation zone (Fig. 3c). This can explain both the northward velocities in the shear zone and the divergent displacement and dike intrusion in the Higashi-Izu Monogenetic Volcano Group.

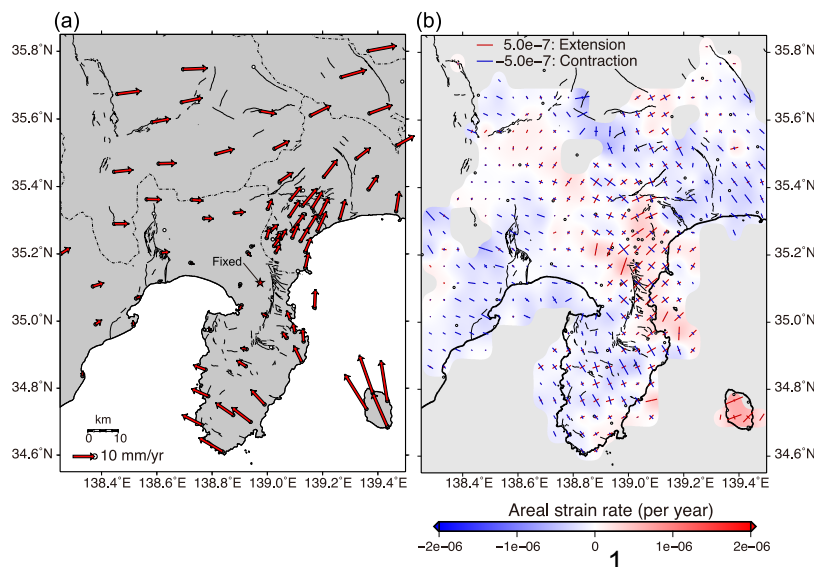


Fig 1. (a) GNSS velocity vectors and (b) distribution of principal and areal strain rates during 2016-2018. Velocity vectors indicate relative velocities with respect to the GEONET Kannami site (Fixed site in (a)).

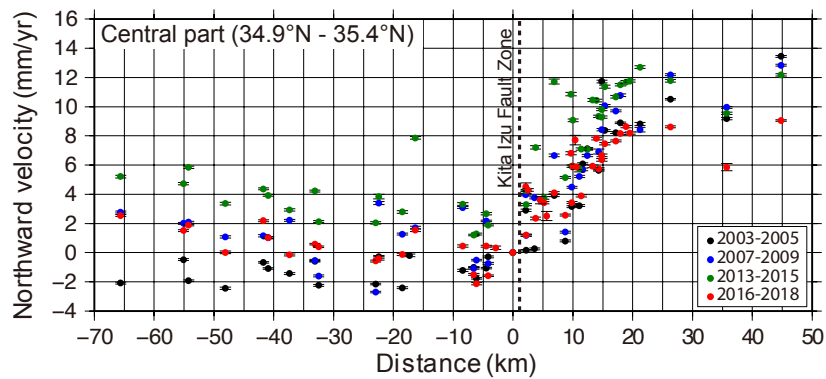


Fig 2. East-west profiles of GNSS northward velocity vectors in the central part (34.9°N - 35.4°N) of the study area. The horizontal axis shows the eastward distance from the Kannami site (Fixed site in Figure 1(a)).

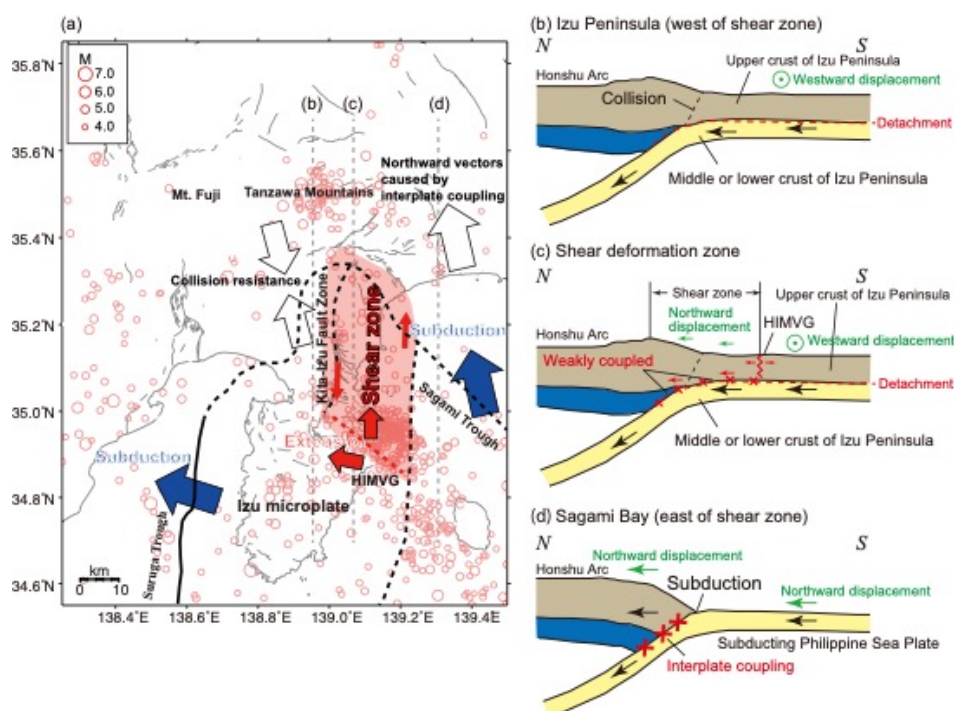


Fig 3. (a) Conceptual diagram of tectonic interpretation of Izu collision zone, with the locations of cross-sections (b), (c), and (d). (b) Because of the collision between the Izu Peninsula and the Honshu arc, the upper crust of the Izu Peninsula cannot move northwards. However, the middle or lower crust of the Izu Peninsula subducts beneath the Honshu arc (Arai et al., 2013). The crust of the Izu Peninsula is assumed to contain a detachment zone (Seno 2005). (c) Beneath the shear zone, it is assumed that the detachment is incomplete, and weak coupling occurs. This causes northward displacement in the shear deformation zone. Moreover, the relative motion between the shear zone and the detached zone causes divergence and dike intrusion at the Higashi-Izu Monogenetic Volcano Group (HIMVG). The weakly coupled zone causes the planarly distributed earthquakes. (d) East of the shear zone, the subducting forearc of the Philippine Sea Plate is coupled with the Honshu arc. This causes northward displacement in the inland area of the Honshu arc.

This presentation is based on the following paper, which was already published;
 Doke et al. (2020) Deformation of the seismogenic zone in the northeastern part of the Izu Peninsula, Japan, inferred from GNSS observations. *Geological Society, London, Special Publications*, **501**, 111-129. <https://doi.org/10.1144/SP501-2019-104>

Sediment properties of submarine mass movement deposits caused by subduction of topographic high at off Kumano region of the Nankai Trough

Rina Fukuchi¹, Mari Hamahashi², Masafumi Murayama³, Kazuya Shiraishi⁴, Yuichi Okuma⁵,
Juichiro Ashi⁵, and Asuka Yamaguchi⁵

¹Dept. Sci Educ, Naruto Univ. of Educ, ²Faculty of Global and Science Studies, Yamaguchi Univ.,

³Center for Advanced Marine Core Research, Kochi Univ., ⁴JAMSTEC, ⁵AORI, Univ. Tokyo

The relationship between changes in the evolutionary process of accretionary prism and seismicity caused by the subduction of topographic highs such as seamounts have many discussions (Scholz and Small, 1997; Cloos, 1992; Cloos and Shreve, 1996; Wang and Bilek, 2014). Recent research has also become clear that the subducting topographic highs are related to slow earthquakes (Sun et al., 2020).

At the Nankai Trough off Kumano, magnetic anomalies in the accretionary prism toe have been shown that a topographic high is subducting beneath the uplifted region in the northwest side coupled with an embayment to the immediate south. International Ocean Discovery Program (IODP) Sites C0006, C0007, and C0024 have been drilled at this location, and their stratigraphy and age have been studied to infer the structural evolution of the frontal wedge (Yamaguchi et al., 2020). On the western side of the drill sites off-Kumano, a submarine landslide topography (~10 km² size) is developed, which is considered to be caused by the subduction of the topographic high.

To investigate the nature of the submarine landslide and the effect of seamount subduction offshore Kumano, KS-22-3 cruise was carried out in March 2022 on the R/V Shinsei Maru, to retrieve surface sediments of the submarine mass movement deposits. The collected piston core sample, which was cored down to 2.8 m below the seafloor, was analyzed by X-ray CT analysis, and split in half for lithological description, smear slide observation, multi-sensor core logger (MSCL), and XRF core scanner (ITRAX) at Kochi Core Center, Japan. Gamma-ray density by MSCL shows values of ~1.5–2.0 g/cm³, increasing with depth from 0 to 1.4 m, with a large error in the measurements due to the distribution of gravels below 1.4 m.

Magnetic susceptibility ranges 0.66–2.9 × 10⁻³ SI, with the highest value at 1.38 m. This peak in magnetic susceptibility may reflect the lithology at 1.38 m which was silty sand with very coarse sand and contains opaque and volcanoclastic (vitric) grains. Gamma-ray density and magnetic susceptibility are generally similar to the values previously obtained from the shallow part of the accretionary frontal margin sites. The gravels between 1.4 and 1.7 m were sandstone, whereas gravels below 1.7 m were mudstone containing dominant greenish clay.

The clay minerals were composed of smectite, illite, and chlorite by using XRD. The muddy gravels are also characterized by a dominance of Ca and Fe, as measured by ITRAX.

Core description and the core sample analysis in this time suggested that the recovered gravels were harder than the matrix and originated from deeper burial depths. A lithological difference of gravels is observed at 1.7 m, possibly inferring a transition of event. But the mass movement deposits are expected to continue to greater depths, as indicated by seismic profile and the observed extent of the topography at the seafloor. Therefore, the submarine landslide topography might have been formed by multiple and/or large-scale landslides.

Further investigation is underway to clarify the origin of the mass transport deposit, by comparing the composition, physical properties, and age of the gravel deposits revealed in this study with the properties of the sediments at the frontal margin of the accretionary prism

previously drilled by IODP.

- Cloos, M. (1992), *Geology*, doi:10.1130/0091-7613(1992)020<0601:TTSZEA>2.3.CO;2
- Cloos, M. and Shreve, R.L. (1996), *Geology*, doi:10.1130/0091-7613(1996)024<0107:SZTATS>2.3.CO;2
- Scholz and Small, (1997) ,*Geology*, doi: 10.1130/0091-7613(1997)025<0487:TEOSSO>2.3.CO;2
- Sun et al. (2020), *Nat. Geosci.*, doi: 10.1038/s41561-020-0542-0
- Yamaguchi et al., 2020 ; IODP Expedition 358 C0024, doi: 10.14379/iodp.proc.358.104.2020
- Wang and Bilek (2014), *Geology*, doi: 10.1130/G31856.1

The role of seamount subduction on the earthquake cycle

Rosalie J. Verwijs, Camilla Catania

EAPS, Massachusetts Institute of Technology

The subduction of seamounts is likely to have a large influence on the slip behavior of megathrusts. These sources of heterogeneity affect the state of stress on the fault interface, fluid flow, and alter the upper plate, but there is no clear answer as to what role a seamount plays in hosting large earthquakes. Generally, large topographic heterogeneities in subduction zones are linked to earthquakes with a very complex source system. However, different studies found conflicting results: seamounts can promote the occurrence of large earthquakes, act as barriers to rupture propagation, or facilitate aseismic slip. These contrasting behaviors may be controlled by competing processes, such as the elastic deformation imparted by the seamount and its effect on hydraulic properties.

We are interested in the role of seamounts on the state of stress, slip stability, and seismic behavior. To investigate this, we combine two numerical models: SULEC, which is a long term model that simulates coupled mechanical and hydrological processes in a subduction zone, and FDRA, a quasi-dynamic rupturing short term code. The stress state output from SULEC, when the fault has reached a quasi-steady state, is used as input for the short term FDRA model.

We have implemented non-planar faults in a halfspace in FDRA, and we present early simulation results investigating the effect of a seamount on the state of stress in an elastic half space. We explore some idealized scenarios to quantify how the seamount affects the state of stress as a function of its dimension and distance from the free surface. These results will inform future, more realistic simulations which will include initial conditions and elastic heterogeneity calculated in SULEC.

Serpentinite carbonation produces rheological heterogeneities at the subduction interface

Samuele Papeschi¹, Paola Vannucchi², Takehiro Hirose¹ & Keishi Okazaki^{1,3}

¹Kochi(X-Star), JAMSTEC ²Dept. Earth Sciences, Univ. Florence, Italy, ³EPS Science Program, Hiroshima Univ.

Slip at the subduction interface is accompanied by contrasting modes of stress release, which include seismic slip, aseismic creep, and geodetically detectable slip accompanied by very low-frequency and low-frequency earthquakes and tremors, known as slow earthquakes. This rheological complexity is in part a direct result of the heterogeneous mixing of different material, which is commonly caused both by sedimentary and tectonic processes in subduction zones. In addition to this, chemical reactions between rocks and fluids can modify enormously the rheology of the subduction interface, for example through carbonation, which can transform nearly monomineralic serpentinites into rheologically heterogeneous mixtures of phyllosilicates and carbonates.

We hereby present the initial results of a study carried out on the Island of Elba (Italy) at the paleo-subduction interface between accreted ophiolitic units and underplated oceanic sediments. Ultramafic rocks, at the base of the upper plate, were sheared during subduction producing mylonitic lizardite- and antigorite-bearing serpentinites. The interaction with subduction-related fluids drove the progressive carbonation of serpentinite and the development of ophicarbonates with different proportions of talc, chlorite, carbonates, and quartz, which were sheared during top-to-E deformation in the Apenninic subduction. Slip within carbonated serpentinites was accommodated by contrasting deformation modes, which produced talc-rich mylonites coexisting with carbonate-rich cataclasites. In this study case, carbonation, not only modified the bulk rheology of the subduction interface but caused the change from nearly monomineralic serpentinites into heterogeneous mixtures of different minerals.

Spatial Relationship of Shallow Slow Earthquake and Strong Negative Velocity Impedance at Hyuga-nada

Yasunori Sawaki¹, Yusuke Yamashita², Shukei Ohyanagi¹, Emmanuel Soliman Garcia², Aki Ito³, Hiroko Sugioka⁴, Tsutomu Takahashi³, Masanao Shinohara⁵, and Yoshihiro Ito²

¹Graduate School of Science, Kyoto Univ., ²DPRI, Kyoto Univ.,

³JAMSTEC, ⁴Graduate School of Science, Kobe Univ., ⁵ERI, Univ. Tokyo

Thanks to seafloor seismic observations including ocean bottom seismograph (OBS) last decade, numerous shallow slow earthquakes have been reported in the Nankai subduction zone. The Hyuga-nada area at the western Nankai attracts our attention in terms of vigorous high activity of slow earthquakes, such as shallow tectonic tremors, and very-low-frequency earthquakes (Tonegawa et al., 2020; Yamashita et al., 2015, 2021). The occurrence of the shallow slow earthquakes in the Hyuga-nada is likely related to the subduction of the Kyushu–Palau Ridge (KPR) (Tonegawa et al., 2020), which leads to the complicated subsurface structure within the overriding plate (e.g., Nishizawa et al., 2009). Recently, Akuhara et al. (in revision) found a prominent low-velocity zone (LVZ) beneath ~3–4 km thick sediment over the KPR, by performing the transdimensional inversion of teleseismic Green’s functions (GFs; Akuhara et al., 2019) and a surface wave dispersion curve from a very dense (radius of ~2 km) array observation. Here we computed receiver functions (RFs) and GFs using widely distributed networks of broadband and short-period OBSs starting from 2014 to constrain the lateral distribution of the LVZ around the KPR concerning shallow slow earthquake activities.

The computed RF/GF traces showed significant phases with successive negative and positive amplitudes around 2-s lapse time. Assuming that RF/GF phases were attributed to *P*-to-*S* conversions beneath an OBS station, these successive phases showed a distinctive negative velocity impedance above a positive velocity impedance. This suggests the presence of the LVZ above the KPR (Akuhara et al., in revision) with ~100 km width around the source region of shallow slow earthquakes. We also found the lateral depth variation of the LVZ; the LVZ likely deepens towards the plate interface at the eastern end of the area with tectonic tremor activities in May 2015 (Yamashita et al., 2021). We will further discuss the spatial relationship between the LVZ and shallow slow earthquake events and related fluid processes.

[Acknowledgements]

We would like to appreciate the support for the seafloor observation projects by the Ministry of Education, Culture, Sports, Science, and Technology: “Research Project for Disaster Prevention on the great Earthquakes along the Nankai Trough” and “Science of Slow Earthquakes” in Grant-in-Aid for Scientific Research on Innovative Area.

Relating permeability and geophysical properties with asperity contact

Kazuki Sawayama¹ and Takeshi Tsuji²

¹BGRL, Dept. Science, Kyoto Univ., ²School of Eng., Univ. Tokyo

The crustal permeability anisotropy could be one possible cause of the occurrence of the slow earthquake and its spatio-temporal variations. Recent observations have revealed microtremors that cannot be explained by mineral dehydration, and it has been interpreted that differences in permeability at plate boundaries increase fluid pressure. Considering the heterogeneous asperity distribution in seismogenic zones, the asperity contact may affect such permeability differences. Many experimental studies have shown that the permeability in the weakly contacted discontinuity (i.e., faulted rock) is highly stress-dependent, whereas the permeability in strongly contacted fracture becomes almost constant. Given that slow earthquakes are sensitive to changes in ambient stress, the small changes in stress can trigger the change in such a contact state, causing drastic changes in permeability. Although in-situ permeability measurements are not accessible, geophysical properties (e.g., electrical resistivity, seismic velocity & amplitude) have the potential to estimate crustal permeability differences. In fact, recent observations have detected changes in electrical resistivity and seismic velocity due to crustal stress changes, possibly linked to permeability. This study verified how amount of the permeability change is induced by the asperity contact state based on numerical simulations of the digital rock. To propose a model to estimate crustal permeability changes from observed geophysical properties, we also investigated the changes in electrical and elastic properties at elevated asperity contact ratio of various fracture models.

We prepared a synthesized fault plane with controlled roughness based on the fractional Brownian motion and natural rough surfaces of natural rock fractures. For each fracture model, we applied various shear displacements and simulated the elastic-fully plastic deformation of the asperities by a half-space-based dry contact model, up to ~ 2.2 GPa of the normal loading. We adopted 125 GPa of Young's modulus based on the stress-strain experiment of fresh gabbro under high pressure. Based on deformed rough surfaces, we conducted fluid flow simulations by the lattice Boltzmann method. The size of the digital rock model is 24×24 mm with a $25 \mu\text{m}$ square grid. The provision of a constant body force from the inlet to the outlet boundaries and the periodic boundary along the fracture plane allowed us to simulate the fracture flows in the directions perpendicular to the shear direction. The permeability was then estimated from the macroscopic flow velocity, where we assumed Darcy flow and negligible matrix permeability. Geophysical properties are calculated by the finite element method. The electrical resistivity is estimated by simulated electric current associated with applied voltage in the same direction of the fluid flow. The fracture specific stiffness is evaluated by the fracture aperture changes against applied normal stress, and is related to the amplitude of the seismic wave. Each input to the simulation was determined based on laboratory experiments.

As a result, changes in permeability and geophysical properties are correlated with asperity contact (Figure). Their sensitivities against the asperity contact are differed by shear displacements; the rock properties of mated fracture (i.e., joint) have relatively low sensitivity, whereas those of the sheared fracture (i.e., fault) have significant dependence on the contact state. The permeability and resistivity changes against asperity contact show inflections at $\sim 50\%$ of contact. At larger asperity contact, almost no fluid flow is detected. Although

permeability at such conditions cannot be precisely calculated in our numerical model due to the limited voxel size, the permeability must be saturated after this percolation threshold. These results will be beneficial provided geophysical observation data predict permeability change triggered by subsurface stress perturbation.

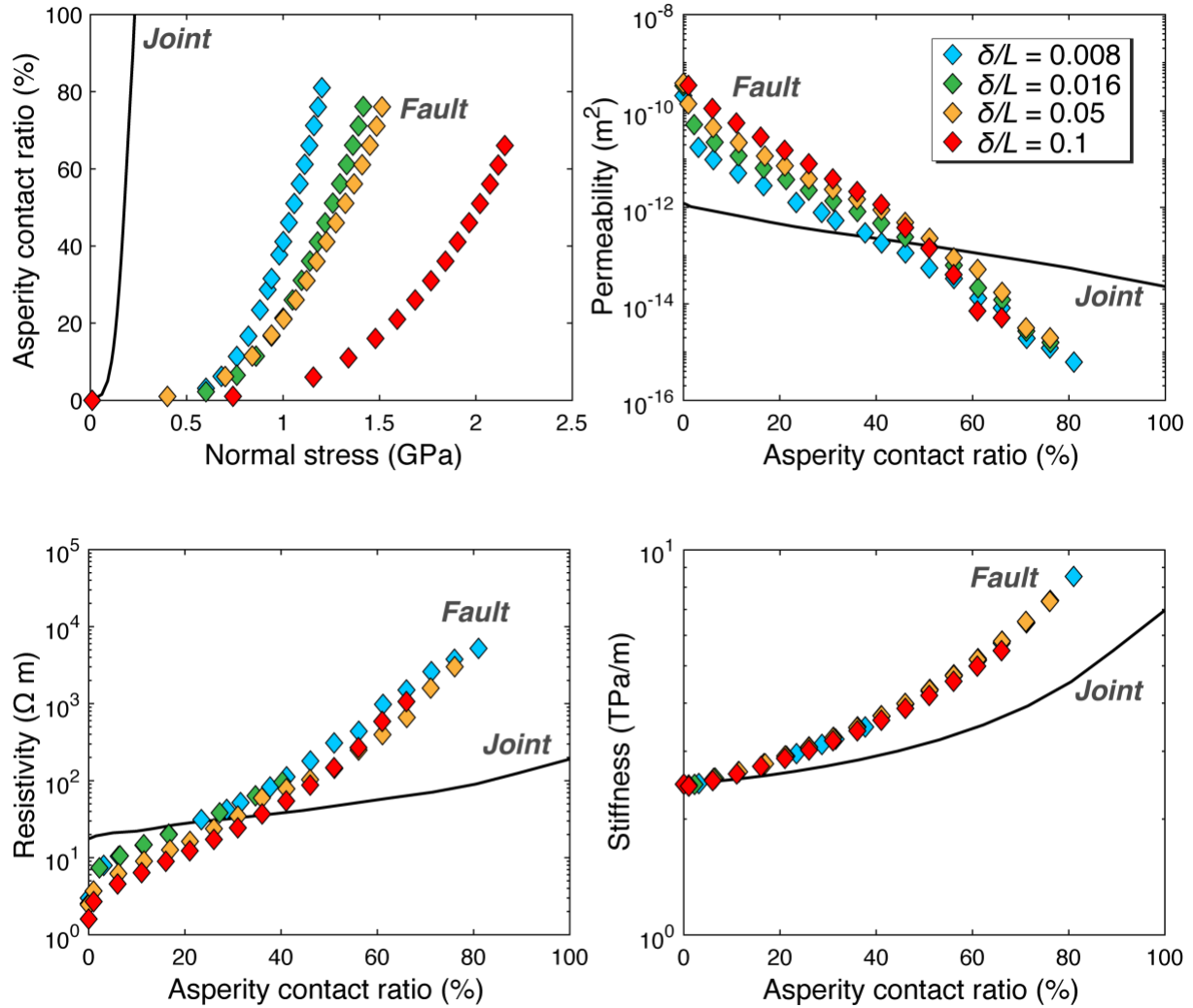


Figure: Plots showing asperity contact ratio versus normal stress, and the changes in permeability, electrical resistivity and fracture specific stiffness as a function of asperity contact ratio. The colour indicates different shear displacement ratios (δ/L), where fracture length L is fixed to be 24 mm in our calculations.

Structural features of the uppermost Philippine Sea Plate beneath the Kii Peninsula, central Japan

Katsuhiko Shiomi¹

¹ National Research Institute for Earth Science and Disaster Resilience

The structural feature of the Kii Peninsula is one of the keys to studying the source models of megathrust earthquakes in the Nankai Trough. In this study, we applied the harmonic decomposition (HD) analysis method (Bianchi *et al.*, 2010, doi: 10.1029/2009JB007061) to the receiver functions (RFs) at the stations in the Kii Peninsula and found that the subducting slab could be divided into distinct areas in terms of its plunge azimuth and the anisotropic feature in the oceanic crust. We confirmed that these segmentations corresponded well with the features of the intraslab seismicity and the deep tectonic tremor activity.

We used high S/N waveforms by teleseismic events with $M \geq 5.8$ observed at NIED Hi-net/F-net, JMA, ERI, DPRI, AIST, and MLIT stations in the Kii Peninsula. Applying a $f_c = 1.0$ Hz low-pass filter to the seismograms, we estimated RFs at each station. Using the three-dimensional velocity model by Matsubara *et al.* (2019, doi: 10.5772/intechopen.86936), we estimated the depth of the distinct velocity interface beneath each station. The velocity interface was located at ~ 30 km depth along the Pacific coast and deeper toward the inland area. Based on the comparison with the previous models (e.g., Shiomi *et al.*, 2008, doi: 10.1111/j.1365-246X.2008.03786.x), we concluded that the velocity interface was the Moho within the subducting Philippine Sea slab. Next, we applied the HD analysis to the RFs for the target depth of the slab Moho at each station. To estimate the plunge azimuth of the dipping slab Moho, we evaluated the principal axis of the particle motion for the first-order harmonic components with a time window from -0.2 to 0.2 s, where 0 s is the arrival time of the converted phase at the slab Moho. We used the second-order harmonics for a time window from -0.7 to -0.3 s to investigate anisotropic features of the oceanic crust. To evaluate the stability of the HD analysis, we applied 500-time bootstrap resampling to the RF dataset at each station and estimated the average and standard deviation σ . In the process of the bootstrap resampling, the result in which the amplitude of the unmodeled component was larger than that of the modeled component was rejected. For the station in which more than 300 results were rejected in the bootstrap test or which the estimation error 2σ exceeded 22.5° , we classified them as "unstable."

Figure 1 indicates the results of the HD analysis. Although the HD analysis was applied to each station independently, the neighboring stations showed similar results. The slab Moho in central Mie and Nara Prefectures inclined to the northwest, and the direction changed to the north in central Wakayama Prefecture. This feature is well coincident with the previous models. At five stations in northern Mie Prefecture, the plunge azimuths of the slab Moho were "unstable." According to the slab Moho geometry proposed by Shiomi *et al.* (2008), the interval

of the iso-depths was relatively wide in this region. Considering this feature and our results, the slab in this region may be a very low dip angle. On the other hand, the slab Moho beneath southern Wakayama and southern Mie Prefectures was dipping to the northeast, which is inconsistent with the previous models. The northern edge of this area corresponds well with the southern limit of the active tremor region. Within the region, where many stations indicated the northeast dipping slab Moho, two stations, E.HGU and E.KTU showed different results. The deeper extension of these two stations corresponds to the location of a small gap in the belt-like tremor zone. Next, we confirmed the anisotropic features of the oceanic crust (Figure 1b). In the up-dip region of the tremor zone, the fast axes are directed parallel to the strike of the slab iso-depth. In the northeastern Kii Peninsula, the fast axes were directed to the NE-SW even in the down-dip region. However, the axes showed various directions in the central and western peninsula. This feature may be affected by the valley-like shape of the subducting PHS. The region where the change of the anisotropic feature appeared corresponds well with the region where the location of intraslab seismicity transitions from the oceanic crust to the oceanic mantle (e.g., Shiomi & Park, 2008; doi: 10.1029/2007JB005535). Therefore, phase transitions of slab materials under complex stress fields may have been observed.

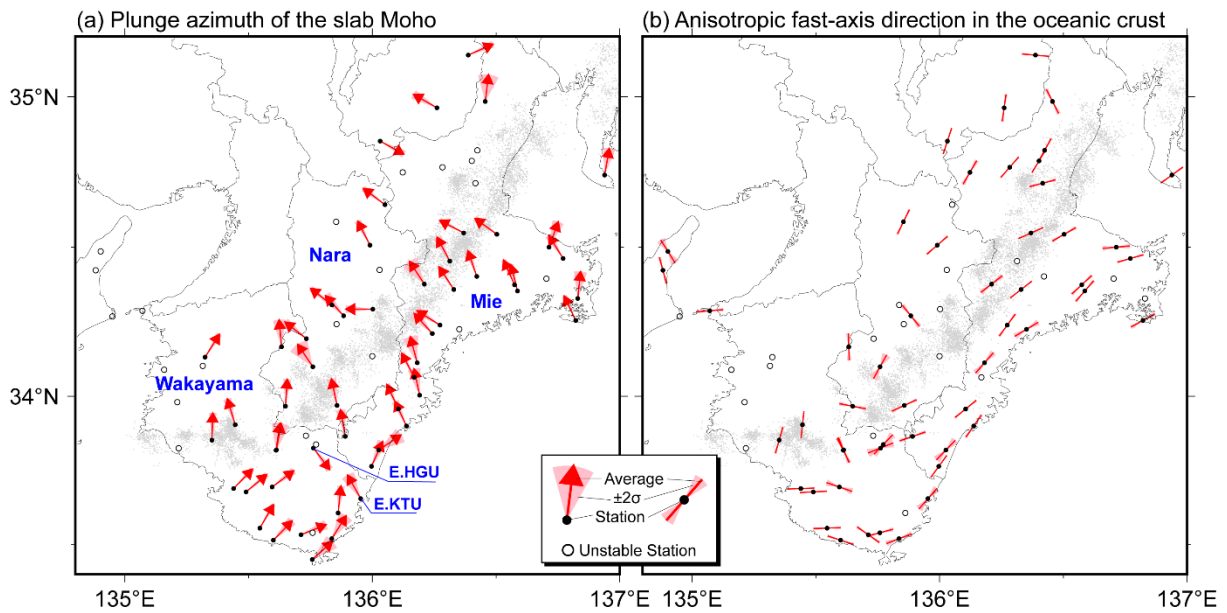


Figure 1 (a) Plunge azimuths of the Moho within the Philippine Sea slab estimated from the receiver functions' first-order harmonic components. The direction of the arrowhead indicates the deeper side. (b) Anisotropic fast axis directions within the oceanic crust of the slab estimated from the receiver functions' second-order harmonic components. Results with $\pm 2\sigma \leq 45^\circ$ are indicated in both figures.

Acknowledgements: We used the PDE Bulletin provided by the USGS, and the local hypocenter catalog jointly constructed by JMA, MEXT and other related institutes. Waveform data by NIED Hi-net/F-net, JMA, ERI, DPRI, AIST, and MLIT were used in this study. We are grateful to Jeffrey Park for making his program code for the HD analysis available.

Detectability of very low frequency earthquakes in Nankai

Shunsuke Taekemura¹, Satoru Baba², Suguru Yabe³, Yusuke Yamashita⁴,
Katsuhiko Shiomi⁵ and Takanori Matsuzawa⁵

¹ERI, Univ. Tokyo, ²JAMSTEC, ³AIST, ⁴DPRI, Kyoto Univ., ⁵NIED

To discuss source physics and seismicity of interplate slips, especially for slow earthquakes, the detectable limit of seismic phenomena is important. In Nankai, southwest Japan, the detectable limit of geodetic signatures due to interplate slips of both slow and fast earthquakes has been evaluated (Suito, 2016; Agata et al., 2019). In this study, we evaluated the spatial variation of detectable limits of very low frequency earthquakes (VLFs) in Nankai based on F-net/DONET broadband seismometers and numerical simulations using the 3D velocity model.

Green's functions from the plate boundary of the Philippine Sea plate were evaluated by the reciprocal calculations via the OpenSWPC (Maeda et al., 2017). We employed the regional 3D velocity model of Koketsu et al. (2012), assuming the minimum *S*-wave velocity of 1.5 km/s and assumed source grids on the plate boundary by a uniform interval of 0.05°. Focal mechanisms on each source grid are similar to those in Baba et al. (2020). We prepared the synthetic VLFE waveforms with various-duration boxcar functions. Maximum amplitudes of VLFs at a certain station are controlled mainly by moment rate (M_0/t) if we assume w^{-1} -type moment rate functions (w : angular frequency), such as the Brownian walk model and boxcar function. Ide (2008) and Ide & Maury (2018) demonstrated that the Brownian walk model could practically reproduce the characteristics of observed seismic slow earthquakes (tremors and VLFs). Thus, we employed the boxcar functions with durations of 5-200 s and M_w of 2.5-5 as w^{-1} -type moment rate functions to simplify the evaluation of detectable limits of VLFs.

To evaluate detectable limits by inland F-net broadband station around the Nankai, the analysis frequency range of F-net is 0.02-0.05 Hz, and amplitude thresholds of F-net horizontal and vertical components are assumed to be 5 and 3 nm/s, respectively. When there are three or more stations where the maximum amplitude in any of the components exceeds the thresholds, the VLFE is considered detectable. We determined the detectable limit at a certain source grid as the lowest moment rate from the detectable VLFs. Expected detectable limits of deep VLFs by inland F-net seismometers are $10^{12.5}$ - $10^{12.7}$ Nm/s beneath Shikoku and Kii. Inland F-net, which locate far from shallow VLFE sources, can detect shallow VLFs with $10^{13.0}$ - $10^{13.3}$ Nm/s. Expected detectable limits of shallow VLFs ($\sim 10^{13}$ Nm/s) well correspond with smaller shallow VLFs in the catalog of Takemura et al. (2022ab).

Then, we added onshore DONET broadband seismometers. DONET1 (22 stations) was deployed southeast off the Kii Peninsula, and DONET2 (29 stations) was deployed off the Kii Channel. The distance between DONET1 and DONET2 is approximately 60 km. Four or five stations of DONET are connected to one node. Inter-station distances within a node and inter-node distances are approximately 10 and 30 km, respectively. Due to characteristics noise in ocean bottom seismometers (Webb 1998), the analysis frequency range of DONET is 0.03-0.05 Hz, and amplitude thresholds of DONET horizontal and vertical components are assumed to be

30 and 3 nm/s, respectively. By introducing DONET, detectable limits of shallow VLFs beneath DONET stations are improved to approximately $10^{12.6}$ Nm/s. In the region between DONET1 and DONET2 and inter-node regions, detectable limits were not improved compared with those by inland F-net only. This is caused by large noise amplitudes in horizontal components and propagation features of shallow VLFE waves around DONET. As shown in Toh et al. (2018), amplitudes of shallow VLFE signals at stations with epicentral distances larger than 20 km become several ten times smaller than those just above shallow VLFE sources. Although near-source records from DONET allow us to investigate detailed hypocenter determination and source analysis of shallow VLFs (e.g., Toh et al., 2020; Yamamoto et al., 2022), inland F-net data is better for comprehensive monitoring of VLFs in Nankai.

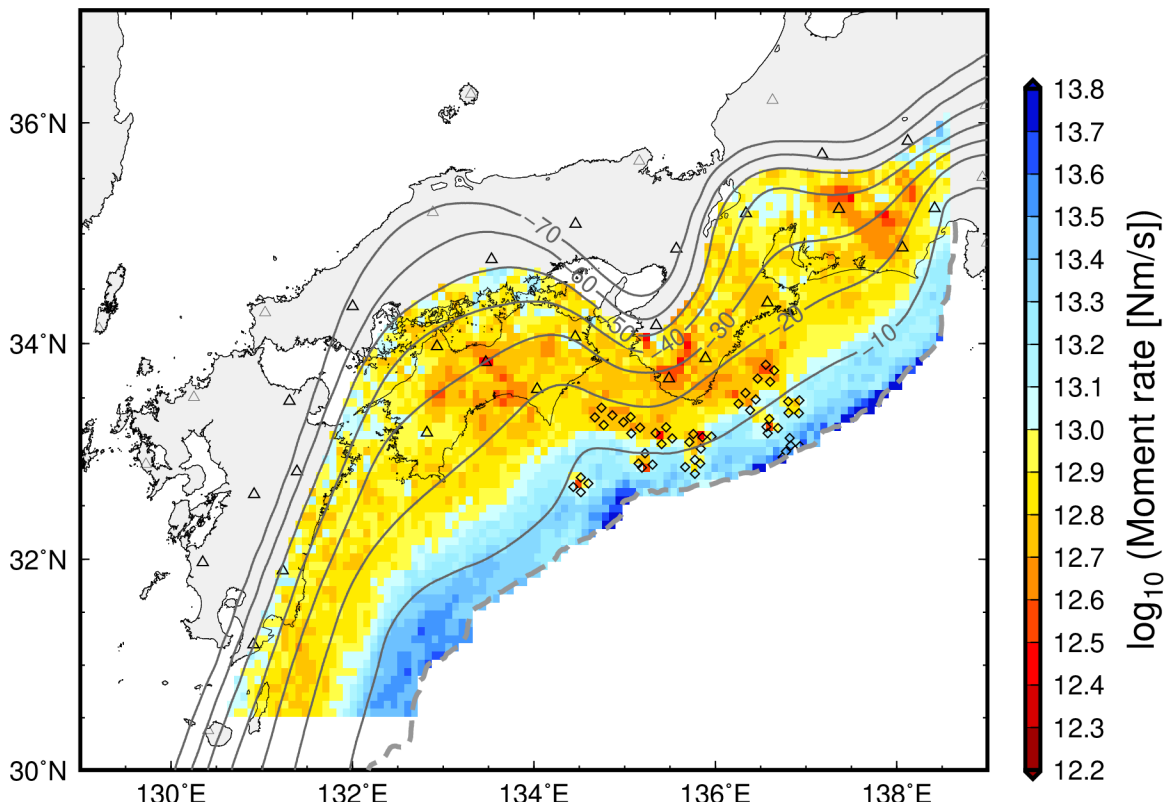


Figure. Spatial variation of the detectable limits of very low frequency earthquakes in Nankai. The contour lines in the map are the upper surface of the Philippine Sea Plate by Koketsu et al. (2012). The black open triangles and diamonds are the used F-net and DONET stations, respectively.

Estimation of the crustal deformation using radiated energy of tectonic tremors in the northern Kii Peninsula, Nankai subduction zone

Tsukasa Yamamoto¹, Yoshihiro Hiramatsu¹

¹Kanazawa University

Monitoring slip and seismic activity in the transition zone at a subducting plate is important to understand the seismogenic process at shallow plate boundaries. Tectonic tremors and short-term SSEs have been known to occur in spatio-temporal synchrony as episodic tremor and slip (ETS) events. Maeda and Obara (2009) reported that the scaled energy between the accumulated radiated energy of tremors and the seismic moment of a slow slip event is almost constant. On the other hand, slip without tremors has also been observed (e.g. Wech and Bartlow, 2014). The northern Kii Peninsula is one of the most active regions of ETS events in the Nankai subduction zone. Recently, Nakamoto et al. (2021) estimated radiated energy of tremors for ETS events beneath the northern Kii Peninsula by using waveform data recorded by a seismic array, providing suitable data to examine the relationship between the radiated energy of tremors and slips. The objective of this study is to estimate the amount of crustal deformation using the source location and radiative energy of tremors.

We used the epicenter and radiated energy of tremors estimated from seismic waveform data of the array observation network of the National Institute of Advanced Industrial Science and Technology (AIST) (Nakamoto et al., 2021). Among the ETSs reported in Nakamoto et al. (2021), we select ETSs which include sufficiently large clusters of tremors and only one short-term SSE estimated from geodetic data. We used the plate interface model of Shiomi et al. (2008) and set subfaults of a size of 10 km by 10 km and distribute tremors to each subfault to obtain the cumulative radiated energy for each subfault. We estimated the slip of each subfault from the conversion of the cumulative radiated energy to seismic moment by using scaled energy. For each ETS, the scaled energy was calculated as the ratio of the cumulative radiated energy to the seismic moment of a short-term SSE. The crustal deformation is then calculated using the fault parameters and slip of each subfault. First, we assume that the scaled energy is spatially homogeneous for each ETS event. We set the strike, dip, and slip for each subfault as follows: (1) consistent strike and dip with the plate interface model and the rake of 90°, (2) the same strike, dip, and rake as those of the short-term SSEs estimated geodetically, (3) consistent strike and dip with the plate interface model, and rake which minimizes the difference between the observed and calculated tilts change, (4) consistent strike and dip with the plate interface model, and the rake of which the azimuth of slip is constant; (5) using the plate interface model of Iwasaki et al. (2015) and use the same conditions as those in (1).

For each ETS, the amount of tilt estimated from the cumulative radiated energy of the tremors

differed by a several factors under all conditions compared to the observed values. To quantitatively evaluate the difference between the observed and calculated tilts, we use the L2 norm of the difference between the observed and calculated tilts of the east-west and north-south component. We find that the case (3) shows the smallest L2 norm. To examine the effect of a heterogeneous spatial distribution of scaled energy, we define high radiated energy regions where the cumulative energy of tremors in all ETSs exceeds 1.0×10^8 J on a subfault and varies the scaled energy in the high radiated energy regions, 0.1, 0.2, 0.5, 1, 10, 20, and 50 times higher than that of the other regions for the case (1). As a result, the L2 norm becomes the minimum when the scaled energy is one time, i.e., the same value as the other regions. Therefore, we suggest that the scaled energy is spatially homogeneously distributed in the analyzed region.

Spatio-temporal seismic velocity change near the Japan-Kuril trenches junction revealed from long-term dense-OBS network observation

Takehiro Sato¹, Ryosuke Azuma¹, Ryota Takagi¹, Ryota Hino¹, Masanao Shinohara²

¹Tohoku University, ²ERI, Univ. Tokyo

Seismic interferometry (SI) is often used to detect the temporal change in seismic velocity caused by large earthquakes because SI can obtain Green's functions with high temporal resolution. Recent studies using SI succeeded to detect seismic velocity changes associated with regular and slow earthquakes (e.g., Tonegawa et al., 2022). In the Japan-Kuril trenches junction, a dense array composed of 42 ocean bottom seismometers (OBSs), equipped with three-components 1 Hz velocity sensors, and observed waveforms were recorded with a 200-Hz sampling rate, were in place in 2006–2007. During the observation, three tectonic tremor activities (Kawakubo et al., 2021), two large earthquakes off the Kuril Islands (Lay et al., 2009), and a local moderate earthquake (Mj 6.2) have happened and possibly brought seismic velocity change. We examined the temporal changes in seismic velocity related to those activities by seismic interferometry.

We computed nine-component single-station cross-correlation functions (CCFs) from three-component continuous records (Hobiger et al., 2014; Uemura et al., 2018). The frequency range is 1–2 Hz, where the spectral amplitude is stable in time. The velocity changes were estimated from 15-days-averaged CCFs by assuming a homogeneous velocity change around a station.

We detected several temporal changes in seismic velocity, exceeding estimation error, during the observation period. The most remarkable change is the coseismic drop of 0.05–0.2% and following recovery, coincident with the Mj 6.2 event, at sites near the epicenter. The detected coseismic velocity drop would be explained as damage to the subsurface structure by strong ground shaking. In addition, several velocity reduction events with smaller magnitude, ~0.02–0.05%, were identified. The tremor activities, the local earthquake, and the teleseismic large earthquakes are supposed to be candidates of the causes of the velocity reduction. We plan to investigate the relationship of those reduction events with the ground motions to see whether the strong ground motion by the local and the teleseismic earthquakes account for the reduction.

POSTER

Strain Partitioning and Interseismic Fault Behavior Along the Caribbean-South American Transform Plate Boundary: Creeping and Locked Faults, and Fast and Slow (?) Earthquakes

Higgins, M.^{1,2}, La Femina, P.¹, **Weber, J.**³, Geirsson, H.⁴, Ryan, G.⁵, and
Wauthier, C.¹

¹Dept. of Geosciences, The Pennsylvania State University, University Park, PA USA, ²Department of Geology, Florida International University, Miami, FL USA, ³Department of Geology, Grand Valley State University, Allendale, MI USA, ⁴Institute of Earth Sciences, University of Iceland, Reykjavik, Iceland, ⁵Seismic Research Centre, University of the West Indies, Ste. Augustine, Trinidad, West Indies

We combined Global Positioning System and Interferometric Synthetic Aperture Radar (InSAR) data to characterize the interseismic behavior (i.e., locked or creeping), and strain partitioning for the faults along the ~900 km long Caribbean-South American transform plate boundary. Interseismic strain is distributed mainly on three faults, the San Sebastian, El Pilar, and Central Range faults, but partitioning occurs across multiple faults in the west (San Sebastian and La Victoria faults) and east (Sub-Tobago Terrane, Central Range, and South Coast faults). In northern Venezuela, slip is partitioned on the San Sebastian (16.4 ± 1.7 mm/yr) and La Victoria (4.3 ± 0.9 mm/yr) faults. In north-eastern Venezuela, the El Pilar fault accommodates slip at a rate of 18.6 ± 1.8 mm/yr. In Trinidad and Tobago, slip is partitioned between the Sub-Tobago Terrane (3.0 ± 0.1 mm/yr), Central Range (14.5 ± 2.0 mm/yr), and South Coast (3.0 ± 0.1 mm/yr) faults. The La Victoria, San Sebastian, the western El Pilar segment, and Sub-Tobago Terrane faults are locked to depths of 16.2 ± 4.0 km, 7.7 ± 5.2 km, 6.7 ± 2.8 km, and 8.0 ± 0.2 km, respectively. The eastern segment of the El Pilar, the Central Range, and the South Coast faults all creep. Our new InSAR results indicate that the entire Central Range Fault is creeping. The locked western segment of this transform plate boundary may be capable of producing a Mw 8 earthquake, which is a significant finding regarding seismic hazard and risk. We are also currently evaluating cGPS time-series to determine whether slow slip earthquakes also occur – e.g., in creep-to-locked transition zones – along this ~900 km long transform plate boundary.

An improved method of mitigating orbital errors in multiple SAR interferometric pairs analysis for slow crustal deformation measurement

Qian XU

ERI, Univ. Tokyo

It is challenging to precisely measure the slow crustal deformation rate using SAR data. The long-wavelength orbital errors, owing to the uncertainties in satellite orbit vectors, commonly exist in SAR interferograms, which degrade the precision of the InSAR products and become the main barrier of extracting interseismic tectonic deformation. Here, I propose a novel temporal network orbital correction method that is able to isolate the far-fault tectonic deformation from the mixed long-wavelength signals based on its spatio-temporal characteristic. The proposed approach could effectively separate the subtle tectonic deformation from glaring orbital errors without ancillary data, and enhance the availability of InSAR technology for slow crustal deformation measurement. The reliability and effectiveness of this method have been validated by the synthetic data and real Sentinel-1 SAR images. A case of extracting the interseismic deformation along the Tuosuo Lake segment of the Kunlun fault (China) is given. The derived InSAR velocity fields clearly present the predominant left-lateral strike-slip motions of the Tuosuo Lake segment. The fault-parallel velocity differences across the fault between areas ~50 km away from the fault trace are found to be 5-6 mm/yr. The estimated average surface creep rate of 0.3 mm/yr indicates that the Kunlun Tuosuo Lake segment is highly-locked with the risk of future seismic hazard.

Slow stick-slips on a meter-scale laboratory fault

Futoshi Yamashita¹, Kurama Okubo¹, and Eiichi Fukuyama^{2,1}

¹NIED, ²Graduate School of Engineering, Kyoto Univ.

Fault slip mode is dominantly controlled by the balance between the elastic loading stiffness k and the rheological critical stiffness k_c . When $k_c > k$, the system is unstable, which corresponds to the regular earthquake on the natural fault. As k_c decreases, the system goes to more stable. When $k_c \sim k$, the system falls into the boundary between unstable and stable, and the episodic slow slips arise on the fault. It is considered that such a slip behavior is closely related to the slow earthquakes in nature. In centimeter-scale laboratory experiments, slow stick-slip events, whose peak slip velocity is lower than the regular stick-slip events, were observed by tuning the stiffness balance at around $k_c \sim k$ (e.g., Leeman et al., 2016, Nature Communications; Leeman et al., 2018, JGR; Tinti et al. 2016, JGR). Here we report that similar slip behaviors were observed even on a meter-scale laboratory fault.

The meter-scale experiments were carried out with the large-scale rock friction apparatus at NIED (Yamashita et al., 2015, Nature). The fault dimension was 1.0 m in length by 0.1 m in width. We distributed metagabbro particles ground with a jet mill as the simulated gouge (mean diameter: 12 μm , maximum diameter: 75 μm) as homogeneously as possible over the fault before each experiment. The initial thickness before the compression was 3 mm. The driver blocks were also metagabbro. We first applied normal stress on the fault, and then sheared at a constant loading velocity. The normal stress (σ) and the shear stress (τ) were individually monitored by load cells.

In all experiments, the initial fault slips were stable. But in some cases, the observed τ/σ started to oscillate at some shear displacement, that is, the stable sliding transitioned to the slow stick-slips. The experimental conditions, under which the slow stick-slip was observed, are shown in Table 1, though the amplitude of τ/σ oscillation was tiny in the experiment LB21-0015. As shown in Table 1, the maximum amplitude of τ/σ oscillation, which corresponds to half of the maximum strength drop and called A_{max} here, is larger when the loading velocity is larger for the same normal stress.

We then examined if the frictional parameters can be constrained by numerical simulations of slow stick-slips. Following Urata et al. (2017, PAGEOPH), we assumed a spring-slider model with one-degree-freedom. The fault slip was assumed to obey Slip law of rate- and state-dependent frictional (RSF) law. With the same experimental settings, the velocity step change tests were carried out and RSF parameters were estimated (Shimoda et al., 2020, SSJ meeting; Yamashita et al., 2022, JpGU meeting); $(a, b, D_c) = (0.004156, 0.004983, 23.9 \mu\text{m})$. We fixed the RSF parameters a and b at the estimated ones and searched for optimum D_c values that can simulate the slow stick-slips whose A_{max} is closest to the observed one. As the results, we obtained 6 μm for the optimum D_c .

While this D_c is the best for reproducing the observed A_{max} , it cannot simulate the initial stable sliding. The transition from the stable sliding to the slow stick-slip suggests that k_c gradually increased. We consider that it is basically due to a decrease in D_c with the shear displacement (e.g., Marone and Kilgore, 1993, Nature), and D_c might be large at the initial stage of the

experiments as suggested by the estimate based on the velocity step change tests.

It should be noted that the slow stick-slips went back to the stable sliding except for the experiment LB21-018 before the shear displacement reached its limit (400 mm). Such behaviors were not observed in the small-scale experiments, and therefore the large fault area and/or the large slip displacement could decrease k_c again and then cause such behaviors. We will investigate its mechanism by analyzing the local strain data and the microstructure of the gouge layer sampled after each experiment.

Table 1. Experimental conditions

ID	Normal stress (MPa)	Loading velocity (mm/s)	Maximum amplitude of τ/σ oscillation, A_{\max}
LB21-0012	1.3	10	0.031884
LB21-0013	1.3	15	0.055662
LB21-0014	1.3	30	0.099488
LB21-0015	2.7	5	0.001645
LB21-0016	2.7	10	0.008367
LB21-0017	2.7	15	0.028781
LB21-0018	2.7	30	0.045639

Effect of fluid flow on fault healing

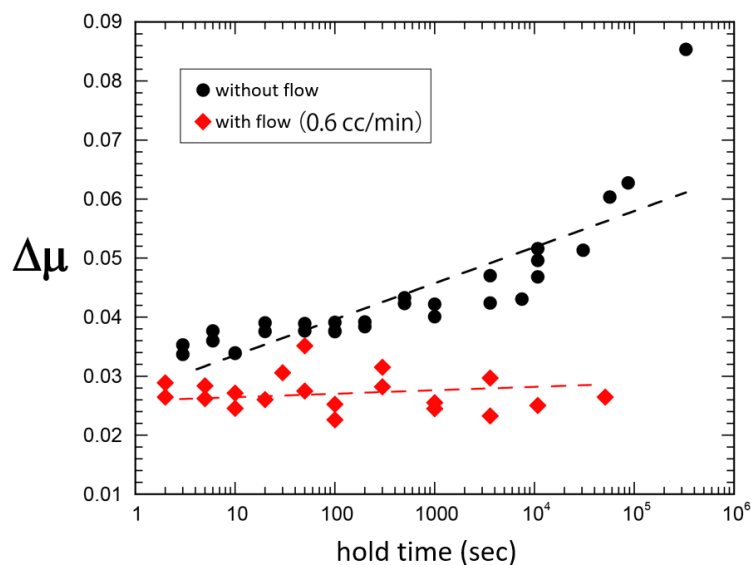
Yohei Hamada¹, Takehiro Hirose¹, Wataru Tanikawa¹

¹JAMSTEC, Kochi

Various seismological and geological observations have focused on the role of fluids in the generation of earthquake, including slow slip. A recent scientific drilling project found the existence of high-pressure aquifer in slow slip regions. The fluid in the fault may not only reduce the fault strength by producing high pore pressure but may also control the process of fault strength recovery through physico-chemical interaction with the fault material. Here, we conduct laboratory friction experiments to verify the hypothesis that the flow of water suppresses the increase of fault strength. We performed slide-hold-slide tests under the condition of water flow (flow SHS test) using a fluid pressure-controlled rotary shear apparatus installed in JAMSTEC Kochi.

Ceramic ball (30 - 1000 μm) and crushed Indian sandstone (125-250 μm) were used as simulated fault gouge, and the flow SHS tests were performed under the condition of flowing water at a flow rate of 0.0cc/min and 0.6 cc/min to compare the strength recovery rate. The experiment was conducted under the conditions of a slip velocity of 5 $\mu\text{m/s}$, normal stress of 3 MPa, water pressure of 0.3 - 1.5 MPa, and a hold time of 2 seconds to 72 hours.

In the case without the flow, the frictional strength recovered in proportion to the logarithm of time, as in previous studies (e.g. Dietrich, 1972; black dots in the figure). On the other hand, the frictional strength did not almost recover in the presence of flow (red squares). The water pressure tended to gradually increase with the hold time. When the strength recovery is expressed by the effective friction coefficient, the increase rate of the friction coefficient was almost the same as that when there was no flow. This result was obtained for both ceramic and natural sand, confirming that this inhibition of strength recovery occurs independently of the interaction between the fluid and the gouge. Furthermore, there was an increase in fluid pressure over time, which suggests that the increase in contact area may have blocked the flow path, thereby causing an increase in fluid pressure and consequently no apparent strength recovery. The presentation will include a preliminary discussion of the torque control experiments.



Preliminary analysis of continuous gravity measurement data obtained in a slow slip area in the Ryukyu Trench

Yuichi Hiramatsu¹, Yoshiyuki Tanaka¹, and Akio Kobayashi²

¹Department of Earth Planetary and Science, The University of Tokyo

²Meteorological Research Institute, Japan Meteorological Agency

Seismological studies have revealed that high-pressure crustal fluids cause slow slip events (SSEs) on the plate interface along the circum-Pacific subduction zones. In the Tokai area in Japan, gravity anomalies synchronized with long-term SSEs (duration of ~5 years) were detected by absolute gravimeters, suggesting that fluids could migrate up-dip along the plate interface during the SSEs. However, the temporal resolution of the gravimetry was 1 year, which was insufficient to know whether similar gravity anomalies occur during SSEs with shorter durations. In Ishigaki Island in the Ryukyu Trench, SSEs with durations of ~1 month have occurred approximately twice a year. We initiated a continuous measurement using two gPhoneX gravimeters in January 2020.

We report a preliminary analysis result of gravity data obtained till June 2022. We removed noises from earthquakes and typhoons and corrected for the effects of atmospheric pressure, tides and polar motion. The entire observation period was divided into a few-month periods and an instrumental drift during each period was removed with a quadratic function. The residual changes from both gravimeters agreed within ~1 microGal.

To discuss gravity anomalies associated with SSEs, we need to remove groundwater effect. We initiated continuous groundwater observation near the gravity site in March 2022. We found a good correspondence between the groundwater levels and the tidal levels observed at the Ishigaki Port. The non-tidal changes of the groundwater amounted to +/- 10 cm and were considered too small to detect with the gravity observation. Next, we physically modeled gravity changes due to precipitation with the GWATER-1D incorporating daily weather data. The model well explained the increases in gravity just after rainfall events but underestimated the subsequent decreases. We found that patterns of the increases and decreases in gravity were different depending on total amount of rainfall and durations of rainfall events. We are trying to use these patterns to improve the model prediction.

**Subduction–accretion–exhumation processes in the subduction zone:
Example from the Cretaceous subduction complexes
on the central Kii Peninsula, SW Japan**

Yusuke Shimura¹, Tetsuya Tokiwa², Makoto Takeuchi^{1,3}

¹Geological Survey of Japan, AIST,

²Faculty of Science, Shinshu Univ.,

³Graduate School of Environmental Studies, Nagoya Univ.

Ancient high-*P*/low-*T* metamorphic and accretionary complexes have formed respectively in the deep and shallow parts of the subduction zone. The two complexes have recorded evidence of slow to fast slips occurred in the subduction plate boundary. Many researchers have studied for these complexes in terms of lithology, geological structure, and their evolution, and they have discussed about linkage with a generation of several types of earthquakes in the subduction plate boundary. However, these earthquakes have occurred frequently on the forearc region, and therefore, the nature of the geological formation processes on the forearc region is essential for comprehensive understanding of the earthquakes in the subduction zone. The present study focuses on the Cretaceous subduction complexes in SW Japan, namely the Sanbagawa high-*P*/low-*T* Metamorphic Complex and the Shimanto Accretionary Complex. These ancient complexes have been well studied by kinematic, thermal, geochronological, and geochemical investigations with respect to understanding earthquake generation, but a series of the tectonic processes has not yet been clarified. We conducted lithological, structural, chronological, and thermal studies for the Cretaceous subduction complexes located on the central Kii Peninsula, SW Japan, and aimed to elucidate their subduction, accretion, and exhumation processes.

The Cretaceous subduction complexes on the central Kii Peninsula are divided into eight formations in descending order of structural position: Kosoku, Iro, Mugitani, Kogurisu, Atarashi, Takaharagawa, Akataki, and Makio formations. The eight formations can be grouped three types in terms of lithological and structural characteristics: Sanbagawa type (Kosoku and Iro formations), Mugitani type (Mugitani, Kogurisu, and Atarashi formations), and Shimanto type (Takaharagawa, Akataki, and Makio formations). The Sanbagawa type of formations records exhumation-related deformation, which produced schistosity, stretching lineation, and folds. The Mugitani type of formations records both earlier accretion-related deformation which produced block-in-matrix structures and later exhumation-related deformation. The Shimanto type of formations records accretion-related deformation. Each type of formations shows the Aptian to Maastrichtian in the depositional age of clastic rocks, which is younger in descending order of structural position. In addition, the Sanbagawa, Mugitani, and Shimanto types of formations show the peak temperatures of 280–440 °C, 280–290 °C, and ca. 280 °C, respectively, showing that higher temperatures of types are found at structurally higher position. We assume that the Cretaceous subduction complexes show the large-scale tectonic juxtapositions of complexes, which resulted the types of formations representing deeper facies in the subduction zone at higher structural levels. These types of formations are in fault contact with each other, and thus, the accumulation of the slow to fast slips on the forearc region have likely generated these geological structures.

Development of UAV technology to realize high-frequency GNSS-A observation: preparation

Yusuke Yokota¹, Takenori Hashimoto², Shusaku Yamaura², Masata Kaneda²,
Taichi Kawakami³, Yoshiaki Hirakawa⁴, and Takumi Matsuda⁵

¹IIS, Univ. Tokyo, ²SELAB, Co., Ltd., ³Kaiyodenshi, Co., Ltd., ⁴Yokohama National Univ.,
⁵Meiji Univ.

GNSS-A is a technology that realizes steady seafloor geodetic observation. It corresponds to the GNSS observation in the land area. Since the latter half of the 20th century, long-term slow slip events (year-scale) have been detected using the GNSS (Ozawa et al., 2002, Science), but shallow undersea trench-region SSEs only recently have been detected using the GNSS-A (Yokota & Ishikawa, 2020, Sci Adv). It has already been shown that the current vessel observations lack accuracy and frequency, and do not have sufficient detection capability (Yokota et al., 2021, PEPS). Observation methods using second-generation sea-surface platforms such as a wave-glider and a buoy have been proposed and studied (Tadokoro et al., 2020, FES; Iinuma et al., 2021, FES; Sakic et al., 2021, FES), but there is a problem with their ability to maintain a sea surface in areas with strong tidal currents. Therefore, research is underway to apply the sea surface landing type UAV as a third-generation platform to underwater and seafloor observations (e.g., Yokota & Matsuda, 2021, RS). Here, we will focus on the flying boat type UAV and introduce the preparation research for its realization.

SELAB's flying boat type sea-surface landing UAV HAMADORI can take off and land only on the surface of the water, and its application to transportation, fisheries, and others ... is already underway. The biggest consideration in UAV observation is the weight of the equipment, and it is desirable to keep it below 10 kg in consideration of the 100 km-flight. In general, the internal processing equipment, the parts that generate the acoustic signal, the sonar that transmits the signal together weigh tens of kilograms. Here, these were designed to be lightweight and to be installed on the body of the UAV. The operation test in the water tank has been completed, and after the final construction and mounting, the test in the actual sea area is planned. Two observation sites are planned to be added to the Nankai Trough area for this research.

At the same time, it is difficult to detect SSE unless the observation accuracy similar to that of vessel observation can be obtained. Regarding the estimation of underwater disturbance, which is the largest error factor of GNSS-A, the influence has been reduced by modeling a series of studies (Yokota et al., 2018, MGR; Yokota & Ishikawa, 2019, SNAS; Yokota, 2019, JMASJ; Yokota et al., 2020, FES; Yokota et al., 2022, under review; Watanabe et al., 2022, under review). On the other hand, there is the bias error including signal reading error, angle dependence, and device dependence due to the finite size of a sonar. It has a particularly large effect on vertical component. Currently, we are studying a method for correcting these errors, and preparations for experimental verification are underway.

Acknowledgement:

This study is supported by ERI JURP 2022-Y-KOBO25 in Earthquake Research Institute, the University of Tokyo, by the University of Tokyo Excellent Young Researcher project, by SECOM science and technology foundation, and by JSPS KAKENHI Grant Number JP21H05200 in Grant-in-Aid for Transformative Research Areas (A) "Science of Slow-to-Fast Earthquakes."

Tremor-like behavior in nucleation of laboratory earthquakes

Tetsuo Yamaguchi¹, Taihei Fukudome²,

¹Dept. Biomaterial Sciences, Univ. Tokyo, ²Dept. Mechanical Engineering, Kyushu Univ.

The question of whether slow slip terminates as a single event or it triggers fast rupture is one of the most important problems in science of slow earthquakes. In this study, we conducted laboratory experiments by using compliant polymer gels having controlled surface asperities as analogue materials, and observed nucleation behavior for a giant rupture event with the high-speed imaging and the digital image correlation technique. We found that, a slow nucleation process grows in an oscillatory manner (i.e., slow slip accompanies tremor) and its duration is inversely proportional to the one-third of the driving velocity.

To understand the mechanisms, we first determined the frictional constitutive law with thin gels and observed a non-monotonic driving-velocity dependence; the friction increases and then decreases as the driving velocity increases. Based on the obtained frictional constitutive law, we conducted the finite difference simulations for the analogue fault in heterogeneous normal stress conditions. As a result, we reproduced the slow oscillatory nucleation for a giant and fast slip. This suggests that the viscoelastic relaxation of gels and heterogeneous fault structures play an essential role in the generation of oscillatory nucleation.

Seismicity of regular and slow events in relation to seamount subduction in the Hikurangi subduction margin, New Zealand

Kimihiko Mochizuki¹, Yusuke Yamashita², Tomoaki Yamada¹, Emily Warren-Smith³,
Katie Jacobs³, Martha Savage⁴, Laura Wallace³, Stuart Henrys³, Towako Aoyama¹ and
Masanao Shinohara¹

¹ERI, Univ. Tokyo, ²DPRI, Kyoto Univ., ³GNS Science, ⁴Victoria Univ. Wellington

Onshore GNSS observation in the North Island of New Zealand has revealed episodic slow slip events (SSE) along the Hikurangi subduction margin. The recurrence interval, depth distribution and duration of the SSEs vary along the margin. The most distinctive and abrupt change in such SSE characteristics occurs at a marked change in plate coupling in the central part of the margin. To the north, SSEs occur at ~1-2 year intervals along the shallow part of the plate interface (< 12 km depth). To the south, SSE slip distribution occurs at much deeper depths (> 25 km), and the slip duration is longer. Although several subducted seamounts with dimensions of ~20 km have been identified along the margin by seismic surveys, the long-wavelength plate interface geometry does not show noticeable variations across this transition zone. Therefore, the along-strike temperature and lithostatic pressure conditions are considered uniform. While both changes in incoming plate roughness and upper-plate lithology have been suggested to explain the transition, the controlling factors of the plate coupling and slip behavior of the plate interface remain enigmatic.

We conducted offshore seismic observations using ocean bottom seismometers (OBS) along the Hikurangi margin. We collected three years of passive seismic data in a northern part and one year across the transition zone. SSEs with magnitudes as large as M6.8 occurred during each observation period, and we successfully observed burst-type repeating earthquakes and tectonic tremors accompanying the SSEs.

In a northern part of the Hikurangi margin, we found that both burst-type repeating earthquakes and tectonic tremor appeared to start near the end of each SSE cycle. Seismic and electromagnetic surveys have consistently shown that there exists a core with high seismic velocities and high resistivities in the down-dip side within the subducted seamount. Both activities were distributed on the up-dip side of the core of the subducted seamount; the repeating earthquakes were located closer to the core and the tremor more distributed further up-dip. Both activities may have been separated in space while active synchronously in time.

For our most recent research project, PULSE (Physical processes UnderLying Slow Earthquakes), we deployed 5 short-period and 5 broadband ocean bottom seismometers (OBS) for a one-year offshore observation from October 2020 to October 2021. PULSE aimed to capture the next occurrence (previously 2016) of slow slip and accompanying seismicity activity in the transition region. In May 2021, an SSE occurred to the north of the plate coupling transition zone directly beneath the OBS network. The OBS data revealed two sequences of tremor activities in relation to the SSE. The first sequence appears to have started in February 2021, about three months before the SSE, and the activity became most intense at the end of March, stopping in mid-April. The second sequence appears to be coincident with the May 2021 SSE, but the intensity appears much weaker than the first sequence. The tremor distribution shows a sharp along-dip boundary coincident with the direction of plate convergence. A recent tomographic study has revealed a subducted seamount at depth along the plate interface, and its subducting trace may be a cause of such a sharp boundary.

Locating tectonic tremors with uncertainty estimates: optimizing inter-station measurements, wave propagation-based quality control, and Bayesian inversion

Takeshi Akuhara¹, Yusuke Yamashita², Hiroko Sugioka³, and Masanao Shinohara¹

¹ERI, Univ. Tokyo, ²DPRI, Kyoto Univ., ³Kobe Univ.

Locating tectonic tremors is challenging because of emergent onsets on their seismic records. Relative arrival time measurements and seismic amplitudes have often been used for this location problem. The resulting hypocenters have illuminated various aspects of source processes, including along-strike migration. Nevertheless, few studies have estimated their location errors in a satisfactory manner: the location errors should reflect uncertainties of observation data without any subjective criteria. Additionally, for shallow tectonic tremors occurring offshore, the soft seafloor sediment amplifies seismic waves and delays their arrival, which could bias hypocenter estimates. Improper error assessments may obscure important second-order features in hypocenters or even cause misinterpretation.

We present a novel locating technique that addresses error estimations in an objective way. Data used are arrival time and amplitude differences between station pairs. We first optimize the $N(N - 1)/2$ inter-station measurements to obtain N station-specific relative measurements, where N is the number of stations. This optimization involves only a simple algebraic calculation, and uncertainties of the measurements can be estimated without any subjective criteria. The resulting N measurements and uncertainties are used as inputs to the later inversion analysis.

The N station-specific measurements help intuitively capture seismic wave propagation better than original inter-station data. Assuming the source beneath the station of the maximum amplitude or the earliest arrival, we can obtain the time–distance and amplitude–distance relationship of the wave propagation, which offers the first-order approximation of wave propagation speed (i.e., shear wave velocity, V_S) and attenuation strength (i.e., quality factor, Q_S). We use these estimated V_S and Q_S values as wave propagation-based quality control factors that can effectively reject events with unreasonable measurements.

Finally, we simultaneously solve multiple hypocenters (x, y, z), site amplification and delay factors, and background V_S and Q_S using the Bayesian interface. The added model parameters other than hypocenters can mitigate biases from our insufficient knowledge of subsurface structures. The Markov-chain Monte Carlo (MCMC) method is used for the probabilistic sampling of the posterior and is augmented with a parallel tempering scheme. After a sufficient number of iterations, the aggregation of MCMC samples converges to the posterior probability, from which any statistics can be extracted.

We tested the proposed technique using 20 consecutive days of seismic records from an intensive tremor activity that occurred off the Kii Peninsula in 2020–2021. We used the seismic network of 24 permanent stations from DONET and 15 campaign stations. We extract 300 s long time windows with 50% overlap from the continuous records and convert them to band-passed, smoothed envelopes. Detection of tremors involves inter-station waveform correlation: time windows with a correlation coefficient higher than the 98th percentile for at least 400 station pairs are subject to the proposed location process.

A closer look at the optimization results will help understand the effectiveness of this approach. In successful cases, the optimized arrival time and amplitude data reflect a seismic

wave propagating radially from the epicenter, allowing the quantification of V_S and Q_S based on the distance plot (Figure 1). For the quality control, we used V_S of 2.0–3.5 km/s and Q_S of 100–300 as acceptance criteria. We obtained 338 events through this process.

Hypocenters determined by the Bayesian inversion successfully illuminate the details of tremor activity (Figure 2). In the southwestern part, tremors are distributed in several clusters separated from each other. In the northeastern part, tremors occur in a narrow band elongating to the ENE–WSW direction. Typical location errors (i.e., 2σ) are ± 1 km horizontally and ± 2 km vertically under sufficient station coverage. The errors tend to be magnified outside the station network, as naturally anticipated.

The estimated amplitude and time correction factors differ significantly from place to place, and V_S and Q_S are well constrained by the prior probability. Conversely, hypocenter determination would be significantly biased without careful treatment of these factors. To the best knowledge, for the first time, this study located tremor, with uncertainties estimated and bias from unknown subsurface structures mitigated. We believe that precise, less-biased hypocenters determined in this way can illuminate important features in source processes and their relation to the structural heterogeneities.

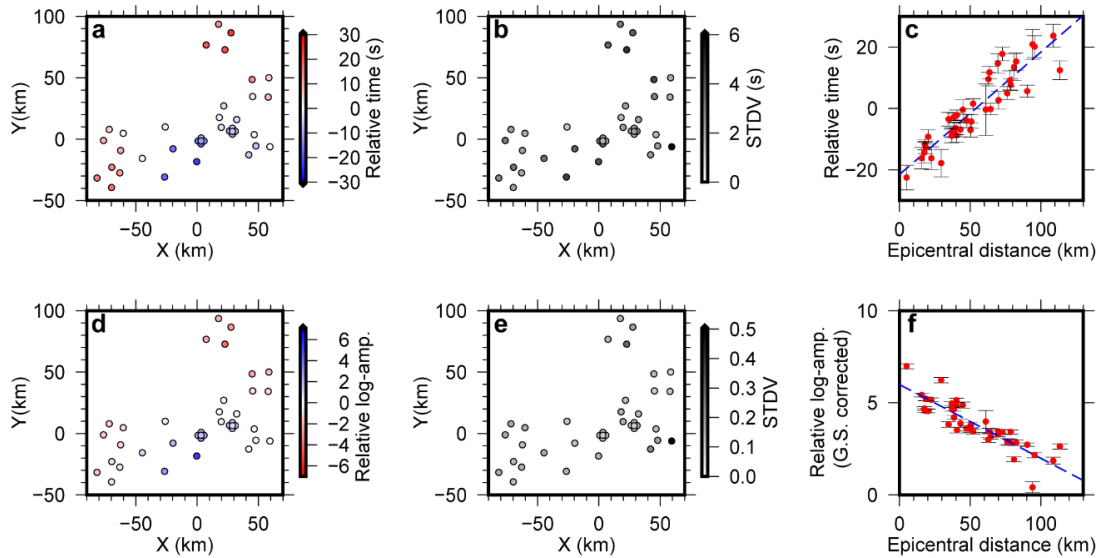


Figure 1. Example of optimization for an event: (a–c) arrival time and (d–f) amplitude data. (a, d) Optimized data at each station. (b, e) Standard deviations. (c, f) Distance plot.

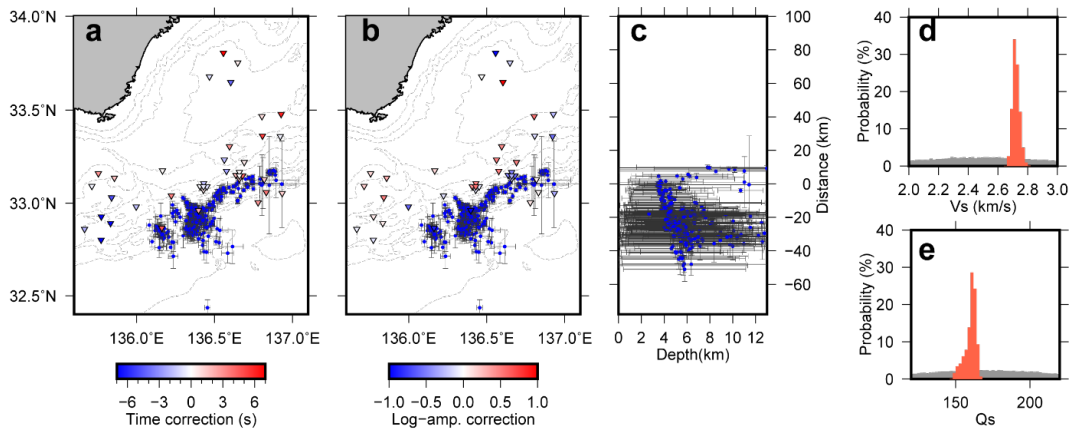


Figure 2. Bayesian inversion results. (a–c) Blue dots show hypocenters, with the error bars denoting uncertainties of $\pm 2\sigma$. Inverted triangles show stations with color showing (a) time correction or (b) log-amplitude correction resulting from the inversion. (d–e) Estimated (d) V_S and (e) Q_S . Gray and red histograms show the prior and posterior probabilities, respectively.

Explaining the First-order Source Characteristics of Slow Slip Events and Tremors with a Frictional-Viscous Faulting Model

Baoning Wu^{1,2}, David Oglesby², Abhijit Ghosh², Gareth Funning²

¹Department of Earth Sciences, University of Southern California, USA,

²Department of Earth and Planetary Sciences, University of California Riverside, USA,

We consider a frictional-viscous fault zone model to explain the first-order source characteristics of slow slip events (SSEs). The frictional-viscous model is inspired by the recent geological observations that imply the occurrence of SSEs in fault zones with a finite thickness of ~hundreds of meters. The bulk matrix of the fault zone deforms viscously, while pervasive frictional surfaces are distributed in the viscous matrix. To simultaneously consider both the 10s-kilometer-scale rupture propagation and the 100s-meter-scale fault zone features in the same model, we treat a fault zone as a zero-thickness "surface" embedded in an elastic medium. The "frictional-viscous" characteristics are parameterized into a constitutive relation where fault strength is partitioned into a frictional and a linear viscous component in parallel (e.g., Ando et al., 2010; Nakata et al. 2011; Ando et al., 2012).

We explored the above model setup both analytically and numerically. Two key parameters in the frictional-viscous model are the viscous coefficient η_v and the event stress drop. The present frictional-viscous model can simultaneously explain various kinematic source parameters for SSEs to first order when the viscous coefficient η_v is about 10^4 to 10^5 times of $\frac{\mu}{2\beta}$, and the average stress drop in a slip transient is about 10 kPa. μ is the shear modulus and β is the shear wave speed. $\frac{\mu}{2\beta}$ is often called the radiation damping factor, which reflects the intrinsic slip-rate-damping strength of the elastic system. The characteristic kinematic source parameters of SSEs that are explained by the above model parameters include the slip rate ($\sim 10^{-8}$ m/s), rupture propagation speed ($\sim 10^{-2}$ m/s), rise time and source duration (\sim days), diffusive migration diffusivity ($\sim 10^3$ m²/s), and radiation energy to moment ratio (10^{-9}). This frictional-viscous model can also explain the shorter inter-event interval and lower average stress drop observed in subduction zone SSEs, compared to what is observed in the fast earthquakes at the seismogenic depth, and why the differences are both ~ 100 fold for event interval and stress drop. These agreements imply that the frictional-viscous model is a promising representation of the actual SSE source processes.

The present model provides many hypotheses, which can be further tested with future geophysical, geological, and experimental data. For example, our results imply that the frictional-viscous model has a moment-duration scaling relation of $M_0 \sim T^3$ for slow slip events. Also, to explain the observed kinematic source parameters of SSE, the effective viscosity of the shear zone in the model need to be $\sim 10^{12}$ to 10^{14} Pa*s (assuming shear zone width = 100m), which is significantly lower than the typical ambient rock viscosity (usually above 10^{18} Pa*s).

(Below is a poster made at 08/20 for abstract submission, will be updated by the time of the workshop)

Explaining Slow Slip Events and Tremors with a Frictional-Viscous Faulting Model

Baoqing Wu^{1,2}, David Oglesby², Abhijit Ghosh², and Gareth Funning²

¹Department of Earth Sciences, University of Southern California, ²Department of Earth and Planetary Sciences, University of California, Riverside

REF: Baoqing Wu's PhD dissertation Email: baoqingw@usc.edu

Twitter: @BaoqingWu

[Survey] which slow EQ statement you like more?

1. "There are two fundamentally different slip phenomena, a slow earthquake and a fast earthquake."
2. "Slow earthquake is a transitional slip phenomenon between fast earthquake and stable slip"

Tomoo Nishikawa
@nishik_lab

1. Explaining SSEs with classic EQ models is non-trivial

actual fault with width \rightarrow **model simplification** \rightarrow **"frictional-only" fault boundary condition**

- In a classic earthquake model, "faults" are simplified as surfaces. The shear resistance that a fault applies on the medium is assumed to be frictional, and it can be described with a friction law (e.g., rate-and-state, slip weakening).
- To first-order, this classic model can explain the seismic and geodetic characteristics of regular fast earthquakes well.
- However, to explain slow slip events (SSEs), the parameter ranges allowed in these classic models are often narrow.

2. Vision from geologists: a frictional-viscous zone

- Recent geological observations that imply the occurrence of SSEs in fault zones with a finite thickness of ~hundreds of meters. The bulk matrix of the fault zone deforms viscously, while pervasive frictional deformation features are distributed in the viscous matrix (e.g., Fagereng and Sibson, 2010; Schmidt and Platt, 2021; Kirkpatrick et al., 2021). However, what mechanisms allow transient deformation features to communicate within a more distributed shear zone is still an open question (e.g., Behr and Burgmann, 2021).

Summary and model predictions

- This model can simultaneously explain viscous kinematic source parameters for SSEs to 1st order when $\eta_V \sim 10^4(4-5) \mu(2\theta)$ and $\Delta\tau \sim 10$ kPa.
- The explained SSE features include slip rate ($\sim 10^{-4}-8$ m/s), rupture speed ($\sim 10^{-1}-2$ m/s), rise time-source duration (\sim days), migration diffusivity ($\sim 10^{-1}-3$ m²/s), EMO ($10^{-4}-9$), and shorter event interval and lower $\Delta\tau$.
- Model prediction: The effective viscosity of the shear zone needs to be $\sim 10^{12}-10^{14}$ Pa·s (assuming shear zone width = 100m).

3. One way to model a frictional-viscous fault

- These 3D features can be parameterized as "friction law" on a 2D fault. The total fault strength equals the sum of the frictional and viscous strength components. The frictional strength can experience a sudden drop (slip-weakening), while the viscous strength increases linearly with slip rate V (Ando et al., 2010).
- Such a boundary condition is equivalent to a mechanical system where the frictional and viscous force act in parallel. It has been proposed by many studies, e.g. Ando et al., 2010; Lavier et al., 2013; Beall et al., 2019.
- However, the rupture dynamics under this boundary condition have not been fully quantified.

Effective friction law:

$T_{elastic} < f_0$, fault stays locked, and $V=0$;
 $T_{elastic} > f_0$, fault starts to slip, and we have
 $T_{elastic} = f_0 - (f_0 - f_1) \frac{D}{D_0} = \eta_0 + \eta_1 \cdot V$, when $D \leq D_0$
 $T_{elastic} = f_1 + \eta_1 \cdot V$, when $D > D_0$

Two KEY "friction law" parameters:
 $\Delta\tau$: frictional strength drop
 η_1 : viscous coefficient

4. Quantifying first-order rupture features with BIEs

One method to evaluate the interaction between fault and elastic medium is to analyze the elastodynamic boundary integral equations (BIEs). By coupling BIEs and the frictional-viscous boundary conditions, one may approximate the first order rupture features and obtain some useful analytical relations.

$$\Delta\tau \approx \frac{D}{L}, \quad V_r \approx \left(1 + \frac{\eta_1}{\beta}\right) \left(1 + \frac{\eta_0}{\mu(2\theta)}\right)^{-1} \cdot 2\beta$$

$$V \approx \left(1 + \frac{\eta_0}{\mu(2\theta)}\right)^{-1} \frac{\Delta\Delta\tau}{\mu} \cdot \beta, \quad M_0 \approx \Delta\tau \cdot \left(1 + \frac{\eta_0}{\mu(2\theta)}\right)^{-1} \cdot \beta^3 \cdot T_0^3$$

$$E \approx \Delta\tau \cdot \left(1 + \frac{\eta_0}{\mu(2\theta)}\right)^{-1}, \quad D_r \approx C \cdot \frac{\Delta\tau}{T_0} \cdot \left(1 + \frac{\eta_0}{\mu(2\theta)}\right)^{-1} \cdot L \cdot 2\beta$$

(μ is shear modulus, β is shear wave velocity)

- η_1 affects the source kinematics through $\left(1 + \frac{\eta_0}{\mu(2\theta)}\right)^{-1}$
- As η_1 increases $\rightarrow V$ and V_r decreases, T increases
- MO-T scaling remains $M_0 \propto T^3$
- When $\eta_0 \approx 10^4 - 10^6 \mu(2\theta)$ & $\Delta\tau \approx 10$ kPa, all these kinematic parameters are simultaneously explained with the frictional-viscous model.

6. Shorter event interval & smaller $\Delta\tau$

- Stress amplification effect:** the actual shear stress on the frictional contact builds up significantly faster than the average shear stress on the fault, because the friction force is small.
- As a result, a frictional-viscous fault would have a shorter event interval and a smaller average stress drop.

5. Validating the analytical relations with 3D BEM dynamic rupture simulations

Simulations setup:

Slip rate/shear stress along AA', spatial(x)-temporal(y) evolutions:

- We validate our analytical derivations with 3D dynamic rupture simulations using boundary element method (BEM).
- We consider a planar fault embedded in a homogeneous elastic whole space. We use the elastodynamic stress transfer functions derived in Tada, (2005).
- Although the numerical simulations cannot test the parameter space where η_1 is as large as $10^4 \mu(2\theta)$, they do support the trends in rupture behaviors that are suggested by the analytical solutions.

7. Diffusive tremor migration with $Df \sim 10^{-3} \text{ m}^2/\text{s}$

Observations in Ando et al. 2012:

Our analytical relations:

Numerical models, yielding stress 10 times higher in the nucleation zone:

- Diffusive tremor migration ($\times^2=Df-t$) are often observed in ETS with $Df \sim 10^{-3}-4$ m²/s (Ide 2010; Ando et al., 2012; Creager et al., 2020). Ando et al. (2012) show that such diffusive migrations can be explained with the presented frictional-viscous model.
- We obtain the same results as Ando et al. (2012). In addition, we show that the required η_1 is $10^4 - 10^6 \mu(2\theta)$, consistent with the η_1 inferred from other SSE rupture features.

Can we use electrical conductivity to help understand the earthquake-induced stress-cycle in the ductile region beneath the Alpine Fault, New Zealand?

T. Grant Caldwell¹, Ted Bertrand¹, Wiebke Heise¹, Yasuo Ogawa², Stephen Bannister¹, Sandra Bourguignon¹, John Haines¹, Laura Wallace¹, Susan Ellis¹, Sandra Piazzolo³, Virginia Toy⁴,
Phaedra Upton¹

¹GNS Science, New Zealand, ²Tokyo Institute of Technology, ³University of Leeds, ⁴Johannes Gutenberg Universität-Mainz.

In the Southern Alps (New Zealand), 3D inversion modelling of MT data and micro-earthquake data from a closely spaced array of seismometers shows that a dipping electrically conductive zone is located immediately below the seismogenic region of the crust at the down-dip projection of the Alpine Fault. There is a strong correlation between the spatial extent of the conductor and surface strain-rates derived from GPS data suggesting the conductive zone is a consequence of the ongoing ductile deformation. The conductivity image also shows a remarkable resemblance to model calculations of accumulated (ductile) creep between major Alpine Fault earthquakes. The simplest interpretation of these correlations is that the conductive zone is produced when creep deformation connects small amounts of saline fluid present at the mineral grain-boundaries.

However, the mechanism by which the enhanced conductivity is produced at mid-crustal depths is poorly understood. Based on observations of the fault rocks being exhumed along the Alpine Fault we think that the most plausible mechanism is pressure-solution-creep associated with the latter stages of fault rock mylonitization. The dissolution-precipitation chemistry at the grain boundaries would provide additional charge carriers enhancing the conductivity of the grain boundary fluid and explain the correlation observed between the conductivity and the surface strain rate.

Since creep depends on differential stress, the question that arises is whether it would be possible to turn the conductivity image into a stress image. This will only be possible if we have a clear understanding of the mechanisms producing the conductivity and deformation. Laboratory-based studies of the electrical properties of materials undergoing ductile deformation at mid-crustal temperatures and pressures are needed to develop this understanding. However, if the relationship between the conductance and creep rate can be established we would have a new way of assessing the stress in the ductile region beneath the Alpine Fault and thus a new window into the mechanics of the earthquake cycle.

The Evolution of Slip Events Inferred from Cascadia Tremor

Joan Gomberg, Aaron Wech
US Geological Survey

Hazardous, fast slipping, seismogenic earthquakes grow by rupturing additional fault area, and when resolvable do so in a seemingly complex manner. The more leisurely growth of slowly slipping, nearly aseismic earthquakes (SSEs) provides opportunities to observe how ruptures initiate, grow, and stop. We analyze a new catalog of seismic tremor location and radiated energy measurements to constrain the evolution of the area and energy of hundreds of SSEs in the Cascadia subduction zone. We find that when we remove intermittent pauses in tremor activity, the areal growth patterns of all events become nearly uniform. This growth may be described by a power-law relationship with exponents indicative of a diffusive-like slip process in which slip rate slows as the event grows (assuming proportional propagation and slip rates). We suggest that removal of pauses removes unsteady slip front propagation and reveals the underlying universality in growth. The uniformity suggests that all ruptures grow identically, and their eventual size is controlled by external factors. We also show that SSEs are not simply a sum of smaller independent events (i.e., slip is hysteretic). Preliminary analysis of the progression of radiated energies shows that while some SSEs are significantly more energetic than others, when de-meaned and pauses are removed, the same remarkable uniformity in growth patterns emerges. In contrast to theoretical expectations of seismic efficiency increasing with propagation velocity, we find no systematic differences in radiated energy before or after pauses or for tremors on newly ruptured or re-ruptured areas, nor do tremors become quieter as SSEs grow and propagation velocities slow. Notably, energies appear modulated ubiquitously at a tidal frequency of 12.4 hours, confirming prior inferences of SSEs occurring on extremely weak faults.

Frictional properties of input sediments to the North Sumatra subduction zone

Junli Zhang¹, Katja Stanislowski¹, and Matt J. Ikari¹

¹MARUM—Center for Marine Environmental Sciences, University of Bremen

The 2004 great Sumatra-Andaman earthquake showed that coseismic slip propagates to the trench, and causes large tsunamis. Recent scientific drilling results reveal that a prefan pelagic stratigraphic formation (Unit III) is most likely to be the horizon that hosts the coseismic fault rupture. To understand its frictional behavior, previous friction experiments have been conducted, but mainly focused on Subunit IIIB. In this study, we filled this gap by conducting velocity step friction experiments on intact samples recovered from Subunit IIIA.

The velocity step friction experiments were conducted under 10 MPa effective normal stress and the shear velocity ranges from the plate tectonic driving rate (1.6 nm/s) at the North Sumatra subduction zone to the maximum velocity that the instrument allows (50 $\mu\text{m/s}$). Two samples were selected, a claystone and a silty claystone. Our X-ray diffraction (XRD) results show that the mineral composition of the claystone is 70% phyllosilicates, 16% quartz, 8% feldspar, 4% epidote and 2% other minor minerals, while the major components of silty claystone are 54% phyllosilicates, 29% quartz and 14% feldspar. Friction experiments reveal that the claystone is relatively weak with a residual friction coefficient $\mu_r = 0.23$, whereas the silty claystone is frictionally strong ($\mu_r = 0.46$). The claystone is velocity-strengthening for all velocity steps and switches from slip-strengthening at 1.6-5 nm/s to slip-weakening at 0.016-0.5 $\mu\text{m/s}$ and then to slip-strengthening or slip-neutral at 1.6-50 $\mu\text{m/s}$. In contrast, the silty claystone is velocity-weakening for most velocity steps and slip-weakening for all the velocities, which may facilitate unstable sliding. Also, we observed several spontaneous stress drops in the silty claystone and interpreted them as slow slip events (SSEs). The peak velocity of the laboratory SSEs ranges between 1.5- and 2.4-times the plate convergence rate, similar to the inferred slow slip rates on the Sunda megathrust from numerical modeling studies. Collectively, our findings suggest that Subunit IIIA could host coseismic slip and possibly SSEs in the North Sumatra subduction zone.

Spatiotemporal distribution of tectonic tremors accompanying 2014 and 2019 SSE in the north of the Hikurangi Subduction Zone

Towako Aoyama^{1,3}, Kimihiro Mochizuki¹, Yusuke Yamashita², Tomoaki Yamada¹

¹ ERI, Univ. Tokyo, ² DPRI, Kyoto Univ., ³ Dept. EPS, Univ. Tokyo

The Hikurangi margin is located off the east coast of the North Island of New Zealand, where the Pacific Plate subducts beneath the Australian Plate. Large slow slip events (SSEs) occur more frequently in the margin than in other subduction zones. In addition, this region is characterized by a very shallow subducting plate interface, making it one of the best areas to reveal relationships between SSEs and accompanying earthquakes. In 2014-2015, Hikurangi Ocean Bottom Investigation of Tremor and Slow Slip (HOBITSS) experiment deployed Ocean Bottom Seismometers (OBSs) and Absolute Pressure Gauges (APGs). During the observation, a large SSE occurred beneath the HOBITSS network in September 2014, and its slip distribution was obtained using data from onshore GNSS stations and offshore APGs (Wallace et al., 2016). And tectonic tremors accompanying the SSE occurred on the down-dip side of a subducted seamount within the SSE slip region (Todd et al., 2018). Another offshore seismic observation was conducted around the seamount from 2018 to 2019 using 5 OBSs. A large SSE occurred in March 2019 under the network and tectonic tremor activity was detected by Yamashita et al. (2019). However, since different methods were used to detect tectonic tremors accompanying the 2014 and 2019 SSEs, the magnitude and spatiotemporal distribution of the activity are not directly comparable. Therefore, in this study, we applied to the 2019 OBS data the same envelope correlation method (ECM) as used by Yamashita et al. (2021) to detect tectonic tremor activity in 2019, and to reveal the differences in order to understand the characteristics of tectonic tremor activity in the northern Hikurangi margin.

Todd et al. (2019) performed event detection on two months of HOBITSS OBS data from September to October 2014 and discriminated between normal earthquakes and tectonic tremors by amplitude ratios in two frequency bands, the 4-10 Hz band and the 12-20 Hz band. They applied an ECM to determine hypocenters of 120 tectonic tremors.

Yamashita et al. (2021) detected tectonic tremors using waveforms of the 2-4 Hz frequency band. By applying an ECM, they determined hypocenters of more than 1,700 tectonic tremors while their depth were fixed at the plate interface.

In this study, the ECM method was applied to the waveforms in the 2-4 Hz frequency band recorded by 7 OBSs deployed in 2014-2015, including five short-period (1 Hz) OBSs and two broadband OBSs, to determine tectonic tremors. Because earthquakes can be included in the detected events, events listed in the earthquake catalog by GeoNet, the New Zealand onshore seismic network, were removed. In order to confirm whether the waveform records of the short-period OBS and broadband OBS were correlated, these procedures were applied to three different OBS combinations: a) only 5 short-period OBS stations, b) 5 short-period OBS stations and 1 broadband OBS station, and c) 5 short-period OBS stations and 2 broadband OBS stations. The results showed that the correlation between the waveforms was approximately equal for all three combinations.

As a result, approximately 2,000 events (more than 10 times as many as those determined by Todd et al. (2018)) were detected in all three combinations. The detected tectonic tremor activity became more active toward the end of the SSE period (late September to early October). When compared to the epicenters of the 120 events detected by Todd et al. (2018), the epicenters of the events detected here were generally distributed to the south. On the other hand, no tectonic tremors, which had been detected around a seamount located to the southeast of the observation network, were detected.

Formation and transport of silica particles in supercritical and vapor conditions and its implications to fracture sealing

Atsushi Okamoto¹, Jumpei Sugioka¹, Takamasa Niibe¹

¹Graduate School of Env., Univ. Tohoku

Ubiquitous occurrences of quartz veins in the crusts and subduction zones at the depths of ordinary and slow earthquakes suggest an importance of sealing of faults and fractures by silica precipitation. However, it is not easy to know how porosity structure in a fracture evolves by silica precipitation. In particular, quartz veins do not always show growth from the pre-existing quartz grains on the fracture wall, but also shows the blocky texture that is filled by equant quartz grains. Such texture suggests that fracture can be sealed regardless the wall rock minerals, via nucleation of quartz crystals. Weatherley and Hanley (2013) suggested that silica precipitation occurs instantaneously at the fault jog at the time of earthquakes due to dilatancy, and Amagai et al. (2019) experimentally revealed that amorphous silica nanoparticles forms by flash vaporization, and these particles are quickly transformed to quartz under supercritical conditions. However, it is still unclear whether ‘flashing’ is important in natural quartz vein formation, as the amount of silica precipitated by flashing is small compared to the open space volume in a fracture. As such the formation mechanism of blocky quartz veins and its impact on the hydrology of the fractures are still poorly understood.

In this study, we conducted the hydrothermal flow-through experiments on silica precipitation induced by drop of fluid density with increasing temperature; from liquid to supercritical fluid conditions (SCF: from 300 °C to 430 °C at 25 MPa, for 1h, 6h, 12h), and from liquid to vapor (LV; from 200 °C to 375 °C at 10 MPa for 6h). We did not use the rock or quartz substrate, and high Si solution (Si~300 mg/kgH₂O, Al~3-5 mg/kgH₂O) was prepared by dissolutions of quartz ± granite ± albite. During the experiments, fluid flowed upward at the constant rate of 0.1 ml/min, and silica particles were caught by 24 stainless meshes placed at the interval of 1 cm. We found the systematic variation of silica minerals in time and space. In the SCF runs, an onset of silica precipitation is largely consistent with the position at the drop of fluid density with increasing temperature (~10cm from inlet). Amorphous silica particles with size of <10 μm formed throughout the flow path after 1h, whereas quartz as well as cristobalite appeared after 6h and 12 h and some shows bi-pyramidal euhedral quartz shapes with size of ~ 50 μm and quartz formed within the cristobalite particles. In LV runs, the silica precipitates are more concentrated into the narrow regions, and fine particles of both amorphous silica and quartz crystals formed. We also conducted the sealing experiment with filling alumina balls along the flow paths. We found that silica (metastable phases and quartz) attached the alumina balls and clogged the flow path. In a case, we found that characteristic oscillation of fluid pressure with saw tooth pattern. Our results imply that a rapid decompression in faults causes quartz particles, via formation of metastable silica particles and rapid transformation to quartz (within a few hours) by continuous supply the liquid or supercritical fluids. These silica particles could clog fractures locally, and the repeat of breakdown and clogging may produce oscillation of fluid pressure before complete sealing.

Weatherley, D.K., Henley, R.W., 2013. Flash vaporization during earthquakes evidenced by gold deposits. *Nature Geoscience*, 6, 294.

Amagai T, Okamoto A, Niibe T, Hirano N, Motomiya K, Tsuchiya N, 2019. *Scientific Reports*, 9: 9738

“Stew and slide” friction and fluid-flow experiments on incoming sediments from the Japan trench

Keishi Okazaki^{1,2}, Mizuki Ueda¹, Yohei Hamada², Asuka Yamaguchi³, Ikuo Katayama¹

¹Earth and Planetary Systems Science Program, Hiroshima University, ²Kochi Institute for Core Sample Research, X-star, JAMSTEC, ³AORI, the University of Tokyo

By the current technology, it is quite challenging to obtain the fault materials directly from the hypocenters of megathrust earthquakes, while we can collect incoming sediments from outer-rise regions at the subduction zones that will reach the seismogenic zone in the future. We have been conducting friction and fluid-flow experiments on incoming sediments at high pressure and temperature conditions. A piston core sample of hemipelagic sediments obtained during the cruise KS-15-3 was used in the experiments. The hemipelagic sediments sample is mainly composed of clay minerals, terrigenous grains and biogenic opal. To synthesize the fault materials supposing to exist at the hypocenters of megathrust earthquakes and to understand how their frictional and hydraulic properties evolve with diagenetic/metamorphic reactions with subduction, we first cooked the sediments at temperatures 100–230°C for 10 minutes to 27 hours with intermitted permeability measurements, then applied shear deformation to the sediments with sliding-velocity steps. Permeability of the sediments decreased about an order of magnitude due to an initial compaction by the pressurization to the confining pressure of 150MPa and the pore fluid pressure of 58MPa. Permeability was further decreased by another order of magnitude by the cooking at the temperature of 100°C for 220 minutes. Frictional behavior of the incoming sediments shows a velocity strengthening behavior at a room temperature, whereas that gradually changes to a velocity weakening, which behavior potentially induces seismic slips, with increasing temperature. Comparison of the fault stiffness and the effective normal stress among laboratory, and natural small, large and slow earthquakes indicates that the spectrum of slip behaviors could occur by different fault stiffness (i.e., host rock properties) and effective normal stress (i.e., host rock elastic and hydraulic properties) even with a same frictional property.

Frictional properties of basalt: Effects of the seamount subduction on earthquake generation

Michiyo Sawai¹, Tomoya Hiramatsu¹, Souta Wada¹ and Kyuichi Kanagawa¹

¹Chiba University

Subducted seamounts are thought to affect seismic faulting along a subduction zone megathrust by increasing the normal stress on the subduction interface and to act as asperities (e.g., Cloos, 1992). There is also a possibility that they act as barriers for rupture propagation due to the large resistance (e.g., Kodaira et al., 2000). On the other hand, recent studies suggested that they may promote creep or slow slip behavior (e.g., Mochizuki et al., 2008). In spite of many studies on subducting seamounts, frictional properties of seamount materials are still poorly understood. In this study, we have conducted friction experiments to determine the friction parameter ($a - b$) (rate dependence of steady-state friction) and investigated how this parameter changes with temperature.

We conducted friction experiments on gouge of basalt cored from ~200 mbsf (meters below seafloor) of the Takuyo-Daisan Guyot at Site 879 of ODP Leg 144, at a confining pressure of 150 MPa, pore pressures of 100 MPa, temperatures of 25–200°C, and axial displacement rates changed stepwise among 0.1, 1 and 10 $\mu\text{m/s}$, by using a gas-medium, triaxial apparatus installed at Chiba University.

The results show that steady-state friction decrease with increasing temperature toward 100°C, then increase at $\geq 150^\circ\text{C}$. Unstable stick-slips were observed at 200°C. At low temperatures of $\leq 50^\circ\text{C}$, ($a - b$) values of the basalt gouge are positive and do not change noticeably. However, the gouges show neutral to negative values of ($a - b$) at temperatures of $\geq 100^\circ\text{C}$. Thus ($a - b$) value of the basalt gouge likely changes from positive to negative with increasing temperature. Our results suggest that a seamount may be a site of earthquake nucleation at depths with temperatures of $\geq 150^\circ\text{C}$.

Numerical simulation with a multiscale circular patch model in the northern segment along the Japan Trench

Ryoko Nakata¹, Takane Hori², Hideo Aochi^{3,4}, and Satoshi Ide¹

¹Dept. EPS, Univ. Tokyo, ²JAMSTEC, ³BRGM, France, ⁴ENS-CNRS PSL, France

In subduction zone, various magnitude and types of earthquakes occurred such as megathrust earthquake, tsunami earthquakes, repeating earthquakes and imperfect repeating earthquakes. To reproduce some of them, we have approximated spatial heterogeneity as circular or rectangular patches and treated them as one- or two-hierarchical structure. However, it is important to explain various phenomena by including hierarchical characteristics. Then, we conducted numerical simulations of earthquake generation cycles by adopting a multiscale patch model. Here, we performed off Sanriku region where various earthquakes have been observed. For example, in the northern segment of the Japan Trench, at the shallow area, $M \sim 8$ earthquakes such as the 1896 Meiji-Sanriku earthquake ($M_w 8.1$) [Tanioka & Satake, 1996; Satake et al., 2017] occurred, and at deeper area, smaller magnitude of earthquakes, repeating earthquakes, and slow slips [Uchida et al., 2016] occurred.

Our simulation is based on the rate- and state-dependent friction (RSF) law that represents the process of stress accumulation and release on the plate interface. We used the same equations, initial conditions, seismic radiation damping term, plate geometry, and plate convergence rate as in our previous study [Nakata et al., 2016; 2021]. In this study, a multiscale circular patch model [Ide & Aochi, 2013] was adopted to represent the spatial heterogeneity of seismic events with $M \geq 5.6$ in the northern segment. For the Meiji Sanriku earthquake, we used that of the second-level patch with a radius (r) of 100 km from Ide & Aochi [2013]. For $M_j = 7.1-7.6$ and $6.6-7.2$ earthquakes, we used the third ($r = 50$ km) and fourth-level patches ($r = 25$ km) from Ide & Aochi [2013]. In addition, we added smaller earthquakes. For fifth-level patches with a radius of 12 km, corresponding to events of $M_j 5.6-6.5$ earthquakes, we used hypocenters determined by JMA since 1923. We assumed heterogeneity of the characteristic slip distance, L and uniform A-B.

In tentative results, $M_{6.2-7.4}$ earthquakes sometimes occurred only on the marginal area. And $M > 8$ earthquakes ruptured almost all patches with recurrence interval of a few decades during approximately 130 years. Because the large and small patches overlapped to each other, they formed a larger patch. Then, no small earthquakes occurred at the central area during $M > 8$ earthquake cycle. This situation is inconsistent with the observations. Now we are examining how to load and rupture each patch separately. Simple approach of earthquake cycle simulation based on RSF law with multiscale patches may not be able to explain observed multiscale seismicity. It may require major modifications.

Automatic classification of fast and slow earthquake signals from continuous records using an unsupervised machine learning algorithm

Yuki Kodera¹

¹MRI, JMA

Continuous seismic waveforms recorded in a seismometer include various earthquake signals such as ordinary fast earthquakes and slow earthquakes like tectonic tremors. If the automatic classification of continuous records is possible, that would enable us to handle a large amount of seismic data and to understand geophysical phenomena around a target seismometer. In this study, we propose an unsupervised machine learning algorithm to perform automatic classification of continuous records using frequency and time domain characteristics. The unsupervised approach has an advantage in that the algorithm does not require prior knowledge (e.g., template) of what kind of signals are included in the record.

Our proposed algorithm uses running spectra as features. Running spectra are obtained with a 4-s time window and are converted into 10-dimensional vectors with a filter bank. Then the vectors are compressed to 2000 representative points after performing the vector quantization. Finally, the representative points are clustered by the Ward hierarchical clustering algorithm in the space mapped by the kernel principal component analysis based on a Markov chain transition matrix.

The proposed algorithm was applied to a one-week-long continuous record of a temporary ocean-bottom seismometer deployed to observe aftershocks of the 2004 M7.4 off the Kii Peninsula earthquake (Yamazaki et al., 2008). The record includes many shallow tectonic tremors in addition to aftershocks (Tamaribuchi et al., 2019). The dendrogram generated by the hierarchical clustering algorithm showed that (1) aftershocks with large amplitudes were separated from other signals when the dendrogram was cut at 1/2 of the maximum height and (2) tectonic tremors with large amplitudes were separated from background noises and classified into a unique class when the dendrogram was cut at 1/4. Those results indicate that, although there remains an issue of how to cut the dendrogram appropriately, fast and slow earthquake signals on continuous records could be extracted and classified automatically by the hierarchical clustering algorithm, without labeled datasets or templates.

Strongly scattering medium along slow earthquake fault zones, inferred by the new observations of short-duration tremors

Akiko Toh¹, Yann Capdeville², Wu-cheng Chi³, Satoshi Ide¹

¹Dept. EPS, Univ. Tokyo, ²Nantes Université, CNRS, ³IES, Academia Sinica

At least two types of seismic events occur in shallow subduction zones; ordinary earthquakes and tremors. They are classified based on waveforms, and tremors show longer signal duration. To date, the difference between the two has been solely attributed to their seismic source process. Thus, tremors' long signals were considered to reflect a long source process.

Here, we report that we found some tremors exhibiting short-duration signals directly above the source while exhibiting the typical long-duration signals at far offsets. These observations have become available thanks to ocean bottom seismometers that record tremors close to the source. We refer to this type of tremor as a "short-duration tremor". The short-duration tremors cannot be explained by the long source time process. Therefore, we need a new mechanism that explains the observations by which the long-duration signals can be produced from the short source time processes suggested by the short-duration signals.

We propose a mechanism where an anomalous structure that prolongs seismic signals is vertically localized around the seismic source. With such a structure, seismic waves recorded directly above the source should hardly propagate through the structure, so their signal duration would remain short. On the other hand, the structure would prolong the seismic waves that depart the source horizontally toward distant stations since they would propagate through the structure long distances. Although there are numerous possible structures, we consider a structure in which many small inclusions with ultra-low S-wave velocities are distributed around the epicentre. We performed simulations in elastic wave propagation using a 2D spectral element method. The obtained synthetic waveforms qualitatively captured the features of the short-duration tremors.

The inclusions in our model could be seismic expressions of recently geologically detected aquifers in the tremor source region. Further, since tremors are regarded as the smallest member of slow-earthquakes of various sizes which share the same fault zone, this structure around tremor sources can potentially be a controlling factor of slow-earthquakes.

Seismic and aseismic behavior in The Pichilemu crustal fault system during the post-seismic period of the 2010 Mw8.8 Maule Earthquake

Kellen Azúa¹, Francisco Pastén-Araya², Sergio Ruiz¹

¹Geophysical Department, University of Chile, Santiago, Chile, ²Department of Civil Engineering, UCM, Talca, Chile

In recent years, attempts have been made to establish the relationship or connection between aseismic and seismic slip in space and time, especially in the afterslip of the large megathrust earthquakes. It is known that afterslip is a product of ordinary earthquakes (aftershocks) and aseismic slip. However, it has not been possible to clarify what type of signal (seismic or aseismic) predominates over time, what mechanisms generate them, and why they are separated spatially. For this reason, we study the post-seismic behavior of the 2010 Mw 8.8 Maule earthquake, specifically in the area near Pichilemu Fault System (PFS), in order to characterize the seismic behavior of this area after this mega-earthquake. Using two dense networks of temporal stations, IMAD and Chile RAMP, which were active several months after the mainshock, we built a robust catalog of events using the envelope and cross-correlation techniques. Then, we relocated them manually to identify potential low-frequency earthquakes (LFEs) and ordinary earthquakes location around the PFS area. Analyzing the frequency content of the earthquakes, preliminary results show differences in the behavior of these two kinds of events. For earthquakes of similar duration, magnitude and location, we observed different frequency behaviors, some controlled by high frequencies as usual in ordinary earthquakes and others dominated by low frequencies (possible LFEs). These first results suggest that the afterslip of the Maule earthquake could be concentrated in the interface as well as in the PFS. Furthermore, this could indicate a heterogeneous seismogenic behavior of the PF, indicating possible mechanical, frictional, or rheological variations in the PFS during the afterslip of the Maule earthquake.

Imaging the changes in the migration patterns of deep LFE caused by the occurrence of the 2010 L-SSE in Western Shikoku, Japan.

Anca Opris¹, Keisuke Ariyoshi¹, Takahiro Hatano², Takane Hori¹

¹JAMSTEC, ²Dept of Earth and Space Science, Osaka University

It is well known that the periodicity and migration patterns of deep tremor episodes show significant heterogeneities, manifested in the segmentation across the strike of the subduction area (Obara 2010), which is believed to be determined by structural and frictional inhomogeneous properties of the plate interface (Ide 2012). ETS episodes have very complex migration pattern consisting of: (1) concentrated bursts cascading along the strike of the subducting plate, (2) parabolic or linear propagation pattern (Ide, 2010, Ando et al., 2012) and (3) rapid tremor reversal (Houston et al., 2011), including up-dip and down-dip very fast migration. We developed a imaging method for objectively quantifying and imaging the migration of ETS episodes from the generalized version of the two-point cross-correlation integral of Grassberger and Procaccia (1983), using the method described by Tosi et al. (2008) to quantify the space-time correlations in deep low frequency earthquake occurrence. We applied our method to a LFE catalogue (Mizuno et al., 2019) covering a time period of 3 years, from January 2009 to December 2011. Each LFE has a duration of about few-seconds, allowing us to approximate events as a point-process. The space-time combined correlation integral $Cc(\tau, r)$ is a measure of the fraction of the number of the LFE pairs shorter than time interval τ and distance r . After we compute the inter-event times and inter-event distances between all pairs of LFE's in each data set and calculate $Cc(\tau, r)$ at an equal interval in logarithmic time and space, in order to extract the space-time pattern as it evolves in time, we discretize the $Cc(\tau, r)$ in respect to the time step, for each distance (Figure 1).

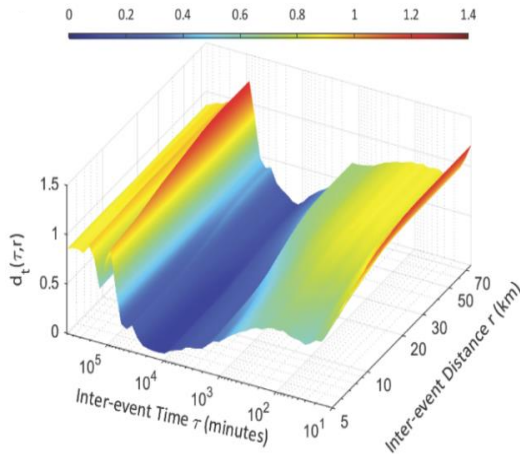


Figure 1. Space-time plot indicating the correlations between LFE pairs, from highly clustered power-law burst (red) towards quiescent times (blue), where $d_t(\tau, r) = \log(Cc(\tau, r)) / \log(\tau)$.

This coefficient is a direct measure of the fractal behaviour as it evolves in space-time, capturing the transition from highly clustered bursts towards quiescence behaviour (Idehara et al., 2014), where the exponent is close to 0. The intermediate range values ($0.4 < d_t < 0.8$) corresponds to the transition between the power-law bursts and the quiescence interval, ultimately reflecting the macroscopic behaviour of ETS episodes, which show a clear tendency of chain-reaction or cascade parabolic propagation over large distances, as proposed by Ide (2010), Ariyoshi et al. (2012), Ando et al. (2012). by plotting the gradient of $d_t(\tau, r)$ in respect to the inter-event distance. Next, for imaging this transition domain, we define the *correlation coefficient*

as the local slope between the temporal gradient and the logarithm of distance step r .

In 2010, a long-term slow slip event (L-SSE) occurred in the western part of Shikoku (Ozawa et al., 2013). To quantify the changes in LFE clustering behaviour caused by the nearby L-SSE, we divided each data set corresponding to Bungo Channel and West Shikoku segments into 3 data sets corresponding to before, during and after 2010 (Figure 2). Although very large ETS episode propagate from Bungo Channel to West Shikoku segment, sometimes with a temporal delay, the smaller clusters tend to show only local propagation. The gradient of $d_i(\tau, r)$ varies between 0 and 1, with high clustering intervals corresponding to the largest values. Modelling under the assumption of steady-state diffusion ($D=\text{constant}$) was performed by least-square fitting to the propagation front, indicating values between $10^4 \text{ m}^2/\text{s}$, similar to previously reported values (Ide et al. 2010, Kato et al., 2020, etc.). This fit can be improved by considering an empirical general equation for the migration front $R = a_1\sqrt{t} + a_2t^{\text{beta}}$ (De Barros et al., 2021), where the second term accounts for the observed acceleration in the propagation of LFE bursts. Values close to 0.5 indicate diffusive behaviour, while small a_2 or beta coefficient suggest low critical stress and can be omitted, as is seen in the case of both segments in 2010. Due to the occurrence of the L-SSE, the stress in the LFE region is released in bursts lasting about 1 day in Bungo Channel and up to 5 days in West Shikoku, without developing in large ETS episodes. In contrast, the before and after space-time pattern shows longer spatio-temporal correlations, with beta approaching 0.5, indicating clear parabolic propagation. The correlation coefficient is also a good indication of the clustering exponent, thus indicating the LFE density variation in space-time. Considering that the LFE count is a direct indication of the energy released during ETS episodes, it can be used to solve the unsteady-state diffusion equation to directly estimate physical parameters associated with anomalous stress diffusion.

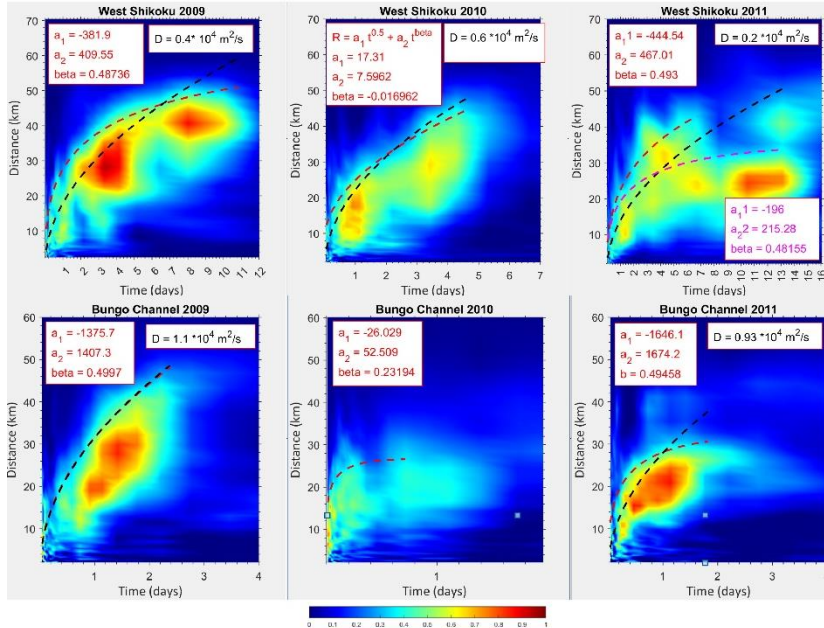


Figure 2. Space-time pattern revealed by the correlation coefficient d_{st} . Upper panel shows the macroscopic propagation pattern for West Shikoku segment, for LFE events occurring 1 year before the 2010 long-term SSE, during and 1 year afterwards, respectively (from left to right). Similarly, the down panel shows the pattern in Bungo Channel segment. The black dotted line indicates a steady-state diffusive front ($R = \sqrt{Dt}$) of coefficient D indicated in the upper right corner, while the red dotted shows the least square error fit for $R = a_1\sqrt{t} + a_2t^{\text{beta}}$.

Deep-learning algorithms have the potential to model and predict complex systems which might be difficult to model using large temporal and spatial data. For a LFE catalog with more than 500,000 events (Kato and Nakamura, 2020), we could further investigate space-time behavior of LFE clusters using PINN's (physics informed neural network algorithms) which allow data-driven discovery of physical parameters (diffusion, velocity, stress drop) by solving partial differential equations such as Fokker–Planck equation (FPE). Alternatively, it is more efficient to solve the inverse problem, which is to derive the terms of the FPE directly from the observation data. It requires no prior knowledge except assuming the observed data satisfies FPE, enabling us to uncover the unknown mechanisms behind the migration processes and whether or not we can identify heterogeneous or stressed regions within the subduction zone.

P-S travel time of low SNR events using polarization detection

Jingyi Sun¹, Yusuke Mukuhira¹, Takayuki Nagata², Taku Nonomura², Hirokazu Moriya³,
Takatoshi Ito⁽¹⁾

¹Institute of fluid science, Tohoku University,

²Department of Aerospace Engineering, Tohoku University,

³School of Engineering, Tohoku University.

Detecting low signal-to-noise ratio (SNR) microseismic events provides a way to understand subsurface reservoirs. We present a feasible method to detect S-wave arrivals of low SNR events. We introduce 3D particle motion analysis to characterize the polarization of the waveform. We capture the direct S-wave particle motion depicting the planar shape (planarity) and the P-wave arrival polarization perpendicular to the S-wave arrival polarization (perpendicularity). Previous studies have introduced spectral matrix (SPM) analysis to characterize 3D particle motion in the time and frequency domains and have detected P-wave arrivals for low SNR microseismic events. SPM analysis can detect coherent seismic arrivals but is insufficient to measure S-wave arrivals.

To distinguish S-wave from noise and to detect S-wave arrivals, we introduce the time delay coordinates of the SPM. We refer to the new SPM matrix as the extended spectral matrix (Ext-SPM). We evaluate the planarity and perpendicularity of the polarization in the time and frequency domains by introducing Ext-SPM analysis methods and combining them into a characteristic function. Then, we set a threshold of the characteristic function to detect the S-wave arrival time. The P-S travel time is the difference between the P-wave and S-wave arrival times. The P-S travel time result allows us to locate the hypocenter of the event. We apply our method to field data recorded at the Groningen field in the Netherlands to detect catalog events as well as low SNR events. In addition to this, we also try to apply our method to slow earthquake events.

Zhang et al., 2019 proposed a rapid seismic correlation and localization (REAL) method that focuses on correlating the arrivals of different phases and locating seismic events by calculating P and S pickup counts and travel time residuals. We also experimented with using P-S travel times to locate those detected events.

Determination of the non-slipperiest sand in Japan based on the double direct rotary shear experiment

Wataru Tanikawa¹, Manami Kitamura², Osamu Tada³, Riko Nakamura⁴, Harue Osada¹,
Yohei Hamada¹, Takehiro Hirose¹

¹JAMSTEC, ²AIST, ³Marine Work Japan Ltd., ⁴Kochi Univ.

In the summer of 2021, we held a scientific event called "Non-Slippery Sand Koshien" that determines "the non-slipperiest sand in Japan" as a part of JAMSTEC's 50th anniversary celebrations (<https://www.jamstec.go.jp/50th/suberanai/>). The goal of this event was to determine the least slippery sand among 50 types of sand or rocks (beach sand, volcanic ash, granite etc.) selected by the general public. A friction of fault rock is difficult to predict because it is influenced by various factors (mineral composition, grain size/shape), therefore, the mechanical data obtained from this event will lead to an understanding of the diversity of friction and earthquake process.

To determine the winner (= the least slippery sand), friction experiments of powdered materials were carried out using a rotary shear apparatus. Two different granular materials (about 1g with less than 1mm of grain size) were placed between two parallel layered simulated fault planes (25 mm diameter circles), and the same shear stresses were applied simultaneously to the granular materials (Figure 1). At the beginning of the game, the shear stress was increased at a constant acceleration (4 Nm/min) while the vertical stress was fixed at 4 MPa. When the rotation speed reached 0.1 rpm, the rotation was kept a constant of 0.1 rpm. As the frictional resistance of the granular material on the rotated side is relatively lower than that on the non-rotating side, the measured shear stress corresponds to that of the sliding side. To investigate the reason that the sand won the match, the relationship between the mineral composition, particle size, and grain density, and the shear stress were evaluated.

The winner of the match was "the powdered oyster shells cultivated in Wakasa Bay (Fukui Prefecture)". The sand particles that won the match tended to have a higher maximum shear stress. In particular, mechanically crushed powders from solidified rocks (igneous rocks, sedimentary rocks, and ores) showed higher maximum shear stress than natural granular materials such as beach sand and river sand. Granular materials with lower quartz content, larger average grain size, and larger specific surface area showed higher peak friction and tended to win the match. The major difference between artificially crushed sand and natural sand is that the former has an angular particle shape and the latter has rounded shape. The winner of "the crushed oyster shell" is partly composed by a flat-shaped grains that increases the contact surface area between grain particles. That could be one of the reasons for the win.

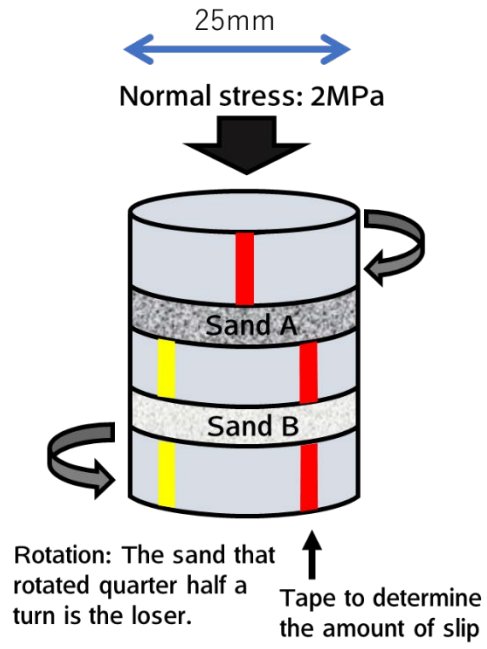
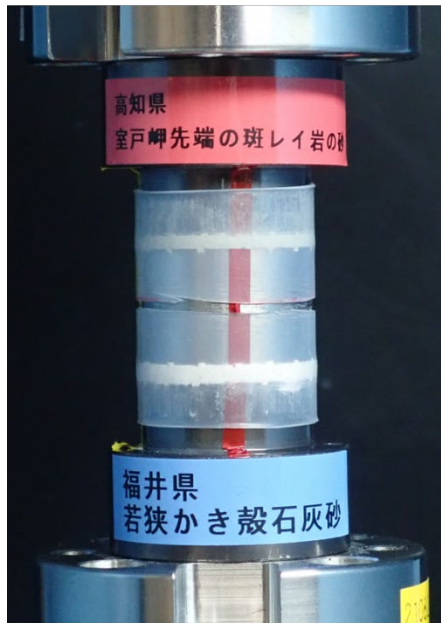


Figure 1. A photo and a sketch of the match to determine less slipperier sand (higher friction) using a biaxial deformation apparatus including triaxial pressure vessel.

Possible low velocity zone in the overriding plate beneath the Tosabae-Trough in the central-western Nankai Trough

Yasuyuki Nakamura¹, Kazuya Shiraishi¹, Gou Fujie¹, Shuichi Kodaira¹, and Gaku Kimura¹

¹JAMSTEC

To understand the structural characteristics related to the various slip styles along the plate boundary in the Nankai Trough subduction zone, we conducted seismic reflection profiling along densely spaced survey lines in the central-western Nankai Trough. Seismic data obtained along ~4 km spaced survey lines were processed with pre-stack depth migration (PreSDM). A three-dimensional depth map of subducting Philippine Sea plate was created from the interpretation of each PreSDM profile. The plate depth map showed an apparent arcuate depression on the surface of the Philippine Sea plate which runs ~100 km along the Tosabae Trough from off Kii Channel to off Cape Muroto. Velocity models previously derived from a nearby refraction seismic survey line showed a low-velocity zone in the hanging wall beneath the Tosabae Trough. Additionally, a recent result from full-waveform inversion (FWI) of the Ocean Bottom Seismograph data along a survey line off Cape Muroto also showed a prominent low-velocity zone in the overriding plate beneath the Tosabae Trough. The velocities in the deeper part of the overriding plate were not precisely constrained in the PreSDM analysis. We interpreted that the apparent depression illustrated on the plate depth map could actually indicate the low-velocity zone in the hanging wall sediments beneath the Tosabae Trough. The low velocities might be caused by faulting beneath the Tosabae Trough, such as the Kumano Basin Edge Fault zone suggested in the off Kumano area. This low-velocity zone is located at the boundary between the large slip zone of the 1946 Nankai earthquake and the zone with slow earthquake activity. The low-velocity zone in the overriding plate might constrain the up-dip limit of the megathrust rupture zone.

Investigate slow earthquakes variability and interaction with earthquake ruptures in Cascadia subduction zone

Zhen Liu¹, Yingdi Luo²

¹Jet Propulsion Laboratory, California Institute of Technology, Pasadena, USA

²JIFRESSE, University of California, Los Angeles, USA

Slow earthquakes such as tremor and slow-slip (ETS) along the Cascadia subduction zone display considerable variability at different spatiotemporal scales despite semi-regular recurrence and an intriguing increase of events frequency with depth. However, what causes such variability, especially the depth-dependent behavior remains elusive. We develop a laboratory-based rate-and-state asperity-in-matrix subduction fault model, supported by geological observations of exhumed fault with heterogeneous frictional properties and pore pressure variation to investigate the underlying processes of the observed ETS variability. We find that the depth-dependent variation of effective normal stress (pore pressure) is one important factor in controlling ETS behaviors, allowing us to reproduce the observed complexity of the ETS patterns and depth-frequency scaling that agrees quantitatively well with the observations. Based on the developed ETS zone model, we consider three downdip seismogenic extension and ETS transition scenarios and investigate how different transition configuration affects slow earthquake evolution and interaction with megathrust rupture throughout an earthquake cycle.